IUSS
Scuola Universitaria Superiore Pavia

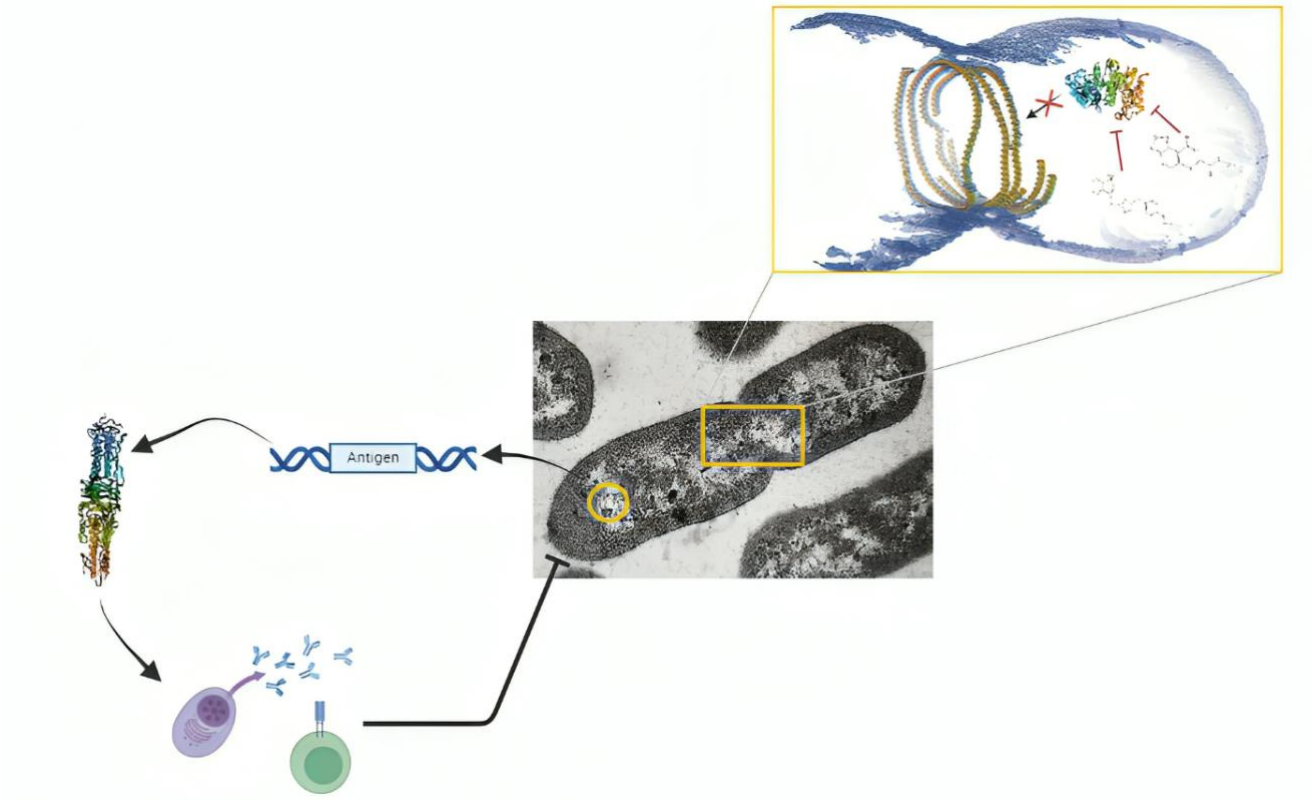

Scuola Universitaria Superiore IUSS Pavia

Novel approaches to manage antimicrobial resistances: a story of vaccine research and divisome inhibition

A Thesis Submitted in Partial Fulfilment of the Requirements

for the Degree of Doctor of Philosophy in

BIOMOLECULAR SCIENCE AND BIOTECHNOLOGY

by

Samuele Irudal

Supervisor: Silvia Buroni,

March 2024

Scuola Universitaria Superiore IUSS Pavia

Novel approaches to manage antimicrobial resistances: a story of vaccine research and divisome inhibition

A Thesis Submitted in Partial Fulfilment of the Requirements
for the Degree of Doctor of Philosophy in

BIOMOLECULAR SCIENCE AND BIOTECHNOLOGY

by

Samuele Irudal
Supervisor: Silvia Buroni, Department of Biology and Biotechnology

May 2024

Abstract

In recent years, the bacterial Multi-Drug Resistance phenotype has become a considerable burden in clinics as treatment success strictly depends on how an infection responds to a drug; unfortunately, the number of effective antibiotics is inevitably decreasing while few or none have been newly commercialized. In light of this, new approaches and alternative bacterial targets are necessary to balance such a delicate situation. Reverse vaccinology has proved useful in cases where vaccine discovery would be difficult; thus, this approach has been applied to the case of *Burkholderia cepacia* complex (Bcc) bacteria, a group of highly resistant Gram-negatives affecting mainly immunocompromised, and people with Cystic Fibrosis. The genomes of 26 *Burkholderia* strains, mainly belonging to the Bcc, were analysed and compared to identify highly conserved and potentially immunogenic proteins involved in virulence. Three candidates were selected, i.e., BCAL1524, BCAM0949, and BCAS0335, and their localization inside the bacterial cells was validated. Furthermore, their involvement in virulence was studied by creating deletion mutants and by characterizing: mutants antimicrobial resistance profile; auto-aggregation and biofilm formation; swimming motility and symptoms development in *Galleria mellonella*; in addition, as BCAM0949 exploited similarities with *Pseudomonas aeruginosa* EstA and LipC, its lipolytic and rhamnolipid production activity were investigated too. The data obtained suggest that BCAL1524 and BCAS0335 share a relevant involvement mainly in the establishment of *in vivo* infection; the lipase BCAM0949 mediates multiple phenotypes, among them swimming motility and biofilm and rhamnolipid production, which can be all linked to the lipid metabolism.

Another valuable strategy resides in targeting alternative bacterial structures respect to existing ones, such as the divisome. The filament temperature sensitive Z (FtsZ) protein is a highly-conserved target, providing an interesting platform for drug development in particular against the ESKAPE pathogens – which includes *Enterococcus spp.*, *Staphylococcus* aureus, *Klebsiella pneumoniae*, *Acinetobacter baumannii, Pseudomonas aeruginosa* and *Enterobacter spp.*, all known to acquire antibiotic resistance easily and to avoid drug treatment

effectively. Here, the C109 compound and a series of predicted inhibitory compounds were investigated for their FtsZ inhibitory activity against *Acinetobacter baumannii* and *Staphylococcus aureus*, respectively, by analysing the GTPase and polymerization activity *in vitro*. The antibiofilm activity of the C109 compound was tested on different *A. baumannii* strains, including three clinical isolates, showing variable inhibitory effects on sessile bacteria by blocking both FtsZ GTPase and polymerization activity. Regarding *S. aureus,* one of the predicted compounds, called C11, was found to efficiently inhibit bacterial growth at low concentrations by acting on FtsZ polymerization and to decrease *G. mellonella* death upon *S. aureus* infection. To conclude, the results obtained confirm how important to study of FtsZ inhibitory compounds is, in the particular context of nosocomial infections frequently characterized by drug-resistance.

ACKNOWLEDGEMENTS

Non sono mai stato bravo con ringraziamenti, né a farli e tantomeno a riceverli. Sono convinto che le persone che abbiano partecipato a questo "viaggio" sappiano da loro del contributo datomi, e non si sentiranno offese se non ricordate nella classica "lista della spesa" che spesso caratterizza questa sezione. Una volta arrivato a Pavia, dovetti rivedere e cambiare il mio modo di approcciarmi alla materia ed alla vita di laboratorio; è stato difficile, lungo e molte sono state le notti insonni (De André, 1971). Perché il percorso accademico prevede anche questo: molte soddisfazioni, molta crescita e molte esperienze, ma qual è il prezzo da pagare? Alla fine dei conti cosa resta?

Sicuramente le relazioni create sono quelle ci si porterà poi dietro, a prescindere dal percorso scelto dopo il dottorato; ovviamente, data l'eterogeneità del luogo di lavoro, i legami creati sono dei più diversi e disparati. C'è chi ha sempre una parola di conforto o di incoraggiamento, memore dell'esperienza pregressa; c'è chi invece ha consigli e suggerimenti preziosi, maturati con gli anni. Persone così diverse hanno impatti diversi, plasmano il carattere e a volte anche l'animo; per questo lasciano un segno che non sia solo nel ricordo. Come previsto, tutte queste persone hanno partecipato e partecipano alla mia crescita, rendendomi quello che forse può essere definito un "buon ricercatore". Grazie. Un grazie in particolare va a tutti gli studenti, sia triennali che magistrali, che mi hanno arricchito con i loro dubbi e le loro curiosità; spero di aver lasciato loro qualcosa sotto l'aspetto scientifico ma soprattutto sotto quello umano.

A tutta la mia famiglia va un ringraziamento speciale, per il sostegno e la motivazione che non hanno mai esitato a mostrarmi; la vostra fiducia è stata il mio punto di riferimento quando tutto il resto si muoveva troppo velocemente. Grazie anche per tutti i salva-pranzo del lunedì.

Table of Contents

LIST OF FIGURES

LIST OF TABLES

Introduction

ANTIBIOTICS, AN OVERVIEW

Antibiotic discovery lowered significantly mortality associated with infectious diseases, increasing the average life expectancy from 47 to 76.4 years in developed countries (https://www.cdc.gov/nchs/fastats/deaths.htm). The so-called antibiotic era started in the 1945 after global commercialization of Penicillin G, and witnessed its peak between the 1950s and the 1970s when a large number of antibiotics were discovered (Adedeji, 2016); according to their distinctive backbone, 12 major antibiotic classes are present, many of them isolated from different sources during the XX century (Powers, 2004). Different bacterial compartments can be targeted (Kapoor *et al.*, 2017): β-lactams and glycopeptides interfere with peptidoglycan synthesis, directly by targeting the enzymes involved (the Penicillin Binding Proteins) (Bush and Bradford, 2016) or by binding the D-ala-D-ala dimer precursor (Zeng *et al.*, 2016); aminoglycosides and macrolides block protein synthesis via 30S (Krause *et al.*, 2016) and 50S ribosome subunit inhibition (Vázquez-Laslop and Mankin, 2018), respectively, leading to cell death or growth impairment; trimethoprim and sulphonamides prevent folate production by acting on different step of the relative enzymatic pathway (Sköld and Swedberg, 2017); ansamycins, as rifamycin, inhibit bacterial RNA polymerase by forming a stable complex with its target, exerting a bactericidal activity (Goldstein, 2014); quinolones act on gyrase and topoisomerase IV converting them into toxic enzymes able to fragment the chromosome (Aldred *et al*, 2014); daptomycin, a lipopeptide, lead to membrane disruption by forming pore structures in Gram-positive membrane, with subsequent ion leak and depolarization (Miller *et al.*, 2016); polymyxin, another lipopeptide, possesses a hydrophobic tail linked to a positively-charged ring that allows interaction with the negatively-charged Lipopolysaccharide (LPS) and the subsequent insertion in the Gram-negative outer membrane, resulting in cell lysis

(Mohapatra *et al.*, 2021). Despite their number and chemical variability, the pace at which new antibacterial classes were produced rapidly decreased; the focus was therefore moved to the modification of already-known compounds and the rational synthesis of new molecules (Durand *et al.*, 2018). In particular, the click-chemistry approach, granting Sharpless the Nobel prize in 2022, relies its efficacy on functional groups present on the original backbone to bind two or more compounds (Demko and Sharpless, 2002); recently, Silverman *et al.*, (2017), managed to produce a series of vancomycin head-to-head dimers with increased potency against methicillin-resistant *Staphylococcus aureus* (MRSA) and vancomycin-resistant *Enterococci* (VRE). Moreover, the *in situ* click chemistry variant takes advantage of candidate precursors binding conformation in the target protein to guide linkage, in a faster and more efficient way (Glassford *et al.*, 2016). Instead, rational drug design relies on the *de novo* construction of chemical entities following a set of rules (such as Lipinski's rules), which determine activity against a target, non-toxicity, and other pharmacokinetic properties (Lewis, 2013); some examples are a series of arylquinoline compounds active against *Mycobacterium tuberculosis* H37Rv (Jain *et al.*, 2013) and the ETX0462 compound active *in vitro* and *in vivo* against ESKAPE (*Enterococcus faecium*, *Staphylococcus aureus*, *Klebsiella pneumoniae*, *Acinetobacter baumannii*, *Pseudomonas aeruginosa*, and *Enterobacter* spp.) pathogens (Durand-Reville *et al.*, 2021). Unfortunately, only a small number of the active molecules listed before were able to reach the market as production and clinical development costs are usually not counterbalanced by a sufficient economic return (Rex and Outterson, 2016). Future advances in the use of artificial intelligence, such as AlphaFold 2.0, may provide a cheaper, more efficient way to fill the gap between research and industry (Wong *et al.*, 2022). Surely, nowadays the market is witnessing a paucity of new antibacterial compounds which will be hardly recovered (Powers, 2004), while of great concern is the increasing rate of unsuccessful treatment caused by antibiotic resistance.

Novel approaches to manage antimicrobial resistances: a story of vaccine research and divisome inhibition.

ANTIBIOTIC RESISTANCE

Penicillin was first released in 1941 and no more than one year later the first penicillin-resistant *S. aureus* was identified (Center for Disease Control and Prevention, 2019); the trend was maintained also for other major antibiotics (**Figure 1**), e.g. resistance to methicillin and

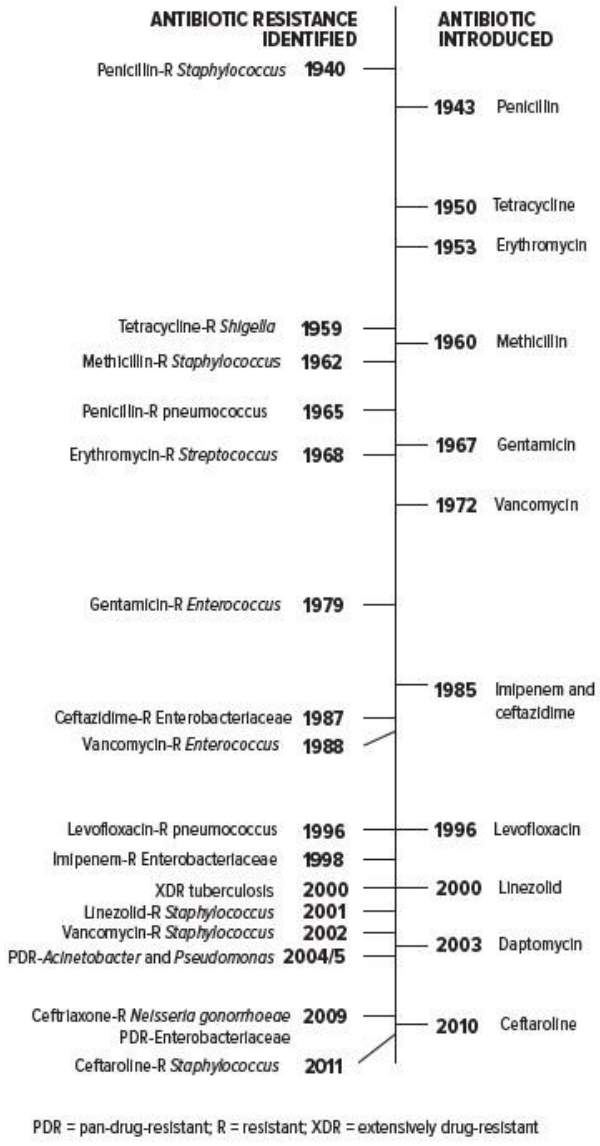

Figure 1: Timeline of antibiotics discovery and reported resistances (Ventola, 2015).

ceftazidime avibactam arose the same year the Food and Drug Administration (FDA) approved them; in contrast, it took over 40 years to observe vancomycin-resistant *S. aureus*. Interestingly, antibiotic resistance is a very ancient fact (Durand *et al.*, 2018); it is well-known that antibiotics are naturally produced as an effect of the competition between microorganisms, which have to thrive in the natural environment. Consequently, species able to produce antimicrobials need to avoid self-toxicity by producing resistance genes usually located within a biosynthetic antibiotic operon (Davies, 1994). In 2006, D'Costa *et al.* proposed the existence of the resistome, a "reservoir of resistance determinants that can be mobilized into the microbial community", after the identification of resistance genes in an environment where no antibiotic pressure was present; in addition, multiple multi-drug resistant (MDR) bacterial species were identified in archaeological sites as well as permafrost samples (Durand *et al.*, 2018). Since the transfer of resistome genes from environmental species to human pathogens has been proved (Jiang *et al.,* 2017), it is reasonable to suspect a role in MDR insurgence played by antibiotic use and overuse in clinical and agricultural settings (Waglechner and Wright, 2017).

As antimicrobials can target many distinct pathways in bacterial cells, bacteria evolved multiple ways to prevent self-toxicity and to proliferate under selective conditions (**Figure 2**).

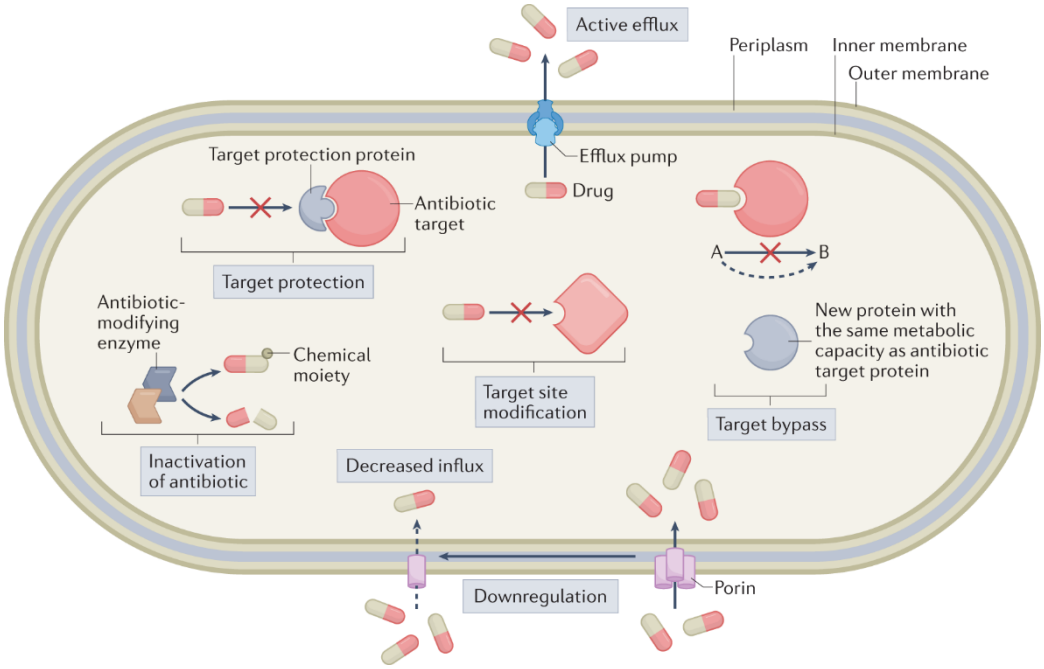

Figure 2: Schematic representation of the known antimicrobial resistance mechanisms (Darby et al., 2023).

Intrinsic resistance relies on proper structural and functional characteristics of the bacteria, for example, lack of cell wall or the presence of outer membrane which limits antibiotic diffusion; acquired resistance refers to naturally susceptible bacteria acquiring resistance determinants from other resistant bacteria, commonly via Horizontal Gene Transfer (HGT) (Sun *et al.*, 2019). The most ancient antibiotic resistance gene class identified, *bla*$_{OXA}$, is dated back to at least millions of years ago (Barlow and Hall, 2002) and encodes a β-lactamase, the most common resistance mechanism found in Gram-positive and -negative bacteria (Abushaheen *et al.*, 2020); these extracellular or periplasmic enzymes can hydrolyse the amide bond inside the β-lactam ring, inactivating it. Another class of enzymes directly acting on the

antibiotic is the aminoglycoside-modifying one (AME): according to the type of modification, it is divided into aminoglycoside O-phosphotransferases (APHs), N-acetyl transferases (AACs), and O-nucleotidyl transferases (ANTs); such modifications prevent the substrate from interacting with the 30S ribosome subunit (Krause *et al.*, 2016). A further adaptive mechanism consists of target modification, resulting in the antibiotic inability to recognize it: to note, variants exist of the PBPs which have lower affinity for penicillin (King *et al.*, 2014); trimethoprim resistance in *S. aureus* arises from a single-point mutation in the dihydrofolate reductase (*dhfr*) chromosomal gene (Abushaheen *et al.*, 2020); topoisomerase IV mutations, as well as *gyrA* and *gyrB* ones, reduce quinolone affinity to the enzyme-DNA complex (Aldred *et al.*, 2014); LPS structure and charge variation causes instead polymyxin resistance (Mohapatra *et al.*, 2021).

Alteration in membrane permeability represents one more mechanism to prevent compound entry and accumulation inside the cells; it relies mainly on the presence of a series of efflux pumps, which can increase the active antibiotic efflux outside the cell (Du *et al.*, 2018). Five different pump families are present with redundant or cooperative functionality: on one hand, the ATP-binding cassette (ABC) family, which activity is powered by ATP; on the other hand, the major facilitator superfamily (MFS), the multidrug and toxin extrusion family (MATE), the small multidrug resistance family (SMR) and the resistant-nodulation-cell division (RND) superfamily are all sustained by the transmembrane ion gradients (Du *et al.*, 2018). Considering their affinity for diverse harmful metabolic wastes and hazardous compounds, the presence of efflux pumps is usually correlated to the MDR phenotype. In Gram-negative bacteria, the RND family system is well-known and conserved (Nikaido and Takatsuka, 2009); its members are tripartite, formed by an inner membrane protein (IMP), a periplasmic membrane fusion protein (MFP) and an outer membrane protein (OMP). There is a high homology between RND pumps in different bacterial species and each component is required and necessary for drug export. ABC

pumps mediate solutes import and export: they possess transmembrane domains with substrate-binding and nucleotide-binding domains and are divided into homodimeric and heterodimeric groups (Du *et al.*, 2018); the latter is usually associated with intrinsic and acquired antibiotic resistance in Gram-positive bacteria. The MFS family is the most diverse and largest group of transporters, found in all organisms; it is composed of uniporters, symporters, and antiporters, while multidrug efflux is conferred by drug:H^+ antiporters 1 (DHA1) and 2 (DHA2) families. Bacterial MATE transporters are categorized into the NorM and DinF families, which employ H^+ and Na^+ gradients to efflux cationic and polyaromatic drugs (Du *et al.*, 2018). Finally, SMR proteins are small channels, functioning as homodimers or heterodimers and conferring resistance to lipophilic cations and quaternary ammonium compounds (Du *et al.*, 2018).

This vast asset of antimicrobial resistance proteins originates from years of adaptation and competition, where antibiotic pressure was low compared to nowadays clinical settings; today, the risk to generate multi-drug resistance pathogens is much higher, especially in fragile patients whose survival relies on drug administration.

Chapter 1

CYSTIC FIBROSIS AND CFTR CHANNEL MUTATIONS

Cystic fibrosis (CF) is an autosomal recessive life-threatening disease, with an incidence between 1/3000 and 1/6000 live births in the Caucasian population (Scotet *et al.*, 2020) and a worldwide estimation of 105.000 affected patients (https://www.cff.org/intro-cf/about-cystic-fibrosis). When first described by Andersen in 1938 (Andersen, 1938) life expectancy did not exceed the first year of life, while today the median age survival is near to 50 years. The responsible gene, *CFTR* (Cystic Fibrosis Transmembrane Regulator), was cloned and characterized over 30 years ago, thus increasing the management of CF (Kerem *et al.*, 1989; Riordan *et al.,* 1989). *CFTR* is located on chromosome 7 (7q31.2); it is 189 kb long and composed of 27 exons, encoding a protein of 1480 amino acids (Bear *et al*, 1992). It belongs to the ABC transporters, but differently from them, CFTR pumps anions (specifically Cl^-) down their electrochemical gradient through a channel pore (Csanady *et al.*, 2019). This channel is composed of two transmembrane domains (TMDs), each containing six transmembrane helices and two nucleotide-binding domains (NTBs), linked in a single polypeptide chain; further, the two NTBs are linked by a cytosolic regulatory (R) domain. Two processes regulate channel gating: to be active, the R domain has to be phosphorylated by cAMP-dependant protein kinase (PKA); then, ATP has to bind cytosolic NTBs to allow anions efflux.

More than 2.000 mutations can affect CFTR (http://www.genet.sickkids.on.ca/), while roughly 200 are known to cause CF (Csanady *et al.,* 2019). According to how they affect the protein, seven classes of mutations have been proposed as reported in **Figure 3** (De Boeck and Amaral, 2016): class I includes mainly missense mutations, often leading to mRNA degradation; class II, as F508del, affects correct protein folding and maturation, as traffic to the membrane is impaired; G551D is a class III mutation impairing channel

gating, while conductance is influenced in class IV mutations; class V mutations causes a reduction in the normal level of CFTR protein, as

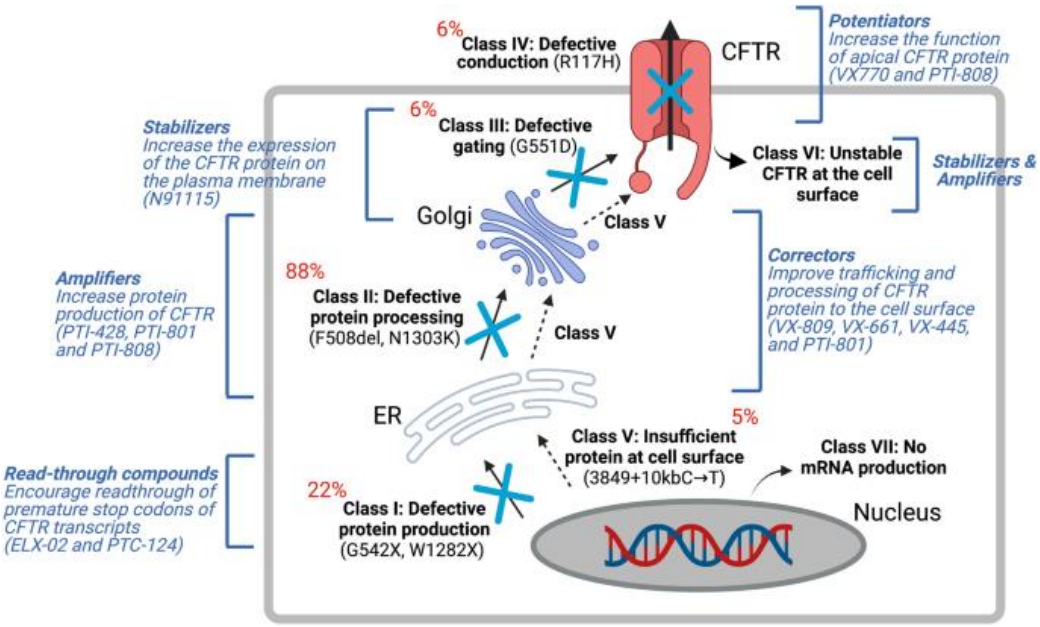

Figure 3: Summary on the mutations affecting CFTR channel (Lee et al., 2021).

they can lead to alternative splicing events originating both normal and aberrant mRNA; class VI reduces protein half-life in the membrane and, finally, class VII mutations consist in the so-called unrescuable mutations, caused by large gene deletions.

CF pathophysiology and inflammation control

Nevertheless, all the previously mentioned mutations result in unbalanced $Cl^-/HCO3^-$ efflux and increased Na^+ retention into the cellular space (Yu and Sharma, 2022); as a consequence, water resorption driven by osmotic pressure is increased giving rise to more viscous secretions. This thickened mucus leads to mucous plugging and obstructive pathologies (Yu and Sharma, 2022): in the pancreas, pancreatic juices cannot balance the acidic stomach chime thus preventing nutrients absorption; pancreatic autodigestion may even occur, with the involvement of the endocrine pancreas in chronic cases

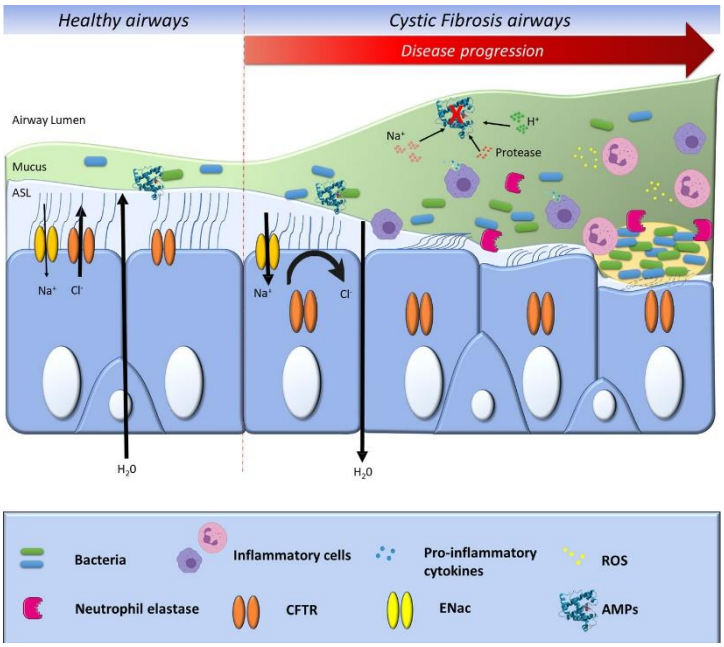

Figure 4: Graphical representation on CF lung disease progression (Mitri et al., 2020).

and the development of CF-related diabetes; meconium ileus at birth and intestinal obstruction during adult life are the main intestinal complications, while biliary and hepatic ducts occlusion can originate in the liver. In the lung, the disease is consequent to infection and inflammatory process (**Figure 4**). Mucus cannot be properly eliminated by mucociliary movement, so it can sustain opportunistic infections in the

airways as it is stacked in the bronchioles; indeed, the leading cause of death remains respiratory failure, with lethality of 44.4 % (Cystic Fibrosis Foundation, 2021) and 56.82 % (European Cystic Fibrosis Society, 2022) in USA and Europe, respectively. Clearance depends on the airway surface liquid (ASL), composed of two separate phases: a viscous one, trapping particulates on the upper face, and a lower, more fluid one, the periciliary layer (PL), which facilitates the movement of the cilia (Knowles and Boucher, 2002); increased water resorption in

the PL leads therefore to increased fluid density and impaired ciliary movement. Furthermore, the altered pH reduces the activity of antimicrobial peptides (AMPs) such as LL-37 and β-defensin-3, highly effective against *Pseudomonas aeruginosa* and *Staphylococcus aureus*, as experimentally proved by Alaiwa *et al.* (2014).

The neutrophilic infiltration and release of IL-8, along with IL-17, IL-1β, and IL-6, produce a perpetual condition of inflammation (Roesch *et al.*, 2018), which results in an increased mucous secretion and structural damage; thus, pulmonary function gradually decreases and eventually lung transplantation has to be considered. In parallel, increased elastase serine protease concentration correlates with a decrease in lung functions; as a consequence, lung structure deteriorates due to side-effect degradation of fibronectin and elastin as well as metalloprotease 9 activation (Cohen-Cymberknoh *et al.*, 2013). Other cell types, namely M1-macrophages and polarized Th2-, Th17- and Th22-lymphocytes, help to maintain the pro-inflammatory environment (Cohen-Cymberknoh *et al.*, 2013); airway epithelial cells can also stimulate such unbalance by producing TNFα (Cigana *et al.*, 2007).

In this light, the necessity to contain inflammation becomes pivotal: classical anti-inflammatory drugs include glucocorticoids, COX-1 and COX-2 inhibitors such as ibuprofen, and macrolides which can act on different layers of the inflammatory response; their usage has to be carefully monitored as side effects can range from gastro-intestinal complications to further dysregulated immune response (Balfour-Lynn *et al.*, 2006; Varrassi *et al.,* 2020). Nevertheless, to effectively reduce the rate of lung decline, inhaled corticosteroids and azithromycin are usually administered (Mitri *et al.*, 2020). Other treatments are under study, including immunomodulatory antibodies, anti-proteases, and gene-expression modulating compounds, which could carry new possibilities to effectively manage this pathology (Mitri *et al.*, 2020).

CFTR specific therapies

Thanks to the development of targeted therapies, CF became a chronic disease, with psychological, clinical, and economic burdens. The so-called modulators enhance or restore the correct expression of the *CFTR* gene affected by specific mutations (Lopes-Pacheco, 2020); according to their effect, they have been divided into five categories: potentiators can restore conductance and channel gating; correctors act on post-translational modifications and trafficking to the plasma membrane; stabilizers increase CFTR half-life and reduce its turnover; read-through agents and non-sense mediated inhibitors prevent premature termination and non-sense mediated decay, which decrease the quantity of CFTR transcript inside the cell (Lopes-Pacheco, 2020).

Currently, only four modulators have reached the market for the treatment of CF. In 2012 ivacaftor (Kalydeco®), a potentiator, was the first drug approved for ≥ 6 y/o patients with at least one G551D mutation (Barry *et al.*, 2014); thanks to its efficacy, its approval was extended to other additional 38 CF-causing mutations (Durmowicz *et al.,* 2018). A first-generation corrector, lumacaftor, was approved in 2015 for lumacaftor/ivacaftor (Orkambi®) co-treatment for ≥ 12 y/o patients carrying homozygous F508del (Wainwright *et al.,* 2015); for heterozygous F508del mutation with residual activity *in trans*, the combination with the second-generation corrector tezacaftor/ivacaftor (Symdeko®) was approved for ≥ 6 y/o patients in 2018 (Rowe *et al.*, 2017); both combinations were able to increase the level of active channel at the membrane. To further increase the therapeutic responsiveness in the case of F508del, the first triple combination tezacaftor/ivacaftor/elexacaftor (Trikafta®) was approved (Keating *et al.*, 2018) for ≥ 12 y/o patients, providing the same benefits of Symdeko® and Orkambi®. Despite these four medications could not restore the CFTR function, a protective effect against severe CF symptoms and rapid lung and pancreas deterioration was achieved, thus contributing to the development of future improved therapies. Due to the high number of different mutations, access, and side effects,

approximately 10% of people with CF (pwCF) is not eligible for treatment (Kramer-Golinkoff *et al.*, 2022); this percentage is expected to further decrease as a large number of other promising modulators is currently tested in clinical trials.

INFECTION IN CYSTIC FIBROSIS

Along with excessive inflammation, recurrent bacterial infections have to be promptly managed and controlled. As previously said, the lower respiratory tract cannot be maintained sterile due to the lack of mucociliary clearance, which fails to prevent bacteria colonization from the upper respiratory tract; additionally, the abnormal chronic inflammatory response fails to efficiently resolve infection (Henderson *et al.*, 2022). Such a condition promotes microenvironment variations, resulting in a hypoxic mucus layer sustaining bacteria organization in biofilm; in addition, this polymeric extracellular matrix protects from the host immune response and administered antibiotics, contributing to the establishment of opportunistic infections.

Biofilm in CF lungs is a complex structure undergoing continuous evolution from childhood to adulthood and it is composed of different bacteria whose interactions range from synergy to competition (Thornton and Parkins, 2023). During infancy and childhood, the presence of *Haemophilus influenzae* and *S. aureus* is characteristic, eventually supplanted in adulthood by Gram-negatives such as *P. aeruginosa* and *Burkholderia cepacia* complex bacteria. These bacteria have been considered indicators of lung function decline since their prevalence and abundance vary according to the advancing disease severity, while frequent and recurrent exposure to antibiotics may function as a promoting factor for airway dominance.

Staphylococcus aureus

S. aureus is a Gram-positive bacterium reaching its highest prevalence in childhood, and its acquisition is usually due to nasal colonization. In 2019 its overall prevalence in Europe was stable, 36.39% in children

and 35.98% in adults (European Cystic Fibrosis Society, 2022), while in the US the prevalence referred to 2021 peaked at 80% in the 6 to 10 y/o cohort and then decreased up to 10% in the ≥ 45 y/o cohort (Cystic Fibrosis Foundation, 2021); the reason of this frequency has to be found in the efficient early eradication strategies directed against other pathogens and in *S. aureus* rapid adaptation, aggregation and biofilm formation (Høiby, 2002). Additionally, clinical outcomes are influenced by *S. aureus* phenotypic divergence as mutations in metabolic genes promote Small Colony Variant (SCV) transformation and resistance to host defences and antibiotic pressure; consequently, SCV has been associated with worse lung function, chronic infection, and co-occurrent proliferation in the presence of *P. aeruginosa* or other pathogens (Junge *et al.*, 2016). Even though less present, MRSA still represents a risk for excess-associated mortality and further accelerated lung function decline (Thornton and Parkins*,* 2023; Rumpf *et al.,* 2021); clinical concern arises from its beta-lactams and fifth-generation cephalosporine resistance, mainly mediated by the acquisition of *mecA* gene. MRSA diffusion follows *S. aureus* one, with 5% and 18% of patients colonized in Europe and the US, respectively (European Cystic Fibrosis Society, 2022; Cystic Fibrosis Foundation, 2021). Up to now, no international eradication guideline is available, as clinical trials failed to demonstrate slower lung disease progression; nevertheless, different studies reported reduced exacerbation frequency and decreased rate of persistence after vancomycin inhalation therapy (Dezube *et al.,* 2019; Jennings *et al.,* 2014).

Haemophilus influenzae

Haemophilus influenzae, a Gram-negative coccobacillus, is medially more prevalent in the first 5 years of life (21.8%) than in adulthood (8.4%) and its presence in the lower tract is associated with local inflammation (Cystic Fibrosis Foundation, 2021; European Cystic Fibrosis Society, 2022). It possesses several factors involved in adhesion and persistence, while infections are usually transient and rarely persistence in the airway of a single strain is observed (Román *et al.,* 2004); in fact,

hypermutability phenotypic adaptation allows great diversity and, in part, resistance to different classes of antibiotics. Given its high turnover, no culture-specific therapy is available.

Pseudomonas aeruginosa

Pseudomonas aeruginosa, a Gram-negative bacillus, is the most prevalent bacterium in adults with an abundance peak between 41 and 50%, while a lower prevalence between 10 and 20% is observed in < 18 y/o (Cystic Fibrosis Foundation, 2021; European Cystic Fibrosis Society, 2022); this increase during lifetime is parallel to the decrease of *S. aureus* and *H. influenzae*, driven by antibiotic therapy to eradicate early airway colonizers and by bacterial exposure from soil and aquatic environments (Parkins *et al.,* 2018). Person-to-person transmission is possible, as several epidemic strains are shared exclusively in pwCF and many of them are associated with worse outcomes; during chronic infections, strains rapidly evolve to adapt to the host environment, even by acquiring mutations. The well-known transition to mucoid phenotype is indicative of rapid clinical decline and fitness advantages (Pritt *et al.,* 2007) since increased production of alginate, Pel, and Psl exopolysaccharides promotes the establishment and persistence of the infection through biofilm formation. Overall, the clinical impacts of *P. aeruginosa* chronic infection include frequent pulmonary exacerbation, lung function decline, lower nutritional state, faster progression to stage 4 lung disease and death; besides, early-age colonization is linked to a 10-year reduced survival on average, compared to uncolonized patients (Thornton and Parkins, 2023). Considering the outcomes, early eradication therapy is the golden standard to prevent chronic *P. aeruginosa*, with guidelines prescribing inhalation of colistin, tobramycin and/or aztreonam, or oral ciprofloxacin (Mogayzel *et al.*, 2014); different studies, such as the Early *Pseudomonas* Infection Control and the Trial for Optimal Therapy for *Pseudomonas* Eradication in Cystic Fibrosis, contributed to shed light on the best regimens to adopt (Treggiari *et al.,* 2011; Langton Hewer *et al.,* 2021), but once long-term

efficacy was evaluated, no benefit in clinical response was highlighted (Mayer-Hamblet *et al.,* 2015).

Stenotrophomonas maltophilia

Stenotrophomonas maltophilia is a Gram-negative bacterium that emerged as a CF pathogen thanks to the increased patients' life expectancy, with an overall incidence between 5 and 10% (Cystic Fibrosis Foundation, 2021; European Cystic Fibrosis Society, 2022); this rise in recent times has to be attributed mainly to the increased administration of antipseudomonal drugs (Amin *et al.,* 2020). It is not clear if *S. maltophilia* infection could have an impact on people experiencing higher rates of lung function declines and more advanced disease (Berdah *et al.,* 2018), yet Waters *et al.* (2011) pinpointed that chronic infection represented an independent risk factor for severe pulmonary exacerbation. No consensus guidelines are available and treatments usually rely on fluoroquinolones, next-generation β-lactams, β-lactamase inhibitors combinations (Amin *et al.,* 2020).

Achromobacter spp.

Achromobacter spp. are Gram-negative bacteria usually recovered from the environment, and isolation in clinical settings usually depends on the correct distinction from *P. aeruginosa* and on antibiotic usage (Tetart *et al.,* 2019). This group possesses high diversity as many species are as prevalent in pwCF as the historically most known one, *A. xyloxidans* (Edwards *et al.,* 2017); in total, the prevalence of the entire genus ranges from 3 to 7% (Cystic Fibrosis Foundation, 2021; European Cystic Fibrosis Society, 2022). Different intrinsic characteristics, such as the ability to form a biofilm, intrinsic antibiotic resistance, and hypermutability enable survival and lung disease progression, as confirmed in adults and children by Recio *et al.* (2018) and Sunman *et al.* (2022). Person-to-person diffusion and clonality have been suspected, while even if no eradication protocol is present, inhalation therapy with colistin, ceftazidime, and tobramycin efficiently kept patients free from infection after 3 years (Wang *et al.,* 2013).

Nontuberculous mycobacteria

Nontuberculous mycobacteria (NTM) are a group of heterogeneous environmental bacteria, with an increasing prevalence ranging from 4.8 to 9.76% (Cystic Fibrosis Foundation, 2021; European Cystic Fibrosis Society, 2022). Historically, they have been divided into "rapid" and "slow" growers, while their presence may be associated with a range of conditions, from asymptomatic to severe disease (Griffith *et al.,* 2007); similarly to *S. maltophilia*, increased isolation rate could be due to improvement in pwCF life expectancy and more accurate detection techniques, along with a heightened clinician awareness. The geographic distribution reflects NTM diversity, as *M. avium* complex (MAC) is diffused in North America and *M. abscessus* complex (MABSC) is more frequent in Western Europe and Israel; in parallel, MABSC-positive patients usually present more severe and even fatal lung disease compared to MAC-positive patients. Risk factors include age and, even if unclear, co-infection and drug exposure (Levy *et al.,* 2008). Survival relies on timely and accurate diagnosis, and treatments can be long and arduous, with a chance of significant side effects; guidelines for pulmonary infection prescribe administration of rifamycin, ethambutol, and macrolides, but emerging treatments include a combination of β-lactams, β-lactamase inhibitors, tetracycline derivatives, and oxazolidinones (Johnson *et al.,* 2023).

The *Burkholderia cepacia* complex

The *Burkholderia cepacia* complex (Bcc) is a group of over 20 Gram-negative species closely related (**Table 1**), isolated both in the environment and in clinical settings (Depoorter *et al.,* 2020; Peeters *et al.,* 2013); of particular interest, *B. cenocepacia* and *B. multivorans* are commonly identified in pwCF (LiPuma, 2010). During the last years, the incidence in children was around 1-2%, while it increased up to 4% in adults (Cystic Fibrosis Foundation, 2021; European Cystic Fibrosis Society, 2022). Despite the low incidence, Bcc bacteria, and in particular *B. cenocepacia*, have been associated with increased overall mortality and rapid respiratory decline with an increased pulmonary exacerbation

frequency compared to *P. aeruginosa* (Jones *et al.,* 2004); usually infection precludes lung transplantation, as rapid decline and higher mortality are likely to occur after that (Murray *et al.,* 2008). In parallel, the rare cepacia syndrome shows a near-uniform fatality, characterized by rapid necrotizing pneumonia with or without septicaemia. Differently from *P. aeruginosa*, patient-to-patient transmission is prevalent and raised concern in the diffusion of epidemic clones, in particular the ET-12 one, which originated in Canada during the 80s and further spread in Europe after patients attended a summer camp (Mahenthiralingam *et al.,* 2005); thus, early diagnosis and eradication therapies are the leading edges to prevent chronic infection. More recently, the presence of *B. cenocepacia* epidemic strains decreased in favour of the increased identification rate of *B. multivorans* mainly in the UK, Spain, and the USA (Kenna *et al.,* 2017; Medina-Pascual *et al.,* 2012; LiPuma et al., 2010). Treatment options partially overlap with *P. aeruginosa* ones: combinations containing third-generation cephalosporins (ceftazidime-tazobactam) or carbapenems (meropenem-vaborbactam) are elective, although Bcc basal antibiotic resistance and ability to acquire it may lead to fewer options (Lord *et al.,* 2020).

The species belonging to the Bcc carry complex genomes ranging from 6 to 9 Mb, among the largest identified until now, organized in three chromosomes: chromosome 1 (c1) (3.3-3.9 Mb), chromosome 2 (c2) (2.4-3.6 Mb) and chromosome 3 (c3) (0.5-1.4 Mb). Differently from c1 and c2, c3 was proved to be non-essential and therefore is now considered a mega-plasmid, conferring competitive advantages to the bacteria in its natural habitat (Agnoli *et al.,* 2012). They can rapidly adapt by acquiring mutations and possess great metabolic variability, which is reflected in their wide phenotypic plasticity. This characteristic made possible different biological applications, e.g. plant growth promotion and phytopathogen control (Chen *et al.,* 2020; Jung *et al.,* 2018) and sludge, soil, and wastewater bioremediation (Cauduro *et al.,* 2023; He *et al.,* 2022). Nevertheless, their resistance to heavy metals and xenobiotics is one of the leading causes of pharmaceutical products and

disinfectants contamination (Tavares *et al.,* 2020; Eissa *et al.,* 2016), which can result in nosocomial and even multi-center outbreaks since patients debilitated and elderly with CF or Chronic Granulomatous Disease (CGD) are the most endangered.

Species name	Reference
Burkholderia aenigmatica	Depoorter *et al.,* 2020
Burkholderia ambifaria	Coenye *et al.,* 2001a
Burkholderia anthina	Vandamme *et al.,* 2002
Burkholderia arboris	Vanlaere *et al.,* 2008
Burkholderia catarinensis	Bach *et al.,* 2017
Burkholderia cenocepacia	Vandamme *et al.,* 2003
Burkholderia cepacia	Yabuuchi *et al.,* 1992
Burkholderia contaminans	Vanlaere *et al.,* 2009
Burkholderia diffusa	Vanlaere *et al.,* 2008
Burkholderia dolosa	Vermis *et al.,* 2004
Burkholderia lata	Vanlaere *et al.,* 2009
Burkholderia latens	Vanlaere *et al.,* 2008
Burkholderia metallica	Vanlaere *et al.,* 2008
Burkholderia multivorans	Vandamme *et al.,* 1997
Burkholderia paludis	Ong *et al.,* 2016
Burkholderia pseudomultivorans	Peeters *et al.,* 2013
Burkholderia puraquae	Martina *et al.,* 2018
Burkholderia pyrrocinia	Vandamme *et al.,* 2002
Burkholderia seminalis	Vanlaere *et al.,* 2008
Burkholderia stabilis	Vandamme *et al.,* 2000
Burkholderia stagnalis	De Smet *et al.,* 2015

continue

Burkholderia territorii	De Smet *et al.,* 2015
Burkholderia ubonensis	Yabuuchi *et al.,* 2000
Burkholderia vietnamiensis	Gillis *et al.,* 1995

Table 1: **List of bacteria included in the *Burkholderia cepacia* complex**

When first isolated in 1977, *B. cepacia* was grouped in the *Pseudomonas* genus (namely *P. cepacia*), while lately all the isolates were simply recognized as a single *B. cepacia* species (Laraya-Cuasay *et al.,* 1977). From mid-1990 the presence of multiple different species inside *B. cepacia* became clear, thus proposing five genomovars – genotypically different but phenotypically similar groups (Vandamme *et al.,* 1997), organized under the name *Burkholderia cepacia* complex. Over time, more species were added to the Bcc, many of them with involvement in clinical settings; in this light, taxonomy and species identification grew pivotal, considering the high level of similarity shared between the species. Automated and manual phenotypic identification, using VITEK 2 or Phoenix systems, is not suitable due to the high similarity of biochemical results between the species (Furlan *et al.,* 2019). *recA* sequencing is valuable for identification at the genus level, while it may fail for species identification, as sequence identity ranges from 94 to 95% (Coenye *et al.,* 2001b); similarly, 16S rRNA and *hisA* sequencing suffer the same limitations as above (Jin *et al.,* 2020; Papaleo *et al.,* 2010). Nevertheless, *recA* analysis is still more reliable than the emerging matrix-assisted laser desorption ionization-time-of-flight mass spectrometry (MALDI-TOF MS), as it failed to distinguish at the species level a set of previously *recA*-identified Bcc strains (Gautam *et al.,* 2017). To conclude, the most precise taxonomic identification tool used today is multilocus sequence analysis (MLSA), since it utilizes nucleotide sequences of different housekeeping alleles, such as *tpD*, *gltB*, *gyrB*, *recA*, *lepA, phaC,* and *trpB* genes, to discriminate Bcc members even at the strain level (Baldwin *et al.,* 2005).

Burkholderia cenocepacia

The most studied bacterium of the Bcc, *B. cenocepacia*, represents a major threat for pwCF; according to *recA* sequence similarity, the most pathogenic strains have been divided into subgroup IIIA, IIIB, and IIID, while IIIC includes the environmental ones (Drevinek *et al.*, 2008a). In addition to *recA*, the *B. cepacia* Epidemic Strain Marker (BCESM) provides a valuable tool to identify and classify virulent epidemic strains, as it correlates with virulence, transmissibility, and mortality; it is part of a low-GC-content genomic island long 31.7 kb and encoding 35 predicted coding sequences, including genes involved in quorum-sensing, DNA-mobilization, and transcriptional regulation, but no virulence factors (Drevinek *et al.*, 2008a).

The Edinburgh-Toronto lineage (ET-12) is the first transatlantic lineage identified, originated in North America and diffused in Europe in 1989 (Drevinek and Mahenthiralingam, 2010; Mahenthiralingam *et al.,* 2005). The strains belonging to this group are rarely isolated in the environment, suggesting a definite shift towards host-associated pathogen life; *B. cenocepacia* J3125 and K56-2 are the most studied strains, as their multi-drug resistance profiles and clinical impact are particularly relevant. Differently from the other epidemic lineages, the ET-12 possesses the major cable pilin subunit *cblA* (Mahenthiralingam *et al.,* 1996).

Along with ET-12, two other strain types, the Canadian RAPD 01 and the European CZI, were isolated in 1996 and 2005 (Drevinek e*t al.,* 2005; Mahenthiralingam *et al.,* 1996). They were later identified as the same ST-32 lineage thus raising the possibility of an intercontinental spread, but no epidemiological link has been highlighted today. As ET-12, they belong to subgroup IIIA. In parallel, in the USA the most prevalent *B. cenocepacia* epidemic clones belong to subgroup IIIB and include the PHDC strain and the Midwest clone, isolated in 2001 and 1988 (Chen *et al.,* 2001; LiPuma *et al.,* 1988). While the Midwest clone caused several infections in the Great Lake region, PHDC has been

endemic for at least 20 years in different CF centres and raised concerns as it was the first to be identified from agricultural soil too (LiPuma *et al.,* 2002). Moreover, the PHDC strain has been the second confirmed transcontinental strain as it was identified also in European pwCF (Coenye *et al.,* 2004).

B. cenocepacia J2315 and K56-2 genomes

B. cenocepacia J2315 transmissibility and virulence raised concern during many outbreaks in Canada and Europe, thus increasing the interest in gaining knowledge about its genetics and pathogenicity; therefore, it was the first Bcc strain to be fully sequenced (Holden *et al.,* 2009). *B. cenocepacia* J2315 genome is one of the largest among Gram-negatives, 8.06 Mb long and with a GC content of 66.9%; it is composed of three circular chromosomes and the pBCJ2315 plasmid, carrying 3537, 2849, 776 and 99 coding sequences respectively, of which 126 are pseudogenes or partial genes. While c1 contains mainly CDSs involved in cell division, basal metabolism, and other core function genes, c2 and c3 contain a greater proportion of accessory and unidentified genes; in particular, c1 carries a 57-kb duplicated region which localizes on different locations on the chromosome, each of them containing 57 CDSs and thus resulting in increased gene dosage. When compared, the genome of J2315 shared up to 78% of orthologs CDSs with Bcc, with the greatest conservation on the largest chromosome; the remaining 21% of the DNA in J2315 consists in regions of difference (RODs) (Holden *et al.,* 2009). These regions are likely originated from recent horizontal gene transfer and include mainly lineage-specific DNA indels and allelic variants (11.7%) and genomic islands (9.3%), characterized by abnormal GC content and by CDSs showing similarities with genes associated with mobile genetic elements, such as transposons and plasmids; indeed, the presence of fourteen horizontally-transferred unique putative genomic islands has been correlated with J2315 virulence and pathogenicity. The best described is the 44-kb *cenocepacia* island (cci), with stress response regulators and genes involved in arsenic and antibiotic resistance, amino acid and fatty

acid metabolism, and different regulators, including an *N*-acyl-homoserine lactones (AHLs)-dependent quorum-sensing systems (Baldwin *et al.,* 2004); moreover, the *Burkholderia cepacia* epidemic strain marker (BECSM) was identified inside the cci, allowing a useful tool to distinguish epidemic strains. Along with gene acquisition, the loss of genes played a rather significant role in the pathogenicity of this strain, as proved by J2315 ability to persist in a harsh environment and to chronicize. A similar behaviour has been observed in *P. aeruginosa*, as loss of genes involved in LPS production conferred protection from the immune system and establishment of chronic lung infection (Marzhoseyni *et al*., 2023).

After more than ten years, the genome of the K56-2 strain was completely sequenced too (García-Romero and Valvano, 2020). Genome organization is maintained as in J2315, with a mean GC content of 66% and a length of 7.7 Mb: c1, c2, and c3 carry 3337, 2880, and 651 genes respectively, while the smaller replicon, identified as a plasmid, carries 106 genes and share a 99.9 % of identity with pJ2315.

B. cenocepacia virulence factors

B. cenocepacia infections are amongst the most feared among pwCF, as they are associated with rapid lung deterioration, reduced survival, and an overall worst outcome; a wide range of virulence factors contribute to such phenotype (**Figure 5**), allowing an efficient adaptation to the stressful lung environment.

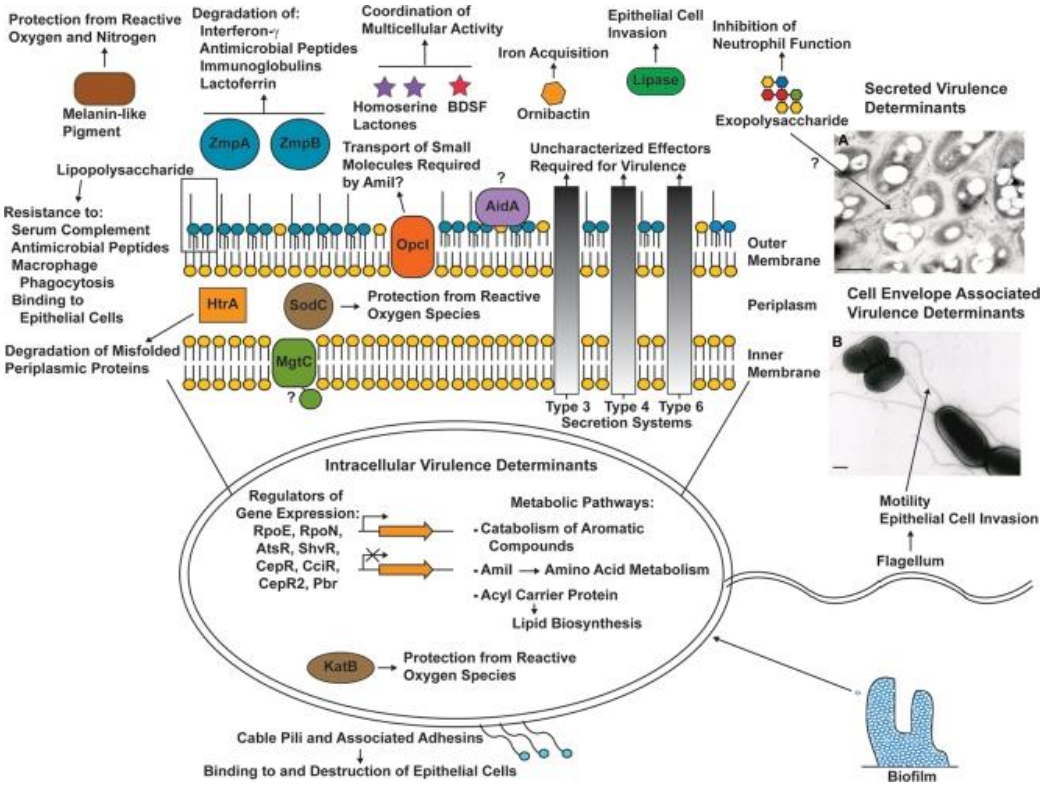

Figure 5: Summary of the principal virulence factors identified in B. cenocepacia (Loutet and Valvano, 2010).

Quorum-sensing (QS) regulates multiple genes through two diffusible molecules, the N-acyl homoserine lactone (AHL) and cis-2-dodecenoic acid (*Burkholderia* diffusible factor, BDSF), both produced in a cell density-dependent manner (Schmid *et al.,* 2017). AHL acts through an AHL synthase CepI and a regulator CepR, belonging to the LuxIR-

family; eventually, additional components, such as the CciI synthase and the CciR regulator, may be present, located on the genomic island II. In 2009 a third orphan regulator, named CepR2, has been identified as adjacent to no AHL synthase (Malott *et al.,* 2009). Analogously, BDSF is synthesized by the bifunctional crotonase RpfF and exerts its activity by binding to the RpfR receptor, lowering the intracellular c-di-GMP concentration and upregulating different virulence factors, some of them shared with the AHLs systems (Schmid *et al.,* 2017). Genes regulated by QS include those for protease production, siderophore synthesis, motility, biofilm formation, and secretion systems (Piochon e*t al.,* 2020); in the K56-2 strain, CepR mainly functions as a positive regulator upregulating downstream genes, while CciR acts as an inhibitor of gene expression.

As *B. cenocepacia* growth strictly depends on iron availability, especially in a nutrient-depleted environment such as the lung, different secreted siderophores act to scavenge free iron from the surrounding, e.g. ornibactin, the biologically more important siderophore, and pyochelin (Visser *et al.,* 2004). In the human host, iron is usually in complex with proteins like transferrin or heme which make it more soluble; as free iron is insoluble, low-molecular-weight chelators produced by bacteria allow transport and solubilization. Interestingly, some J2315 strains defective for a gene involved in pyochelin biosynthesis have been reported to be able to produce this chelator in an iron-deficient medium, meaning that the entire pathway may still be functional (Jaiyesimi *et al.,* 2021).

On the outer membrane surface, one of the major components is lipopolysaccharide (LPS). Interestingly, LPS can be modified with a variety of sugar modifications, resulting in adaptation to chronic infection, persistence, and increased resistance to charged antimicrobial peptides (Loutet *et al.,* 2006). J2315 does not possess the O antigen at all, leading to an adaptive phenotype during infection and a consequent shift towards chronicization. Capsular exopolysaccharide (EPS) is

another factor playing a significant role in chronicity; the most abundant one is cepacian, which appears to enhance the virulence once expressed. As the O antigen, cepacian expression is lost in the J2315 strain (Drevinek and Mahenthiralingam, 2010).

B. cenocepacia is characterized by intrinsic resistance to β-lactams, polymyxins, and aminoglycosides, and it can acquire *in vivo* resistance to virtually all antibiotic classes (Sass *et al.,* 2011). It possesses a variety of antibiotic-modifying enzymes, such as β-lactamases, and dihydrofolate reductase, alternative drug targets, active efflux pumps, and decreased cell wall permeability (Rhodes and Schweizer, 2016). Among them, the most versatile resistance mechanisms are the efflux pumps, especially the well-studied RND efflux transporters (Buroni *et al.,* 2014; Guglierame *et al.,* 2006); their expression usually varies according to the concentration of the substrate. Additionally, RND pumps involvement is dependent on the physiological growth of the bacteria (planktonic or sessile).

Adherence and motility are two determinant factors for epithelial lung cell invasion; as the flagellum allows movement through different density media, it also serves as an adhesin to contact host cells (Pimenta *et al.,* 2021a). While transcriptome analysis in *P. aeruginosa* pointed to a decreased expression in motility-associated genes during chronic infection, an opposite trend was reported in *B. cenocepacia* in agreement with its ability to cause life-threatening septicaemia. Genes involved in the synthesis and assembly of flagella are usually organized in clusters, since the J2315 strain possesses five of them distributed on chromosome 1 and, eventually, additional genes are present on chromosomes 2 and 3 (Holden *et al.,* 2009); of note, flagellar gene transcription is quorum-sensing dependent (O'Grady *et al.,* 2009). Unique to ET-12 lineage is the presence of the 22-KDa adhesin AdhA in association with the cable pili CblA, which has been reported to be essential for invasion; further analyses demonstrated how AdhA

expression increases during growth in sputum, shedding light on its role during infection (Drevinek *et al.,* 2008b).

B. cenocepacia can produce biofilm on both abiotic and biotic surfaces (Coenye *et al.,* 2001b). Once adhered, sessile cells start producing polysaccharides in response to intercellular communication, thus organizing in microcolonies that entrap nutrients and bacteria; progressively, the amount of matrix increases leading to biofilm maturation and subsequent dispersion. Biofilm production is mainly regulated by the AHL-mediated QS system (Schmid *et al.,* 2017) and the c-di-GMP dependent sigma factor RpoN (Fazli *et al.,* 2017), while it relies on cell adhesion via flagella or pili and on iron availability (Berlutti *et al.,* 2005). EPS is one of its major components granting mechanical stability and attachment, both providing a physical barrier impairing leucocytes extravasation and protecting bacteria from immune system recognition and environmental stresses (Murphy and Caraher, 2015). Moreover, this matrix allows the differentiation of persister cells, i.e. a subpopulation of cells characterized by a lower basal metabolism and by resistance to antibiotics.

Despite the factors involved in persistence are not fully understood, toxin-antitoxin modules (TA) are thought to participate in this process (Van Acker *et al.,* 2014). Usually organized in operons, they consist of a stable toxin coupled with an unstable antitoxin; this latter is degraded under stress conditions resulting in the increased concentration of the cognate toxin. Such unbalance inhibits some important basal cellular functions, switching to the characteristic antibiotic-insensitive state of persister cells.

Other pathogenicity factors include exoproducts, such as zinc metalloproteases and lipases (Mullen *et al.,* 2007; Straus *et al.,* 1992). Zinc metalloproteases, such as ZmpA and ZmpB, disrupt tissue integrity and host defence mechanisms by cleaving different cytokines, lactoferrin, collagen, and human immunoglobulin, and by inactivating mammalian

protease inhibitors (Kooi *et al.,* 2006). Despite the lipases have been studied for their biotechnological applications, little is known about their role in virulence; nevertheless, the presence of lipases is correlated to increased epithelial cell invasion rate and with inhibition of alveolar macrophage phagocytosis. To survive internalization, *B. cenocepacia* can also rely on different factors: a type IV secretion system prevents endosome-lysosome fusion, inhibiting bacteria degradation (Sajjan *et al.,* 2008); cytoplasmic SodB and periplasmic SodC superoxide dismutases and KatA and KatB catalase-peroxidases confer resistance to the oxidative stress generated inside cells and phagocytes, easing bacterial survival inside phagosome; *B. cenocepacia* melanin-like pigment acts as a scavenger for oxidative species, attenuating the oxidative burst (Keith *et al.,* 2007); the sigma factor RpoE and its homolog genes are activated in case of osmotic stress and macrophages, delaying phagolysosomal fusion (Flannagan *et al.,* 2008).

This wide variety of factors is indicative of a bacterium adapted to stressful environments, which evolved different mechanisms to survive and persist despite the harsh conditions of the host; exploiting such an arsenal would provide new options for targeted therapy and preventive strategies.

B. cenocepacia **canonical and alternative treatments**

As stated before, there is no standard approved drug therapy as data correlating antibiotic resistance *in vivo* and *in vitro* are still lacking; therefore, no information is available on the duration and efficacy of mono vs. combined antibiotic therapy. Nevertheless, combinations of first- and second-line β-lactams are preferred as trimethoprim-sulfamethoxazole moderate toxicity cannot be ignored; in parallel, inhalation therapy with aztreonam and tobramycin efficiently counteracted *B. cenocepacia* chronic infection, but no improvement in lung function could be observed (Waters *et al.,* 2017; Tullis *et al.,* 2014). Simultaneous administration of corticosteroids and immunosuppressors, as IFN-γ, may adjuvate antibiotic efficacy by

modulating the host response to infection, in particular in the case of cepacia syndrome (Assani *et al.,* 2014; Gilchrist *et al.,* 2012).

Recently, a newly developed alginate oligosaccharide (OligoG) has shown antibiotic potentiation through biofilm disruption, but further studies are needed to define the impact on bacteria load (Fischer *et al.,* 2022); on the contrary, phage therapy alone or in synergy with antibiotics produced a significant decrease in *B. cenocepacia* CFU, even when treating antibiotic-resistant cells (Mankovich *et al.,* 2023). As an upstream approach to interfere with different virulence factors, quorum sensing inhibitors (QSI) have been developed and studied: many of them are analogues of AHL, obtained by modifying the lactone moiety (Brackman *et al.,* 2012); lately, a new family of diketopiperazines was found to inhibit the activity of CepI synthase, hindering proteases and siderophores production as well as biofilm formation, and showing *in vivo* activity in a *Caenorhabditis elegans* infection model (Scoffone *et al.,* 2016). To conclude, the benzothiazole derivative C109 has been proven to interact with *B. cenocepacia* divisome protein FtsZ, a homolog of human tubulin involved in the bacterial division; such compound inhibited GTPase activity and polymerization *in vitro*, while inducing bacteria filamentation and death (Hogan *et al.,* 2018).

Novel approaches to manage antimicrobial resistances: a story of vaccine research and divisome inhibition.

A VACCINE FOR BCC

Much progress was made in the past years which shed light on Bcc pathogenesis, virulence factors, host-pathogen interactions, and host immune response (**Figure 6**); despite all, there have been slow

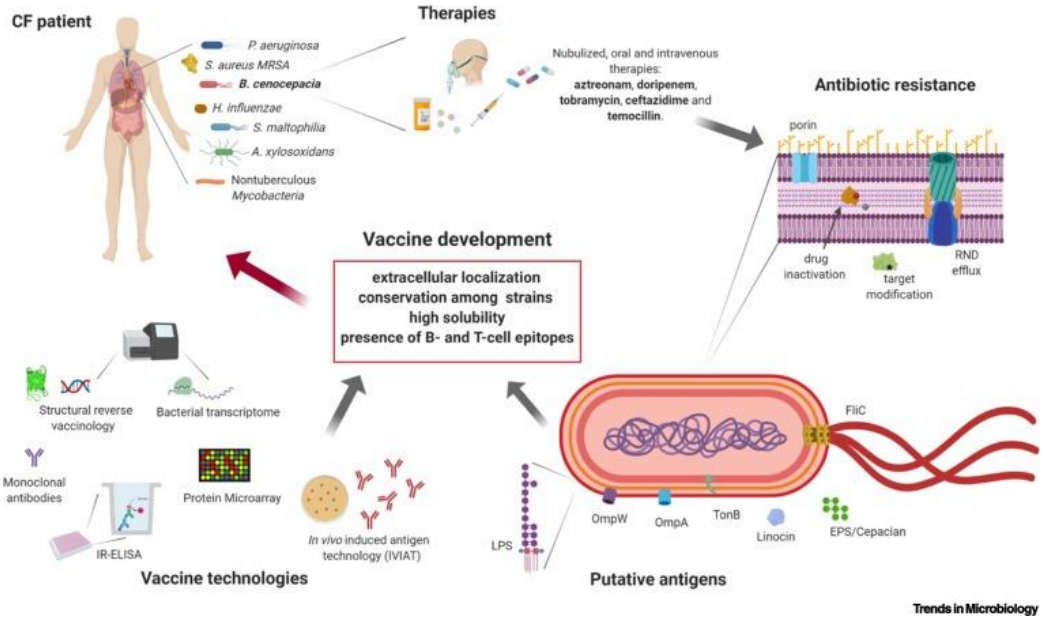

Figure 6: Advancements, strategies and critical steps in managing B. cenocepacia infection. (Scoffone et al., 2020)

advances from the clinical point of view and chances of successful treatment strictly depend on the identification. Moreover, no further steps were made in the development of a vaccine since different challenges have to be overwhelmed, e.g. proper safety and efficacy and long-lasting immunity against chronic and acute infections (Wang *et al.,* 2020); of note, *Burkholderia* is known to survive intracellularly and therefore its antigens have limited visibility to the immune system. As a consequence, full protection against intracellular bacteria would require not only the presence of neutralizing antibodies but also an appropriate cellular immune response.

Classical vaccine discovery approaches

While no literature is present on heat-killed vaccines, different groups focused on the development of subunit-based ones as multiple membrane proteins could be identified via genome-available information. Bertot *et al.* (2007) were able to induce mucosal and systemic immunization in rats by administering a mixture of outer membrane proteins (OMPs) from *B. multivorans* in combination with the adjuvant adamantylamide dipeptide; in a mouse model of chronic infection, the production OMP-specific secretory IgA was involved in the enhanced clearance of *B. multivorans* from lungs and reduced disease signs. In addition, protection against *B. cenocepacia* challenge was observed, suggesting a cross-protective role towards other Bcc pathogens.

Later in 2010, Makidon *et al.* expanded the previous study by producing an OMP-nanoemulsion (OMP-NE) intranasal formulation obtained from *B. multivorans*, which elicited IgA and IgG-mediated protection without any bias between Th1 and Th2 response; moreover, cross-protection was observed against other *B. cenocepacia* strains. In particular, a 17 kDa OmpA-like protein was found to be immunodominant and widely conserved among Bcc and non-Bcc strains, remarking its involvement in cross-reactivity and its potential for future vaccine development. Another 24 kDa OmpA-like protein, namely BCAL2958, was identified in *B. cenocepacia* J2315 and among 6 other different Bcc species (Sousa *et al.,* 2016); once expressed and purified, it was able to interact with IgG in sera from pwCF previously experiencing respiratory infection by Bcc, meaning that antibodies anti-BCAL2958 were produced during the infection. Furthermore, the purified protein was able to stimulate neutrophils production *in vitro*, increasing the secretion of TNFα, nitric oxide (NO), and elastase; parallelly, myeloperoxidase and catalase secretion was enhanced, reducing the level of extracellular H_2O_2. Such an effect on neutrophils is thought to have a downstream effect on dendritic cells and monocytes, which are

stimulated to differentiate into mature antigen-presenting cells (Cerutti *et al.,* 2013).

A surfomics approach allowed the identification and the isolation of 16 extracellular proteins expressed by *B. cenocepacia* J2315 (Sousa *et al.,* 2020a), by treating bacteria with trypsin and analysing the following amino acid fragments via liquid-chromatography–tandem mass spectrometry. One of them, the OmpA-like BCAL2645 protein, was immunoreactive against sera from pwCF with anterior Bcc infection (Seixas *et al.,* 2021); its expression was increased in growth conditions mimicking CF lungs and its microaerophilic environment, and a raised polyclonal anti-BCAL2645 antibody was able to inhibit *B. cenocepacia* K56-2 adhesion and invasion on CFBE41o- bronchial epithelial cells. Once the gene encoding the protein was deleted, the relative mutant produced a thinner biofilm compared to the wild-type strain.

Analogously, Sousa *et al.,* (2020b) developed an immunoproteomic approach to identify *B. cenocepacia* J2315 proteins stimulating the humoral immune response of the CF host; basically, supernatant from bacteria grown in artificial sputum medium (ASM) was incubated with serum samples from pwCF chronically infected by Bcc, detecting 9 immunoreactive and extracellular proteins conserved across Bcc genomes. Among them, a group of proteins including the phage-shock protein PspA (BCAL2022), the chaperone GroEL (BCAL3146) and the ferredoxin-NADP reductase Fpr (BCAL0536) have been identified also in outer membrane vesicles (OMVs) in *B. pseudomallei*; OMVs are nonreplicating particles produced by Gram-negatives following stress stimuli and are known to contain highly immunogenic proteins which may be used as vaccines (Toyofuku *et al.,* 2023). Nevertheless, further studies regarding the protective role in mice have to be performed.

With a different immunoproteomic technique, linocin and OmpW were identified (McClean *et al.,* 2016): proteins from different strains of *B. cenocepacia* and *B. multivorans* were first blotted on a 2D blot and then

incubated with CF lung epithelial cells or with sera from pwCF infected by Bcc; by merging the data, linocin and OmpW were isolated as both immunoreactive and involved in cell adhesion. Like the previous proteins, they were able to elicit a potent humoral response *in vivo*. Mice immunized with recombinant OmpW or linocin were protected against *B. multivorans* and *B. cenocepacia* challenge, inducing a mixed Th1/Th2/Th17 response and stimulating IL-6, IL10, and IL-17 production, which are likely to protect from extracellular and intracellular bacteria. When overexpressed in *Escherichia coli*, linocin and OmpW conferred enhanced attachment to lung cells, confirming their role as adhesins.

As interfering with adhesion proved to be an efficient way to provide host protection from infection, trimeric autotransporter adhesins (TAAs) acquired even more importance for vaccine study (Thibau *et al.,* 2020). TAAs are a class of highly conserved adhesins present exclusively in Gram-negatives and with a unique head-stalk-structure composed of three identical proteins; many of them, as *Salmonella enterica* SadA, *Haemophilus influenzae* Hia and above all *Neisseria meningitidis* NadA, which is one of the main antigens in 4CMenB vaccine, showed remarkable immunogenicity. In Bcc, two of the first studied TAAs were BCAM0223 and BCAM0224 (Mil-Homens *et al.,* 2014; Mil-Homens and Fialho, 2012); different phenotypes were attenuated upon their inactivation, namely hemagglutination, biofilm formation, adherence to vitronectin and human bronchial cells, virulence in *G. mellonella* and resistance to human serum, suggesting that these two virulence factors are involved in infection establishment. Relevantly, the eligibility of TAA BCAM2418 as a vaccine candidate was studied later by Pimenta *et al.,* (2021b). First, antibodies anti-TAA were generated by immunizing goats with a BCAM2418 N-terminal fragment; then, co-incubation with *B. cenocepacia* K56-2 and J2315, *B. multivorans* VC13401, and *B. contaminans* IST408 was performed in an adhesion assay with mucin or bronchial epithelial cells; in all the cases, adhesion decreased in a dose-dependent manner highlighting the cross-

protection provided by the antibody. Moreover, *G. mellonella* protection from *B. cenocepacia* K56-2 was successfully achieved when bacteria were pre-incubated with the anti-BCAM2418 antibody, but no benefit was reported in the case of the other *Burkholderia* strains.

Live-attenuated vaccination relies on the administration of a weakened form of the bacteria causing the disease (Detmer and Glenting, 2006); in this case, considering that the context is similar to the one of the natural infection, it should create a strong and long-lasting immunity by stimulating $CD8^+$ cytotoxic T cells and T-dependent antibody response. To date, only one potential live attenuated vaccine could be produced by studying the *B. cenocepacia tonB*-deficient mutant (Pradenas *et al.,* 2017); *tonB* encodes an essential membrane energy protein that modulates all the outer membrane receptors involved in iron acquisition, thus allowing its capture and entry. Interestingly, the *tonB* mutant showed decreased growth and virulence when infected in BALB/c mice after growing in LB medium without iron supplement, with all the mice surviving after six days. In addition, 87.5% of the mice survived after 6 days to a lethal dose of *B. cenocepacia* K56-2 following intranasal immunization with the *tonB* mutant strain, while 71.4% successfully cleared bacteria from their lungs. Antibody titration showed high levels of IgG and IgG2a; the latter represents a marker of a Th1-driven immune response, meaning that protection was achieved even if only a cellular immune response was induced. Taking into consideration the bias towards the Th2 immune response characterizing pwCF lungs, triggering a Th1 response against *B. cenocepacia* could be advantageous in this context to achieve a more balanced Th1/Th2 response (Moser *et al.,* 2002).

THE REVERSE VACCINOLOGY APPROACH

Dealing with classical vaccine discovery can be expensive and time-consuming and requires growing the pathogens *in vitro*. In the case of attenuated vaccine, identifying a proper mutant requires extensive trials and errors as no basic physiological mechanism has to be harmed

(Detmer and Glenting, 2006); hence, the right virulence factors need to be identified to impair virulence without hampering immunogenicity. On the other hand, a subunit vaccine requires the separation of each component of the pathogen one by one and the possibility to purify these antigens in quantity suitable for vaccine testing (Rappuoli, 2000). While the previously reported studies addressed these problems in different ways, just one group adopted a genomic approach (Alsowayeh *et al.,* 2022).

The reverse vaccinology (RV) approach takes advantage of the annotated genome of the pathogen to catalogue virtually all its protein

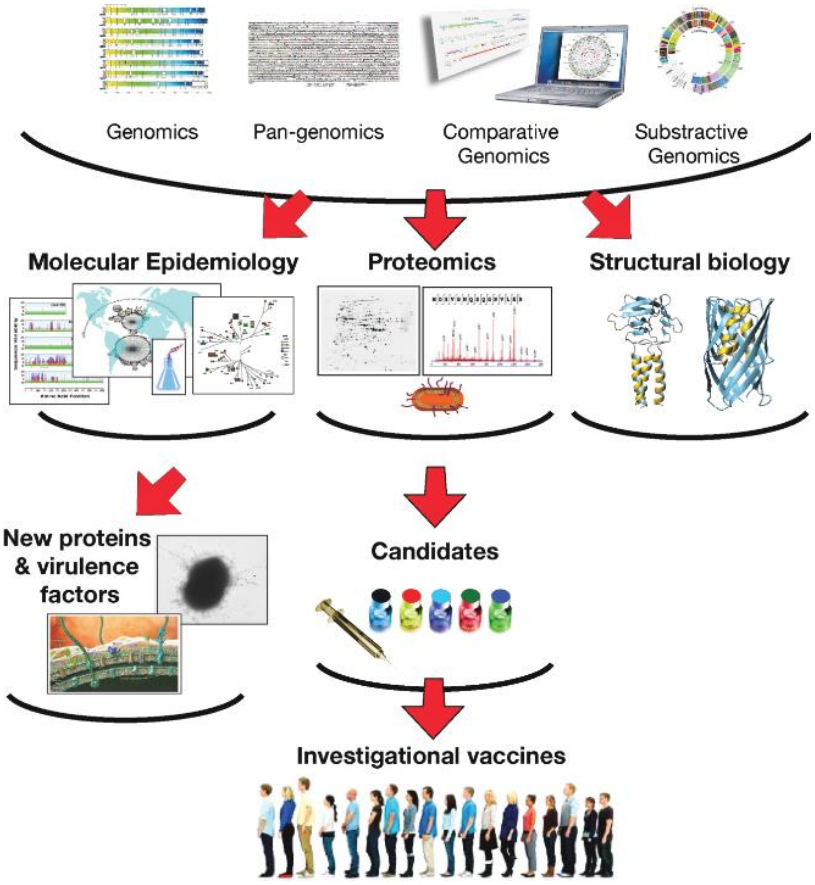

Figure 7: Overview of Reverse Vaccinology (Seib et al., 2012).

antigens (**Figure 7**) (Rappuoli, 2000). Starting from the genetic sequence, it makes use of bioinformatics tools aimed at predicting those antigens that are likely to be vaccine candidates, evaluating important features such as structure, immunogenicity, conservation across the strains, and localization in bacteria; moreover, the identification of similar proteins in other bacterial species help shedding light on the role played in the pathogen of interest. Since 2005, this approach has been widely used to study highly infective vector-borne viruses, pathogenic *E. coli,* and A and B group *Streptococcus* (Chong and Khan, 2019; Moriel *et al.,* 2010; Maione *et al.,* 2005).

Over time, an increasing number of pipelines have been proposed to facilitate the RV process of predicting antigens (Goodswen *et al.,* 2023), usually differing in the bioinformatics tools employed in the four different stages (**Figure 8**). Stage #1 refers to input data gathering and preparation and depends on the presence of protein sequences or eventually of genome sequence; in the latter case, additional steps as predicting the encoded genes and translating them to protein sequences need to be performed. In parallel, other specific analyses have to be considered, e.g. conservation among the strains, toxicity, and protein homology with the human host. Stage #2 aims to identify which of the proteins are naturally exposed to the immune system and evaluates, among all, subcellular localization, antigenicity, and transmembrane domains. Epitope prediction consists in identifying epitopes able to contact B- and T-cells by highlighting only the small part of the peptide involved in the interaction; it is the main point of stage #3 and it is functional for multi epitope-vaccine candidates. To conclude, stage #4 consists in verifying how the vaccine construct might interact with its targets and relies on molecular docking and *in silico* cloning.

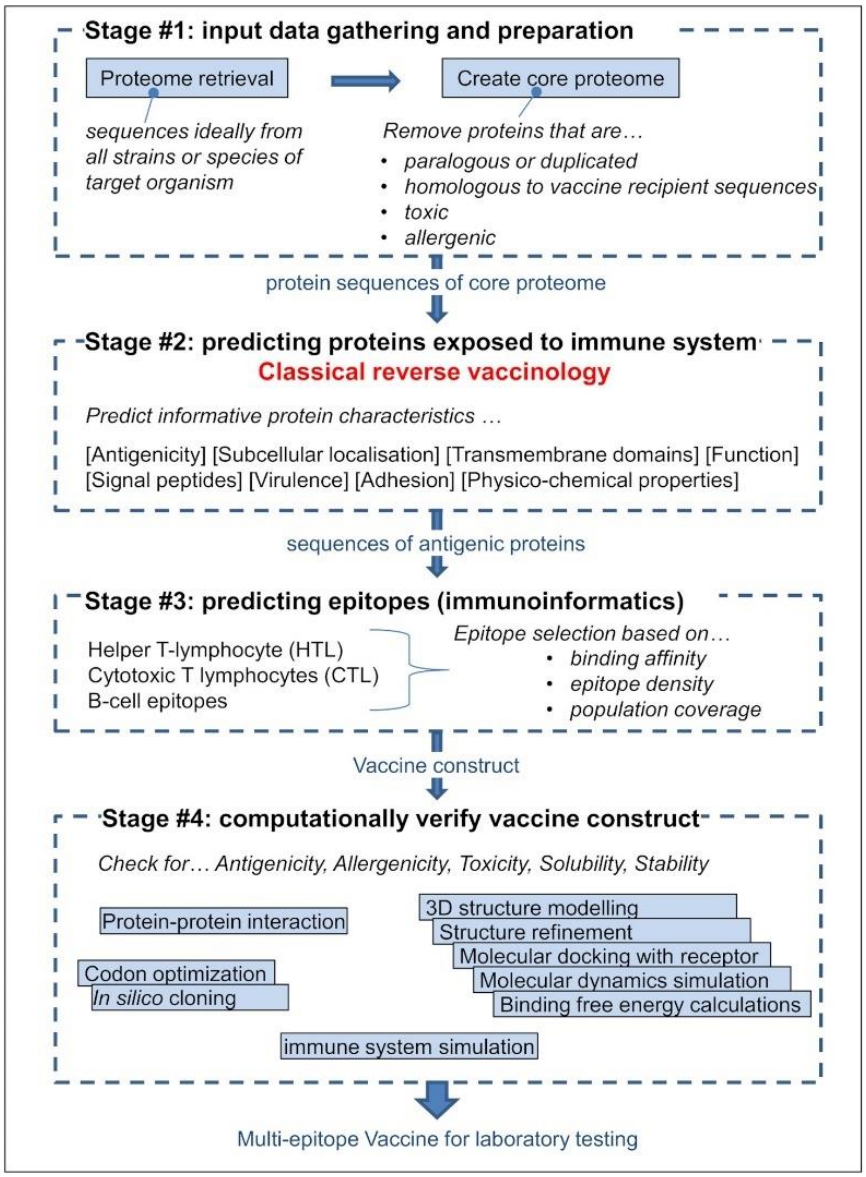

Figure 8: General workflow for vaccine candidates identification according to reverse vaccinology. (Goodswen et al., 2023)

The RV approach was successfully applied for the first time in bacteria for *Neisseria meningitidis* infection; strains of this pathogen are classified into six serogroups (A, B, C, W, X, and Y) associated with invasive disease, which can still cause meningitis and septicaemia worldwide despite the availability of effective vaccines (Feavers and Maiden, 2017). Infants less than 1 year are at higher risk as the infection is characterized by rapid onset and non-specific symptoms. For 40 years, purified capsular polysaccharides were employed, such as bivalent and tetravalent vaccines, following replaced by polysaccharide conjugate formulations protecting by serogroups A, C, W, and Y. In 2000, Pizza *et al.* sequenced the entire MenB genome and identified 28 proteins able to induce bactericidal antibodies production; in 2006 the *Neisseria* heparin-binding antigen NHBA, the *Neisseria* adhesin NadA and the factor H binding protein FHbp were selected as the most promising candidates (Giuliani *et al.,* 2006) and, once combined with the OMVs inside the MenZB™ vaccine (Oster *et al.,* 2005), the final 4CMenB formulation was approved in Europe in 2013 (Vesikari *et al.,* 2013). To note, the three antigens identified are exposed in the outer membrane.

Considering the efficacy of this method, Alsowayeh *et al.* (2022) resorted to RV to identify novel antigen candidates in *B. cepacia* strains; by analysing their proteomes, 28966 core proteins were identified, 3684 of which were non-redundant. Localization prediction revealed that 75 proteins were periplasmic, 31 were in the outer membrane and 18 were extracellular; in total, 23 of them were categorized as virulence factors after a BLASTp search. Furthermore, ProtParam and HMMTOP 2.0 analysis tools were applied to estimate solubility and length, as well as to predict transmembrane helices. Specifically, high solubility, molecular weight less than 110 kDa and presence of 1 transmembrane helix at most are characteristics required for optimal purification and for the exclusion of membrane channels. To avoid autoimmune reactions, the shortlisted proteins were blasted against the human proteome, and the less similar candidates were selected; finally, according to antigenicity and B- and T-cell epitopes prediction, a

flagellar hook basal body complex protein (FliE), a fimbria biogenesis outer membrane usher protein, a flagellar hook protein (FlgE), a cytochrome c4 and a Type IV pilus secretin (PliQ) were chosen. *In silico*, a chimeric vaccine peptide formed of 14 epitopes linked to the cholera toxin B subunit adjuvant was constructed, and a docking analysis was performed to evaluate the binding energy to Toll-like receptor-4 (TLR-4), MHC-I, and MHC-II; this resulted in the low net binding free energy of the TLR-4-, MHC-I- and MHC-II-vaccine complexes and therefore in a favourable predicted interaction between the vaccine and its immunological targets.

Reverse vaccinology has demonstrated higher speed and efficiency compared to traditional methods in identifying novel epitopes, mainly due to significant advancements in whole-genome sequencing software and techniques; unfortunately, most of the beneficial discoveries in this area are based on *in silico* predictions. However, further validation of these epitopes is crucial, both in preclinical and clinical phases, to determine their effectiveness in stimulating the immune response. Numerous potential targets have already been identified, and many epitopes have been evaluated, leading to the design of various putative vaccines, including multi-epitope vaccines that could offer wide protection against multiple bacteria.

Chapter 2

THE ESKAPE GROUP OF PATHOGENS

In clinics, one of the most feared groups of pathogens is the ESKAPE one; it is a group of six highly virulent and antibiotic-resistant Gram-positive and -negative nosocomial bacteria, comprising *Enterococcus faecium*, *Staphylococcus aureus, Klebsiella pneumoniae*, *Acinetobacter baumannii, Pseudomonas aeruginosa,* and *Enterobacter spp.* (De Oliveira *et al.,* 2020). Sometimes, also *E. coli* is included in the acronym as growing evidence is showing how its acquired resistance can endanger patients' life (Kritsotakis *et al.,* 2022). Due to their trend in acquiring mutations and mobile genetic elements, WHO designated ESKAPE as a "priority status" for the urgent development of new antimicrobials (WHO, 2017); to date, studies reported resistance mechanisms against lipopeptides, oxazolidinones, macrolides, tetracyclines and fluoroquinolones, and even against last line antibiotics including glycopeptides, carbapenems and polymyxins (De Oliveira *et al.,* 2020). Their diffusion is mainly correlated with poor patient care and failure to use personal protective equipment; inadequate stewardship practices can therefore facilitate the diffusion of MDR strains following improper antibiotic prescription, as for the presence of unqualified personnel (Watkins *et al.,* 2022). Overall, critically ill and immunocompromised patients are at higher risk of infection, in particular in the case of mechanical ventilation or peripherally inserted central catheters that provide a substrate for biofilm formation (El-Mahallawy *et al.,* 2016) and increase the chance of bacteraemia and septicaemia. As said before, the presence of a biofilm usually hampers complete eradication and poses the basis for persister cells formation and lower antibiotic sensitivity. Unfortunately, the worries about ESKAPE are not limited to the hospital setting alone, but they are correlated with global health threats (Collignon and McEwen, 2019); in fact, the problem is spread to wherever antimicrobials are used, i.e.

farms, animals, and aquaculture environments (**Figure 9**). Wastewater and manure runoff, therefore, became the central hub where multi-drug resistance bacteria are conveyed and can further diffuse. Raising

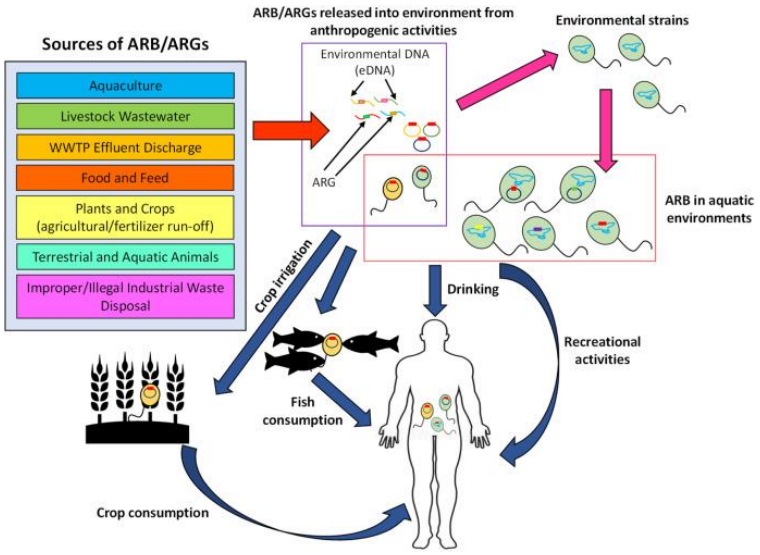

Figure 9: Involvement of the environmental context in antibiotic resistant bacteria (ARB) and antibiotic resistance genes (ARGs) diffusion (Denissen et al., 2022)

awareness of such a view is the goal of the "One Health" approach, pointing to design and implement "programs, policies, legislation, and research in which multiple sectors communicate and work together to achieve better public health outcomes" (WHO, 2017), involving the effort of multiple health professions to achieve optimal health for wildlife, plants, people and environment. From this point of view, the problem of antibiotic resistance acquires also ethical implications becoming everyone's problem.

Following, a list of the ESKAPE pathogens is reported; *P. aeruginosa* and *S. aureus* will not be subject matter as already deepened previously.

Enterococcus faecium

It is a Gram-positive coccus, most commonly involved in hospital-acquired infections (HAIs) in immunocompromised patients (De

Oliveira *et al.,* 2020); it often exhibits resistance to β-lactam antibiotics, such as penicillin and meropenem, and ultimately resistance towards vancomycin has been reported giving rise to vancomycin-resistant *E. faecium* (VRE) strains. In Europe and US, the percentage of VRE increased to 16.8% and 14%, respectively, in 2020 (ECDC, 2022; CDC, 2022); in particular, clonal complex 17 (CC17) strains have been associated with outbreaks in Asia, Europe, South America, and Australia. VRE outbreaks last on average 11 months, longer than the other ESKAPE; management of infected patients requires efforts as the need for contact precautions and isolation rooms become imperative, while treatment relies on expensive and less efficient second-line antibiotics as daptomycin and tigecycline (Prasad *et al.,* 2012). VRE display an extended ability to develop and share resistance through HGT; virulence phenotypes range from hemagglutination to thick biofilm formation, which allows growth on various medical devices. Bloodstream infections can lead to nausea, vomiting, fever and body aches, lower back or abdominal pain, and fatigue.

Klebsiella pneumoniae

K. pneumoniae is a Gram-negative rod-shaped bacterium belonging to the *Enterobacterales.* It has been able to develop resistance against all known antimicrobials (De Oliveira *et al.,* 2021); prevalence from 3 to 5% has been reported in Western countries, but an increase of up to 45% has been observed in developing countries (Mohd-Asri *et al.,* 2021); mortality rate often exceeds 40%, and it has been associated with carbapenem-resistant *K. pneumoniae* strains (CRKP). Since 2001, when carbapenemases were first identified in the US, CRKP spread caused invasive infections in Europe, China, the US, and across the Indian Ocean rim; recently, AMR hypervirulent *K. pneumoniae* is emerging in both low- and high-income countries, showing a hypermucoviscous phenotype associated to K1 and K2 capsular serotypes. Other common virulence factors include iron uptake systems, LPS, adhesins, and exopolysaccharides (Riwu *et al.,* 2022). In this case drugs with a risk of toxicity, e.g. polymyxins or aminoglycosides, have to be considered as

treatment options; symptoms are usually overlapping VRE ones, even if in case of respiratory infection a characteristic sputum is produced (Sanivarapu and Gibson, 2023).

Acinetobacter spp.

Quite common in hospitals, they are Gram-negative coccobacilli; like *K. pneumoniae*, their persistence in clinical settings allowed the development of resistance against virtually all antibiotics (De Oliveira *et al.,* 2021). They possess a high tolerance to pHs, temperature, dry environments, and low nutrient conditions, promoting their survival in disinfectants and on different surfaces. Since the 1970s, the most common bacterium isolated in temperate climates is *A. baumannii*. MDR and carbapenem-resistant strains (CRAB) are characterized by resistance to carbapenems, fluoroquinolones, and aminoglycosides, with a prevalence of more than 50% in Europe and the US compared to non-resistant *Acinetobacter* strains (ECDC, 2022; CDC, 2022), four times higher than the resistance rate observed in *K. pneumoniae*. Such an increase occurred between 2011 and 2016, when three CRAB clonal lineages - CC1, CC2, and CC3 - spread globally and mainly in Western countries, even with peaks up to 90% in Turkey and Greece; unfortunately, the presence of some pandrug-resistant isolates makes impossible the treatment with last-resort polymyxin- and carbapenem-class antibiotics, leaving with no valuable options. *A. baumannii* causes a range of diseases from bloodstream infection to pneumonia and meningitidis, and symptoms are not easily distinguishable from the ones of the other ESKAPE; it encodes different virulence factors, including various efflux pumps, protein secretion and nutrient-acquisition systems, biofilm production, and quorum sensing (Dehbanipour and Ghalavand, 2022).

Enterobacter spp.

This group includes *E. aerogenes* and *E. cloacae*, two Gram-negative bacilli representing a significant threat to neonatal wards (De Oliveira *et al.,* 2021); while *E. aerogenes* has been the most clinically prevalent

Enterobacter from the 1990s to 2003, *E. cloacae* and *E. cloacae* complex acquired importance in 2010. This latter spread across the US, following the dissemination of hospital-associated carbapenem-resistant *E. cloacae* ST78 and ST178 strains and now reached global diffusion; moreover, the emergence of pandrug-resistant *E. aerogenes* harbouring subpopulations of colistin-resistant bacteria was reported in 2005 (Thiolas *et al.,* 2005), making tigecycline the only effective antibiotic. Bloodstream and local infections are predominant; fimbriae are the prevalent virulence factors followed by type VI secretion systems and siderophores.

FINDING ALTERNATIVE WAYS

As ESKAPE pathogens have a high tendency to acquire antibiotic resistance, different solutions have been considered (Mulani *et al.,* 2019). An increasing number of bacteriophage preparations underwent clinical phase studies since 2015, thus representing a promising therapy for AMR infection; examples include NCT00945087 and NCT02116010, designed for postoperative respiratory infections and wound infections respectively (https://clinicaltrials.gov/). Phages have multiple pros, e.g. their host specificity prevents damage to normal flora, they can rapidly grow in the host bacteria, they mutate alongside their host, and can be successfully combined with antibiotics (Mulani *et al.,* 2019); unfortunately, some cons have still to be considered as phages can be even strain-specific, monophage therapy usually requires prior *in vitro* testing on the disease-causing bacteria and, to avoid the exchange of antibiotic resistance and virulence genes, phage genome has to be fully characterized. In addition, limitations may arise regarding administration and entry routes.

Antimicrobial peptides (AMPs) are characterized by their positively charged and short structure and are produced by all living forms (Wang *et al.,* 2010); both natural and bioengineered AMPs exist with proven antibacterial, anti-inflammatory, antibiofilm, and wound healing abilities. Histatin-5, WLBU-2 and LL-37 show up to 90% biofilm

inhibition and more than 70% of bactericidal activity against ESKAPE *in vitro* (Mulani *et al.,* 2019), while the lactoferrin derivative HLR1r and the natural peptide PT-13 act as anti-infective against MRSA and *S. aureus in vivo*. Nevertheless, crucial factors hamper the *in vivo* efficacy of AMPs, e.g. tendency to be degraded by tissue proteases, cytotoxicity to mammalian cells, and salt-dependent activity, along with high production cost.

Thanks to their ability to produce ROS, metal nanoparticles, such as AgNPs, have shown promising results due to their ability to damage cell membrane, cell wall, cellular proteins, or DNA (Dakal *et al.,* 2016). No toxicity has been associated with prolonged administration and efficacy was reported in the case of planktonic and sessile bacteria; besides, AgNPs have been widely explored as composite hydrogels or dressing for topic treatment promoting re-epithelization and wound healing. Examples of already commercialized formulations are Aquacel® and Articoat™; as pathogens can develop resistance to AgNPs after repeated exposure at subinhibitory concentrations, combination with antibiotics results in increased therapeutic efficacy and reduced administration dose (Mulani *et al.,* 2019).

Compounds targeting bacterial virulence factors are useful to reduce antibiotic load and preserve beneficial flora (Maura *et al.,* 2016). Anti-virulence approaches do not affect pathogen viability and as a result impose a lower selective pressure compared to antibiotics, penalizing persistence mechanisms and the evolution of resistance. Different candidates have been identified by screening natural products, modifying native ligands, and simulating *in silico* docking; usually, ESKAPE virulence can be targeted in three main ways, e.g. specific virulence factors, such as type III secretion systems (T3SS) (Goldberg *et al.,* 2022); master virulence regulators, as quorum sensing (Beenker *et al.,* 2023); resistance to host defences and antibiotics, as biofilm and capsule (Bamunuarachchi *et al*., 2021). Many anti-virulence compounds are natural ones; in particular, menthol, garlic, and black pepper

essential oils are well-tolerated and are effective against T3SS, enterotoxins, and biofilm formation, but their usage is usually limited to topical application. Biofilm formation and motility can be impaired in ESKAPE pathogens by targeting cyclic-di-GMP signalling (Hengge *et al.,* 2023); both alkaloids and flavonoids can indeed inhibit phosphodiesterases. Comparable results can be obtained with quinones and terpenoids interfering with RhlR, LasR, and MvfR QS systems, therefore their combination with antibiotics may provide successful therapies against persister cells. Sometimes, as in the case of the quorum quencher furanone C-30, resistances may still arise usually linked to the presence of mutated efflux pump repressors or to the physical separation between sensitive and resistant cells, a feature already observed in biofilm (Maura *et al.,* 2016).

To date, no anti-virulence drugs have been approved for ESKAPE pathogens, while only a few reached the clinical trial phase. Despite their attractivity, further research is needed to define their pharmacodynamics and bioavailability.

The bacterial divisome

The bacterial divisome is a highly dynamic macromolecular complex characterized by a dozen specific cell division proteins assembling in a time-dependent manner (Sass and Brötz-Oesterhelt*,* 2013); divisome formation is the first step for cell division and FtsZ, a structural homolog of eukaryotic tubulin, is its most critical component. Namely filamentous temperature-sensitive Z, this protein can polymerize in a GTP-dependent manner leading to the formation of the Z-ring, serving as a scaffold to recruit the other proteins; GTPase activity is therefore required for monomers polymerization. Nevertheless, to direct the Z-ring to the membrane, a protein called FtsA has to be present along with ATP (Loose and Mitchison, 2014); following ATP binding, FtsA polymerizes in a ring structure and coordinates FtsZ polymerization, while it is essential to bind late division factors, such as FtsK and FtsN (Nierhaus *et al.,* 2022). Similarly to FtsZ, FtsA possesses ATPase activity

which is required for its remodelling. Upstream, two other factors have been reported to prevent misplacement away from midcell (Gamba *et al.,* 2009): Noc is a specific effector of nucleoid occlusion, precisely a non-specific DNA binding protein and an FtsZ antagonist, which prevents the assembling of the division machinery near the nucleoid (Wu and Errington, 2004); MinC facilitates unbundling by preventing FtsZ lateral filaments interaction and inhibiting its GTPase activity (Dajkovic *et al.,* 2008).

In *E. coli,* divisome formation can be divided into two temporally distinct stages (**Figure 10**) (Du and Lutkenhaus, 2017): first, Z-ring is formed at the future division site with the help of its anchors FtsA and ZipA; ring formation is then enhanced by different functionally

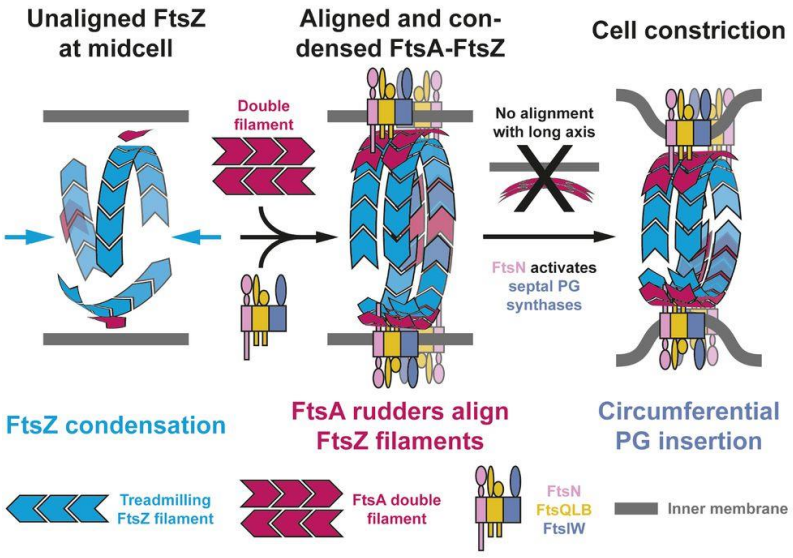

Figure 10: Divisome formation and ring constriction in E. coli model. (Du and Lutkenhaus, 2017)

redundant proteins called Zaps (ZapA, ZapC, and ZapD), directly contacting FtsZ. Zaps act by laterally crosslinking FtsZ monomers and ZapA, in particular, antagonizes MinC; moreover, the ABC-transporter FtsEX colocalizes to the ring as it participates in the control of the periplasmic peptidoglycan hydrolase activities. The second stage starts

after a temporal delay, when 7 essential division proteins, namely FtsK, FtsQ, FtsL, FtsB, FtsW, FtsI, and FtsN, are recruited simultaneously; septal peptidoglycan is synthesized once FtsN arrives and is followed by the recruitment of other cell wall remodelling enzymes, coordinating cell wall synthesis and leading to cell constriction and separation.

FtsZ as a therapeutic target

FtsZ has been lately identified as the central pacemaker protein in many bacteria divisome, thus explaining its high conservation rate (Sass and Brötz-Oesterhelt, 2013); by comparing crystal structures of a variety of homologs, two independently folding domains were identified, the N-terminal and the C-terminal, linked by the central H7 core helix, with a total of 23 residues. FtsZ is a structural homolog of human tubulin and its weight is approximately 40000 Da (Han *et al.,* 2021); its binding to GTP or GDP requires the presence of K^+ and Mg^{2+}. The N-terminal domain hosts the nucleotide-binding pocket (NBP) and, in parallel, the C-terminal domain forms the T7 tubulin-like catalytic synergy loop and a flexible region serving as binding site for the various cell division proteins. Once GTP contacts the NBP, the head-to-tail association of FtsZ monomers enables the formation of single-stranded protofilaments, which laterally interact with each other to eventually form the Z-ring. The T7-loop plays a key role, as its insertion in the NBP of the next FtsZ subunit triggers FtsZ GTPase activity; in fact, catalytic activity is only possible when two adjacent FtsZ monomers are joined together. In turn, the hydrolysis of GTP to GDP favours the disassembly of the protofilaments and promotes the rapid FtsZ turnover between the Z-ring and the cytoplasmic pool; such remodelling is necessary for the constriction of the ring and cell division. Therefore, there are two possible ways to interfere with divisome formation: first, interfering with the GTPase activity would perturbate ring assembly/disassembly, preventing constriction; second, polymerization can be blocked, thus reducing protofilaments formation (Han *et al.,* 2021). To date, a series of FtsZ inhibitors, including natural products and synthetic small molecules, able to induce bacteria cell

death by binding to the NBP in the N terminus or to the C domain have been described (Tripathy and Sahu, 2019); in both cases inhibition results in bacterial filamentation and eventual cell death.

Cinnamaldehyde, a chalcone, showed MIC values ≤1 μg/ml against *E. coli* and MRSA and impaired the GTPase activity and Z-ring assembly by interfering with the T7 loop (Domadia *et al.,* 2007); it showed a dose-dependent effect on GTPase activity, with an IC_{50} value of 5.81 ± 2.2 μM. Further, a library of derivatives was produced to highlight the importance of substitutions on the benzene ring. 9-phenoxy alkyl berberine derivatives were able to inhibit both antibiotic-susceptible and -resistant *S. aureus* strains with MIC values between 2 and 8 μg/ml, impairing the GTPase activity with relative IC_{50} values ranging from 37.8 to 63.7 μM (Sun *et al.,* 2014). The synthetic benzamide compound PC190723 and its derivatives, along with a MIC ≤2 μg/ml against *S. aureus*, showed enlargement and killing of staphylococci *in vivo*, by acting on the polymerization state; co-crystallization performed on PC190723 and FtsZ confirmed benzamide binding close to the T7 loop (Matsui *et al.,* 2012). A series of 4- and 5-substituted 1-phenyl naphthalenes were reported to be active against methicillin-sensitive (MSSA) and -resistant *S. aureus* and VRE, with MICs between 0.5 and 2 μg/ml; similar to PC190723, the antibacterial activity was due to the increased FtsZ polymerization and to the later protofilaments instability (Kelley *et al.,* 2013).

The C109 compound

The benzothiadiazole compound C109 (**Figure 11**), synthesized by Makarov *et al.* (2006), gained interest as broad-spectrum antimicrobials in 2018, when Hogan *et al.* studied its efficacy against different ESKAPE pathogens and *B. cenocepacia*, among the others. C109

administration caused filamentation in *B. cenocepacia* at 8 mg/L and a reduced biofilm formation at 4 mg/L. A knockdown mutant library was

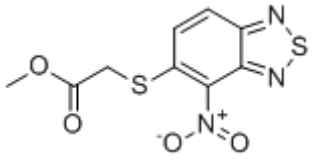

Figure 11: The benzothiadiazole compound C109.

produced in *B. cenocepacia* K56-2 which led to the identification of a strain hypersusceptible to C109 upon *ftsZ* minimal expression; *ftsZ* conditional deletion produced the same filamentation phenotype, thus confirming the target. Moreover, FtsZ mislocalization was confirmed by creating a FtsZ-GFP fusion protein. Purified *B. cenocepacia* FtsZ revealed that the GTPase activity was decreased upon incubation with C109, with an IC_{50} of 8.2 ± 1.3 μM, and that polymerization was impaired in a dose-dependent manner; as the affinity for GTP did not change, it was concluded that C109 functioned as a non-competitive inhibitor. An additive effect was confirmed when C109 was combined with meropenem, tobramycin, and ceftazidime, among others.

Later, Chiarelli *et al.* (2020) further characterized C109 against purified *P. aeruginosa* FtsZ; while kinetic parameters were comparable to the ones previously seen, the IC_{50} was lower than the one reported for *B. cenocepacia* FtsZ. Despite all, C109 MIC against *P. aeruginosa* was 128 mg/L and a checkerboard assay with C109 in combination with the efflux pump inhibitor PaβN MC-207.110 proved the involvement of an efflux system in the resistance phenotype.

Finally, Trespidi *et al.* (2021) focused on C109 as an antistaphylococcal agent; different MSSA and MRSA strains were evaluated for their susceptibility, yielding mean MIC values of 4 and 2 mg/L, respectively. Biofilm formation was inhibited at 0.125 mg/L , as a less structured biofilm having fewer cells was produced upon C109 addition. Once the

activity of purified *S. aureus* FtsZ was assessed, the reported IC_{50} was 1.5 μM but, differently from *B. cenocepacia*, polymerization was not affected.

Overall, C109 has proven to be an effective strategy against different pathogens, in virtue of both its antibiofilm and divisome inhibitor activity, as for its additive effect when a PEGylated nanocrystal formulation was administered combined with antibiotics (Costabile *et al.,* 2020); nevertheless, some pathogens as *P. aeruginosa* are naturally resistant due to the presence of efflux pump systems. As it possesses lower toxicity towards human cells compared to other FtsZ inhibitors, its application against other pathogens may give an additional tool to combat infection. Regardless, the different studies on this compound confirmed how researching new molecules to inhibit FtsZ protein and the entire divisome as well is worth.

Aims of the Work

Antimicrobial resistance (AMR) is nowadays considered a plague that will hardly be dammed in the future; since the number of newly discovered antibiotics is decreasing and the already produced ones are becoming less efficient, alternative strategies to counteract infection are necessary, particularly in patients subjected to continuous antibiotic treatments; this is the case of people with Cystic Fibrosis (pwCF), who may experience respiratory failure caused by chronic lung infections. In particular, a rapid lung function decrease is associated with *Burkholderia cepacia* complex bacteria – a group of Gram-negatives highly resistant to antibiotics whose eradication is usually difficult. Since no vaccine is available, the Reverse Vaccinology approach may aid in identifying potential new antigens for vaccine production.

In this work, the RV approach has been applied to identify a set of antigens belonging to different classes; three of them were selected and the corresponding genes were deleted by double-recombination in the *B. cenocepacia* K56-2 strain to study their role. 2D-SDS PAGE analysis was performed to confirm their subcellular localization, and their involvement in different virulence aspects, i.e. antibiotic resistance, biofilm formation, auto-aggregation, swimming motility, and symptoms production in *G. mellonella,* was studied; in addition, the lipolytic activity and rhamnolipid production of one of them was investigated too.

ESKAPE (*Enterococcus faecium, Staphylococcus aureus, Klebsiella pneumoniae, Acinetobacter baumannii, Pseudomonas aeruginosa,* and *Enterobacter spp.*) pathogens group is one of the most feared in clinics, as it comprises antibiotic-resistant and highly virulent Gram-positive and -negative bacteria (De Oliveira *et al.*, 2020) designated as a "priority status" by WHO in 2017.

New cellular targets, such as Filament-temperature sensitive (Fts) proteins, are drawing attention as they coordinate cellular division; one of them, FtsZ, is a widely-conserved essential protein whose inhibition leads to bacteria filamentation and death.

Among the studied inhibitors, the C109 compound has been proven to inhibit FtsZ from *B. cenocepacia, P. aeruginosa,* and *S. aureus* (Trespidi *et al.,* 2021; Chiarelli *et al.,* 2020; Hogan *et al.,* 2018). Here, its ability to inhibit *Acinetobacter baumannii* FtsZ has been investigated through GTPase activity and sedimentation assay; quantitative and qualitative Confocal Laser Microscopy Laser analysis was performed to study its antibiofilm activity on ATCC 19606 and the clinical strains 560380, MO5, and HU5.

To predict other possible FtsZ inhibitory compounds, a set of twelve chemical entities predicted to interact with *S. aureus* FtsZ were studied. To validate FtsZ as a target, GTPase activity assay was performed, and their MICs against *S. aureus* ATCC 25923 were further determined. One of them was studied evaluating its FtsZ polymerization inhibitory activity and its antimicrobial potency against *S. aureus* by kill-curve assay and infection in *G. mellonella*.

Materials and methods

IDENTIFICATION OF THE ANTIGEN CANDIDATES

The complete genomes of the following *Burkholderia cepacia* complex strains (**Table 2**) were automatically annotated using Rapid Annotation Subsystem Technology (RAST) (Aziz *et al.*, 2008).

Strain	Source
***B. ambifaria* AMMD**	cell culture
***B. anthina* AZ-4-10-S1-D7**	soil
***B. cepacia* ATCC25416**	wash glove
***B. cenocepacia* J2315**	CF sputum
***B. cenocepacia* DDS-22E-1**	aerosol sample
***B. cenocepacia* H111**	CF patient
***B. cenocepacia* HI12424**	cell culture
***B. cenocepacia* MSMB384WGS**	water
***B. cenocepacia* VC12308**	CF sputum
***B. cenocepacia* YG-3**	cell culture
***B. contaminans* SK875**	pig with swine respiratory disease
***B. diffusa* RF2-nonBP9**	soil
***B. dolosa* AU0158**	CF patient
***B. lata* A05**	blood of patient with cepacia syndrome

continue

***B. latens* AU17928**	CF maxillary sinus
***B. gladioli* ATCC10248**	plant
***B. glumae* 257SH-1**	rice panicles
***B. metallica* FL-6-5-30-S1-D7**	soil
***B. multivorans* ATCCBAA-247**	CF patient
***B. pyrrocinia* DSM10685**	soil
***B. seminalis* FL-5-4-10S1-D7**	soil
***B. stabilis* ATCC BAA-67**	CF sputum
***B. stagnalis* MSMB735WGS**	soil
***B. territorii* RF8-non-BP5**	soil
***B. ubonensis* MSMB1471WGS**	soil
***B. vietnamiensis* AU1233**	CF blood

Table 2: List of the annotated Burkholderia genomes employed for the analysis.

Proteins were filtered according to: conservation among the different strains higher than 65%; conservation with *E. coli* K12 non-pathogenic strain lower than 30%, to prioritize Bcc-specific proteins; length of the amino acid sequence higher than 230 aa, as this is the length predicted for an extracellular protein to behave as an antigen; proteins with an identity equal to 100% in all pathogenic strains were excluded, as they are not immunologically selected. Proteins were then subjected to localization prediction analysis with pSORT (Yu *et al.,* 2010) and functional prediction with InterProScan (Jones *et al.*, 2014). A BLAST analysis was performed to exclude proteins with homology with human ones (Altschul *et al.*, 1990); transmembrane prediction tools, i.e.

TMHMM (Krogh *et al.*, 2001), Phobius (Käll *et al.,* 2004), and HMMTOP (Tusnády and Simon, 2001), were then employed to assess the number of transmembrane domain. The antigenicity of the selected proteins was analysed using Vaxign (He *et al.*, 2010) and VaxiJen (Doytchinova and Flower, 2007): the antigenicity score values were accepted when greater than or equal to 90.9 or 0.5, respectively. If available, structural information was collected from RCSB PDB (Berman *et al.,* 2000). A synthetic flowchart of the antigen discovery pipeline is presented in **Figure 12**.

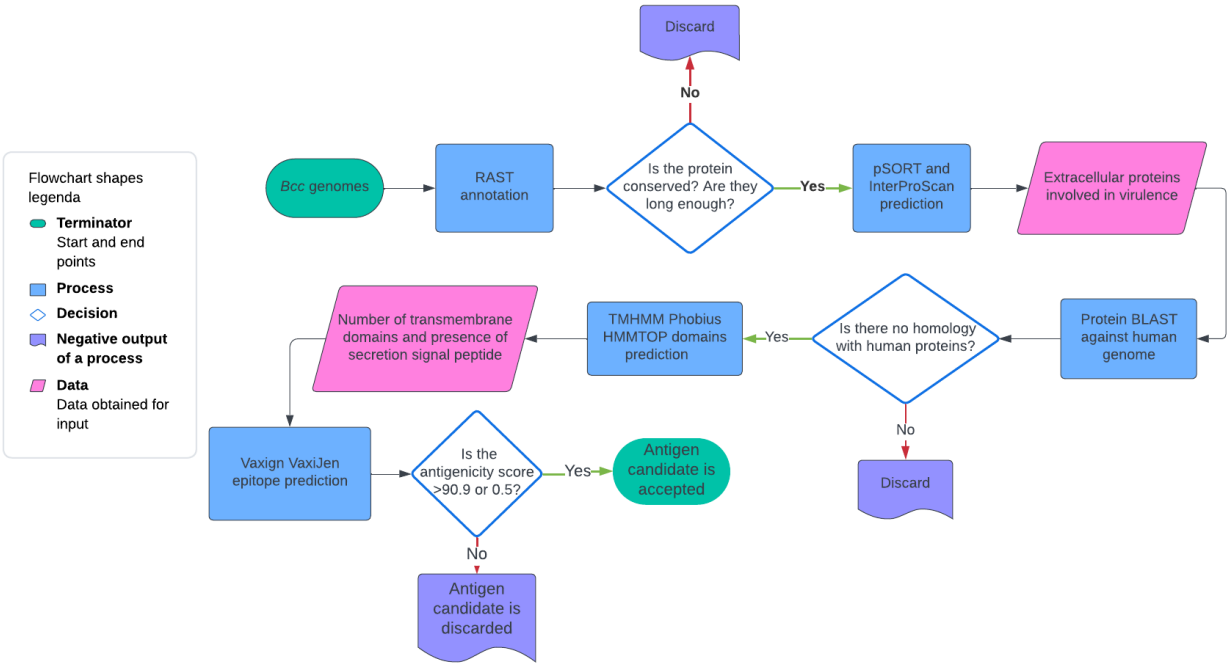

Figure 12: Synthetic flowchart describing bioinformatic pipeline employed to select antigen candidates. Created in Lucid (lucid.co).

BACTERIAL STRAINS AND PLASMIDS

Bacterial strains and plasmids are listed in **Table 3**.

Strain	Relevant genotype	Reference
***Burkholderia cenocepacia* K56-2**	WT strain	Laboratory collection
Δ*BCAL1524*	K56-2 Δ*Bcal1524*	This work
Δ*BCAM0949*	K56-2 Δ*Bcam0949*	This work
Δ*BCAS0335*	K56-2 Δ*Bcas0335*	This work
K56-2 pAP20	WT strain with the empty pAP20 plasmid	This work
Δ*BCAL1524* pAP20	Δ*Bcal1524* with the empty pAP20 plasmid	This work
Δ*BCAM0949* pAP20	Δ*Bcam0949* with the empty pAP20 plasmid	This work
Δ*BCAS0335* pAP20	Δ*Bcas0335* with the empty pAP20 plasmid	This work
Δ*BCAL1524* pAP20-*1524*	Δ*Bcal1524* complemented with the pAP20 *Bcal1524* plasmid	This work
Δ*BCAM0949* pAP20-*0949*	Δ*Bcam0949* complemented with the pAP20 *Bcam0949* plasmid	This work
Δ*BCAM0949* pAP20-*0949-0950*	Δ*Bcam0949* complemented with the pAP20 *Bcam0949-0950* plasmid	This work
Δ*BCAS0335* pAP20-*0335*	Δ*Bcas0335* complemented with the pAP20 *Bcas0335* plasmid	This work

continue

K56-2 pSCRhaB2	WT strain with the empty pSCRhaB2 plasmid	This work
Δ*BCAL1524* pSCRhaB2	Δ*Bcak1524* with the empty pSCRhaB2 plasmid	This work
Δ*BCAM0949* pSCRhaB2	Δ*Bcam0949* with the empty pSCRhaB2 plasmid	This work
Δ*BCAS0335* pSCRhaB2	Δ*Bcas0335* with the empty pSCRhaB2 plasmid	This work
Δ*BCAL1524* pSCRhaB2-*1524*	Δ*Bcal1524* complemented with the pSCRhaB2 *Bcal1524* plasmid	This work
Δ*BCAM0949* pSCRhaB2-*0949*	Δ*Bcam0949* complemented with the pSCRhaB2 *Bcam0949* plasmid	This work
Δ*BCAM0949* pSCRhaB2-*0949-0950*	Δ*Bcam0949* complemented with the pSCRhaB2 *Bcam0949-0950* plasmid	This work
Δ*BCAS0335* pSCRhaB2-*0335*	Δ*Bcas0335* complemented with the pSCRhaB2 *Bcas0335* plasmid	This work
***Escherichia coli* SY327**	*⊿(lac pro) argE(Am) recA56 rif^R nalAλ pir*	Laboratory collection
***E. coli* DH5α**	*F- Φ80lacZ⊿M15 ⊿(lacZYA-argF) U169 recA1 endA1 hsdR17(rK- mK+) phoA supE44 thi-1 gyrA96 relA1λ-*	Laboratory collection
***E. coli* BL21 DE3**	*fhuA2 [lon] ompT gal (λ DE3) [dcm] ΔhsdS* *λ DE3 = λ sBamHI0 ΔEcoRI-B int:lacI::PlacUV5::T7 gene1) i21 Δnin5*	Laboratory collection

continue

A. baumannii ATCC 19606	Reference strain	Laboratory collection
A. baumannii 560380	A representative strain of ST 2 clone	Clinical isolates
A. baumannii MO5	A representative strain of ST 78 clone	Clinical isolates
A. baumannii HU5	Unknown ST	Clinical isolates
S. aureus ATCC 25923	Reference strain	Laboratory collection
Plasmids		
pET-SUMO	*Km^R; expression plasmid; possess inducible lacO promoter and His (6X) and SUMO tag*	Invitrogen
pET-SUMO-*BCAL1524*	*pET-SUMO carrying the 1584 bp long BCAL1524 gene*	This work
pET-SUMO-*BCAM0949*	*pET-SUMO carrying the 1017 bp BCAM0949 lipase*	This work
pET-SUMO-*BCAS0335*	*pET-SUMO carrying the 1001 bp long N-terminal fragment of the BCAS0335 gene*	This work
pET-SUMO FtsZAb	*pET-SUMO carrying the 1167 bp long FtsZAb gene*	This work
pET-SUMO FtsZSa	*pET-SUMO carrying the 1173 bp long FtsZSa gene*	Trespidi *et al.*, 2021
pGPI-*Sce*I-XCm	*Cm^R, Tp^R;* mobilizable suicide vector*;* carries the I-*Sce*I recognition site, the *R6Ky* origin of replication and a *xylE* reporter gene	Hamad *et al.*, 2010

continue

pGPI-*Sce*I-XCm-*ΔBCAL1524*	pGPI-*Sce*I-Xcm containing the 5'- and 3'-flanking regions of *BCAL1524* for deletion	This work
pGPI-*Sce*I-XCm-*ΔBCAM0949*	pGPI-*SceI*-Xcm containing the 5'- and 3'-flanking regions of *BCAM0949* for deletion	This work
pGPI-*Sce*I-Xcm-*ΔBCAS0335*	pGPI-*Sce*I-Xcm containing 5'- and 3'-flanking regions of *BCAS033*5 for deletion	This work
pDAI-*Sce*I	*Tet*^{R}*;* mobilizable broad host range plasmid; carries the gene for the I-*Sce*I homing endonuclease	Flannagan *et al.*, 2008
pRK2013	*Kan*^{R}*; RK2*-derived helper plasmid carrying the *tra* and *mob* genes for mobilization of plasmids containing *oriT*	Figurski and Helinski, 1979
pAP20	*ori*PBBR1PDHFR *Cm*^{R}*; Cm* duplicated region deleted	Law *et al.*, 2008
pAP20-*1524*	*pAP20* carrying the functional *BCAL1524* gene	This work
pAP20-*0949*	*pAP20* carrying the functional *BCAM0949* gene	This work
pAP20-*0949-0950*	*pAP20* carrying the functional *BCAM0949-0950* operon	This work
pAP20-*0335*	*pAP20* carrying the functional *BCAS0335* gene	This work

continue		
pSCRhaB2	*oripBBR1 rha*R *rhaS PrhaB* Tp^R *mob*+ opposite orientation of the *dhfr* cassette	Cardona *et al.*, 2005
pSCRhaB2-*1524*	*pSCRhaB2* carrying the functional *BCAL1524* gene	This work
pSCRhaB2-*0949*	*pSCRhaB2* carrying the functional *BCAM0949* gene	This work
pSCRhaB2-*0949-0950*	*pSCRhaB2* carrying the functional *BCAM0949-0950* operon	This work
pSCRhaB2-*0335*	*pSCRhaB2* carrying the functional *BCAS0335* gene	This work

Table 3: List of bacterial strains and plasmids used. Cm^R, chloramphenicol resistance; Kan^R, kanamycin resistance; Rif^R, rifampicin resistance; Tet^R, tetracycline resistance; Tp^R, trimethoprim resistance.

B. cenocepacia was grown in LB broth (Difco) or artificial sputum medium (ASM) (Kirchner et al., 2012), with shaking at 200 rpm at 37°C or on LB agar plates. Possibly, cultures were supplemented with antibiotics, i.e.: tetracycline (10 mg/L for *E. coli* and 250 mg/L for *B. cenocepacia*), kanamycin (50 mg/L), trimethoprim (50 mg/L for *E. coli* and 200 mg/L for *B. cenocepacia*), chloramphenicol (34 mg/L for *E. coli* and 400 mg/L for *B. cenocepacia*) and ampicillin (200 mg/L). Antibiotics were purchased from Merck-Millipore.

Acinetobacter baumannii ATCC 19606, 560380, MO5 and HU5 clinical isolates and *Staphylococcus aureus* ATCC 25923 were cultured in Mueller-Hinton (MH), Mueller-Hinton II (MHII) (Difco), tryptic soy broth (TSB) (Difco) or Luria-Bertani broth at 37°C, 200 rpm. *E. coli* BL21(DE3) strain was grown in LB broth at 200 rpm, 37°C or on LB agar plates, and was used for recombinant protein expression. To select

the bacteria carrying the recombinant pET-SUMO plasmids, kanamycin was used at a concentration of 50 mg/L.

MOLECULAR BIOLOGY TECHNIQUES

***BCAL1524, BCAM0949* and *BCAS0335* genes**

To express and purify each protein, the *BCAL1524* (1584 bp), *BCAM0949* (1017 bp) and *BCAS0335* N-terminal fragment (1001 bp) were amplified using *B. cenocepacia* K56-2 genomic DNA as template. HotStar HiFidelity Polymerase kit (Qiagen) was employed for the PCR amplification step, using the primers listed in **Table 4**. Fragments were cloned into the pET-SUMO vector (Invitrogen) using Gibson® assembly kit (New England Biolabs).

To delete each target gene, the upstream and downstream DNA sequences flanking the corresponding gene were amplified, using the primers listed in **Table 4**, and cloned into pGPI-*Sce*I-Xcm suicide vector, using the Gibson® assembly kit. Gene deletions were performed as described by Hamad *et al*., (2010), and confirmed by PCR amplifications and sequencing; mutant strains were then cured by growing them in LB broth, until pDAI-*Sce*I was lost.

To complement each deleted strains, the *BCAL1524* (1716 bp), *BCAM0949* (1137 bp), *BCAS0335* (3636 bp) genes and the *BCAM0949-0950* operon (2175 bp) were amplified using *B. cenocepacia* K56-2 genomic DNA as template and cloned into pAP20 (Law *et al.,* 2008) and pSCRhaB2 (Cardona *et al.,* 2005) using the Gibson® assembly kit. *BCAM0949* is in operon with the downstream *BCAM0950* chaperone gene, and the presence of the two genes may be required to efficiently complement the observed phenotypes (Papadopoulos *et al.,* 2022; Putra *et al.,* 2019). The vectors were introduced into the mutant strains by conjugation. During complementation experiments, the expression of genes cloned into pSCRhaB2 was induced with 0.01% rhamnose.

BCAL1524

- **pET-SUMO-*BCAL1524***

pET-SUMO-*BCAL1524*For

5'-gaacagattggtggtatgGGTTCCGGCTCCATCAGCCAGGGTC-3'

pET-SUMO-*BCAL1524*Rev

5'-tacctaagcttgtctttaCTTGCCGTGCGTGCCGCCGAGCAGG-3'

- **pGPI-*Sce*I-Xcm-*ΔBCAL1524***

Upstream fragment (541 bp)	Downstream fragment (537 bp)
***Δ1524*For**	***Δ1524*For2**
5'-caatattgcatgcggtaccCGTAGTGTACCGAACCGTACATTTCC-3'	**5'-gacattaaggttatccctggcggcacgcacggcaagTAATCCGAC-3'**
***Δ1524*Rev**	***Δ1524*Rev2**
5'-cttgccgtgcgtgccgccAGGGATAACCTTAATGTCCATTTCGTC -3'	**5'-caagcttcttctagaCTGGTCGCACCGACGACGTTGCCGAG -3'**

- **Deletion check**

***Δ1524*checkFor**

5'-CCTTGCTCACGATTTGATGCAAG-3'

***Δ1524*checkRev**

5'-GAGCTCGACGGTCAAGGCGCTG-3'

- **pAP20-*1524***

pAP20-*1524*For

5'-gattcacaagaaggattcggATGGACATTAAGGTTATCCCTC-3'

continue

pAP20-*1524*Rev

5'-cttgcatgcctgcaggtcgact*TTACTTGCCGTGCGTGCCGCCG-3'

- **pSCRhaB2-*1524***

pSCRhaB2-*1524*For

5'-gaaattcagcaggatcacat*ATGGACATTAAGGTTATCCCTCATGG-3'

pSCRhaB2-*1524*Rev

5'- ctgcaggtcgactctagag*TTACTTGCCGTGCGTGCCGCC -3'

BCAM0949

- **pET-SUMO-*BCAM0949***

pET-SUMO-*BCAM0949*For

5'-gaacagattggtggtatg*ACGACCGCGCTGACGACGCTCGCGAC -3'

pET-SUMO-*BCAM0949*Rev

5'-tacctaagcttgtct*TCACACGCCCGCGAGCTTCAGCCGGTTCG -3'

- **pGPI-*Sce*I-Xcm-*ΔBCAM0949***

Upstream fragment (541 bp)	Downstream fragment (542 bp)
***Δ0949*For**	***Δ0949*For2**
5'-caatattgcatgcggtaccGCAGCATCGCTATGCGCTGAACGAG-3'	**5'-ccaaatcgatgcgttccctgaagctcgcgggcgtgTGATCGATG-3'**

continue

***Δ0949*Rev**

5'-cacgcccgcgagcttcagGGAACGCATCGATTTGGCCATGCATGTTC -3'

***Δ0949*Rev2**

5'-caagcttcttctagaGGACTTGTCGACCGCACCGGCGTCG -3'

- **Deletion check**

***Δ0949*checkFor**

5'-GCGTCGAGACGTCGCTCGCGTATGCGTG-3'

***Δ0949*check Rev**

5'-GCTCGGCGACTGGAGCCAGCCGTTCTTC-3'

- **pAP20-*0949***

pAP20-*0949*For 5'-gattcacaagaaggattcggATGGCCAAATCGATGCGTTCC-3'

pAP20-*0949*Rev 5'-cttgcatgcctgcaggtcgactTCACACGCCCGCGAGCTTCAG-3'

- **pAP20-*0949-0950***

pAP20-*0949*For

5'-gattcacaagaaggattcggATGGCCAAATCGATGCGTTCC-3'

pAP20-*0949-0950*Rev

5'-CCTTCACGTGCCGCCATCGATCACACGCCCGCGAGCTTCAG-3'

pAP20-*0949-0950*For2

5'-AGCTCGCGGGCGTGTGATCGATGGCGGCACGTGAAGGGCGC-3'

pAP20-*0949-0950*Rev 2

5'- cttgcatgcctgcaggtcgactTCAATGCGCGCTGCCCGCG-3'

continue

- **pSCRhaB2-*0949***

pSCRhaB2-*0949*For

5'- gaaattcagcaggatcacatATGGCCAAATCGATGCGTTCC-3'

pSCRhaB2-*0949*Rev

5'- ctgcaggtcgactctagagTCACACGCCCGCGAGCTTCAG-3'

- **pSCRhaB2-*0949-0950***

pSCRhaB2-*0949*For

5'- gaaattcagcaggatcacatATGGCCAAATCGATGCGTTCC-3'

pSCRhaB2-*0949-0950*Rev

5'- CCTTCACGTGCCGCCATCGATCACACGCCCGCGAGCTTCAG -3'

pSCRhaB2-*0949-0950*For2

5'-AGCTCGCGGGCGTGTGATCGATGGCGGCACGTGAAGGGCGC-3'

pSCRhaB2-*0949-0950*Rev2

5'- ctgcaggtcgactctagagTCACACGCCCGCGAGCTTCAG-3'

BCAS0335

- **pET-SUMO-*BCAS0335***

pET-SUMO-*BCAS0335*For

5'-gaacagattggtggtatgACGACCGCGCTGACGACGCTCGCGAC -3'

pET-SUMO-*BCAS0335*Rev

5'-tacctaagcttgtctTCACACGCCCGCGAGCTTCAGCCGGTTCG -3'

continue

- **pGPI-*Sce*I-Xcm-*ΔBCAS0335***

Upstream fragment (550 bp)	Downstream fragment (548 bp)
***Δ0335*For**	***Δ0335*For2**
5'-caatattgcatgcggtaccGTCCGAACTTTGAACGACGGGTGGC-3'	**5'-gaagaggaagcagatttcgggtgcgggttatcagttctgaTGCAGG-3'**
***Δ0335*Rev**	***Δ0335*Rev2**
5'-gaactgataacccgcaccCGAAATCTGCTTCCTCTTCATGGTCTTC -3'	**5'-ccaagcttcttctagaCGGGCGTTTGAGGATCCAGGATTTTTC -3'**

- **Deletion check**

***Δ0335*checkFor 5'-CGTTTGCGGAATGTGTGTATTTTGCG-3'**

***Δ0335*checkRev 5'-GAACTGCCGAGTCTCGATGCCGTGCA-3'**

- **pAP20-*0335* complementation**

pAP20-*0335*For 5'-gattcacaagaaggattcggATGAAGAGGAAGCAGATTTCGG-3'

pAP20-*0335*Rev 5'-cttgcatgcctgcaggtcgactTCAGAACTGATAACCCGCACCG-3'

- **pSCRhaB2-*0335* complementation**

pSCRhaB2-*0335*For 5'- gaaattcagcaggatcacatATGAAGAGGAAGCAGATTTCGG -3'

pSCRhaB2-*0335*Rev 5'- gcctgcaggtcgactctagagTCAGAACTGATAACCCGCACCG -3'

Table 4: List of primers used. Lowercase letters represent the base sequence complementary to the plasmid.

***A. baumannii ftsZ* gene**

The entire *ftsZ* gene (1176 bp) was amplified by PCR using *A. baumannii* ATCC19606 genome as template, with the following primers:

FtsZSUMOABfor (5'-CAGAGAACAGATTGGTGGTATGGCCTCATTTGAATTTATAGAAG-3') and FtsZSUMOABrev (5'-ATAAATACCTAAGCTTGTCTTTACTTACGTTGCTGATTTTTCAAG-3'). PCR amplification was performed using PCRBIO HiFi polymerase (PCR Biosystems); the gene fragment was cloned into the linearized pET-SUMO vector (Invitrogen) employing the Gibson® assembly kit (New England Biolabs).

ΔBCAL1524, ΔBCAM0949 AND ΔBCAS0335 GROWTH CURVES

To evaluate any impact the deletion could have on physiological growth, bacteria were grown for 24 hours, in LB or ASM media, and growth was monitored through colony count and optical density (OD_{600}) reading.

EXPRESSION AND PURIFICATION OF THE RECOMBINANT PROTEINS

BCAL1524, BCAM0949 and BCAS0335 proteins

BCAL1524, BCAM0949 and the N-terminal 351 aa long BCAS0335 fragment were expressed as SUMO fusion proteins; *E. coli* BL21 (DE3) was used as the expression host. After transformation, bacteria were grown O/N in LB, inoculated 1:100 and grown in LB up to mid-exponential phase, at 37°C, 200 rpm; induction was achieved by adding 0.5 mM of isopropyl-β-D-thiogalactopyranoside IPTG (Merck-Millipore). BCAL1524 optimal expression was achieved after 3 h induction at 30°C; BCAM0949 and BCAS0335 fragment optimal expression were achieved after 20 h induction at 20°C. Cells were harvested by centrifugation, resuspended in lysis buffer (see **Table 5** for the different recipes) supplemented with 1 mM of nonspecific protease inhibitor phenylmethanesulfonylfluoride (PMSF) (Merck-Millipore) and 6 mg/L DNase I (Merck-Millipore), and lysed by sonication. Lysed bacteria were clarified by centrifugation at 50000 *Xg* for 1 h and the supernatant was loaded on a 1 mL HisTrap FF nickel

column (GE-Healthcare), with a flow rate of 1 mL/min. The same flow rate was maintained for the following steps.

In the case of BCAL1524, the column flowthrough was further incubated with 0.5 mL of Ni Sepharose High Performance resin (GE-Healthcare), O/N in hand-over-hand shaking at 4°C; the protein interacting with the resin was then eluted with the lysis buffer containing from 100 to 500 mM imidazole (PanReac-AppliChem) and subsequently dialyzed against a dialysis buffer without imidazole (**Table x**), O/N, with the addition of the SUMO protease, to remove the tag. A reverse-IMAC was performed to remove the SUMO tag.

BCAM0949 was eluted with the lysis buffer containing from 100 to 35-mM imidazole, and subsequently dialyzed against a dialysis buffer without imidazole (**Table 5**) O/N with the addition of SUMO protease. A reverse-IMAC was performed to remove the SUMO tag.

Finally, BCAS0335 fragment was eluted with the lysis buffer containing from 100 to 350 mM imidazole and subsequently dialyzed against a dialysis buffer without imidazole (**Table 5**) O/N with the addition of the SUMO protease. A reverse-IMAC was performed to remove the SUMO tag. The sample was additionally purified by size exclusion chromatography using a Hiload 16/60 Superdex-75 column (GE-Healthcare) using the buffer reported in **Table 5**.

	BCAL1524	BCAM0949	BCAS0335
Lysis buffer	50 mM TRIS-HCl pH 8 300 mM NaCl 2 mM $MgCl_2$ 10 % glycerol 1 mM DTT 5 mM imidazole	50 mM TRIS-HCl pH 7.5 300 mM NaCl 10% glycerol 1 mM DTT 5 mM imidazole	50 mM TRIS-HCl pH 7.5 350 mM NaCl 10% glycerol 5 mM imidazole
Dialysis buffer	50 mM TRIS-HCl pH 8 150 mM NaCl 2 mM $MgCl_2$ 10 % glycerol 1 mM DTT	50 mM TRIS-HCl pH 7.5 150 mM NaCl 10% glycerol 1 mM DTT	50 mM TRIS-HCl pH 7.5 150 mM NaCl 10% glycerol 1 mM DTT
Gel-Filtration buffer			50 mM TRIS-HCl pH 7.5 100 mM NaCl 10% glycerol

Table 5: Recipes of the buffers used to purify the three recombinant proteins.

A. baumanni and *S. aureus* FtsZ protein

To express the FtszAb, the pET-SUMO-FtsZAb vector was transformed into *E. coli* BL21 (DE3); after transformation, bacteria were grown O/N in LB, inoculated 1:100 and grown in LB up to mid-exponential phase, at 37°C, 200 rpm; induction was achieved by adding 0.5 mM IPTG (Merck-Millipore) and maintaining the temperature at 18°C, O/N, at 200 rpm. Cells were harvested by centrifugation. To purify the FtsZ protein, the pellet was resuspended in a lysis buffer containing 50 mM Tris-HCl pH 8, 300 mM KCl, 5 mM imidazole, 2.5 mM $MgCl_2$, 1 mM DTT and 10% glycerol, supplemented with 1 mM PMSF and lysed by sonication. The lysate was clarified by centrifugation at 48000 *Xg* for 1 h and the supernatant was loaded on a 1 mL HisTrap FF nickel column (GE-Healthcare). The protein was then eluted with the lysis buffer supplemented with 250 mM imidazole. To remove the SUMO tag, the sample was dialyzed O/N at 4°C against a buffer composed of 20 mM Tris-HCl pH 7.8, 100 mM KCl, 2.5 mM $MgCl_2$ and 10% glycerol; SUMO protease was added to remove the SUMO tag with a 1:1000 ratio and by a reverse-IMAC.

FtsZSa was expressed and purified as previously described (Trespidi *et al.,* 2021).

The different purification steps were monitored by 12% acrylamide SDS-PAGE gel analysis. All the proteins were then quantified fluorometrically with Qubit Fluorometric Quantification (Thermo Fisher Scientific Inc.) concentrated to ca. 4 mg/mL and stored at -80°C.

PROTEOMIC ANALYSIS

B. cenocepacia mutants were grown in 50 mL of LB medium for 18 h. Cells were harvested and pellets were employed for membrane extraction; supernatants were subjected to Outer Membrane Vesicles (OMVs) purification. Membrane fractions were prepared according to Biot *et al.* (2013). OMV purification supernatants were collected and filtered through a 0.45 μm cellulose membrane, to completely remove

bacterial cells. A centrifugal filter Amicon® (Merck Millipore) with 100,000 Da NMWL (Nominal Molecular Weight Limit) was used to ultrafiltrate the cell-free supernatants, to a final volume of 1 mL. Analysis of the membrane and OMV fractions was conducted by 2D-PAGE electrophoresis gel. Each sample was precipitated with 10:1 of 2.7 M trichloroacetic acid, incubated in ice for 30' and centrifuged for 15' at 14000 rpm. The pellet was subsequently resuspended in 125 µl of UCD (Urea-CHAPS-Dithioerythtiyol) (8M Urea, 4% CHAPS, 0.1 M dithioerythritol), and 0.7 µl of IPG buffer pH 3-10 (GE-Healthcare) and 0.625 µl of 0.5% bromophenol blue were added; the samples was then incubated for 1 h on an IP strip (pH 3-10). Isoelectric focusing was performed according to the program reported in **Table 6**.

Time	Voltage (V)
1 h	0
8 h	30
1 h	12
30 min	300
3 h	Up to 3500
10'	500
Overnight	7950

Table 6: Isoelectric focusing program.

Next morning, strips were equilibrated 12' with buffer A (50 mM TRIS-HCl pH 6.86, M urea, 2% SDS, 30% glycerol, 0.1 M dithioerythritol) and 5' in buffer B (6 M urea, 2% SDS, 50 mM TRIS-HCl pH 6.8, 0.1 M iodoacetamide 30% glycerol, 125 µL of 0.5% bromophenol blue). Mass-weight separation (second dimension) was performed on

polyacrylamide gels formed by a 5% stacking gel and a 12.5% running gel. 0.5% agarose was dissolved in running buffer to immobilize the strips.

ChemiDoc XRS system (Biorad) was used to digitalize each gel; spots were detected using PDQuest Advanced 8.0.1 software (Biorad) (Martinotti and Ranzato, 2016). Experiments were performed in triplicate.

MINIMUM INHIBITORY CONCENTRATIONS (MICS) EVALUATION

B. cenocepacia WT and ΔBCAL1524, ΔBCAM0949 and ΔBCAS0335 strains

The MIC of ten antibiotics was investigated according to the EUCAST broth microdilution method (EUCAST, 2003), growing bacteria in U-bottom 96-well microtiter plates. LB was used as growth medium, and the final bacterial inoculum was 1 x 10^5 CFU/mL. MIC values were determined by the resazurin method (Martin *et al.,* 2006). Nalidixic acid, amikacin, aztreonam, ciprofloxacin, minocycline, piperacillin and tobramycin were purchased by Merck Millipore, levofloxacin and sparfloxacin by Honeywell Fluka™ and Meropenem by AstraZeneca.

A. baumannii ATCC19606, 560380, MO5 and HU5 and *S. aureus* strains

The MICs of C109 towards *A. baumannii* ATCC 19606 and 560380, MO5 and HU5 clinical isolates were assessed according to the EUCAST guidelines (EUCAST, 2003), in MH broth; C109 (Hogan *et al.,* 2018) was dissolved in pure DMSO (≥99%) and two-fold serially diluted from 64 mg/L to 0.125 mg/L, in MH broth. A final inoculum of 5x10^5 CFU/mL was dispensed in each well of a U-bottom 96-well microtiter plate containing increasing concentrations of C109. After 24 h of incubation at 37°C, MICs were determined by the resazurin method (Elshikh *et al.,* 2016).

The effectiveness of 12 synthetic compounds predicted to inhibit *S. aureus* FtsZ (FtsZSa) was tested against *S. aureus* ATCC 25923 by determining MICs, according to the EUCAST guidelines (EUCAST,

2003). The experiment was performed with the two-fold microdilution method in a U-bottom 96-well microtiter plates, and inoculating 10^5 CFU in MH-II medium, using concentrations ranging from 1 to 128 mg/L. Compounds were dissolved in DMSO (≥99%). The microtiter plates were incubated at 37°C for 2 days and growth was determined by the resazurin method (Elshikh *et al.,* 2016).

BACTERIAL AUTO-AGGREGATION ASSAY

Bacterial aggregation assay was performed according to Bhargava *et al.*, (2016) with some modifications. Cultures were grown in LB broth at 200 rpm and 37°C, up to the late-exponential phase. Each sample was then centrifuged and cells were resuspended in Phosphate Buffer Saline (PBS) (PanReac-Applichem); OD_{600} was measured and adjusted to 3. Samples were incubated at room temperature in static condition, for 16 h; after incubation, 50 μL of the culture were removed from the air-liquid interface and the OD_{600} was measured. The aggregation value was expressed as the percentage respect to the starting OD_{600} = 3.

IN VITRO BIOFILM FORMATION

B. cenocepacia WT and ΔBCAL1524, ΔBCAM0949 and ΔBCAS0335 strains

Strains ability to form biofilm was evaluated on 96-mell microtiter plates, using the crystal violet staining method (Vandecandelaere *et al.,* 2016). Bacteria were cultured O/N at 37°C in LB or ASM and diluted to OD_{600} = 0.05 (1 x 10^7 CFU/mL); 200 μL of culture were then added in the wells of a 96-wells microtiter plate. After 4 h, the supernatant was removed from each well and 200 μl of fresh medium were added; the plate was incubated for 20 h at 37°C. Staining with crystal violet and absorbance measurement at OD_{595} were performed to quantify biofilm mass. Results were reported as the ratio between the absorbance of biofilm and planktonic bacteria.

A. baumannii ATCC19606, 560380, MO5 and HU5 strains

The ability of C109 to inhibit the formation of *A. baumannii* biofilm was evaluated on 96-well microtiter plates, using the crystal violet staining method (Vandecandelaere *et al.,* 2016). Bacteria were cultured O/N at 37°C in MH broth and diluted to OD_{600} = 0.02; 200 µL of culture were then added to the microtiter plate, with or without different concentrations of C109 (2-256 mg/L). After 3 h of incubation, the supernatant was removed and 200 µL of fresh medium containing the same C109 concentration was added to each well and incubated at 37°C for 20 h. Staining with crystal violet and absorbance measurement at OD_{595} were performed to quantify biofilm mass. Results were reported as the ratio between biofilm and planktonic bacteria absorbance.

BIOFILM EVALUATION BY CONFOCAL LASER SCANNING MICROSCOPY

B. cenocepacia WT and ΔBCAM0949 strains

B. cenocepacia WT and ΔBCAM0949 strains were grown O/N in LB and diluted in the same medium to OD_{600} = 0.05 (1 x 10^7 CFU/mL); bacteria were then added to µSlide four chambered coverslip (Ibidi) for 4 h in LB, at 37°C. Medium was removed and fresh LB was added. After O/N incubation the medium was removed, while the biofilm was washed two-times with physiological solution and stained with Syto 9 dye (Invitrogen) with a final concentration of 5 µM. A Leica DMi8 with 500- to 530-nm (green fluorescence representing Syto 9) emission filters and a 63X oil immersion objective were used to take five snapshots at different positions in the confocal field of each chamber. Z-slices were obtained every 0.3 microns. To visualize and analyze biofilm images, ImageJ was used. COMSTAT 2 software (Heydorn *et al.,* 2000) was used to measure biomass, thickness, biofilm distribution and roughness coefficient. Experiments were performed in triplicate.

A. baumannii ATCC19606, 560380, MO5 and HU5 strains

A. baumannii strains were cultured overnight in MH medium and then diluted to an OD_{600} = 0.01 using the same medium. The diluted bacteria

were incubated at 37°C in a four-well chambered coverslip μ-Slide (Ibidi), with or without different concentrations of C109 (16, 64, and 256 mg/L). The compound was dissolved in pure DMSO (≥99.9%); the amount of C109 added was 1/200 of the final volume, as this quantity of DMSO was proven not to affect biofilm formation. After 3 h of incubation, the medium was removed along with non-adherent cells, and fresh medium containing the same C109 concentrations was added to the chambers. Incubation was performed O/N, at 37°C.

Following an O/N incubation, the medium was removed, and the biofilm was washed with 1X phosphate buffer saline and stained with Syto 9 (Invitrogen), at a final concentration of 5 μM. To capture five randomly selected snapshots at different positions within the confocal field of each chamber, a 63X oil immersion objective Leica DMi8 with 500- to 530-nm emission filters (representing green fluorescence from Syto 9) was used. Z-slices were obtained with a frequency of 0.3 microns. ImageJ was employed to visualize and process the biofilm images. The biomass, thickness, biofilm distribution and roughness coefficient were measured using COMSTAT 2 software (Heydorn *et al.,* 2000). All CLSM experiments were performed three times.

SWIMMING MOTILITY ASSAY

Motility assay was performed according to Bernier *et al.,* (2005). 1 μL of the overnight bacterial culture was placed in the middle of a 0.3% agar swimming plate, allowed to dry for 30' at room temperature and incubated at 37°C for 16 h. The diameter of the swimming halo was measured and expressed in mm.

INFECTION IN *GALLERIA MELLONELLA*

B. cenocepacia WT and ΔBCAL1524, ΔBCAM0949 and ΔBCAS0335 strains

Each strain was grown in LB broth at 37°C, 200 rpm, up to OD_{600} = 0.5. Each larva was infected with an injection volume of 10 μL containing 1 x 10^3 CFU of bacteria in physiological solution (PS) (Seed and Dennis, 2008); as a control, larvae were injected with PS alone.

Larvae were kept in the dark at 30°C, housed in petri dishes. Health index score and live/dead count were registered at 24 h, 48 h and 72 h (Tsai *et al.,*2016; Seed and Dennis, 2008). At least 10 larvae were included in each group, divided according to their weight. Experiments were performed in triplicate.

S. aureus ATCC25923 strain

S. aureus ATCC25923 has grown in TSB broth at 37°C, 200 rpm, until OD_{600} = 1.5 (10^8 CFU/ml). Each larva was infected with an injection volume of 10 µL containing 1 x 10^5 CFU in physiological solution (PS) (Ménard *et al.,* 2021); 10 µL of C11 20 mg/kg or 40 mg/kg dissolved in DMSO 4% or 8% were administered 1 hour after infection. A control was performed by injecting the same amount of DMSO. Each group was composed of 10 larvae, divided according to their weight; vitality was checked at 1-, 2- and 3-days post-infection and, eventually, at 6-days post-infection. Experiments were performed in triplicate.

LIPASE ACTIVITY ASSAY

LB agar plates containing 0.5 % tributyrin and 1.5 % agar were inoculated as described by Kugimiya *et al.,* (1986). Lipase activity was assessed by measuring the halo diameter (mm) formed around colonies.

RHAMNOLIPID ASSAY

Strains were grown in 10 mL of LB for 48 h, at 37°C, 200 rpm. To quantify the amount of rhamnolipids in the culture supernatant, the orcinol assay was performed (Rosenau *et al.,* 2010). The supernatant was diluted with distilled water up to a final volume of 500 µL. Each sample was extracted twice with two volumes of diethyl ether; the ether fraction was allowed to evaporate; the pellet was dissolved in 100 µL of distilled water and then mixed with 800 µL of 60% sulphuric acid and 100 µL of 1.6% orcinol. Samples were then incubated at 80°C, for 30' and 175 rpm, and the OD_{421} was then measured. Rhamnolipid concentration was calculated using a rhamnose standard curve, on the assumption that

2.5 μg of rhamnolipids correspond to 1 μg on rhamnose (Wilhelm *et al.,* 2007).

EVALUATION OF *A. BAUMANNII* AND *S. AUREUS* FTSZ GTPASE ACTIVITY AND POLYMERIZATION ASSAY

To evaluate FtsZAb GTPase activity, pyruvate kinase-L-lactic dehydrogenase (PK/LDH) spectrophotometric coupled assay was performed according to Hogan *et al.,* (2018) with some modifications. The reaction mixture was composed of 50 mM MES pH 6.5, 100 mM CH_3CO_2K, 5 mM $Mg(CH_3COO)_2$, 10 U PK/LDH, 0.25 mM phosphoenolpyruvate, 0.25 mM NADH and 4.8 μM of FtsZAb; C109 was added in concentration ranging from 0.5 μM to 100 μM; the reaction started by adding 1 mM GTP. Michaelis-Menten equation was used to fit the data and to determine the kinetic constants; the inhibitory centration that reduced the enzymatic activity by half (IC_{50}) was determined. The experiment was performed in triplicate.

A sedimentation assay was performed to assess FtsZAb polymerization (Hogan *et al.,* 2018). The reaction mixture contained 50 mM MES pH 6.5, 5 mM $Mg(CH_3COO)_2$, 100 mM CH_3CO_2K, 12 μM FtsZAb, and 2 mM GTP or GDP; increasing concentration of C109 were tested. To allow polymerization, the reaction mixtures were incubated at 30°C, 300 rpm for 10', samples were ultracentrifuged at 350000 *Xg*, at 25°C for 10'; the supernatant was separated from the pellet, as this latter contains the protein polymers; polymerization was assessed by analysing the samples by SDS-PAGE on 12% polyacrylamide gels.

S. aures FtsZ GTPase activity was evaluated as previously described, and the 12 compounds were tested at the final concentration of 100 μM. The inhibitory concentration that reduced the enzymatic activity by half (IC_{50}) was determined using Prism 9. The experiment was performed in triplicate.

To evaluate FtsZSa polymerization a light scattering assay was performed by measuring the 90° angle light scattering in a Varian Cary Eclipse Fluorescence Spectrophotometer (both excitation and emission wavelengths 400 nm, slit width 5 nm), as described by Król and Scheffers, (2013). The assay was performed at 30°C, in 150 µL of 50 mM MES pH 6.6, 10 mM $Mg(CH_3COO)_2$, 100 mM CH_3CO_2K, using FtsZ at a final concentration of 12.5 µM. After 2 min incubation, the reaction was initiated adding 1 mM GTP, and the mixture was gently stirred with a pipette tip for data collection. Data was collected every 5 s.

STATISTICAL ANALYSIS

Statistical analyses were performed using Prism 9.0 (GraphPad).

Results

PART I: UNVEILING THE POTENTIAL OF *BURKHOLDERIA CEPACIA* COMPLEX ANTIGENS FOR VACCINE DEVELOPMENT

Burkholderia cepacia complex (Bcc) bacteria are characterised by a marked resistance to xenobiotics and toxic compounds; moreover, an increased risk of developing multi-drug resistance strains is linked to antibiotics administration upon persistent infection, particularly in pwCF (Nye *et al.,* 2022). Eventually, protecting fragile patients from infection would limit drug treatments and decrease the number of untreatable infections. As the interest in developing a vaccine is evident, this thesis applied the reverse vaccinology approach to study putative antigen candidates that could be employed to produce a preventive vaccine against the strains belonging to the Bcc. In the following paragraphs, a list of antigen candidates identified by conservation analysis and predictive tools is reported; additional studies are performed on three of them – i.e.: BCAL1524, BCAM0949 and BCAS0335, including the optimal heterologous expression conditions. Their predicted extracellular localisation and involvement in virulence – precisely, in antibiotic susceptibility, biofilm formation, auto-aggregation, motility and infection in *Galleria mellonella* larvae – have been investigated by abolishing the corresponding genes in *B. cenocepacia* K56-2; furthermore, the role of BCAM0949 as lipase and mediator of rhamnolipid production is clarified and deepened.

IN SILICO ANTIGEN CANDIDATES IDENTIFICATION

An antigen candidate requires many conditions to be met, all of them affecting vaccine efficacy in terms of protection and immunological memory stimulation. Antigens identification was performed by applying the reverse vaccinology approach (Rappuoli, 2000), according to the workflow reported in **Figure 13**.

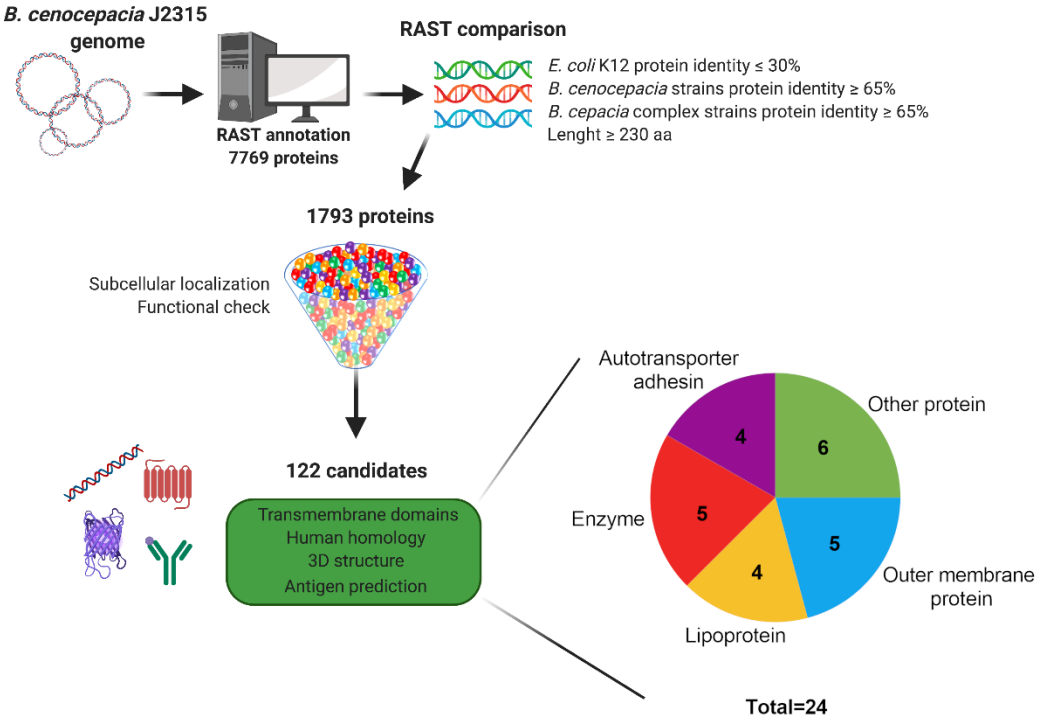

Figure 13: Schematic workflow reporting the different steps of the in silico analysis; B. cenocepacia J2315 was used as a reference. Annotation and comparison were first performed with RAST software, leading to the identification of 7769 proteins, further restricted to 1793 candidates. Then, according to bioinformatics prediction tools and literature reports, the candidates number was further reduced to 122 proteins. Finally, 24 antigens were selected in compliance with the number of transmembrane domains, homology with human host proteins, 3D structure and antigenicity prediction (Irudal et al., 2023).

The obtained shortlist of 24 proteins belonging to different classes is reported in **Table 7**: 5 enzymes, 4 autotransporter-adhesin proteins, 4 lipoproteins, 5 outer membrane proteins and 6 other proteins. To note, BCAM0949, BCAM2418, BCAS0409 and BCAS0236 are involved in cell adhesion and virulence and have already been described (Pimenta *et al.,* 2021, 2020; Guo *et al.,* 2017; Rosales-Reyes *et al.,* 2012). BCAM1514 and BCAS0409 presence has been reported in the outer membrane fraction in the cystic fibrosis niche (Liu *et al.,* 2015), and BCAS0147 is surface exposed (Sousa *et al.,* 2020a).

Protein name	Protein type	Functional prediction	Cellular localization prediction	Length aa	N° of predicted TMD	VaxiJen score	Vaxign-ML Score
BCAL0151	Extracellular ligand binding protein	ABC-type branched-chain amino acid transport systems, periplasmic component	unknown	381	Signal peptide	0.5863	98.9
BCAL0198	Putative outer membrane protein	Outer membrane protein, OmpW	unknown	278	8	0.6727	90.9
BCAL0199	Lipoprotein	DUF2957 domain-containing protein, putative lipoprotein	unknown	414	Signal peptide	0.6030	95.2
BCAL0200	Lipoprotein	DUF2957 domain-containing protein, putative lipoprotein	extracellular	477	≤1	0.7576	90.9
BCAL0358	Enzyme	Peptidase M1 family M1 metallopeptidase	extracellular	723	≤1	0.4835	99.7
BCAL1524	Lipoprotein	Collagen-like triple helix repeat-containing protein	extracellular	558	≤1	0.9966	90.9

continue

BCAL2229	Enzyme	Beta-propeller fold lactonase family protein, surface antigen	extracellular	330	≤1	0.3297	90.9
BCAL2615	Putative outer membrane protein	Putative exported outer membrane porin protein	outer membrane	359	16	0.6883	91.0
BCAL3279	Hypothetical protein	DUF3971 domain-containing protein, Possible exported protein	extracellular	1400	1	0.5901	90.9
BCAL3353	Autotransporter/adhesin protein	Putative outer membrane autotransporter	outer membrane/extracellular	1772	≤1	0.8135	94.9
BCAM0949	Enzyme	LipA triacylglycerol lipase	extracellular	365	1	0.4937	90.9
BCAM1514	Other protein	Outer membrane protein	outer membrane	294	≥1	0.6875	90.9
BCAM1737	Other protein	Alpha-2-macroglobulin	outer membrane	2021	1	0.6400	97.7
BCAM1740	Lipoprotein	Adhesin	extracellular	233	≥1	0.6559	90.9
BCAM1931	Putative outer membrane protein	Outer membrane porin	outer membrane	360	16	0.6868	92.5

continue

BCAM2311	Putative outer membrane protein	Outer membrane porin OmpC	outer membrane	380	16	0.5846	91.4
BCAM2328	Other protein	Coagulation factor 5/8 type-like protein	extracellular	470	1	0.5850	95.4
BCAM2418	Autotransporter/ adhesin protein	Cell surface protein putative haemagglutinin-related autotransporter/ adhesin protein	extracellular	558	1	0.9141	93.5
BCAM2444	Other protein	NHL-superfamily, Six-bladed beta-propeller, TolB-like	extracellular	643	≤1	0.5015	95.0
BCAS0147	Enzyme	YncE super family, beta-propeller fold lactonase family protein	outer membrane/extracellular	397	1	0.6027	90.9
BCAS0236	Autotransporter/ adhesin protein	Putative haemagglutinin-related autotransporter/ adhesin protein	outer membrane/extracellular	1497	≤1	0.8682	92.2
BCAS0321	Autotransporter/ adhesin protein	Autotransporter	outer membrane	4250	≥1	1.115	90.9

continue

BCAS0335	Autotransporter/ adhesin protein	Putative haemagglutinin-related autotransporter/ adhesin protein	extracellular	1198	≤1	0.8436	98.9
BCAS0409	Enzyme	M4 family metallopeptidase	extracellular	566	≤1	0.6513	95.0
BCAS0641	Enzyme	Phosphatase PAP2 family protein	unknown	464	≤1	0.6073	93.9

Table 7: Shortlist reporting the selected antigen candidates.

Among the identified proteins, the collagen-like protein BCAL1524, the lipase LipA BCAM0949 and the trimeric-autotransporter adhesin BCAS0335 were selected.

The first one was chosen since collagen-like proteins contain Gly-X_{aa}-Y_{aa} amino acid repetition, resembling the characteristic collagen-like (CL) domain; they are organized in a triple helix-structure and are widespread in pathogenic bacteria (Rasmussen *et al.,* 2003). They can interact with different host factors as they highly resemble human collagen, thus promoting inflammation, immunoreaction and adhesion (Pilapitiya *et al.,* 2021; Bachert *et al.,* 2015). In addition, mice immunized with *B. pseudomallei* collagen-like protein (Bucl8) produced a high Th2-immune response (Grund *et al.,* 2021), but no studies are present on the role of these proteins in *B. cenocepacia*.

BCAM0949 was chosen because lipases are widespread in clinical *B. cepacia* complex isolates (Mullen *et al.,* 2007); despite the gathered evidence on their role in Bcc infection is little, different studies reported

their involvement in virulence and pathogenesis in *P. aeruginosa* (Tielen *et al.,* 2013; Rosenau *et al.,* 2010).

Trimeric-autotransporter adhesins are pivotal for virulence in a wide range of bacteria (Kiessling *et al.,* 2020). They belong to the V_C secretion system and are formed by a globular head-neck domain, a stalk domain, and a β-barrel anchor domain possessing autotransporter ability. Being trimeric, they require the combination of three separate monomers to adhere through the head domain, whose stabilization is usually linked to the presence of divalent ions inside the stalk domain. In *B. cenocepacia* K56-2 their role as protective antigens has been extensively studied, as they are involved in adhesion and inflammation (Pimenta *et al.* 2020; Mil-Homens *et al.,* 2017; 2014). This led to the choice of BCAS0335 among the antigen candidates to be further characterized.

BCAL1524, BCAM0949 AND *BCAS0335* DELETION MUTANTS' CONSTRUCTION

To characterize the role of these proteins, the wild-type (WT) *B. cenocepacia* K56-2 strain was used to construct the corresponding deletion mutants since it is most amenable to genetic manipulation compared to J2315. Moreover, the two strains share identical aminoacidic sequences of the corresponding protein candidates.

First of all, growth curves were performed both in LB and AS media to characterize the mutants. However, no significant differences in growth rate were highlighted between the WT and each mutant, neither in LB nor in AS media (**Figure 14A, B; Figure 15A, B; Figure 16A, B**).

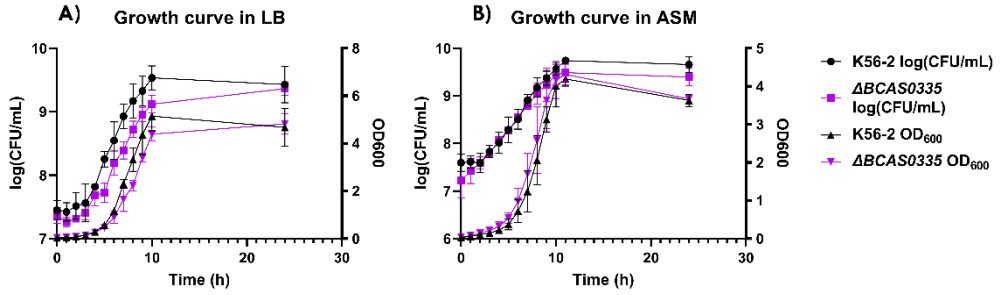

Figure 14: Growth curves of the ΔBCAL1524 mutant strain compared to the WT one, in LB (A) and AS (B) media. Growth was monitored for 24 h, by CFU count and OD_{600} reading. Data are represented as the mean ± SD from three independent experiments.

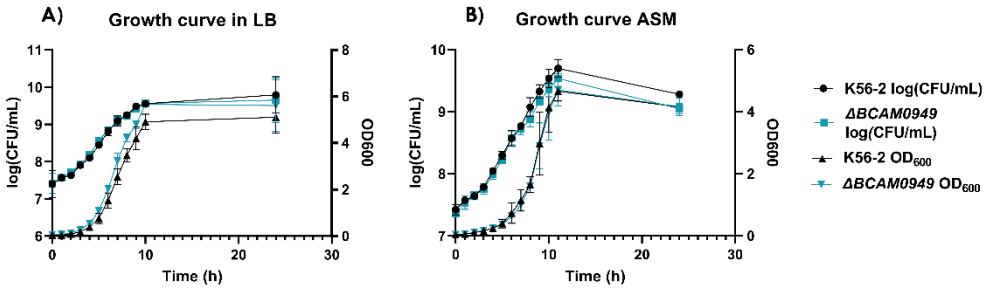

Figure 15: Growth curves of the ΔBCAM0949 mutant strain compared to the WT one, in LB (A) and AS (B) media. Growth was monitored for 24 h, by CFU count and OD_{600} reading. Data are represented as the mean ± SD from three independent experiments.

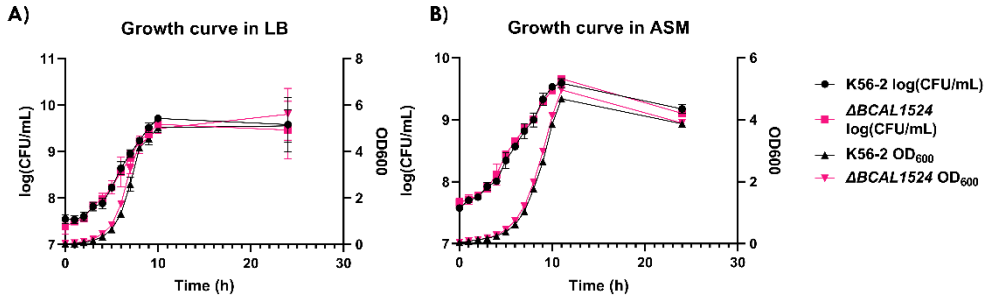

Figure 16: Growth curves of the ΔBCAS0335 mutant strain compared to the WT one, in LB (A) and AS (B) media. Growth was monitored for 24 h, by CFU count and OD_{600} reading. Data are represented as the mean ± SD from three independent experiments.

BCAL1524, BCAM0949 AND BCAS0335 EXPRESSION AND PURIFICATION

Preliminary low-scale expression and purification were performed to evaluate the effort needed to obtain the three antigen candidates in pure form, as good solubility and high yield are essential to large-scale production to assess their role in a mouse model.

To express and purify the antigen candidates, each protein-encoding gene was cloned into the pET-SUMO vector and transformed into the heterologous expression host *E. coli* BL21 (DE3). The expression and purification protocols are reported in the "**Materials and Methods**" section. All the proteins were present in the soluble fraction (**Figures 17, 19** and **21**).

The optimal expression condition for BCAL1524 protein was achieved after three hours of induction with 0.5 mM IPTG, at 20°C and with shaking at 160 rpm. Expression of BCAL1524 yielded a high amount of an unspecific-30 kDa fragment (**Figure 17, A**), which prevented the interaction between our protein of interest and the resin. Therefore, the BCAL1524-rich FT (flowthrough) was further incubated with 0.5 ml of free Ni Sepharose High-Performance resin to enrich the sample (**Figure 17, B**).

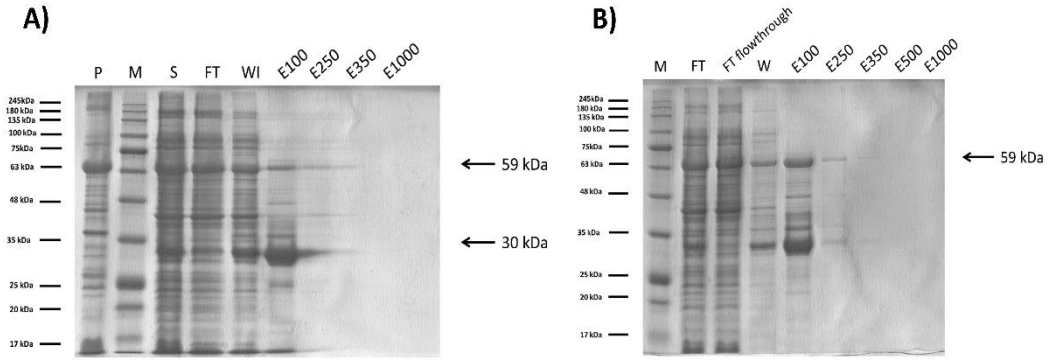

Figure 17: Purification of BCAL1524 (59 kDa) after A) the first Ni-NTA column and B) the flowthrough incubation with free Ni Sepharose High-Performance resin. P: pellet; S: supernatant; M: TriColor Protein Ladder (biotechrabbit™); FT: flowthrough; FT flowthrough: flowthrough from FT; W-WI: washing; E100-1000: elution with 100-1000 mM imidazole.

To remove the SUMO tag, the E100 sample from **Figure 17, B** has been treated with the SUMO protease to obtain the BCAL1524 protein alone (46 kDa); the sample was then reverse-purified using a Ni-NTA column (**Figure 18**).

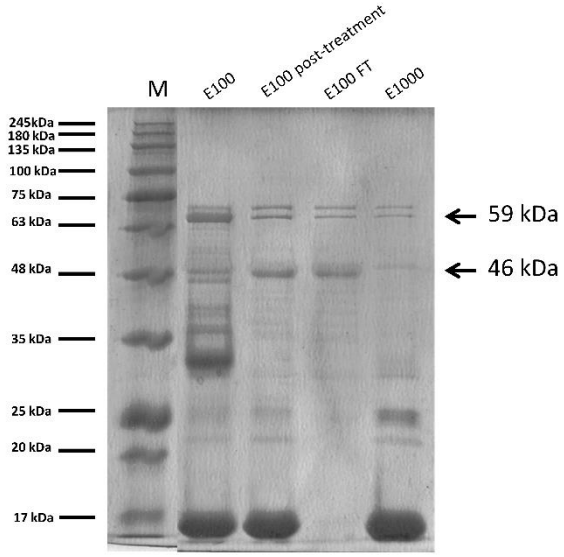

Figure 18: Reverse purification of BCAL1524. M: TriColor Protein Ladder (biotechrabbit™); E100: undigested sample; E100 post-treatment: SUMO-protease digested sample; E100FT: flowthrough from digested E100; E1000: elution with 1000 mM imidazole.

The final yield of the purification process was 1.3 mg/L.

Regarding BCAM0949, the highest amount of protein was achieved after overnight induction with 0.5 mM IPTG, at 20°C and with shaking at 160 rpm.

Despite the large quantity of protein present in the pellet fraction (**Figure 19**), no further enrichment steps were required to increase lipase concentration.

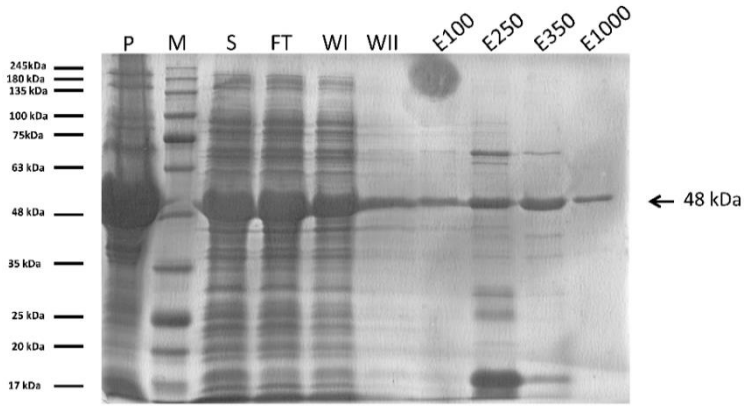

Figure 19: Purification of BCAM0949 (48 kDa). P: pellet; M: TriColor Protein Ladder (biotechrabbit™); S: supernatant; FT: flowthrough; WI-II: washing; E100-1000: elution with 100-1000 mM imidazole.

As the fraction eluted with 350 mM imidazole presented the lowest amount of non-specific protein bands, this sample was digested with the SUMO protease to obtain the BCAM0949 protein alone (35 kDa); the sample was then reverse-purified using a Ni-NTA column (**Figure 19**).

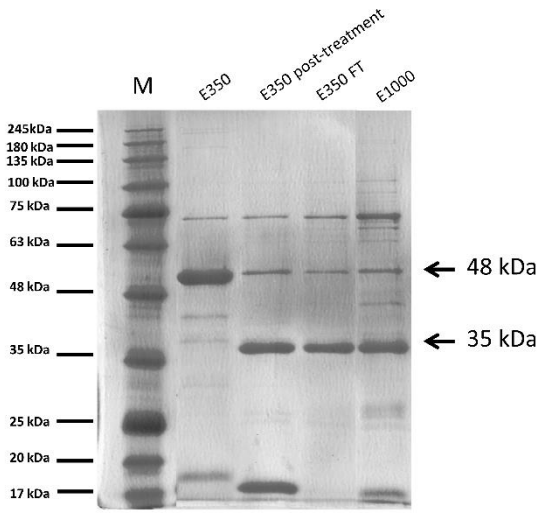

Figure 20: Reverse purification of BCAM0949. M: TriColor Protein Ladder (biotechrabbit™); E350: undigested sample; E350 post-treatment: SUMO-protease digested sample; E350FT: flowthrough from digested E350; E1000: elution with 1000 mM imidazole.

The final yield of the purification process was 1 mg/L.

Finally, the best condition for the expression of BCAS0335 N-terminal fragment was found after overnight induction with 0.5 mM IPTG, at 20°C and with shaking at 160 rpm.

As reported in **Figure 21**, the E100 and E250 eluted samples were the richest in our protein of interest, despite the heavy presence of unwanted unspecific proteins.

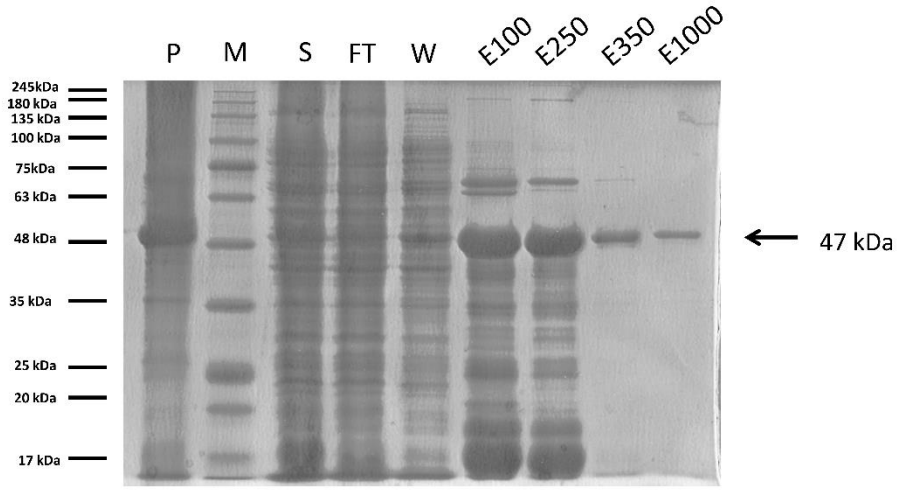

Figure 21: Purification of BCAS0335 (47 kDa). P: pellet; M: TriColor Protein Ladder (biotechrabbit™); S: supernatant; FT: flowthrough; W: washing; E100-1000: elution with 100-1000 mM imidazole.

To obtain the BCAS0335 fragment alone (33 kDa), digestion with the SUMO protease was performed on samples E100 and E250 (**Figure 22**). Both the digested dilutions, especially the E100 one, were visibly clearer after the reverse purification step.

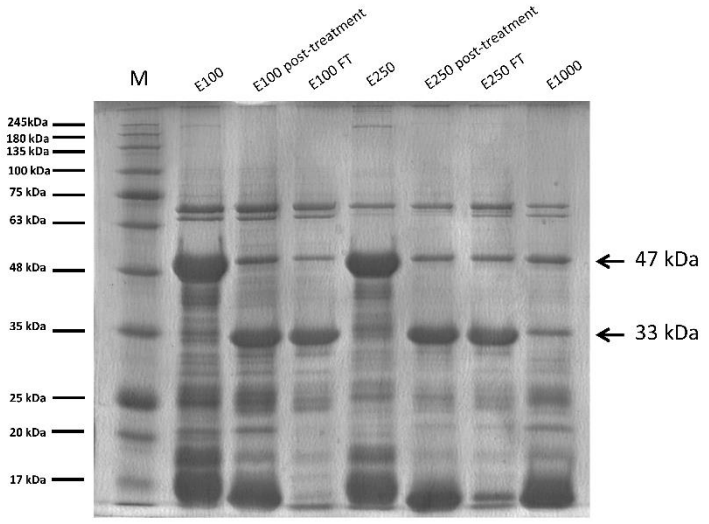

Figure 22: Reverse purification of BCAS0335. M: TriColor Protein Ladder (biotechrabbit™); E100-250: undigested sample; E100-250 post-treatment: SUMO-protease digested sample; E1000FT: flowthrough from digested E350; E1000: elution with 1000 mM imidazole.

To further increase the purity, a size exclusion chromatography (SEC) using a Hiload 16/60 Superdex-75 column was performed (**Figure 23A, B,** and **C**). Size exclusion chromatography allows to fraction a mixed sample according to the weight of the proteins composing it: proteins bigger than the pore size are eluted first, while smaller ones are eluted later. Despite the procedure, SEC did not allowed to achieve higher fraction purity as protein bands with different molecular weights were still present in the same fractions. Such observation may depend on the ability of TAA passenger domain to oligomerize independently on the presence of its relative anchor domain (Cotter *et al.,* 2006); these complexes are therefore heat-resistant and do not disassemble in the presence of reducing agents, usually showing protein bands at molecular weights multiple of the single monomer. This would explain why protein bands of about 70 kDa are present in the same fraction as the BCAS0335 N-terminal fragment.

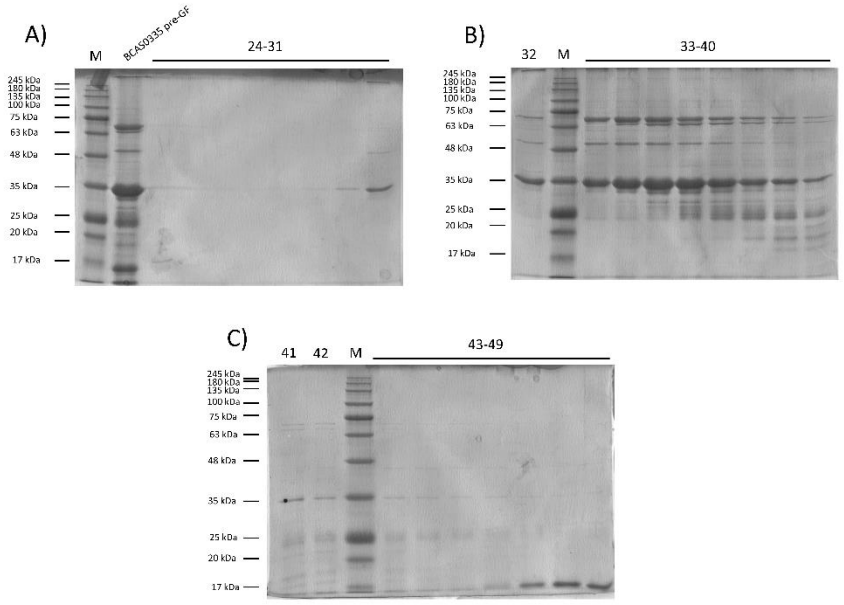

Figure 23: BCAS0335 size exclusion chromatography (SEC). A) Eluted fractions number 24-31; B) Eluted fractions number 32-40; C) Eluted fractions number 41-49. M: TriColor Protein Ladder (biotechrabbit™); BCAS0335 pre-GF: protein sample before SEC; 24-49: number of eluted fractions following SEC.

After the SEC step, fractions were grouped (group A: fractions 31 and 32; group B: fractions from 33 to 36; group C: fractions from 37 to 41) and concentrated.

The final yield of the purification process was 1.5 mg/L.

BCAL1524, BCAM0949 AND BCAS0335 ARE LOCALIZED IN THE OUTER MEMBRANE VESICLE COMPARTMENT

To determine if the antigen candidates are localized on the bacterial surface as predicted by pSORT (Yu et al., 2010), a proteomic analysis was performed on the Outer Membrane Vesicle and membrane fractions obtained from the WT and mutant strains. The spots identified in the WT were superimposed to the ones of each mutant (**Figure 24A, 25A** and **26A)**. The molecular weight (Mr) and isoelectric point (pI) ladders are reported on the y- and x-axis, respectively.

Figure 24 shows a magnification of the 2D gel electrophoresis of the OMVs fraction obtained from the WT and Δ*BCAL1524* strains. In the WT sample (**Figure 24B**), at pI ~8.1 and Mr ~49 kDa (corresponding to BCAL1524 Mr and pI), a spot numbered 7308 was identified with an intensity of 27944.8 mAu; no spot was present at the corresponding coordinates in the Δ*BCAL1524* sample (**Figure 24C**).

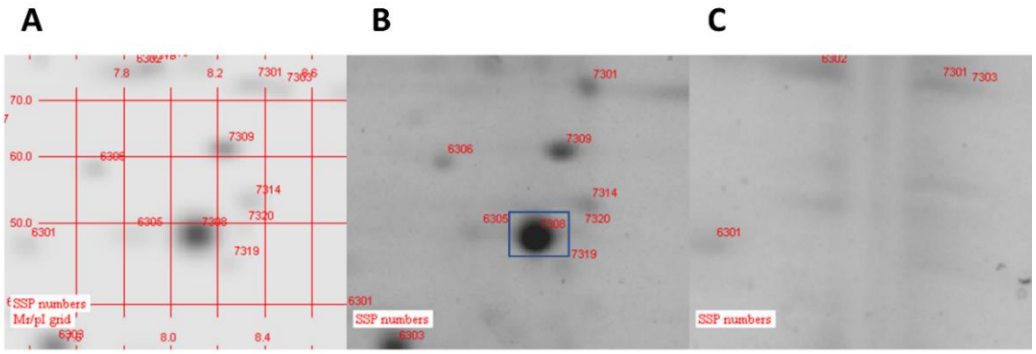

Figure 24: Magnification of the 2D electrophoresis gels. (A) superimposition of WT and ΔBCAL1524 OMVs protein spots; (B) 2D-gel of WT OMVs; (C) 2D-gel of Δ BCAL1524 OMVs. Mr: molecular weight; pI: isoelectric point.

Figure 25B shows the presence of a spot numbered 4301 at pI ~6.4 and Mr ~42 kDa in the WT sample, corresponding to the BCAM0949 protein and with an intensity of 3399.7 mAu; no spot was found at the corresponding coordinates in the Δ*BCAM0949* OMVs (**Figure 25C**).

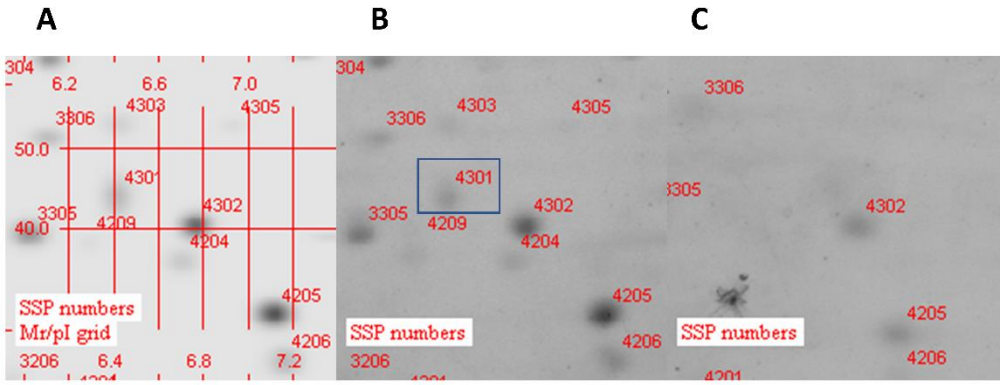

Figure 25: Magnification of the 2D electrophoresis gels. (A) superimposition of WT and ΔBCAM0949 OMVs protein spots; (B) 2D-gel of WT OMVs; (C) 2D-gel of Δ BCAM0949 OMVs. Mr: molecular weight; pI: isoelectric point.

Finally, the presence of BCAS0335 is highlighted in **Figure 26B**, at pI ~5.3 and Mr ~124 kDa and intensity of 4156 mAu; on the other hand, this spot was lacking in Δ*BCAS0335* sample (**Figure 26C**).

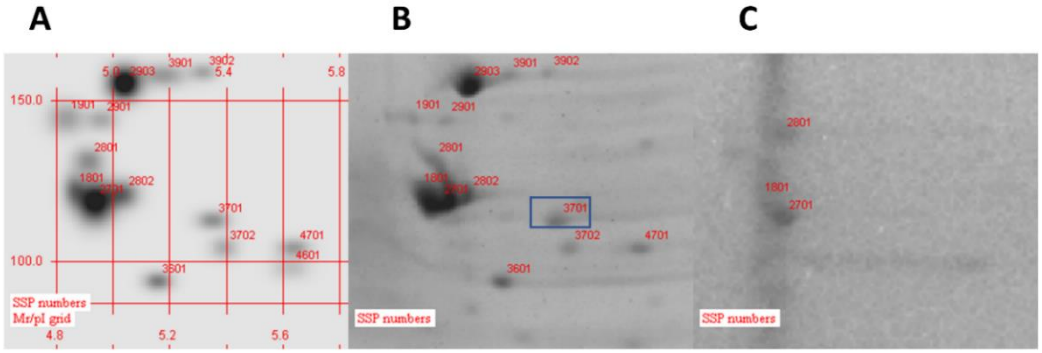

Figure 26: Magnification of the 2D electrophoresis gels. (A) superimposition of WT and ΔBCAS0335 OMVs protein spots; (B) 2D-gel of WT OMVs; (C) 2D-gel of Δ BCAS0335 OMVs. Mr: molecular weight; pI: isoelectric point.

The reported data show that the BCAL1524 collagen-like protein, the BCAM0949 lipase and the BCAS0335 trimeric autotransporter protein are localized in the OMVs compartment under the tested conditions.

ΔBCAM0949 AND *ΔBCAS0335* SHOW DIFFERENT ANTIBIOTIC RESISTANCE COMPARED TO THE WT

To evaluate any involvement of the deleted proteins in antibiotic susceptibility, the MIC of 10 antibiotics was tested using the broth microdilution method, growing bacteria in liquid LB medium. **Table 8** reports the MICs against the WT and the mutant strains: while no differences were found between the WT and Δ*BCAL1524,* the MIC of piperacillin, a β-lactam, was four-fold lower in the case of the lipase mutant (32 mg/L, in bold, vs 128 mg/L).

	Antibiotics									
Strain	*AMK*	*AZT*	*CIP*	*LVX*	*MEM*	*MIN*	*NAL*	*PIP*	*SPX*	*TOB*
WT	≥256	≥256	2	4	8	8	16	128	4	≥256
ΔBCAL1524	≥256	256	2	4	8	4	8	128	4	≥256
ΔBCAM0949	≥256	256	2	4	4	16	16	**32**	4	≥256
ΔBCAS0335	≥256	256	4	4	8	**64**	16	128	4	≥256

Table 8: Minimum Inhibitory Concentrations (mg/L) of 10 antibiotics. AMK: amikacin; AZT: aztreonam; CIP: ciprofloxacin; LVX: levofloxacin; MEM: meropenem; MIN: minocycline; NAL: nalidixic acid; PIP: piperacillin; SPX: sparfloxacin; TOB: tobramycin.

On the other hand, upon *BCAS0335* deletion, the MIC of minocycline, a tetracycline, was eight-fold higher with respect to the WT (8 mg/L, in bold, vs 64 mg/L).

To assess the reliability of the observed phenotypes, the deleted strains were complemented by conjugating a WT copy of the corresponding

gene cloned into the pSCRhaB2 (**Table 9**) plasmid; as control, the WT and the deleted strains were transformed with the empty plasmid to evaluate any impact the plasmids could have on the strain.

	Antibiotics									
Strain	*AMK*	*AZT*	*CIP*	*LVX*	*MEM*	*MIN*	*NAL*	*PIP*	*SPX*	*TOB*
WT pSCRhaB2	≥256	≥256	4	8	16	4	16	128	4	≥256
***ΔBCAL1524* pSCRhaB2**	≥256	≥256	≤2	4	8	≤2	8	128	4	≥256
ΔBCAL1524* pSCRhaB2-*1524	≥256	≥256	≤2	4	16	≤2	16	64	4	≥256
***ΔBCAM0949* pSCRhaB2**	≥256	≥256	≤2	4	8	≤2	16	**16**	4	≥256
ΔBCAM0949* pSCRhaB2-*0949	≥256	≥256	≤2	4	4	≤2	4	**128**	4	≥256
***ΔBCAS0335* pSCRhaB2**	≥256	256	≤2	4	4	**32**	16	64	2	≥256
ΔBCAS0335* pSCRhaB2-*0335	≥256	≥256	≤2	4	8	**4**	8	128	4	≥256

Table 9: Minimum Inhibitory Concentrations (mg/L) of 10 antibiotics against the pSCRhaB2 complemented strains. AMK: amikacin; AZT: aztreonam; CIP: ciprofloxacin; LVX: levofloxacin; MEM: meropenem; MIN: minocycline; NAL: nalidixic acid; PIP: piperacillin; SPX: sparfloxacin; TOB: tobramycin.

As reported in **Table 9**, complementation of Δ*BCAM0949* with the pSCRhaB2-*0949* plasmid efficiently restored the MIC of piperacillin up to the values observed against the WT strain (from 16 mg/L to 128 mg/L); similarly, in the case of Δ*BCAS0335* conjugated with

pSCRhaB2-*0335* the MIC of minocycline decreased to the value observed with the WT (from 32 mg/L to 4 mg/L)

INVOLVEMENT OF BCAL1524, BCAM0949 AND BCAS0335 IN BIOFILM FORMATION

To explore BCAL1524, BCAM0949 and BCAS0335 involvement in *Burkholderia* sessile lifestyle, the crystal violet assay was performed to evaluate biofilm formation in 96-well plates after 48 h of incubation, growing bacteria in LB and AS media. While the Δ*BCAS0335* strain showed a slight decrease in biofilm formation respect to the WT only in LB (**Figure 27A**), Δ*BCAM0949* produced a significantly lower amount of biofilm in both growth media tested (**Figure 27A, B**).

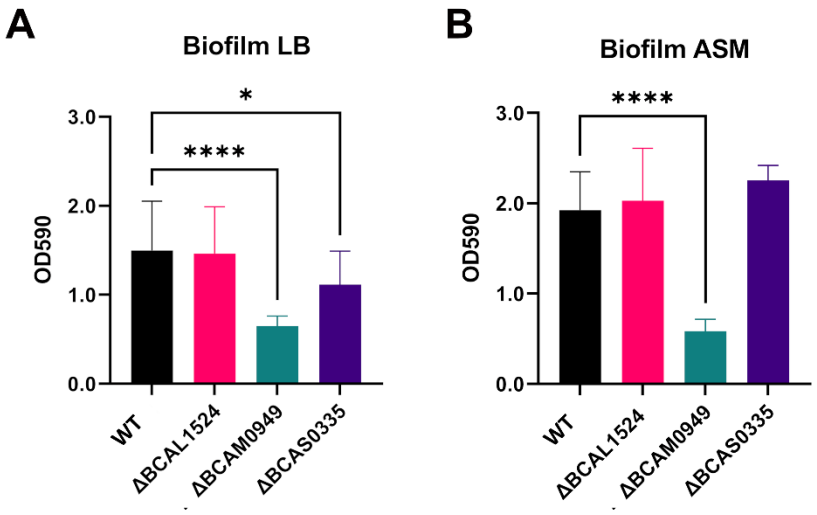

Figure 27: Biofilm formation in (A) LB and (B) ASM of the WT and mutant strains represented as the OD_{590} measured after the crystal violet assay. Data are represented as the mean on ± SD from three independent experiments. (*p < 0.05; **** p< 0.0001 one-way ANOVA test)

Once Δ*BCAM0949* was complemented with the constitutive pAP20-*0949* plasmid, an effective phenotype reversion was obtained, both in LB and AS media (**Figure 28A, B**). On the other hand, Δ*BCAS0335* transformed with the empty plasmid showed no differences in biofilm production compared to the WT pAP20, neither in LB nor AS media (**Figure 28A, B**), but a significant increase in biofilm production was observed once Δ*BCAS0335* was conjugated with pAP20-*0335* both in LB and AS media (**Figure 28A, B**). These data suggest that the lipase and TAA have a role in *Burkholderia* biofilm formation, while BCAL1524 does not seem to be involved in this aspect under the conditions tested.

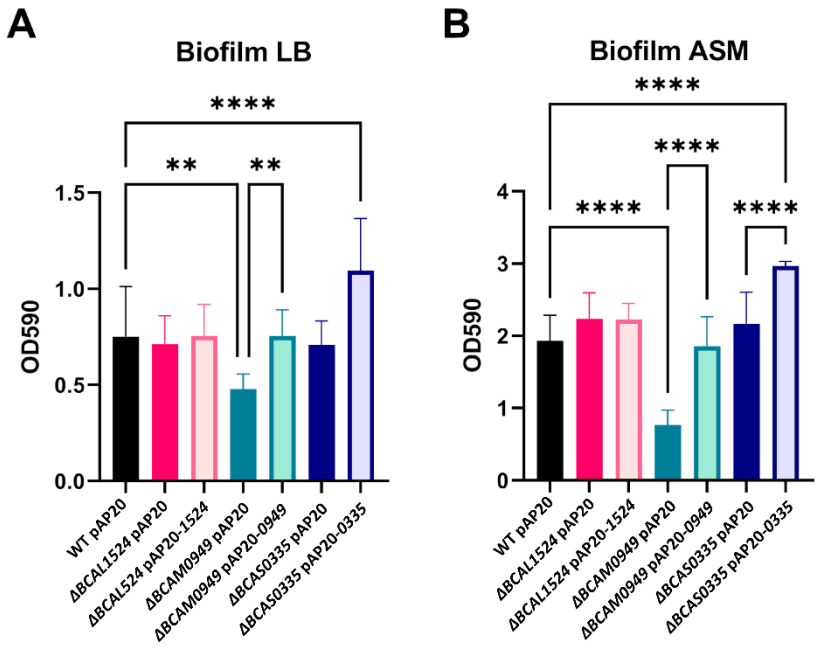

Figure 28: Biofilm formation in (A) LB and (B) AS media of the complemented WT and mutant strains represented as the OD_{590} measured after the crystal violet assay. Data are represented as the mean ± SD from three independent experiments. (**p < 0.01; **** p< 0.0001 one-way ANOVA test)

Considering the difference found in biofilm formation between WT and Δ*BCAM0949,* biofilm characteristics of these strains were evaluated using confocal laser scanning microscopy (CLSM). As shown in **Figure 29A**, once Δ*BCAM0949* was grown in LB and ASM, the produced biofilm resulted less thick and structured compared to the WT one, as confirmed by COMSTAT 2 analysis (**Figure 29B, C**); biomass and average thickness were significantly decreased in Δ*BCAM0949* biofilm, while biofilm roughness was increased, indicating an alteration in biofilm architecture.

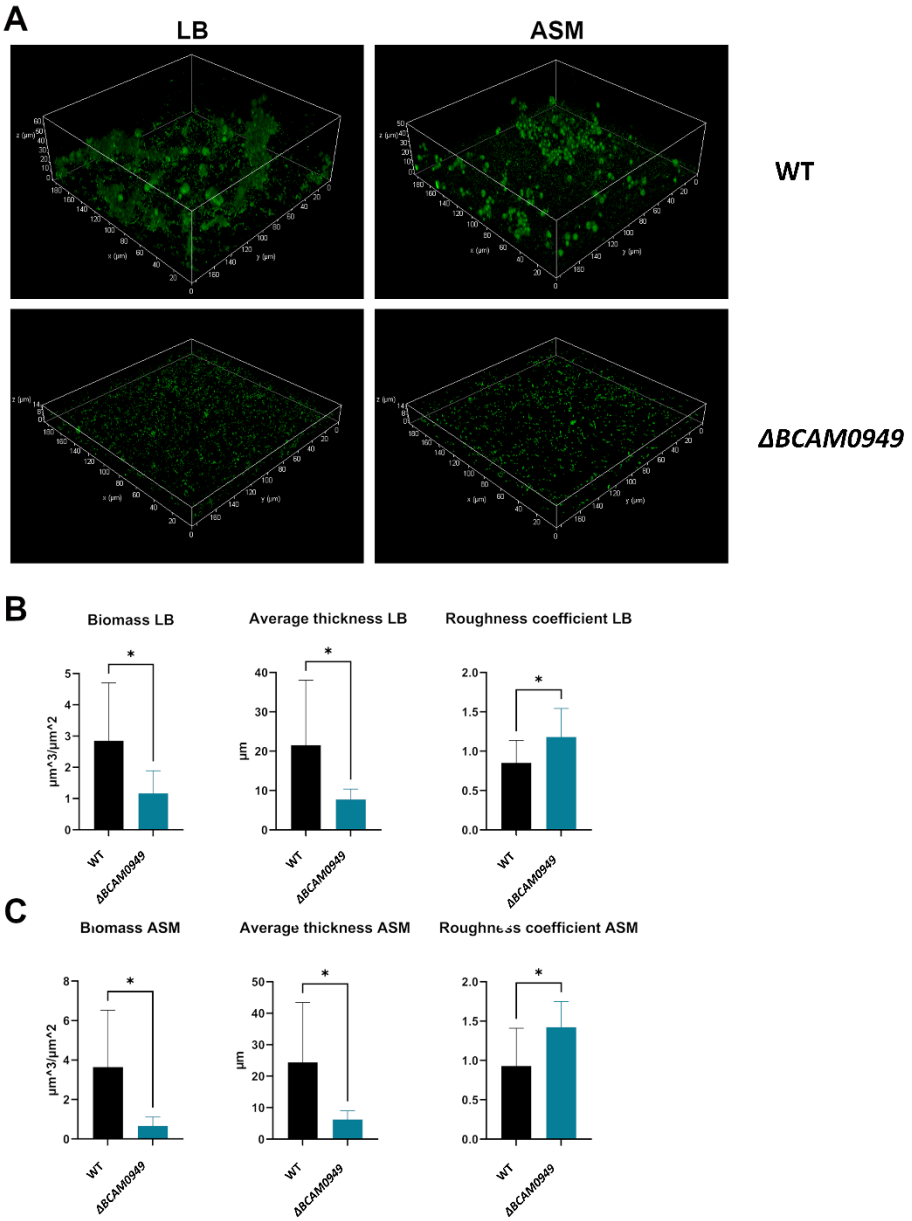

Figure 29: Biofilm evaluation by CLSM. (A) CLSM images of WT and ΔBCAM0949 in LB and ASM; pictures were taken with an overall magnification of 400x and biofilms were grown in chambered slides. Planes at equal distances along the Z-axis of the biofilms were imaged using CLSM; biofilms were grown for 48 h at 37°C, and images were stacked to reconstruct 3D biofilm images. (B, C) COMSTAT 2 qualitative analysis of biofilm properties, showing total biomass, average thickness and roughness coefficient. Data are represented as the mean ± SD obtained from three independent experiments. (*p<0.05 unpaired t test).

In summary, these data support the role of BCAM0949 lipase in *Burkholderia* biofilm formation both quantitatively and qualitatively.

BCAL1524 IS REQUIRED FOR BACTERIAL AUTO-AGGREGATION

Auto-aggregation is a process involved in bacterial colonization and persistence in the host; thus, the influence of the antigen candidates in this phenotype was evaluated using a precipitation-based assay. High precipitation rate is reflected in a decrease in the OD_{600} of the air-liquid interface after 16 h, which is correlated with an increase in bacterial interaction and precipitation. On the contrary, bacterial interaction is impaired when the OD_{600} is higher. The auto-aggregation is quantified as the percentage of the OD_{600} at the air-liquid interface normalized to the initial OD_{600}. For the WT strain, the obtained percentage value was 11.9%; in the case of the Δ*BCAL1524,* Δ*BCAM0949* and Δ*BCAS0335* strains the percentage values were 17.7%, 9.13% and 14.8%, respectively (**Figure 30A, B**).

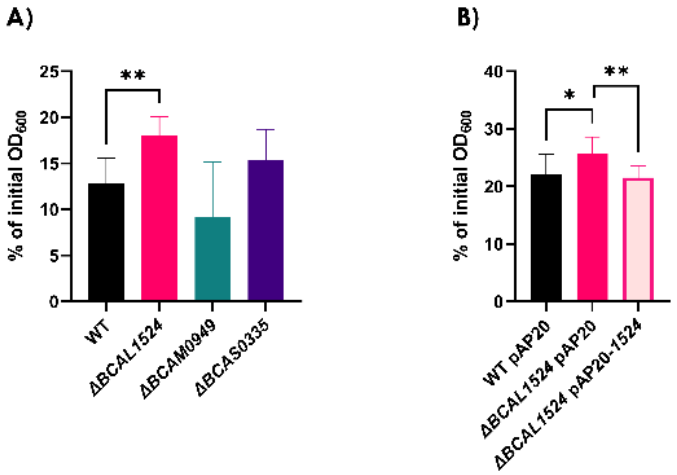

Figure 30: Percentage of initial OD_{600} of A) the WT and mutant strains after 16 h of static incubation and B) WT and mutant strains complemented with the pAP20 plasmids. Data are represented as the mean ± SD obtained from three independent experiments. (* p<0.05; **p<0.01 one-way ANOVA test).

The only significant result was achieved when *BCAL1524* was deleted, since the OD_{600} at the air-liquid interface was higher compared to WT, meaning that the auto-aggregation rate was lower; in contrast, BCAM0949 and BCAS0335 did not influence auto-aggregation. Complementation with the pAP20-*1524* plasmid efficiently restored the auto-aggregation phenotype at the level observed for the WT strain (**Figure 30B**).

BCAM0949 MEDIATES SWIMMING MOTILITY

To diffuse through low viscosity media, bacteria rely on swimming motility. The WT and deleted strains swimming motility was analysed on 0.3% agar plates. The WT halo diameter corresponded to 27.8 mm (**Figure 31A, B**); upon lipase deletion, swimming halo produced by Δ*BCAM0949* was more than halved (10.8 mm), suggesting a nearly-complete abolishment of this phenotype (**Figure 31A, B**). On the contrary, BCAL1524 and BCAS0335 deletion mutants did not show any difference respect to the WT strain (**Figure 31A, B**).

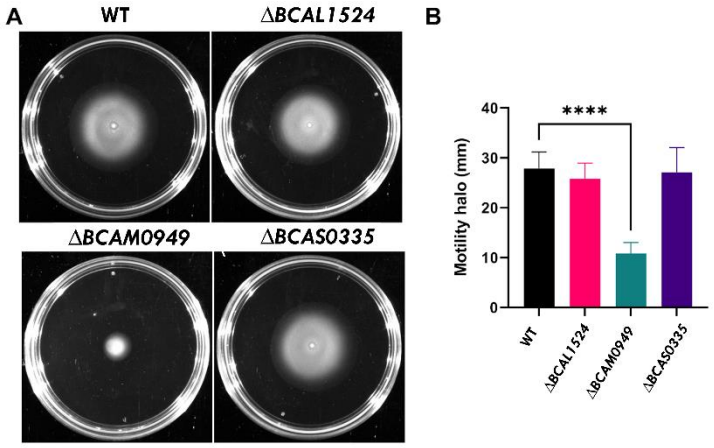

Figure 31: Swimming motility assay on LB 0.3% agar plates. (A) Swimming halos produced by WT and deleted strains. (B) Graphical representation of the produced halos (mm) of WT and deleted strains. Data are represented as the mean ± SD obtained from three independent experiments. (* p<0.0001 one-way ANOVA test).***

In the case of Δ*BCAM0949*, phenotype restoration was achieved only in the presence of the pAP20-*0949-0950* plasmid carrying the lipase in operon with its foldase; indeed, no differences were shown upon complementation of the deleted strain with the pAP20-*0949* (**Figure 32A, B**).

Indeed, literature reports that *Burkholderia territori* LipBT and *P. aeruginosa* LipA lipases need to be co-expressed with their relative

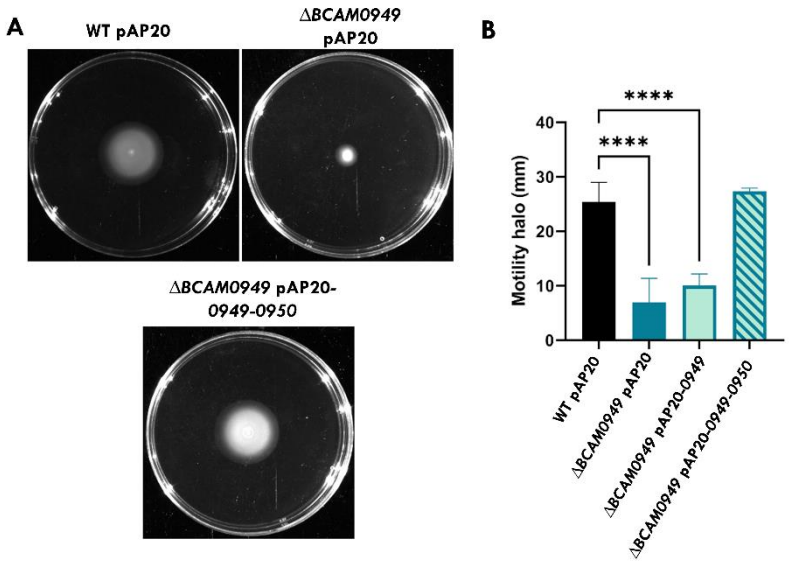

Figure 32: Swimming motility assay on LB 0.3% agar plate WT and mutant strains complemented with the pAP20 plasmids. (A) Swimming halos produced by WT pAP20 and complemented ΔBCAM0949. (B) Graphical representation of the produced halos (mm) of WT pAP20 and complemented ΔBCAM0949. Data are represented as the mean ± SD obtained from three independent experiments. (* p<0.0001 one-way ANOVA test).***

foldases to allow increased intracellular lipase concentration and avoid precipitation, which would be necessary to complement some phenotypes (Papadopoulos *et al.*, 2022; Putra *et al.*, 2019). Therefore, the data suggest a pivotal role sustained by BCAM0949 lipase in this pathway, while BCAL1524 and BCAS0335 have no involvement in swimming motility.

BCAL1524 AND BCAS0335 ARE INVOLVED IN INFECTION ESTABLISHMENT

To evaluate the symptoms produced upon the infection with the *Burkholderia* WT and delete strains, *G. mellonella* animal model was employed. *G. mellonella* larvae are one of the most used insect host to study *Burkholderia* genus infection, as they provide a simple, fast and cost-effective model granting results within 72 hrs. 10^3 CFU of bacteria were used to challenge each larva, and symptoms started to appear 24 hours post-infection (**Figure 33A, B**). To evaluate symptoms progression in infected larvae, the health index (HI) score was calculated (Tsai *et al.,*2016); this score is obtained by assigning a range of values to different phenotypes of the larvae, i.e.: the motility (0 to 3 points), vitality (dead: 0; alive: 2), and melanisation (0 to 4 points). The total score is 9; the higher the evaluated score, the milder the symptoms are. As evident from the higher HI scores, symptoms produced by Δ*BCAL1524* (HI: 6.43) and Δ*BCAS0335* (HI: 6.21) were significantly lower compared to the WT strain (HI: 4.43). At 48 hours post-infection, the HI score of Δ*BCAL1524* (HI: 4.11) and Δ*BCAS0335* (HI: 3.93) infected larvae was still higher than the WT one (HI: 0.76). Interestingly, these larvae showed a melanisation score associated with infection lower than the larvae infected with WT (**Figure 33B**). On the other hand, infection with the Δ*BCAM0949* strain did not produce any significant variation in the HI score compared to the WT strain.

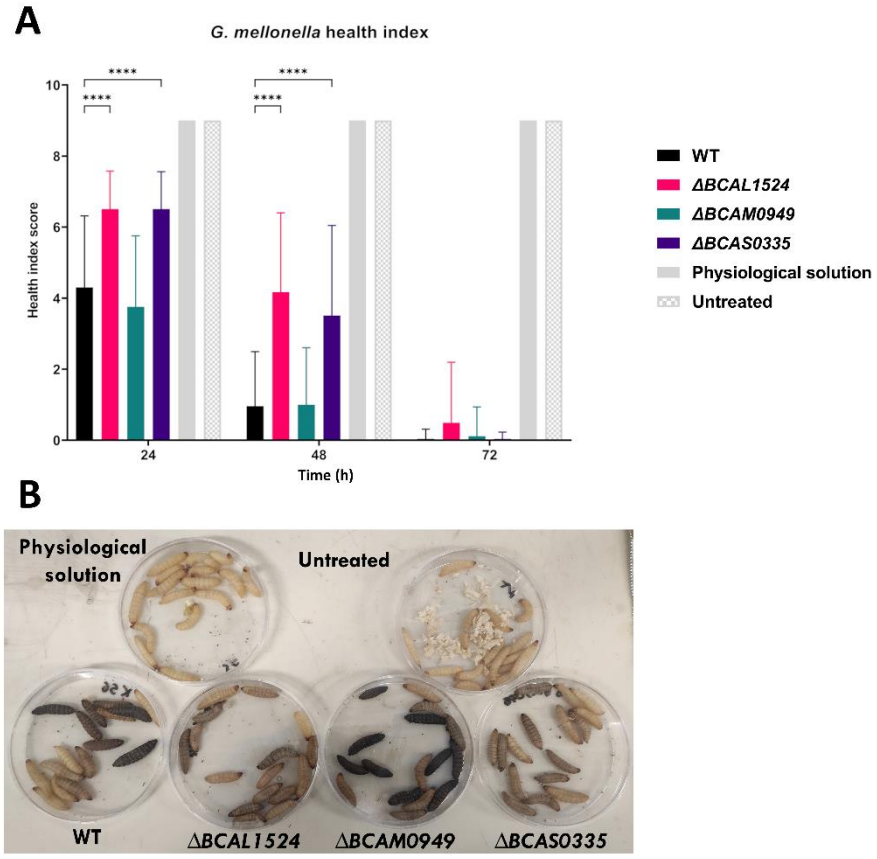

Figure 33: Galleria mellonella infection assay. (A) Health index scores associated with the WT and deleted strains. (B) G. mellonella larvae at 24 hours post-infection. Data are represented as the mean ± SD obtained from three independent experiments. (* p<0.0001 two-way ANOVA test).***

The pAP20 vector was used to complement the observed phenotypes. In the case of Δ*BCAL1524* and Δ*BCAS0335*, complementation was achieved as Δ*BCAL1524* pAP20-*1524* and Δ*BCAS0335* pAP20-*0335* showed HI scores comparable to the WT pAP20 one, at all the time points considered (**Figure 34**).

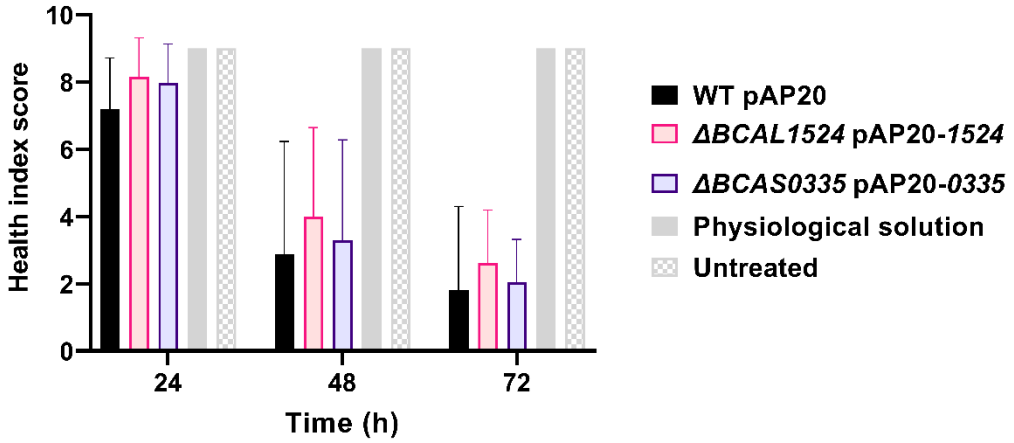

Figure 34: Health index scores associated with the WT and deleted strains, complemented with the pAP20 plasmid. Data are represented as the mean ± SD obtained from three independent experiments.

While the involvement of BCAL1524 and BCAS0335 *in vivo* has been confirmed by the decreased virulence showed by the mutants, the lack of BCAM0949 did not affect the virulence of *B. cenocepacia*.

LIPA POSSESSES LIPOLYTIC ACTIVITY AND IS INVOLVED IN RHAMNOLIPID PRODUCTION

A number of lipases from *P. aeruginosa*, e.g. EstA, are surface-exposed or secreted enzymes characterized by a conserved domain of the triacylglycerol esterase/lipase superfamily (Wilhelm *et al.,* 2007), which was found also in the BCAM0949 protein, we decided to check its lipolytic activity and ability to produce rhamnolipids. The tributyrin agar plate assay was performed to compare the lipolytic activity between the lipase-deleted and complemented strains and the *Burkholderia* WT reference (**Figure 35**). By measuring the diameter produced by each strain, we assessed that Δ*BCAM0949* showed a decreased lipolytic activity compared to the WT (**Figure 35**). The phenotype was not completely abolished, indicating that the bacterium has to possess other lipolytic enzymes such as BCAM2746, BCAM0550 and BCAL1969,

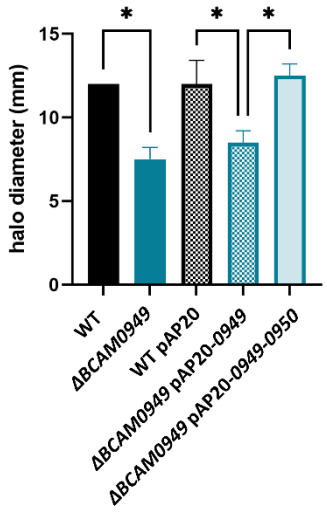

Figure 35: Quantification of lipolytic activity in term of zone of hydrolysis (mm) of WT, ΔBCAM0949 and complemented strains. Data are represented as the mean ± SD obtained from three independent experiments. (*p<0.05; one-way ANOVA test).

among the others. Also in this case, the complementation of the phenotype was achieved by introducing the entire operon into the pAP20 vector (**Figure 35**).

As EstA and LipC are involved in rhamnolipid production in *P. aeruginosa* (Rosenau *et al.,* 2010; Wilhelm *et al.,* 2007), the involvement of BCAM0949 in this aspect was investigated as well. As shown in **Figure 36**, Δ*BCAM0949* produced significantly less rhamnolipids when compared to the WT strain. In addition, even in this case the complementation could be achieved only in the presence of the entire operon, which almost doubled rhamnolipid production with respect to the WT and the WT transformed with the empty pAP20.

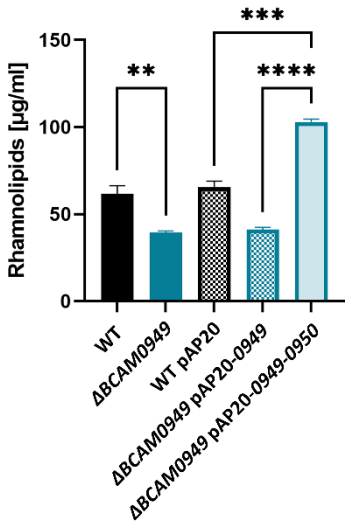

Figure 36: Quantification of rhamnolipid production in WT, ΔBCAM0949 and complemented strains by the Orcinol test. Data are represented as the mean ± SD obtained from three independent experiments. (**p<0.01, ***p<0.001, **** p<0.0001 one-way ANOVA test).

As confirmed by the two previous experiments, BCAM0949 is involved in lipolytic activity and rhamnolipid production, the latter correlated with outer membrane composition, biofilm formation and cell motility, thus demonstrating BCAM0949 involvement in different virulence pathways.

PART II: CHARACTERIZATION OF TWO FTSZ INHIBITORS AGAINST *ACINETOBACTER BAUMANNII* AND *STAPHYLOCOCCUS AUREUS*

ESKAPE bacteria are a group of pathogens prevalently present in hospital settings, associated with nosocomial and opportunistic infections (De Oliveira *et al.,* 2020). As the name indicates, these bacteria are known to easily acquire mutations which allow them to tolerate high antibiotic concentrations, making them a "priority status" as defined by the World Health Organization. Moreover, their ability to produce refractory biofilms on catheters and mechanical ventilation instruments increases the risk of septicaemia, increasing the chance of recurrent infections. Therefore, alternative and conserved drug targets are required for the development of new options, with antibacterial activity on both the sessile and planktonic bacterial lifestyle (Dsouza *et al.,* 2024). Lately, the divisome protein FtsZ attracted the interest of different research groups by virtue of its wide conservation among bacteria and fundamental involvement in bacterial division. In this second part, the FtsZ inhibitory activity of a series of synthetic compounds is investigated against *Acinetobacter baumannii* and *Staphylococcus aureus*. The C109 compound (Hogan *et al.,* 2018) was tested against different *A. baumannii* strains, evaluating the MICs and antibiofilm activity; finally, its activity against the purified FtsZ was shown. Later on, the GTPase inhibitory activity of a group of twelve synthetic compounds, predicted to inhibit *S. aureus* FtsZ, was tested on the purified *S. aureus* FtsZ protein; the MICs of each compound were then evaluated against *S. aureus* ATCC 25923. The FtsZ polymerization inhibitory activity of one of them, C11, was then further investigated by spectrofluorimetry. Finally, the antibacterial activity of C11 against *S. aureus* culture was measured by time-kill assay and infection in the *G. mellonella* animal model.

A. BAUMANNII STRAINS ARE SUSCEPTIBLE TO C109

Four strains of *A. baumannii,* i.e. ATCC 19606, 560380, MO5 and HU5, were selected and tested for C109 susceptibility by microdilution method in MH broth. The four strains are not clonally related and are representative of the following sequence type (ST): *A. baumannii* ATCC 19606 belongs to ST-52, and it is considered the standard reference strain in many laboratories (Artuso *et al*, 2022); 560380 belongs to ST 2 international clone, the most dominant type globally detected (Levy-Blitchtein *et al.,* 2018); MO5 belongs to ST 78 lineage, one of the most diffuse in Italy characterized by being carbapenem-resistance (Shelenkov *et al.,* 2023); sequence type of HU5 is unknown. The Minimum Inhibitory Concentrations (MICs) of C109 toward ATCC 19060 reference strain and 560380 and HU5 clinical isolates was 16 mg/L, while the MIC of C109 against MO5 was 32 mg/L.

C109 HAS ANTIBIOFILM ACTIVITY

The four *A. baumannii* strains were tested for C109 biofilm inhibitory activity, firstly using 96-well microplate crystal violet assay; the compound was tested at concentrations ranging from 2 to 256 mg/L (**Figure 37**). Under the tested conditions, *A. baumannii* ATCC 19606 and M05 produced significantly lower biofilm in the presence of 128 mg/L of C109; in the case of the HU5 strain, biofilm formation significantly decreased when the compound was used at 256 mg/L; finally, 64 mg/L of C109 were enough to significantly alter the biofilm formed by the 560380 strain (**Figure 37**).

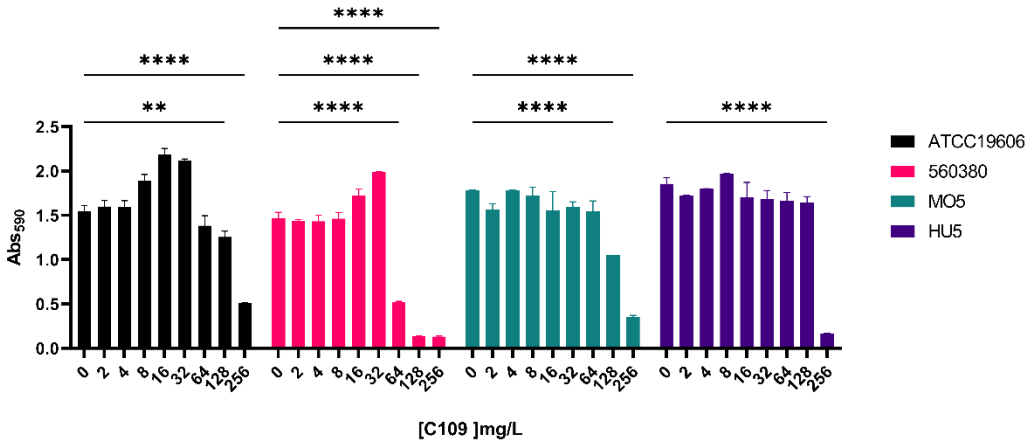

Figure 37: Biofilm formation ability of A. baumannii ATCC 196060 (black), 560380 (pink), MO5 (green) and HU5 (purple). X-axis reports the C109 concentration in mg/L. Data are represented as the mean ± standard error, n=2 (** p < 0.01; **** p < 0.0001 two-way ANOVA test).

To better characterize the effect of C109 on biofilm morphology, confocal laser scanning microscopy (CLSM) analysis was performed. The four strains were statically grown in the presence of 16, 64 and 256 mg/L of C109. As appreciable in **Figure 38**, the biofilm produced by *A. baumannii* ATCC 19606, 560380 and MO5 was qualitatively reduced at 16 mg/L; on the other hand, HU5 biofilm formation was abolished at 64 mg/L, coherently with its susceptibility to the compound (**Figure 38**).

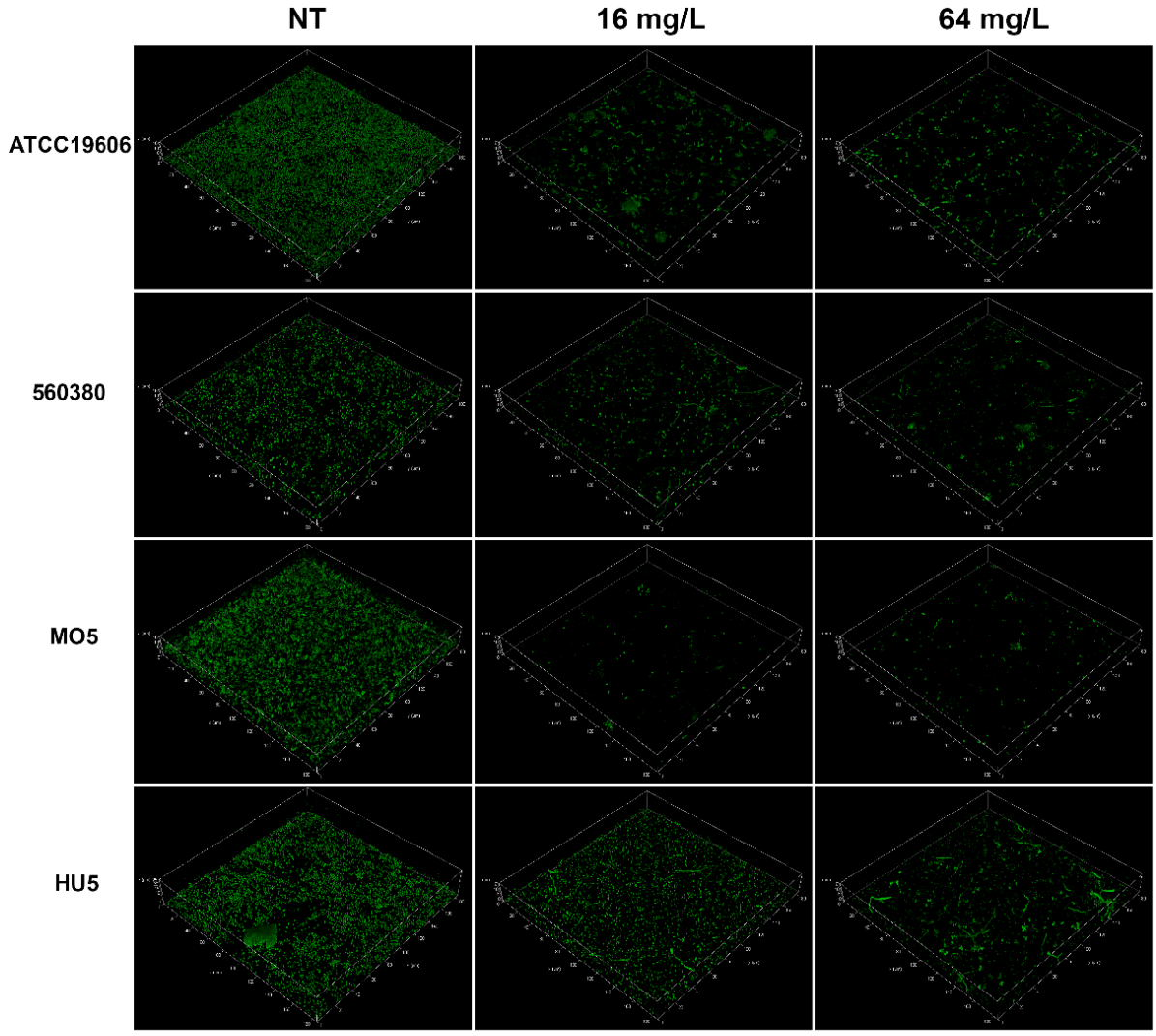

Figure 38: Biofilm evaluation by CLSM. Pictures were taken with an overall magnification of 400x and biofilms were grown in chambered slides. Cells were grown at 37°C overnight in MHII broth with no C109 (NT), 16 mg/L or 64 mg/L of C109. 2D images were stacked to reconstruct the 3D biofilm image. Seventy planes at equal distances along the Z-axis of the biofilm were imaged by CLSM.

COMSTAT 2 analysis was carried out to morphologically analyse the biofilm. ATCC 19606 and 560380 biofilm mass decreased significantly once grown with 16 and 256 mg/L of C109, respectively (**Figure 39A**); on the other hand, MO5 strain biomass slightly decreased only in the presence of 256 mg/L of C109. HU5 biofilm mass was not altered at any concentration tested.

The average thickness of the biofilms produced by ATCC 19606 was indirectly proportional to the C109 concentration used (**Figure 39B**); similarly, in the presence of 16 mg/L of C109, the thickness of 560380 biofilms significantly decreased. No significant variation was observed for the biofilms formed by MO5 and HU5 strains.

The roughness coefficient of the biofilms was analysed too (**Figure 39C**), as it is an indicator of biofilm heterogeneity. An increase in the roughness coefficient, indicative of low homogeneity, was observed in the ATCC 19606 strain after C109 treatment; a similar effect was observed for 560380 at 256 mg/L of C109. No significant variation in the roughness coefficient was observed for the biofilms formed by MO5 and HU5 strains.

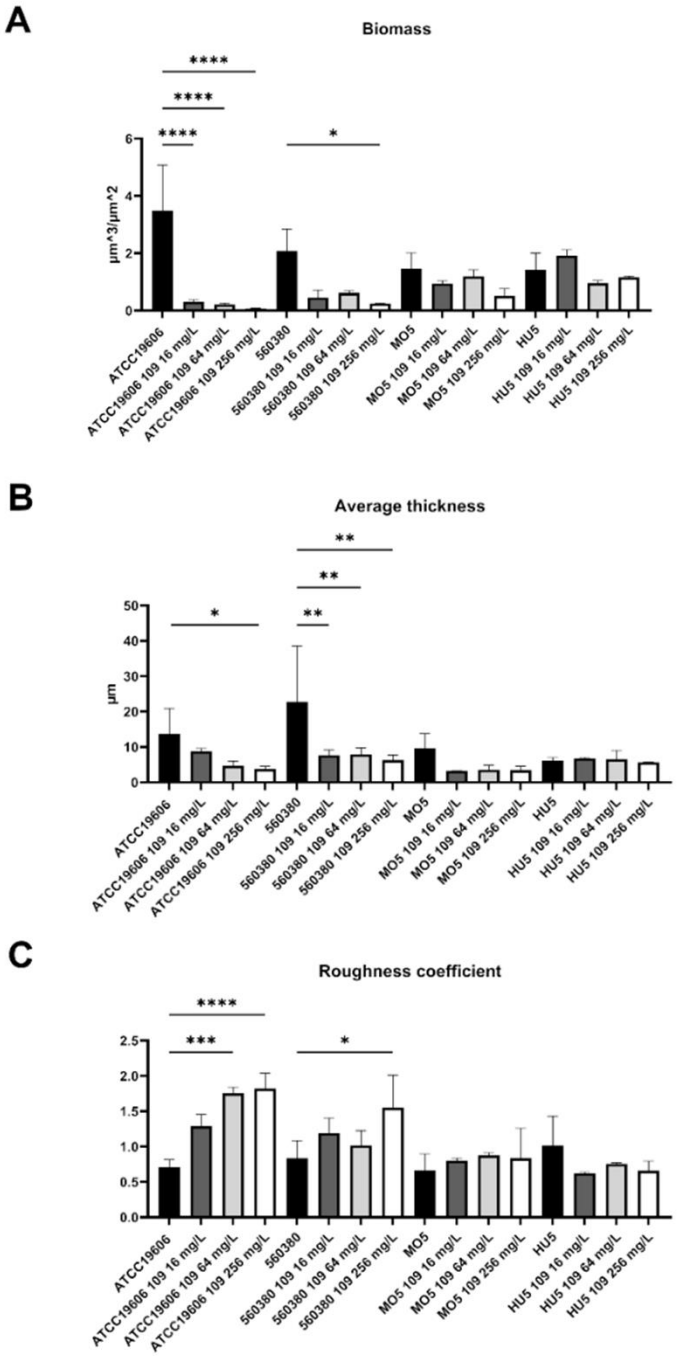

Figure 39: Biofilm morphological analysis by COMSTAT 2. (A) total biomass, (B) average thickness, and (C) roughness coefficient. Data are represented as the mean ± SD obtained from three independent experiments. (* $p < 0.05$, ** $p < 0.01$, *** $p < 0.001$, **** $p < 0.0001$ one-way ANOVA test).

Moreover, the ATCC 19606 and 560380 strain showed a drastic change in the biofilm distribution on the Z-axis upon treatment with 16 mg/L of C109; again, MO5 biofilm distribution was less affected at this concentration (**Figure 40A, B, C**). On the contrary, HU5 biofilm was partially altered at 256 mg/L of C109 (**Figure 40D**).

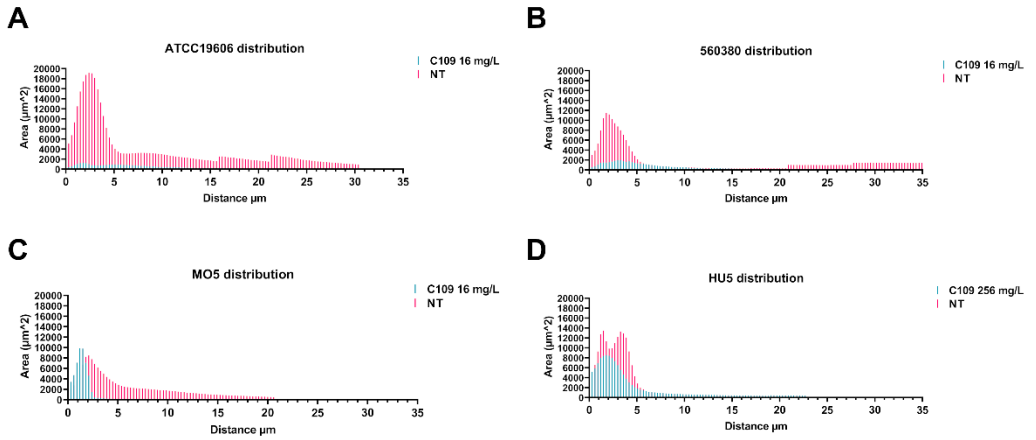

Figure 40: Biofilm morphological analysis by COMSTAT 2. Biofilm distribution in terms of % of area occupied by (A) ATCC 19606, (B) 560380, (C) MO5 and (D) HU5. Data are represented as the mean ± SD obtained from three independent experiments.

Overall, the quantitative and qualitative data obtained demonstrate that C109 was effective in inhibiting biofilm formation in *A. baumannii* ATCC 19606 (128 mg/L), 560380 (128 mg/L) and MO5 (64 mg/L), while a higher concentration was needed for the HU5 strain (256 mg/L). The results were confirmed by CLSM, revealing that 16 mg/L of C109 were enough to alter the biofilm of ATCC 19606, 560380 and MO5; COMSTAT analysis confirmed that the biomass, average thickness and distribution of the biofilms were perturbed at this concentration. On the contrary, MO5 was less sensitive to C109, as a concentration of 256 mg/L was needed to alter the previous biofilm aspects.

A. BAUMANNII FTSZ IS INHIBITED *IN VITRO* BY C109

As previously reported, C109 compound can block the polymerization and GTPase activity of FtsZ in *P. aeruginosa* and *B. cenocepacia* (Chiarelli *et al.,* 2020); on the contrary, only the GTPase activity was impaired by the compound in *S. aureus* (Trespidi *et al.,* 2021). To study its activity against *A. baumannii* FtsZ, the protein was expressed and purified as described in **Materials and Method**. C109 was able to inhibit FtsZ GTPase activity with an IC_{50} of 11.84 μM (**Figure 41A)**. To understand if polymerization could also be influenced by the presence of C109, an *in vitro* sedimentation assay was performed. *A. baumannii* FtsZ is able to polymerize *in vitro* in the presence of its substrate, GTP, but not in the presence of its product, GDP. Upon C109 addition to the reaction at increasing concentration, i.e. 50 and 100 μM, polymerization was reduced already at the lowest concentration used (**Figure 41B, C**).

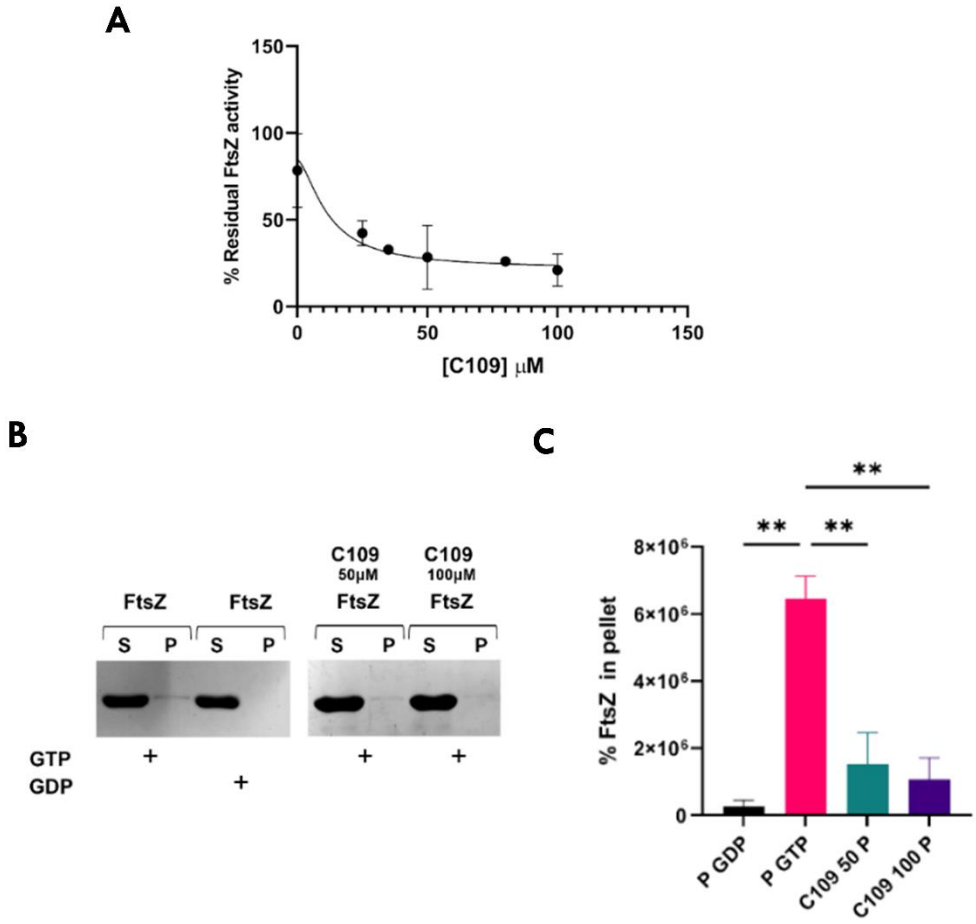

Figure 41: GTPase activity and polymerisation assays on A. baumannii FtsZ in the presence of C109. (A) 50% inhibitory concentration (IC_{50}) of C109 against A. baumannii FtsZ. (B) FtsZ sedimentation assay in the absence or presence of C109, GTP and GDP. P (pellet): unsoluble fraction); S (supernatant): soluble fraction. (C) Relative quantification of FtsZ percentage in the pellet obtained by densitometry analysis. Data are represented as the mean ± SD obtained from three independent experiments; images are representative of at least three different experiments (** p < 0.01 one-way ANOVA test).

To conclude, the data here reported prove that both the GTPase and polymerization activity of *A. baumannii* FtsZ are impaired by C109, as described by Chiarelli *et al.,* (2020) and Hogan *et al.*, (2018) for *B. cenocepacia* and *P. aeruginosa*.

ASSESSMENT OF THE ACTIVITY OF COMPOUNDS PREDICTED TO ACTON *S. AUREUS* FTSZ

The half maximal inhibitory concentration (IC_{50}) of twelve compounds identified by a Virtual Screening approach (in collaboration with Prof. Antonio Coluccia, La Sapienza University, Rome) as able to act on *S. aureus* FtsZ was measured by a pyruvate kinase-L-lactic dehydrogenase (PK/LDH) spectrophotometric coupled assay. Of all tested compounds, C3, C8 and C12 showed a relevant GTPase inhibitory activity (**Table 10**).

Compound	IC_{50}
C109	1.5 μM
C3	14.6 μM
C8	8.4 μM
C12	60 μM

Table 10: Half maximal inhibitory concentration (IC_{50}) of the active compounds. C109 was used as a positive control.

COMPOUND C11 IS ACTIVE AGAINST *S. AUREUS* ATCC 25923

S. aureus ATCC 25923 was tested for compound susceptibility by microdilution method in MH-II broth. The MIC results are reported in **Table 11**. MIC of compound C11 was < 2 mg/L; on the other hand, the MIC of the other compounds was > 256 mg/L.

Compounds	MICs
C1	> 256 mg/L
C2	> 256 mg/L
C3	> 256 mg/L

continue

C4	> 256 mg/L
C5	> 256 mg/L
C6	> 256 mg/L
C7	> 256 mg/L
C8	> 256 mg/L
C9	> 256 mg/L
C10	> 256 mg/L
C11	< 2 mg/L
C12	> 256 mg/L

Table 11: Minimum Inhibitory Concentrations (mg/L) of the 12 compounds.

COMPOUND C11 INHIBITS *S. AUREUS* FTSZ POLYMERIZATION *IN VITRO*

Considering the low MIC value measured for C11 and its inability to block FtsZ GTPase activity, further studies were performed on this compound. The dynamic FtsZ polymerization was assessed by 90° angle light scattering analysis, which finely reflects filament formation

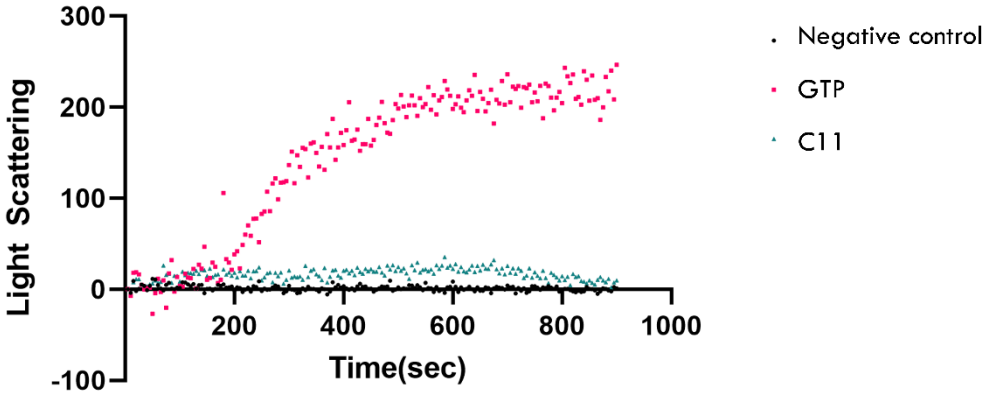

Figure 42: Effect of C11 on the kinetics of S. aureus FtsZ polymerization.

in the presence and in the absence of the inhibitory compound. Once the reaction started in the presence of compound 11 (**Figure 42**), no significant light scattering variation was found (Δmax = 14.11 AU); the light scattering signal was therefore comparable to the negative control in the presence of GDP (Δmax = 1.252 AU). As a positive control, the change in light scattering in the presence of GTP was 230.7 AU. Hence, these results indicate that the presence of C11 abolished FtsZSa polymerization, which is evident by the lack in the light scattering increase between 200 and 600 s.

COMPOUND C11 DELAYS INFECTION IN *G. MELLONELLA*

To test the *in vivo* efficacy of C11, *G. mellonella* larvae were infected with 10^5 CFU of *S. aureus* and the compound was administered 1-hour post-infection with a dosage of 20 mg/kg (2MIC) (**Figure 43**) and 40 mg/kg (4MIC) (**Figure 44**).

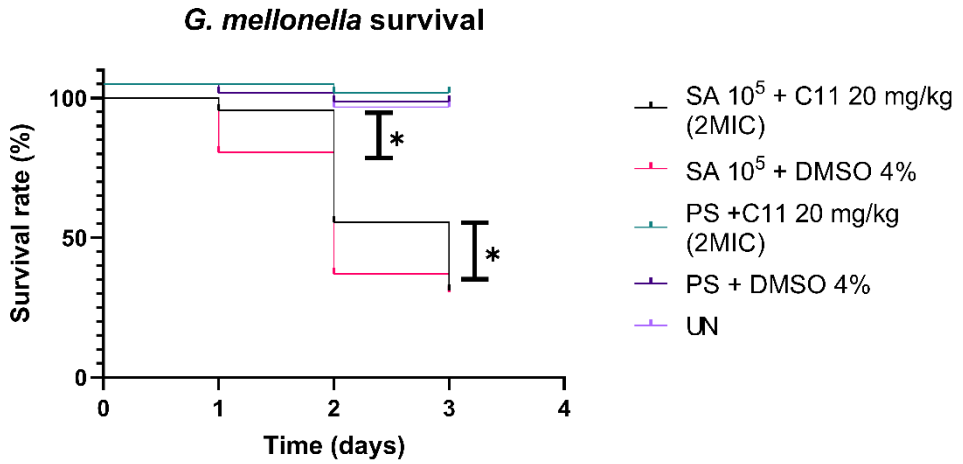

Figure 43: Kaplan-Meyer survival curve of infected Galleria mellonella larvae receiving no treatment (red line) or treatment with C11 20 mg/kg. C11 and DMSO 4% toxicity were evaluated on healthy larvae (green and violet lines), as for general survival of untreated larvae (purple). Green, violet and purple lines are offset 10% from the 100% maximal value to allow better visualisation. Vitality was checked for three days, by measuring the dead/live ratio (*p<0.05, Fisher exact test).

No significant toxicity was found for larvae treated with C11, as vitality was higher than 90 %. On the other hand, once the treatment was administered following the infection, a significant increase in the survival rate was found at 1- and 2-days post-infection (92% and 56% respectively), compared to the mock-treated larvae (80% and 37%. respectively) (**Figure 42**). At 3-days post-infection, no beneficial effect of the treatment could be observed; this observation may be related to the degradation and excretion of the compound over time.

In contrast, the bacteriostatic activity of the compound became more evident when administered at a dosage of 40 mg/kg (**Figure 43**). Compared to the mock-treated group, the survival of the treated larvae was maintained high even at 3-days post-infection (survival rate: 58% vs 32%) and 6-days post-infection (survival rate: 37% vs 19%); the beneficial effect of C11 was confirmed at 2-days post-infection (survival rate: 77% vs 46%), while only a small different was found at 1-day post-infection. Even at

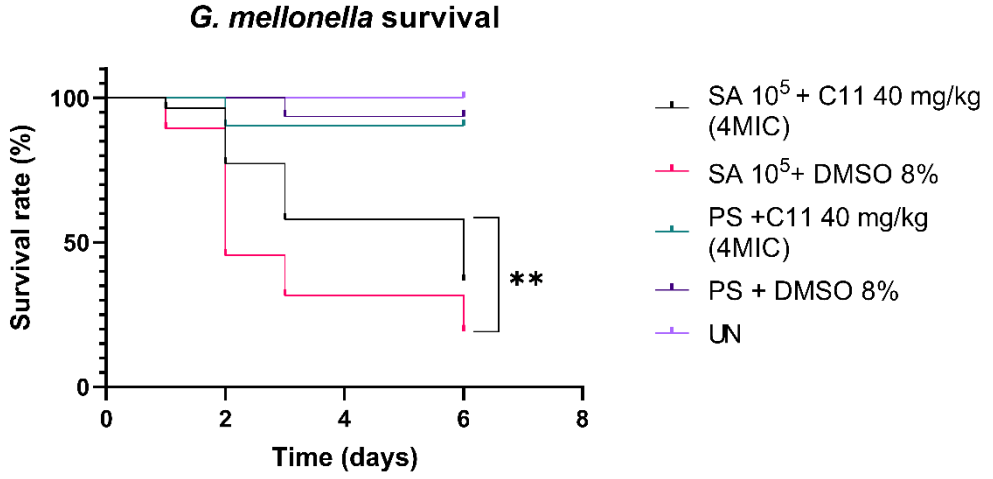

Figure 44: Kaplan-Meyer survival curve of infected Galleria mellonella larvae receiving no treatment (red line) or treatment with C11 40 mg/kg. C11 and DMSO 8% toxicity were evaluated on healthy larvae (green and violet lines), as for general survival of untreated larvae (purple). Vitality was checked for six days, by measuring the dead/live ratio (**p<0.01, Log-rank (Mantel-Cox) test).

these concentrations, neither C11 nor DMSO was toxic as the survival rate is higher than 90 %.

Discussion and future perspectives

In this thesis, the potential of alternative strategies to prevent multi-drug resistance spread has been evaluated. Fragile and immunocompromised people often rely on continuous antibiotic treatments to prevent and cure bacterial infections; unfortunately, considering the pace at which antibiotic-resistant bacteria are identified, new options will be required. This modern problem has been assessed in two ways, by investigating antigens discovery to develop a vaccine against *Burkholderia cepacia* complex bacteria and by studying new divisome inhibitors against two ESKAPE bacteria, namely *Acinetobacter baumannii* and *Staphylococcus aureus*.

In the first part, reverse vaccinology was employed to identify surface-exposed proteins that could serve as ideal antigen candidates for developing a vaccine against *B. cepacia* complex bacteria. This group of bacteria is associated with poor prognosis in people with cystic fibrosis, as recurrent infection can lead to necrotizing pneumonia and septicaemia (Hauser and Orsini, 2015); moreover, considering their high basal antibiotic resistance, empirical treatments are often unsuccessful. Different alternative strategies have been studied so far, e.g.: anti-virulence compounds interfering with the quorum-sensing system (Scoffone *et al.,* 2016), divisome inhibitors (Chiarelli *et al.,* 2020), or bacteriophages (Mankovich *et al.,* 2023). Many groups focused their interest on identifying possible antigens able to elicit a protective immune response, relying mainly on immunoproteomic approaches (Sousa *et al,* 2020a, b; McClean *et al.,* 2016). Noteworthy, a group relied on reverse vaccinology to predict novel antigen candidates (Alsowayeh *et al.*, 2022); still, data have to be experimentally confirmed.

Indeed, reverse vaccinology has proven successful in cases where vaccine development seemed impossible (Masignani *et al.,* 2019), with the most famous example being the 4CMenB vaccine; as highlighted, a suitable vaccine for *Burkholderia cepacia* complex is not available yet.

By selecting gene candidates encoding extracellular proteins predicted to be valuable targets for the immune system, a list of 24 proteins was generated. Among these, three proteins were chosen according to their homology with relevant virulence factors found in other bacteria: BCAL1524, a lipoprotein containing collagen-like triple helix repeats able to interact with host cell receptor; BCAM0949, an extracellular lipase; and BCAS0335, a trimeric autotransporter adhesin (TAA) which interacts with extracellular membrane components and possesses hemagglutinin activity. The *in silico* approach to vaccine design is a relatively new field combining chemical, mathematical and biological approaches, and allowing the screening of a high number of proteins; already deposited data are valuable sources for structural and functional analysis, as they can be employed by prediction tools to model putative proteins. Indeed, structural modelling is the most important step: it can provide information about the 3D structure and therefore on localization and function. In addition, this kind of data is necessary for B- and T-cell epitope prediction, as for antigenicity evaluation. Therefore, deepening the knowledge of the other proteins identified by our analysis would further enhance the predictive power of the protocol.

Usually, directing the immune response towards virulence determinants has been successful in eliciting protective immunity, even if antigens used for vaccine development do not necessarily have to be involved in the establishment of the infection (Delany *et al.*, 2013). Therefore, to study the role of these proteins in virulence, deletion mutants of *B. cenocepacia* K56-2 were produced.

Localization is an important aspect to select an antigen candidate. Since secreted and membrane-associated proteins are the first to interact with the host upon infection, the deleted strains were subjected to a proteomic analysis to support the *in silico* predictions, confirming that the three proteins are localized in the outer membrane vesicles (OMVs) compartments. OMVs play a critical role in virulence and host-

pathogen interaction, as they are needed to establish a favourable colonization niche; they are produced under stress conditions and can carry virulence factors and bioactive molecules that promote bacterial growth and influence host inflammation (Toyofuku *et al.,* 2023). The presence of these three proteins in OMVs suggests their involvement in these pathways. In addition, their localization on the bacterial outer membrane could make them favourite targets for recognition by the host immune system.

Moreover, the protein composition of the outer membrane strongly affects membrane stability and permeability (Delcour, 2009); it is not unusual that deletion of a membrane-associated protein would perturb hydrophobic and hydrophilic antibiotics entry, mediated by lipid and general diffusion porins pathway. Indeed, antibiotic susceptibility tests revealed that BCAM0949 mediates piperacillin resistance, while BCAS0335 affects minocycline sensitivity. Considering the role and localization of these proteins, it is suggested that their absence may alter membrane structure, thereby changing *Burkholderia* antibiotic susceptibility.

Further analyses of virulence determinants indicated that the collagen-like protein BCAL1524 plays a role in bacterial auto-aggregation and *G. mellonella* infection. Auto-aggregation allows bacterial survival inside the host and, in parallel, can stimulate melanisation and encapsulation in *G. mellonella* larvae (Nosanchuk and Casadevall, 2006). Noteworthy, aggregate formation is stimulated in response to stress conditions, which in turn favours dissemination. Melanin production is toxic for larvae, as it correlates with a high level of reactive oxygen species (ROS) (Pereira *et al.,* 2018). Therefore, milder larvae symptoms upon infection can be explained by the decreased melanisation caused by an impaired bacterial aggregation of Δ*BCAL1524*. Since the adhesin BCAS0335 is involved in biofilm formation and contributes to *G. mellonella* infection, it is important to consider that its structure allows to contact different host extracellular matrix components, such as collagen, fibronectin, and

laminin (Kiessling *et al.,* 2020). The higher health index score characterizing larvae infected with the Δ*BCAS0335* strain is compatible with an impaired bacterial adhesion. It is also known that biofilm formation depends, but not exclusively, on adhesins presence (since adhesion to a surface is required for biofilm formation) and growth medium (Hancock *et al.,* 2011). Medium viscosity and nutrient level are indeed important for bacterial sessile lifestyle (Aiyer and Manos, 2022). The presence of extracellular DNA (eDNA) and mucin provides a scaffold for biofilm formation; it could be hypothesized that in these conditions other adhesins or bacterial receptors could intervene to compensate BCAS0335 loss, which is instead required in less dense media. Similarly, while BCAS0335 would be essential for biofilm formation in a nutrient-rich medium, other actors may compensate for its loss during sessile growth in a low-nutrient medium, such as AS one; in fact, the low-nutrient level typical of AS medium stimulates chemotaxis and motility, as for the expression of flagellar proteins (Aiyer and Manos, 2022). This would likely explain the reduced biofilm production observed in the LB medium once *BCAS0335* is deleted. Hence, considering the phenotypes observed in Δ*BCAL1524* and Δ*BCAS0335*, BCAL1524 and BCAS0335 involvement as virulence factors should be further studied to make host-pathogen interaction dynamics clear, also in correlation to the different nutritional levels.

Additionally, the extracellular lipase BCAM0949 is implicated in various virulence pathways, such as biofilm formation and swimming motility. Further investigations confirmed its role as a lipolytic enzyme and revealed its involvement in rhamnolipid production, indicating a similarity to *P. aeruginosa* EstA and LipC, which also requires a cognate foldase LipH to be functional (Rosenau *et al.,* 2010; Wilhelm *et al.,* 2007). Both are involved in virulence. As reported by Rosenau *et al.,* (2010), considering that both EstA and LipC may have access to bacterial outer membrane lipids and that their deletion causes a loss in rhamnolipid production, they could play a role in a regulatory cascade which involves lipids as signalling molecules. Moreover, this phenotype may also

explain the differences found in piperacillin susceptibility and biofilm structure. In the presence of hydrophobic compounds, *P. aeruginosa* rhamnolipids mediate LPS release from the cell surface thus decreasing outer membrane hydrophilicity (Al-Tahhan *et al.,* 2000). On the other hand, rhamnolipids decrease induced by LipA and LipC loss may alter outer membrane hydrophobicity facilitating small hydrophilic molecules diffusion, as piperacillin. Furthermore, maturation of biofilms requires rhamnolipids presence, as they promote cell motility and the maintenance of water-filled channels (Davey *et al.,* 2003). The poorly structured biofilm found in Δ*BCAM0949* is likely the result of rhamnolipids perturbance. Regarding the swimming motility, it is improbable that this phenotype could be dependent on the presence of rhamnolipids, as only the swarming motility was found to be impaired in *P. aeruginosa* and *B. glumae rhlA* mutants (Nickzad *et al.,* 2015; Rosenau *et al.,* 2010). Again, the involvement of LipA in an uncharacterized lipid signalling cascade could justify the unexplained swimming motility phenotype. Therefore, LipA can be considered a pivotal protein in *B. cenocepacia* virulence, able to influence multiple and independent virulence aspects coordinated by membrane lipids. However, further studies are necessary to characterize LipA and the dynamics involving membrane lipid utilization.

Crystallization and interaction studies would be necessary to clarify BCAL1524 and BCAS0335 target recognition. To evaluate the immunogenicity of these antigens *in vivo*, additional experiments in the mouse model will be essential. Based on their potential role in virulence and their surface localization, it is expected that antibodies binding these antigens may impair their function, generating the same phenotype as the isogenic mutant strains: reduced adhesion and biofilm formation, altered membrane permeability, and decreased swimming motility. To conclude, this study lays the groundwork for the future characterization of other novel antigen candidates against the Bcc, eventually leading to the discovery of effective vaccines to avoid *Burkholderia* infections.

In the second part of the thesis, the focus has been on how FtsZ interference can impair bacterial growth, in particular in *A. baumannii* and *S. aureus*. The increase in the rate of antibiotic-resistant isolates has been widely highlighted by the World Health Organization; specifically, the rise of Carbapenem-resistant *A. baumannii* is driving the development of new active compounds. While 2% of healthcare-associated infections are caused by *A. baumannii* (Harding *et al.,* 2018), most frequently the highest mortality rate is associated to bacteraemia and ventilator-associated pneumonia, usually in patients hospitalized for longer periods (Peleg *et al.,* 2008). In addition, the ability of this bacterium to resist hostile environments and persist on abiotic surfaces makes it a dangerous pathogen. *S. aureus* too is mainly associated with hospital-acquired infections, ranging from skin and soft tissue infections to pneumonia, endocarditis, and sepsis. Known to chronically infect non-healing wounds in around 1-2% of the population of developed countries, it is one of the earliest colonizers in pwCF, being present in 20 to 90% of cases; the increasing presence of MRSA raised preoccupations due to its antibiotic resistance, hypermutator phenotype, and adaptation through biofilm formation (Iguchi *et al.,* 2016).

Differently from planktonic cells, bacteria growing as biofilm are characterized by different susceptibility to antibiotics as a consequence of the adopted metabolism; importantly, some cells can switch into slowly replicating persister subpopulations, which could be maintained alive for several generations. Precisely, the adoption of a sessile lifestyle seems to induce cell dormancy by both reducing the metabolic activity and increasing cell adherence via outer membrane and OMPs restyling (Pompilio *et al.,* 2021).

In this context, the conserved protein FtsZ and the entire cell division machinery represent valuable cellular targets for the development of alternative therapeutic strategies. The FtsZ inhibitor C109, previously characterized in our laboratory (Hogan *et al.*, 2018), has proved to

inhibit the growth of more than 100 strains of *A. baumannii* with values ranging from 8 mg/L to 32 mg/L; given the high number of MDR isolates identified, these MICs values are considered valuable. Moreover, a C109 concentration of up to 8MIC was required to impact the biofilm formation of four selected strains. To note, from a qualitative point of view biofilms produced by ATCC 19606, 560380 and MO5 were already affected by a concentration of C109 of 16 mg/L; since 560380 and MO5 strains are the most diffused globally and in Italy, respectively, and their corresponding lineages can harbour carbapenem-resistant strains, the efficacy of this compound provides a valuable choice to manage biofilm formation in the majority of nosocomial infections. The significance of the gathered data relies on the possibility of combining C109 with different antibiotics, e.g.: colistin, ceftazidime and amikacin; by perturbing the very structure of the biofilm, it would allow an increased drug penetration inside the lower layers. In particular, formulations with second-generation β-lactams would prove useful as FtsZ and penicillin-binding proteins participate in the deposition of newly synthesized peptidoglycan (Dik *et al.,* 2019).

As observed for the other Gram-negatives *B. cenocepacia* and *P. aeruginosa*, C109 was able to efficiently decrease both GTPase activity and polymerization of *A. baumannii* FtsZ, meaning that their different FtsZ proteins show a structural homology higher enough to allow a similar C109 inhibitory pattern. Interestingly, this result is in contrast to what was observed in *S. aureus* by Trespidi *et al.,* (2021), where the same compound could only inhibit FtsZ GTPase activity. As highlighted by Battaje *et al.,* (2023), FtsZ proteins from various bacteria show differences in assembly behaviour and kinetic; specifically, the cell wall structures in Gram-positive and Gram-negative bacteria require specific polymerization dynamics and rates of treadmilling. Since Gram-negatives usually present smaller and less conserved inter-domain clefts (Vemula *et al.,* 2023), binding to a nearing less enclosed region or a more conserved one as the nucleotide-binding domain may be favoured. On

the other hand, since in *S. aureus* FtsZ the space between the H7 helix and the C-terminal domain is wider, the compound would possibly accommodate deeply in the cleft, contacting the S9 and S10 folds and stabilizing the C-terminal tail (CTT); this would likely perturb the CTT conformational variation and result in GTP hydrolysis inhibition (Pradhan *et al.,* 2021; Trespidi *et al.,* 2021).

Similarly to *A. baumannii, S. aureus* is mainly associated with hospital-acquired infections, ranging from skin and soft tissue infections to pneumonia, endocarditis, and sepsis. Known to chronically infect non-healing wounds in around 1-2% of the population of developed countries, it is one of the earliest colonizers in pwCF being present from 20 to 90 %. The increasing presence of MRSA raised preoccupations due to its antibiotic resistance, hypermutator phenotype, and adaptation through biofilm formation. Therefore, the role of FtsZ attracted great interest in the study of new strategies to counteract bacterial growth and alter cell division; additionally, bioinformatic analysis is proving useful to rapidly identify potential FtsZ inhibitors from large pools of compounds (Du *et al.,* 2023; Vemula *et al.,* 2023; Qiu *et al.,* 2019).

Computer-aided drug design (CAAD) process can reduce the costs and time involved in researching new drugs (Maia *et al.,* 2020). This *in silico* approach, which relies on molecular modelling techniques, demonstrates how different molecules interact with targets of pharmacological interest; moreover, if the crystal structure of the biological target is lacking, homology modelling can provide one. Despite requiring a high computational cost, simulations performed by CAAD can make a turning point in the early-stage drug discovery process, when little or no information is available.

The CAAD virtual screening was conducted on the FtsZ crystal structure 6KVP (Ferrer-Gonzàlez *et al.,* 2019) to identify potential drug-like inhibitors by Prof. Antonio Coluccia (University La Sapienza, Rome). By screening a library of natural and synthetic molecules, 12

compounds (C1-C12) were identified and further tested for their biological activity.

GTPase activity and/or polymerization inhibition is necessary to perturb Z-ring formation and cellular division; in particular, measuring compounds IC_{50} is functional to understand to which extent GTP hydrolysis is affected by the presence of each compound, thus validating CAAD predictions. C3, C8 and C12 showed a relevant inhibition of GTPase activity, with C8 being the most active one compared to the C109 inhibitor; unfortunately, such an inhibitory effect was not reflected by the MIC value. This should not surprise since the Gram-positive outer membrane presents a thick and multi-layered protective barrier composed of peptidoglycan decorated with polymers of teichoic acids, which make the outer surface negatively charged; similarly, enzymatic degradation of the compounds may play a significant role in their stability and lack of antibacterial activity. Nevertheless, despite GTP hydrolysis being unaffected in the case of C11, this compound was the only one to present a low MIC value (< 2 mg/L) against *S. aureus*. Since CAAD considered not only the catalytic domain but also the polymerization one, filament formation was investigated through 90° light scattering analysis which confirmed FtsZ impairment to assemble. As previously said, polymerization takes place when the FtsZ C-terminal tail domain contacts the N-terminal head domain of another monomer (Tripathy and Sahu, 2019); GTP binding to the nucleotide-binding pocket (NBP) is required for such conformational variation to occur. The T7 loop, located between the helix H and the C-terminal domain, enters the NBP of the following FtsZ monomer and stimulates, in turn, GTP hydrolysis. Compound 24 (Mathew *et al.,* 2016) was able to inhibit the polymerization of *Mycobacterium tuberculosis* FtsZ by contacting the inter-domain cleft (IDC), located between Helix H and the C-terminal domain; on the other hand, phenylpropanoids as chlorogenic and caffeic acids (Hemaiswarya *et al.,* 2011) blocked protofilament formation and GTP hydrolysis of *E. coli* FtsZ by interfering with the T7 loop. Considering

these two examples, we can hypothesize that C11 could selectively interfere with polymerization by interacting with the FtsZ inter-domain cleft; in Gram-positives, the IDC region is wider compared to the one in Gram-negatives, and the dimension and flexibility of C11 may restrict its interaction in the outermost part of the IDC. This behaviour is the opposite of the one observed in the case of the C109 inhibitor, which impaired *S. aureus* FtsZ GTPase activity but not polymerization (Trespidi *et al.,* 2021). In this case, by influencing the C-terminal tail (CTT) conformation in the innermost part of the cleft, FtsZ catalytic activity is indirectly affected (Cohan *et al.,* 2020). Nevertheless, the co-crystal structure of *S. aureus* FtsZ in complex with the C11 compound is required to shed light on the nature of this interaction.

Despite the *in vitro* results, C11 displayed poor efficacy once administrated to infected *G. mellonella* larvae at a dosage of 20 mg/kg (corresponding to 2-fold the MIC value). On the other hand, a dose of 40 mg/kg of the compound was able to significantly increase the survival up to 6-days post-infection, with the best results achieved after 2-days. Animal models are complex systems, and numerous interactions have to be considered; for example, drug stability depends on enzyme degradation and excretion by the host, as for compound structure and charge. As Lipinski's rule of 5 requires (Lewis, 2013), one of the requirements for drug discovery is high lipophilicity expressed as a LogP value less than 5; LogP is the predicted partition coefficient of a solute between octanol and water. Ideally, a value between 1.35 and 1.8 should indicate satisfying oral and intestinal absorption; in the case of C11, the predicted LogP is equal to 3.2 thus indicating a good but not optimal lipophilicity. Still, a compound's chemical property can be altered by complexing it with nanocarriers (Chamundeeswari *et al.,* 2019), e.g.: liposomal and polymeric nanoparticles; these alternative formulations usually increase the bioavailability of the combined active ingredient, protecting the drug from host enzymes and increasing its efficacy. As previously discussed, synergistic activity with other antibiotics may yield more solid results.

Even if FtsZ shares less than 20% of sequence identity with eukaryotic tubulin, they still present a strong structural homology, particularly in their binding domains (Santana-Molina *et al.,* 2023). Recently, Pradhan *et al.,* (2021) described how compounds binding to the FtsZ GTPase domain often result in toxicity in humans, due to the similarities between tubulin and the GTP binding site of FtsZ; on the opposite, targeting the inter-domain cleft would significantly reduce the off-target chance (Pradhan *et al.,* 2021) as this domain is less conserved compared to its the eukaryote counterpart. The low C11 toxicity found in *G. mellonella* larvae can be therefore attributed to that; indeed, a lack of interference with the activity of human tubulin has been shown *in vitro* in our laboratory (data not shown).

The data here obtained reported that C109 represents one of the foremost FtsZ inhibitors to be effective against *A. baumannii*. Being active against clinical isolates, especially for its anti-biofilm activity, makes C109 an interesting alternative strategy against both planktonic and sessile cells. Nevertheless, the importance of the inter-domain cleft is lately attracting interest regarding new FtsZ inhibitors, and studying how the same compound could differentially bind the same target in different bacteria will explain its different modes of action; hence, co-crystallization is required to fully understand the dynamics of such complex interactions. Moreover, C11 represents a valuable FtsZ inhibitor efficient against the Gram-positive *S. aureus* and with poor toxicity in our animal model. In future, investigating its synergistic activity with antibiotics will shed light on its potential as an adjuvant both *in vitro* and *in vivo*; of note, it is of pivotal interest to identify how the compound interacts with FtsZ to better clarify the basis of its biological activity.

References

Abushaheen, M.A., Muzaheed, Fatani, A.J., Alosaimi, M., Mansy, W., George, M., Acharya, S., Rathod, S., Divakar, D.D., Jhugroo, C., Vellappally, S., Khan, A.A., Shaik, J., Jhugroo, P. (2020) Antimicrobial resistance, mechanisms and its clinical significance. *Dis Mon. 66*.

Adedeji, W.A. (2016) The treasure called antibiotics. *Ann Ib Postgrad Med*. *14*, 56-57.

Agnoli, K., Schwager, S., Uehlinger, S., Vergunst, A., Viteri, D.F., Nguyen, D. T., Sokol, P.A., Carlier, A., Eberl, L. (2012) Exposing the third chromosome of *Burkholderia cepacia* complex strains as a virulence plasmid. *Mol Microbiol*. *83*, 362-378.

Aiyer, A., Manos, J. (2022) The use of artificial sputum media to enhance investigation and subsequent treatment of cystic fibrosis bacterial infections. *Microorganisms*. *10*, 1269.

Alaiwa, M.H.A., Reznikov, L.R., Gansemer, N.D., Sheets, K.A., Horswill, A.R., Stoltz, D.A., Zabner, J., Welsh, M.J. (2014) pH modulates the activity and synergism of the airway surface liquid antimicrobials β-defensin-3 and LL-37. *Proc Natl Acad Sci USA. 111*, 18703-18708.

Aldred, K.J., Kerns, R.J., Osheroff, N. (2014) Mechanism of quinolone action and resistance. *Biochem*. *53*, 1565-1574.

Alsowayeh, N., Albutti, A., Al-Shouli, S.T. (2022) Reverse vaccinology and immunoinformatic assisted designing of a multi-epitopes-based vaccine against nosocomial *Burkholderia cepacia*. *Front Microbiol*. *13*, 929400.

Al-Tahhan, R.A., Sandrin, T.R., Bodour, A.A., Maier, R.M. (2000) Rhamnolipid-induced removal of lipopolysaccharide from *Pseudomonas aeruginosa*: effect on cell surface properties and interaction with hydrophobic substrates. *Appl Environ Microb 66*, 3262–3268

Altschul, S.F., Gish, W., Miller, W., Myers, E.W., Lipman, D.J. (1990) Basic local alignment search tool. *J Mol Biol. 215*, 403-410.

Amin, R., Jahnke, N., Waters, V. (2020) Antibiotic treatment for *Stenotrophomonas maltophilia* in people with cystic fibrosis. *Cochrane Database Syst Rev*. *3*, CD009249.

Andersen, D.H. (1938) Cystic fibrosis of the pancreas and its relation to celiac disease: a clinical and pathologic study. *Am J Dis Child. 56,* 344-399.

Artuso, I., Lucidi, M., Visaggio, D., Capecchi, G., Lugli, G.A., Ventura, M., Visca, P. (2022) Genome diversity of domesticated *Acinetobacter baumannii* ATCC 19606^{T} strains. *Microb Genom. 8*, 000749.

References

Assani, K., Tazi, M.F., Amer, A.O., Kopp, B.T. (2014) IFN-γ stimulates autophagy-mediated clearance of *Burkholderia cenocepacia* in human cystic fibrosis macrophages. *PLoS ONE*. *9*, e0213092.

Aziz, R.K., Bartels, D., Best, A.A, DeJongh, M., Disz, T., Edwards, R.A., Formsma, K., Gerdes, S., Glass, E.M., Kubal, M., Meyer, F., Olsen, G.J., Olson, R., Osterman, A.L., Overbeek, R.A., McNeil, L.K., Paarmann, D., Paczian, T., Parrello, B., Pusch, G.D., Reich, C., Stevens, R., Vassieva, O., Vonstein, V., Wilke, A., Zagnitko, O. (2008) The RAST Server: rapid annotations using subsystems technology. *BMC Genomics 9*, 7.

Bach, E., Sant'Anna, F.H., Magrich Dos Passos, J.F., Balsanelli, E., de Baura, V.A., Pedrosa, F.O., de Souza, E.M., Passaglia, L.M.P. (2017) Detection of misidentifications of species from the *Burkholderia cepacia* complex and description of a new member, the soil bacterium *Burkholderia catarinensis* sp. nov. *Pathog Dis*. *75*.

Bachert, B.A., Choi, S.J., Snyder, A.K., Rio, R.V., Durney, B.C., Holland, L.A., Amemiya, K., Welkos, S.L., Bozue, J.A., Cote, C.K., Berisio, R., Lukomski, S. (2015) A unique set of the *Burkholderia* collagen-like proteins provides insight into pathogenesis, genome evolution and niche adaptation, and infection detection. *PLoS One. 10*, e0137578

Baldwin, A., Mahenthiralingam, E., Thickett, K.M., Honeybourne, D., Maiden, M.C., Govan, J.R., Speert, D.P., Lipuma, J.J., Vandamme, P., Dowson, C.G. (2005) Multilocus sequence typing scheme that provides both species and strain differentiation for the *Burkholderia cepacia* complex. *J Clin Microbiol*. *43*, 4665-4673.

Baldwin, A., Sokol, P.A., Parkhill, J., Mahenthiralingam, E. (2004) The *Burkholderia cepacia* epidemic strain marker is part of a novel genomic island encoding both virulence and metabolism-associated genes in *Burkholderia cenocepacia*. *Infect Immun. 72*, 1537-1547.

Balfour-Lynn, I.M., Lees, B., Hall, P., Phillips, G., Khan, M., Flather, M., Elborn, J.S. (2006) Multicenter randomized controlled trial of withdrawal of inhaled corticosteroids in cystic fibrosis. *Am J Respir Crit Care Med. 173*, 1356-1362.

Bamunuarachchi, N.I., Khan, F., Kim, Y.M. (2021) Inhibition of virulence factors and biofilm formation of *Acinetobacter baumannii* by naturally-derived and synthetic drugs. *Curr Drug Targets*. *22*, 734-759.

Barlow, M., Hall, B.G. (2002) Phylogenetic analysis shows that the OXA β-lactamase genes have been on plasmids for millions of years. *J Mol Evol. 55*, 314-321.

Barry, P.J., Plant, B.J., Nair, A., Bicknell, S., Simmonds, N.J., Bell, N.J., Shafi, N.T., Daniels, T., Shelmerdine, S., Felton, I., Gunaratnam, C., Jones, A.M., Horsley, A.R. (2014) Effects of Ivacaftor in patients with cystic fibrosis who carry the G551D mutation and have severe lung disease. *Chest*. *146*, 152-158.

Battaje, R.R., Piyush, R., Pratap, V., Panda, D. (2023) Models versus pathogens: how conserved is the FtsZ in bacteria? *Biosci Rep. 43*, BSR20221664.

Bear, C.E., Li, C.H., Kartner, N., Bridges, R.J., Jensen, T.J., Ramjeesingh, M., Riordan, J.R. (1992) Purification and functional reconstitution of the cystic fibrosis transmembrane conductance regulator (CFTR). *Cell*. *68*, 809-818.

Beenker, W.A.G., Hoeksma, J., Bannier-Hélaouët, M., Clevers, H., den Hertog, J. (2023) Paecilomycone inhibits quorum sensing in Gram-negative bacteria. *Microbiol Spectr*. 11, e0509722.

Berdah, L., Taytard, J., Leyronnas, S., Clement, A., Boelle, P.Y., Corvol, H. (2018) *Stenotrophomonas maltophilia*: a marker of lung disease severity. *Pediatr Pulmonol*. *53*, 426-430.

Berlutti, F., Morea, C., Battistoni, A., Sarli, S., Cipriani, P., Superti, F., Ammendolia, M.G., Valenti, P. (2005) Iron availability influences aggregation, biofilm, adhesion and invasion of *Pseudomonas aeruginosa* and *Burkholderia cenocepacia*. *Int J Immunopathol Pharmacol. 18,* 661-670.

Berman, H.M., Westbrook, J., Feng, Z., Gilliland, G., Bhat, T.N., Weissig, H., Shindyalov, I.N., Bourne, P.E. (2000) The Protein Data Bank. *Nucleic Acids Res. 28,* 235-242.

Bernier, S.P., Sokol, P.A. (2005) Use of suppression-subtractive hybridization to identify genes in the *Burkholderia cepacia* complex that are unique to *Burkholderia cenocepacia*. *J Bacteriol. 187*, 5278-5291.

Bertot, G.M., Restelli, M.A., Galanternik, L., Aranibar Urey, R.C., Valvano, M.A., Grinstein, S. (2007) Nasal immunization with *Burkholderia multivorans* outer membrane proteins and the mucosal adjuvant adamantylamide dipeptide confers efficient protection against experimental lung infections with *B. multivorans* and *B. cenocepacia*. *Infect Immun*. *75*, 2740-2752.

Bhargava, S., Johnson, B.B., Hwang, J., Harris, T.A., George, A.S., Muir, A., Dorff, J., Okeke, I.N. (2009) Heat-resistant agglutinin 1 is an accessory enteroaggregative *Escherichia coli* colonization factor. *J Bacteriol. 191*, 4934-4942.

Biot, F.V., Lopez, M.M., Poyot, T., Neulat-Ripoll, F., Lignon, S., Caclard, A., Thibault, F.M., Peinnequin, A., Pagès, J.M., Valade, E. (2013) Interplay between three RND efflux pumps in doxycycline-selected strains of *Burkholderia thailandensis*. *PloS One. 8*, e84068.

Brackman, G., Risseeuw, M., Celen, S., Cos, P., Maes, L., Nelis, H. J., Van Calenbergh, S., Coenye, T. (2012) Synthesis and evaluation of the quorum sensing inhibitory effect of substituted triazolyl-dihydrofuranones. *Bioorg Med Chem. 20*, 4737-4743.

Buroni, S., Matthijs, N., Spadaro, F., Van Acker, H., Scoffone, V.C., Pasca, M.R., Riccardi, G., Coenye, T. (2014) Differential roles of RND efflux pumps in antimicrobial drug resistance of sessile and planktonic *Burkholderia cenocepacia* cells. *Antimicrob Agents Chemother. 58*, 7424-7429.

Bush, K., Bradford, P.A. (2016) β-Lactams and β-Lactamase inhibitors: an overview. *Cold Spring Harb Perspect Med*. *6*, a025247.

References

Cardona, S.T., Valvano, M.A. (2005) An expression vector containing a rhamnose-inducible promoter provides tightly regulated gene expression in *Burkholderia cenocepacia*. *Plasmid. 54*, 219-228.

Cauduro, G.P., Marmitt, M., Ferraz, M., Arend, S.N., Kern, G., Modolo, R.C.E., Leal, A.L., Valiati, V.H. (2023) *Burkholderia vietnamiensis* G4 as a biological agent in bioremediation processes of polycyclic aromatic hydrocarbons in sludge farms. *Environ Monit Assess. 195*, 116.

Center for Disease Control and Prevention. (2019) Antibiotic resistance threats in the United States. Report 2019. https://www.hhs.gov/sites/default/files/michael-craig-cdc-talk-thursday-am-508.pdf

Center for Disease Control and Prevention. (2022) COVID-19: U.S. impact on antimicrobial resistance. Special report 2022. https://www.cdc.gov/drugresistance/pdf/covid19-impact-report-508.pdf

Cerutti, A., Puga, I., Magri, G. (2013) The B cell helper side of neutrophils. *J Leukoc Biol*. *94*, 677-682.

Chai, W.C., Whittall, J.J., Polyak, S.W., Foo, K., Li, X., Dutschke, C.J., Ogunniyi, A.D., Ma, S., Sykes, M.J., Semple, S.J., Venter, H. (2022) Cinnamaldehyde derivatives act as antimicrobial agents against *Acinetobacter baumannii* through the inhibition of cell division. *Front Microbiol. 29*, 13, 967949.

Chamundeeswari, M., Jeslin, J., Verma, M.L. (2019) Nanocarriers for drug delivery applications. *Environ Chem Lett. 17*, 849–865.

Chen, J.H., Xiang, W., Cao, K.X., Lu, X., Yao, S.C., Hung, D., Huang, R.S., Li, L.B. (2020) Characterization of volatile organic compounds emitted from endophytic *Burkholderia cenocepacia* ETR-B22 by SPME-GC-MS and their inhibitory activity against various plant fungal pathogens. *Molecules*. *25*, 3765.

Chen, J.S., Witzmann, K.A., Spilker, T., Fink, R.J., LiPuma, J.J. (2001) Endemicity and inter-city spread of *Burkholderia cepacia* genomovar III in cystic fibrosis. *J Pediatr. 139*, 643-649.

Chiarelli, L.R., Scoffone, V.C., Trespidi, G., Barbieri, G., Riabova, O., Monakhova, N., Porta, A., Manina, G., Riccardi, G., Makarov, V., Buroni, S. (2020) Chemical, metabolic, and cellular characterization of a FtsZ inhibitor effective against *Burkholderia cenocepacia*. *Front Microbiol*. *11*, 562.

Chong, L.C., Khan, A.M. (2018) Vaccine target discovery. *J Bioinform Comput Biol*. *2019*, 241-251.

Cigana, C., Assael, B.M., Melotti, P. (2007) Azithromycin selectively reduces tumor necrosis factor alpha levels in cystic fibrosis airway epithelial cells. *Antimicrob Agents Chemother*. *51*, 975-981.

Coenye, T., Mahenthiralingam, E., Henry, D., LiPuma, J.J., Laevens, S., Gillis, M., Speert, D.P., Vandamme, P. (2001a) *Burkholderia ambifaria* sp. nov., a novel member of the *Burkholderia cepacia* complex including biocontrol and cystic fibrosis-related isolates. *Int J Syst Evol Microbiol*. *51*, 1481-1490.

Coenye, T., Spilker, T., Van Schoor, A., LiPuma, J.J., Vandamme, P. (2004) Recovery of *Burkholderia cenocepacia* strain PHDC from cystic fibrosis patients in Europe. *Thorax*. *59*, 952-954.

Coenye, T., Vandamme, P., Govan, J.R.W., Lipuma, J.J. (2001b) Taxonomy and identification of the *Burkholderia cepacia* complex. *J Clin Microbiol*. *39*, 3427-3436.

Cohan, M.C., Eddelbuettel, A.M.P., Levin, P.A., Pappu, R.V. (2020) Dissecting the functional contributions of the intrinsically disordered C-terminal tail of *Bacillus subtilis* FtsZ. *J Mol Biol. 432*, 3205-3221.

Cohen-Cymberknoh, M., Kerem, E., Ferkol, T., Elizur, A. (2013) Airway inflammation in cystic fibrosis: molecular mechanisms and clinical implications. *Thorax*. *68*, 1157-1162.

Collignon, P.J., McEwen, S.A. (2019) One Health - Its importance in helping to better control antimicrobial resistance. *Trop Med Infect Dis*. *4*, 22.

Costabile, G., Provenzano, R., Azzalin, A., Scoffone, V.C., Chiarelli, L.R., Rondelli, V., Grillo, I., Zinn, T., Lepioshkin, A., Savina, S., Miro, A., Quaglia, F., Makarov, V., Coenye, T., Brocca, P., Riccardi, G., Buroni, S., Ungaro, F. (2020) PEGylated mucus-penetrating nanocrystals for lung delivery of a new FtsZ inhibitor against *Burkholderia cenocepacia* infection. *Nanomed. 23*, 102-113.

Cotter, S.E., Surana, N.K., Grass, S., St Geme, J.W. 3rd. (2006) Trimeric autotransporters require trimerization of the passenger domain for stability and adhesive activity. *J Bacteriol*. 188, 5400-5407.

Csanády, L., Vergani, P., Gadsby, D.C. (2019) Structure, gating, and regulation of the CFTR anion channel. *Physiol Rev. 99*, 707-738.

Cystic Fibrosis Foundation. (2022) Patient Registry. Report 2021. https://www.cff.org/sites/default/files/2021-11/Patient-Registry-Annual-Data-Report.pdf.

Dajkovic, A., Lan, G., Sun, S.X., Wirtz, D., Lutkenhaus, J. (2008) MinC spatially controls bacterial cytokinesis by antagonizing the scaffolding function of FtsZ. *Curr Biol*. *18*, 235-244.

Dakal, T.C., Kumar, A., Majumdar, R.S., Yadav, V. (2016) Mechanistic basis of antimicrobial actions of silver nanoparticles. *Front Microbiol*. *7*, 1831.

Darby, E.M., Trampari, E., Siasat, P., Gaya, M.S., Alav, I., Webber, M.A., Blair, J.M.A. (2023) Molecular mechanisms of antibiotic resistance revisited. *Nat Rev Microbiol.* 5, 280-295.

Davey, M.E., Caiazza, N.C., O'Toole, G.A. (2003) Rhamnolipid surfactant production affects biofilm architecture in *Pseudomonas aeruginosa* PAO1. *J Bacteriol 185*, 1027–1036.

Davies, J. (1994) Inactivation of antibiotics and the dissemination of resistance genes. *Science*. *264*, 375-382.

References

D'Costa, V.M., McGrann, K.M., Hughes, D.W., Wright, G.D. (2006) Sampling the antibiotic resistome. *Science. 311*, 374-347.

De Boeck, K., Amaral, M.D. (2016) Progress in therapies for cystic fibrosis. *Lancet Respir Med. 4*, 662-674.

Dehbanipour, R., Ghalavand, Z. (2022) *Acinetobacter baumannii*: pathogenesis, virulence factors, novel therapeutic options and mechanisms of resistance to antimicrobial agents with emphasis on tigecycline. *J Clin Pharm Ther*. *47*, 1875-1884.

Delany, I., Rappuoli, R., Seib, K.L. (2013) Vaccines, reverse vaccinology, and bacterial pathogenesis. *Cold Spring Harb Perspect Med*. 3, a012476.

Delcour, A.H. (2009) Outer membrane permeability and antibiotic resistance. *Biochim Biophys Acta*. 1794, 808-816.

Demko, Z. P., Sharpless, K. B. (2002) A click chemistry approach to tetrazoles by huisgen 1,3-dipolar cycloaddition: synthesis of 5-sulfonyl tetrazoles from azides and sulfonyl cyanides. *Angew Chem Int Ed. 41*, 2110-2113.

Denissen, J., Reyneke, B., Waso-Reyneke, M., Havenga, B., Barnard, T., Khan, S., Khan, W. (2022) Prevalence of ESKAPE pathogens in the environment: Antibiotic resistance status, community-acquired infection and risk to human health. *Int J Hyg Environ Health. 244*, 114006.

De Oliveira, D.M.P., Forde, B.M., Kidd, T.J., Harris, P.N.A., Schembri, M.A., Beatson, S.A., Paterson, D.L., Walker, M.J. (2020) Antimicrobial resistance in ESKAPE pathogens. *Clin Microbiol Rev. 33*, e00181-19.

Depoorter, E., De Canck, E., Peeters, C., Wieme, A. D., Cnockaert, M., Zlosnik, J. E. A., LiPuma, J. J., Coenye, T., Vandamme, P. (2020) *Burkholderia cepacia* Complex Taxon K: Where to split? *Front Microbiol. 11,* 1594.

De Smet, B., Mayo, M., Peeters, C., Zlosnik, J.E.A., Spilker, T., Hird, T.J., LiPuma, J.J., Kidd, T.J., Kaestli, M., Ginther, J.L., Wagner, D.M., Keim, P., Bell, S.C., Jacobs, J.A., Currie, B.J., Vandamme, P. (2015) *Burkholderia stagnalis* sp. nov. and *Burkholderia territorii* sp. nov., two novel *Burkholderia cepacia* complex species from environmental and human sources. *Int J Syst Evol Microbiol*. *65*, 2265-2271.

Detmer, A., Glenting, J. (2006) Live bacterial vaccines-a review and identification of potential hazards. *Microb Cell Fact*. *5*, 23.

Dezube, R., Jennings, M.T., Rykiel, M., Diener-West, M., Boyle, M.P., Chmiel, J.F., Dasenbrook, E.C. (2019) Eradication of persistent methicillin-resistant *Staphylococcus aureus* infection in cystic fibrosis. *J Cyst Fibros*. *18*, 357-363.

Dik, D.A., Fisher, J.F., Mobashery, S. (2018) Cell-wall recycling of the Gram-negative bacteria and the nexus to antibiotic resistance. C*hem Rev. 118*, 5952-5984.

Domadia, P., Swarup, S., Bhunia, A., Sivaraman, J., Dasgupta, D. (2007) Inhibition of bacterial cell division protein FtsZ by cinnamaldehyde. *Biochem Pharmacol*. *15*, 74, 831-840.

Doytchinova, I.A., Flower, D.R. (2007) VaxiJen: a server for prediction of protective antigens, tumour antigens and subunit vaccines. *BMC Bioinform. 8*, 4.

Drevinek, P., Baldwin, A., Dowson, C.G., Mahenthiralingam, E. (2008a) Diversity of the *parB* and *repA* genes of the *Burkholderia cepacia* complex and their utility for rapid identification of Burkholderia cenocepacia. *BMC Microbiol*. *8*, 1-10.

Drevinek, P., Holden, M.T.G., Ge, Z., Jones, A.M., Ketchell, I., Gill, R.T., Mahenthiralingam, E. (2008b) Gene expression changes linked to antimicrobial resistance, oxidative stress, iron depletion and retained motility are observed when *Burkholderia cenocepacia* grows in cystic fibrosis sputum. *BMC Infect Dis*. *8*, 1-16.

Drevinek, P., Mahenthiralingam, E. (2010) *Burkholderia cenocepacia* in cystic fibrosis: epidemiology and molecular mechanisms of virulence. *Clin Microbiol Infect*. *16*, 821-830.

Drevinek, P., Vosahlikova, S., Cinek, O., Vavrova, V., Bartosova, J., Pohunek, P., Mahenthiralingam, E. (2005) Widespread clone of *Burkholderia cenocepacia* in cystic fibrosis patients in the Czech Republic. *J Med Microbiol. 54*, 655-659.

Dsouza, F.P., Dinesh, S., Sharma, S. (2024) Understanding the intricacies of microbial biofilm formation and its endurance in chronic infections: a key to advancing biofilm-targeted therapeutic strategies. *Arch Microbiol*. *206*, 85.

Du, D., Wang-Kan, X., Neuberger, A., van Veen, H.W., Pos, K.M., Piddock, L.J.V., Luisi, B.F. (2018) Multidrug efflux pumps: structure, function and regulation. *Nat Rev Microbiol*. *16*, 523-539.

Du, R.L., Chow, H.Y., Chen, Y.W., Chan, P.H., Daniel, R.A., Wong, K.Y (2023)**.** Gossypol acetate: a natural polyphenol derivative with antimicrobial activities against the essential cell division protein FtsZ. *Front Microbiol. 13*, 1080308.

Du, S., Lutkenhaus, J. (2017) Assembly and activation of the *Escherichia coli* divisome. *Mol Microbiol*. 105, 177-187.

Durand, G.A., Raoult, D., Dubourg, G. (2018) Antibiotic discovery: history, methods and perspectives. *Int J Antimicrob Agents. 53*, 371-382.

Durand-Reville, T.F., Miller, A.A., O'Donnell, J.P., Wu, X., Sylvester, M.A., Guler, S., Iyer, R., Shapiro, A.B., Carter, N.M., Velez-Vega, C., Moussa, S.H., McLeod, S.M., Chen, A., Tanudra, A.M., Zhang, J., Comita-Prevoir, J., Romero, J.A., Huynh, H., Ferguson, A.D., Horanyi, P.S., Mayclin, S.J., Heine, H.S., Drusano, G.L., Cummings, J.E., Slayden, R.A., Tommasi, R. A. (2021) Rational design of a new antibiotic class for drug-resistant infections. *Nature*. *597*, 698-702.

References

Durmowicz, A.G., Lim, R., Rogers, H., Rosebraugh, C.J., Chowdhury, B.A. (2018) The U.S. food and drug administration's experience with ivacaftor in cystic fibrosis: establishing efficacy using in vitro data in lieu of a clinical trial. *Ann Am Thorac*. *15*, 1-2.

Edwards, B.D., Greysson-Wong, J., Somayaji, R., Waddell, B., Whelan, F.J., Storey, D.G., Rabin, H.R., Surette, M.G., Parkinsa, M.D. (2017) Prevalence and outcomes of *Achromobacter* species infections in adults with cystic fibrosis: A North American cohort study. *J Clin Microbiol*. *55*, 2074-2085.

Eissa, M.E. (2016) Distribution of bacterial contamination in non-sterile pharmaceutical materials and assessment of its risk to the health of the final consumers quantitatively. *Beni Suef Univ J Basic Appl Sci. 5*, 217-230.

El-Mahallawy, H.A., Hassan, S.S., El-Wakil, M., Moneer, M.M. (2016) Bacteremia due to ESKAPE pathogens: an emerging problem in cancer patients. *J Egypt Natl Canc Inst*. *28*, 157-162.

Elshikh, M., Ahmed, S., Funston, S., Dunlop, P., McGaw, M., Marchant, R., Banat, I.M. (2016) Resazurin-based 96-well plate microdilution method for the determination of minimum inhibitory concentration of biosurfactants. *Biotechnol Lett. 38*, 1015–1019.

EUCAST. (2003) Determination of minimum inhibitory concentrations (MICs) of antibacterial agents by broth dilution. *Clin Microbiol Infect. 9*, 509-515.

European Center for Disease Control and Prevention. (2022) Antimicrobial resistance surveillance in Europe. Report 2020. https://www.ecdc.europa.eu/sites/default/files/documents/Joint-WHO-ECDC-AMR-report-2022.pdf

European Cystic Fibrosis Society. (2022) Patient registry. Report 2020. https://www.ecfs.eu/sites/default/files/ECFSPR_Report_2020_v1.0%20%2807Jun2022%29_website.pdf

Fazli, M., Rybtke, M., Steiner, E., Weidel, E., Berthelsen, J., Groizeleau, J., Bin, W., Zhi, B. Z., Yaming, Z., Kaever, V., Givskov, M., Hartmann, R.W., Eberl, L., Tolker-Nielsen, T. (2017) Regulation of *Burkholderia cenocepacia* biofilm formation by RpoN and the c-di-GMP effector BerB. *Microbiologyopen*. *6*, 1-13.

Feavers, I.M., Maiden, M.C.J. (2017) Recent progress in the prevention of serogroup B meningococcal disease. *Clin Vaccine Immunol*. *24*, e00566-16.

Ferrer-González, E., Fujita, J., Yoshizawa, T., Nelson, J.M., Pilch, A.J., Hillman, E., Ozawa, M., Kuroda, N., Al-Tameemi, H.M., Boyd, J.M., LaVoie, E.J., Matsumura, H., Pilch, D.S. (2019) Structure-guided design of a fluorescent probe for the visualization of FtsZ in clinically important Gram-positive and Gram-negative bacterial pathogens. *Sci Rep. 9*, 20092.

Figurski, D.H., Helinski, D.R. (1979) Replication of an origin-containing derivative of plasmid RK2 dependent on a plasmid function provided in trans. *Proc Natl Acad Sci U.S.A. 76*, 1648-1652.

Fischer, R., Schwarz, C., Weiser, R., Mahenthiralingam, E., Smerud, K., Meland, N., Flaten, H., Rye, P.D. (2022) Evaluating the alginate oligosaccharide (OligoG) as a therapy for Burkholderia cepacia complex cystic fibrosis lung infection. *J Cyst Fibros. 21*, 821-829.

Flannagan, R.S., Linn, T., Valvano, M.A. (2008) A system for the construction of targeted unmarked gene deletions in the genus *Burkholderia*. *Environ Microbiol*. *10*, 1652-1660.

Flannagan, R.S., Valvano, M.A. (2008) *Burkholderia cenocepacia* requires RpoE for growth under stress conditions and delay of phagolysosomal fusion in macrophages. *Microbiol*. *154*, 643-653.

Furlan, J.P.R., Pitondo-Silva, A., Braz, V.S., Gallo, I.F.L., Stehling, E.G. (2019) Evaluation of different molecular and phenotypic methods for identification of environmental *Burkholderia cepacia* complex. *World J Microbiol Biotechnol*. *35*, 1-6.

Gamba, P., Veening, J.W., Saunders, N.J., Hamoen, L.W., Daniel, R.A. (2009) Two-step assembly dynamics of the *Bacillus subtilis* divisome. *J Bacteriol. 191*, 4186-4194.

García-Romero, I., Valvano, M.A. (2020) Complete genome sequence of *Burkholderia cenocepacia* K56-2, an opportunistic pathogen. *Microbiol Resour Announc. 9*, 8-9.

Gautam, V., Sharma, M., Singhal, L., Kumar, S., Kaur, P., Tiwari, R., Ray, P. (2017) MALDI-TOF mass spectrometry: an emerging tool for unequivocal identification of non-fermenting Gram-negative bacilli. *Indian J Med Res*. *145*, 665-672.

Gilchrist, F.J., Webb, A.K., Bright-Thomas, R.J., Jones, A.M. (2012) Successful treatment of cepacia syndrome with a combination of intravenous cyclosporin, antibiotics and oral corticosteroids. *J Cyst Fibros. 11*, 458-460.

Gillis, M., Van, T.V., Bardin, R., Goor, M.A., Hebbar, P.K., Willems, A., Segers, P., Kersters, K., Heulin, T., Fernandez, M.P. (1995) Polyphasic taxonomy in the genus *Burkholderia* leading to an emended description of the genus and proposition of *Burkholderia vietnamiensis* sp. nov. for N2-fixing Isolates from rice in Vietnam. *Int J Syst Evol Microbiol. 45*, 274-289.

Giuliani, M.M., Adu-Bobie, J., Comanducci, M., Aricò, B., Savino, S., Santini, L., Brunelli, B., Bambini, S., Biolchi, A., Capecchi, B., Cartocci, E., Ciucchi, L., Di Marcello, F., Ferlicca, F., Galli, B., Luzzi, E., Masignani, V., Serruto, D., Veggi, D., Contorni, M., Morandi, M., Bartalesi, A., Cinotti, V., Mannucci, D., Titta, F., Ovidi, E., Welsch, J.A., Granoff, D., Rappuoli, R., Pizza, M. (2006) A universal vaccine for serogroup B meningococcus. *Proc Natl Acad Sci USA*. *103*, 10834-10839.

Glassford, I., Teijaro, C.N., Daher, S.S., Weil, A., Small, M.C., Redhu, S.K., Colussi, D.J., Jacobson, M.A., Childers, W.E., Buttaro, B., Nicholson, A.W., MacKerell, A.D. Jr, Cooperman, B.S., Andrade, R.B. (2016) Ribosome-templated azide-alkyne cycloadditions: synthesis of potent macrolide antibiotics by *in situ* click chemistry. *J Am Chem Soc. 9*, 138, 3136-3144.

Goldberg, J.B., Crisan, C.V., Luu, J.M. (2022) *Pseudomonas aeruginosa* antivirulence strategies: targeting the Type III secretion system. *Adv Exp Med Biol*. *1386*, 257-280.

References

Goldstein, B.P. (2014) Resistance to rifampicin: a review. *J Antibiot. 67*, 625-630.

Goodswen, S.J., Kennedy, P.J., Ellis, J.T. (2023) A guide to current methodology and usage of reverse vaccinology towards in silico vaccine discovery. *FEMS Microbiol Rev. 47,* fuad004.

Griffith, D.E., Aksamit, T., Brown-Elliott, B.A., Catanzaro, A., Daley, C., Gordin, F., Holland, S.M., Horsburgh, R., Huitt, G., Iademarco, M.F., Iseman, M., Olivier, K., Ruoss, S., Von Reyn, C.F., Wallace, R.J., Winthrop, K. (2007) An official ATS/IDSA statement: diagnosis, treatment, and prevention of nontuberculous mycobacterial diseases. *Am J Respir Crit Care Med. 175*, 367-416.

Grund, M.E., Kramarska, E., Choi, S.J., McNitt, D.H., Klimko, C.P., Rill, N.O., Dankmeyer, J.L., Shoe, J.L., Hunter, M., Fetterer, D.P., Hedrick, Z.M., Velez, I., Biryukov, S.S., Cote, C.K., Berisio, R., Lukomski, S. (2021) Predictive and experimental immunogenicity of *Burkholderia* collagen-like protein 8-derived antigens. *Vaccines (Basel). 9,* 1219.

Guglierame, P., Pasca, M.R., De Rossi, E., Buroni, S., Arrigo, P., Manina, G., Riccardi, G. (2006) Efflux pump genes of the resistance-nodulation-division family in *Burkholderia cenocepacia* genome. *BMC Microbiol. 6*, 66.

Guo, F.B., Xiong, L., Zhang, K.Y., Dong, C., Zhang, F.Z., Woo, P.C. (2017) Identification and analysis of genomic islands in *Burkholderia cenocepacia* AU 1054 with emphasis on pathogenicity islands. *BMC Microbiol*. *17*, 73.

Hamad, M.A., Skeldon, A.M., Valvano, M.A. (2010) Construction of aminoglycoside-sensitive *Burkholderia cenocepacia* strains for use in studies of intracellular bacteria with the gentamicin protection assay. *Appl Environ Microbiol. 76*, 3170-3176.

Hancock, V., Witsø, I.L., Klemm, P. (2011) Biofilm formation as a function of adhesin, growth medium, substratum and strain type. *Int J Med Microbiol*. *301*, 570-576.

Han, H., Wang, Z., Li, T., Teng, D., Mao, R., Hao, Y., Yang, N., Wang, X., Wang, J. (2021) Recent progress of bacterial FtsZ inhibitors with a focus on peptides. *FEBS J. 288*, 1091-1106.

Harding, C.M., Hennon, S.W., Feldman, M.F. (2018) Uncovering the mechanisms of *Acinetobacter baumannii* virulence. *Nat Rev Microbiol. 16*, 91-102.

Hauser, N., Orsini, J. (2015) Cepacia Syndrome in a non-cystic fibrosis patient. *Case Rep Infect Dis*. *2015*, 537627.

Hemaiswarya, S., Soudaminikkutty, R., Narasumani, M.L., Doble, M. (2011) Phenylpropanoids inhibit protofilament formation of Escherichia coli cell division protein FtsZ. *J Med Microbiol*. *60*, 1317-1325.

Henderson, A.G., Davis, J.M., Keith, J.D., Green, M.E., Oden, A.M., Rowe, S.M., Birket, S.E. (2022) Static mucus impairs bacterial clearance and allows chronic infection with *Pseudomonas aeruginosa* in the cystic fibrosis rat. *Eur Respir J. 3*, 2101032.

Hengge, R., Pruteanu, M., Stülke, J., Tschowri, N., Turgay, K. (2023) Recent advances and perspectives in nucleotide second messenger signaling in bacteria. *Microlife*. *4*, uqad015.

Heydorn, A., Nielsen, A.T., Hentzer, M., Sternberg, C., Givskov, M., Ersbøll, B.K., Molin, S. (2000) Quantification of biofilm structures by the novel computer program COMSTAT. *Microbiology (Readin*g). *146*, 2395-2407.

He, Y., Xiang, Z., Mobley, H.L. (2010) Vaxign: the first web-based vaccine design program for reverse vaccinology and applications for vaccine development. *J Biomed Biotechnol. 2010*, 297505.

He, Y., Yang, L., He, C., Wang, F. (2022) *Burkholderia cepacia* enhanced electrokinetic-permeable reaction barrier for the remediation of lead contaminated soils. *Sustainability (Switzerland)*. *14*, 11440.

Hogan, A.M., Scoffone, V.C., Makarov, V., Gislason, A.S., Tesfu, H., Stietz, M.S., Brassinga, A.K.C., Domaratzki, M., Li, X., Azzalin, A., Biggiogera, M., Riabova, O., Monakhova, N., Chiarelli, L.R., Riccardi, G., Buroni, S., Cardona, S.T. (2018) Competitive fitness of essential gene knockdowns reveals a broad-spectrum antibacterial inhibitor of the cell division protein FtsZ. *Antimicrob Agents Chemother. 62*, e01231-18.

Høiby, N. (2002) Understanding bacterial biofilms in patients with cystic fibrosis: current and innovative approaches to potential therapies. *J Cyst Fibros. 1*, 249-254.

Holden, M.T.G., Seth-Smith, H.M.B., Crossman, L.C., Sebaihia, M., Bentley, S.D., Cerdeño-Tárraga, A.M., Thomson, N.R., Bason, N., Quail, M.A., Sharp, S., Cherevach, I., Churcher, C., Goodhead, I., Hauser, H., Holroyd, N., Mungall, K., Scott, P., Walker, D., White, B., Rose, H., Iversen, P., Mil-Homens, D., Rocha, E.P., Fialho, A.M., Baldwin, A., Dowson, C., Barrell, B.G., Govan, J.R., Vandamme, P., Hart, C.A., Mahenthiralingam, E., Parkhill, J. (2009) The genome of *Burkholderia cenocepacia* J2315, an epidemic pathogen of cystic fibrosis patients. *J Bacteriol Res. 91*, 261-277.

Iguchi, S., Mizutani, T., Hiramatsu, K., Kikuchi, K. (2016) Rapid acquisition of linezolid resistance in methicillin-resistant *Staphylococcus aureus*: role of hypermutation and homologous recombination. *PLoS One. 11*, e0155512.

Irudal, S., Scoffone, V.C., Trespidi, G., Barbieri, G., D'Amato, M., Viglio, S., Pizza, M., Scarselli, M., Riccardi, G., Buroni, S. (2023) Identification by reverse vaccinology of three virulence factors in *Burkholderia cenocepacia* that may represent ideal vaccine antigens. *Vaccines (Basel). 11*, 1039.

Jain, P.P., Degani, M.S., Raju, A., Ray, M., Rajan, M.G.R. (2013) Rational drug design based synthesis of novel arylquinolines as anti-tuberculosis agents. *Bioorganic Med Chem Lett. 23*, 6097-6105.

References

Jaiyesimi, O.A., McAvoy, A.C., Fogg, D.N., Garg, N. (2021) Metabolomic profiling of *Burkholderia cenocepacia* in synthetic cystic fibrosis sputum medium reveals nutrient environment-specific production of virulence factors. *Sci Rep*. *11*, 1-17.

Jennings, M.T., Boyle, M.P., Weaver, D., Callahan, K.A., Dasenbrook, E.C. (2014) Eradication strategy for persistent methicillin-resistant *Staphylococcus aureus* infection in individuals with cystic fibrosis-the PMEP trial: study protocol for a randomized controlled trial. *Trials*. *15*, 223.

Jiang, X., Ellabaan, M.M.H., Charusanti, P., Munck, C., Blin, K., Tong, Y., Weber, T., Sommer, M.O.A., Lee, S.Y. (2017). Dissemination of antibiotic resistance genes from antibiotic producers to pathogens. *Nat Commun. 8*, 1-7.

Jin, Y., Zhou, J., Zhou, J., Hu, M., Zhang, Q., Kong, N., Ren, H., Liang, L., Yue, J. (2020) Genome-based classification of *Burkholderia cepacia* complex provides new insight into its taxonomic status. *Biol Direct*. *15*, 1-14.

Johnson, T.M., Byrd, T.F., Drummond, W.K., Childs-Kean, L.M., Mahoney, M.V., Pearson, J.C., Rivera, C.G. (2023) Contemporary pharmacotherapies for nontuberculosis mycobacterial infections: a narrative review. *Infect Dis Ther*. *12*, 343-365.

Jones, A.M., Dodd, M.E., Govan, J.R.W., Barcus, V., Doherty, C.J., Morris, J., Webb, A.K. (2004) *Burkholderia cenocepacia* and *Burkholderia multivorans*: influence on survival in cystic fibrosis. *Thorax*. *59*, 948-951.

Jones, P., Binns, D., Chang, H.Y., Fraser, M., Li, W., McAnulla, C., McWilliam, H., Maslen, J., Mitchell, A., Nuka, G., Pesseat, S., Quinn, A.F., Sangrador-Vegas, A., Scheremetjew, M., Yong, S.Y., Lopez, R., Hunter, S. (2014) InterProScan 5: genome-scale protein function classification. *Bioinformatics. 30*, 1236-1240.

Jung, B.K., Hong, S.J., Park, G.S., Kim, M.C., Shin, J.H. (2018) Isolation of *Burkholderia cepacia* JBK9 with plant growth-promoting activity while producing pyrrolnitrin antagonistic to plant fungal diseases. *Appl Biol Chem. 61*, 173-180.

Junge, S., Görlich, D., Reijer, M. Den, Wiedemann, B., Tümmler, B., Ellemunter, H., Dübbers, A., Küster, P., Ballmann, M., Koerner-Rettberg, C., Große-Onnebrink, J., Heuer, E., Sextro, W., Mainz, J. G., Hammermann, J., Riethmüller, J., Graepler-Mainka, U.M., Staab, D., Wollschläger, B., Szczepanski, R., Schuster, A., Tegtmeyer, F.K., Sutharsan, S., Wald, A., Nofer, J.R., van Wamel, W., Becker, K., Kahl, B.C. (2016). Factors associated with worse lung function in cystic fibrosis patients with persistent *Staphylococcus aureus*. *PLoS ONE*. *11*, 1-18.

Käll, L., Krogh, A., Sonnhammer, E.L. (2004) A combined transmembrane topology and signal peptide prediction method. *J Mol Biol*, *338*, 1027-1036

Kapoor, G., Saigal, S., Elongavan, A. (2017) Action and resistance mechanisms of antibiotics: a guide for clinicians. *J Anaesthesiol Clin Pharmacol*. 33, 300-305.

Keating, D., Marigowda, G., Burr, L., Daines, C., Mall, M.A., McKone, E.F., Ramsey, B.W., Rowe, S.M., Sass, L.A., Tullis, E., McKee, C. M., Moskowitz, S.M., Robertson, S., Savage, J., Simard, C., Van Goor, F., Waltz, D., Xuan, F., Young, T., Taylor-Cousar, J.L. (2018) VX-445-Tezacaftor-Ivacaftor in patients with cystic fibrosis and one or two Phe508del alleles. *N Engl J Med. 379*, 1612-1620.

Keith, K.E., Killip, L., He, P., Moran, G.R., Valvano, M.A. (2007) *Burkholderia cenocepacia* C5424 produces a pigment with antioxidant properties using a homogentisate intermediate. *J Bacteriol. 189*, 9057-9065.

Kelley, C., Lu, S., Parhi, A., Kaul, M., Pilch, D.S., Lavoie, E.J. (2013) Antimicrobial activity of various 4- and 5-substituted 1-phenylnaphthalenes. *Eur J Med Chem*. *60*, 395-409.

Kenna, D.T.D., Lilley, D., Coward, A., Martin, K., Perry, C., Pike, R., Hill, R., Turton, J.F. (2017) Prevalence of *Burkholderia* species, including members of *Burkholderia cepacia* complex, among UK cystic and non-cystic fibrosis patients. *J Med Microbiol. 66*, 490-501.

Kerem, B., Rommens, J.M., Buchanan, J.A., Markiewicz, D., Cox, T.K., Chakravarti, A., Buchwald, M., Tsui, L.C. (1989) Identification of the cystic fibrosis gene: genetic analysis. *Science*. 245, 1073-1080.

Kiessling, A.R., Malik, A., Goldman, A. (2020) Recent advances in the understanding of trimeric autotransporter adhesins. *Med Microbiol Immunol. 209*, 233-242.

King, D.T., Sobhanifar, S., Strynadka, N.C.J. (2014) The mechanisms of resistance to β-lactam antibiotics. *Handbook of Antimicrobial Resistance*, 1-22.

Kirchner, S., Fothergill, J.L., Wright, E.A., James, C.E., Mowat, E., Winstanley, C. (2012) Use of artificial sputum medium to test antibiotic efficacy against *Pseudomonas aeruginosa* in conditions more relevant to the cystic fibrosis lung. *J Vis Exp. 64*, e3857

Knowles, M.R., Boucher, R.C. (2002) Mucus clearance as a primary innate defense mechanism for mammalian airways. *J Clin Investig. 109*, 571-577.

Kooi, C., Subsin, B., Chen, R., Pohorelic, B., Sokol, P.A. (2006) *Burkholderia cenocepacia* ZmpB is a broad-specificity zinc metalloprotease involved in virulence. *Infect Immun. 74*, 4083-4093.

Kramer-Golinkoff, E., Camacho, A., Kramer, L., Taylor-Cousar, J.L. (2022) A survey: understanding the health and perspectives of people with CF not benefiting from CFTR modulators. *Pediatr Pulmonol*. *57*, 1253-1261.

Krause, K.M., Serio, A.W., Kane, T.R., Connolly, L.E. (2016) Aminoglycosides: an overview. *Cold Spring Harb Perspect Med*. *6*, a027029, 1-18.

Kritsotakis, E.I., Lagoutari, D., Michailellis, E., Georgakakis, I., Gikas, A. (2022) Burden of multidrug and extensively drug-resistant ESKAPEE pathogens in a secondary hospital care setting in Greece. *Epidemiol Infect*. *150*, e170.

References

Krogh, A., Larsson, B., von Heijne, G., Sonnhammer, E.L. (2001) Predicting transmembrane protein topology with a hidden Markov model: application to complete genomes. *J Mol Biol. 305*, 567-580.

Król, E., Scheffers, D.J. (2013) FtsZ polymerization assays: simple protocols and considerations. *J Vis Exp. 81*, e50844.

Kugimiya, W., Otani, Y., Hashimoto, Y., Takagi, Y. (1986) Molecular cloning and nucleotide sequence of the lipase gene from *Pseudomonas fragi*. *Biochem Biophys Res Commun. 141*, 185-190.

Langton Hewer, S.C., Smyth, A.R., Brown, M., Jones, A.P., Hickey, H., Kenna, D., Ashby, D., Thompson, A., Sutton, L., Clayton, D., Arch, B., Tanajewski, Ł., Berdunov, V., Williamson, P.R. (2021) Intravenous or oral antibiotic treatment in adults and children with cystic fibrosis and *Pseudomonas aeruginosa* infection: the TORPEDO-CF RCT. *Health Technol Assess*. *25*, 1-128.

Laraya-Cuasay, L., Lipstein, M., Huang, N. (1977) *Pseudomonas cepacia* in the respiratory flora of patients with cystic fibrosis (CF). *Pediatr Res. 11*, 502.

Law, R.J., Hamlin, J.N., Sivro, A., McCorrister, S.J., Cardama, G.A., Cardona, S.T. (2008) A functional phenylacetic acid catabolic pathway is required for full pathogenicity of *Burkholderia cenocepacia* in the *Caenorhabditis elegans* host model. *J Bacteriol. 190*, 7209-7218.

Lee, J.A., Cho, A., Huang, E.N., Xu, Y., Quach, H., Hu, J., Wong, A.P. (2021) Gene therapy for cystic fibrosis: new tools for precision medicine. *J Transl Med*. *19*, 452.

Levy-Blitchtein, S., Roca, I., Plasencia-Rebata, S., Vicente-Taboada, W., Velásquez-Pomar, J., Muñoz, L., Moreno-Morales, J., Pons, M.J., Del Valle-Mendoza, J., Vila, J. (2018) Emergence and spread of carbapenem-resistant *Acinetobacter baumannii* international clones II and III in Lima, Peru. *Emerg Microbes Infect*. *7*, 119.

Levy, I., Grisaru-Soen, G., Lerner-Geva, L., Kerem, E., Blau, H., Bentur, L., Aviram, M., Rivlin, J., Picard, E., Lavy, A., Yahav, Y., Rahav, G. (2008) Multicenter cross-sectional study of nontuberculous mycobacterial infections among cystic fibrosis patients, Israel. *Emerg Infect Dis*. *14*, 378-384.

Lewis, K. (2013) Platforms for antibiotic discovery. *Nat Rev Drug Discov. 12*, 371-387.

LiPuma, J.J. (2010) The changing microbial epidemiology in cystic fibrosis. *Clin Microbiol Rev*. *23*, 299-323.

LiPuma, J.J., Mortensen, J.E., Dasen, S.E., Edlind, T.D., Schidlow, D.V., Burns, J.L., Stull, T.L. (1988) Ribotype analysis of *Pseudomonas cepacia* from cystic fibrosis treatment centers. *J Pediatr*. *113*, 859-862.

LiPuma, J.J., Spilker, T., Coenye, T., Gonzalez, C.F. (2002) An epidemic *Burkholderia cepacia* complex strain identified in soil. *Lancet*. *359*, 2002-2003.

Liu, H., Ibrahim, M., Qiu, H., Kausar, S., Ilyas, M., Cui, Z., Hussain, A., Li, B., Waheed, A., Zhu, B., Xie, G. (2015) Protein profiling analyses of the outer membrane of *Burkholderia cenocepacia* reveal a niche-specific proteome. *Microb Ecol. 69*, 75–83.

Loose, M., Mitchison, T.J. (2014) The bacterial cell division proteins FtsA and FtsZ self-organize into dynamic cytoskeletal patterns. *Nat Cell Biol*. *16*, 38-46.

Lopes-Pacheco, M. (2020) CFTR modulators: the changing face of cystic fibrosis in the era of precision medicine. *Front Pharmacol*. *10*, 1-29.

Lord, R., Jones, A.M., Horsley, A. (2020) Antibiotic treatment for *Burkholderia cepacia* complex in people with cystic fibrosis experiencing a pulmonary exacerbation. *Cochrane Database Syst Rev*. *4,* CD009529.

Loutet, S.A., Flannagan, R.S., Kooi, C., Sokol, P.A., Valvano, M.A. (2006) A complete lipopolysaccharide inner core oligosaccharide is required for resistance of *Burkholderia cenocepacia* to antimicrobial peptides and bacterial survival in vivo. *J Bacteriol. 188*, 2073-2080.

Loutet, S.A., Valvano, M.A. (2010) A decade of *Burkholderia cenocepacia* virulence determinant research. *Infect Immun*. *78*, 4088-4100.

Mahenthiralingam, E., Campbell, M.E., Henry, D.A., Speert, D.P. (1996) Epidemiology of *Burkholderia cepacia* infection in patients with cystic fibrosis: analysis by randomly amplified polymorphic DNA fingerprinting. *J Clin Microbiol*. *34*, 2914-2920.

Mahenthiralingam, E., Urban, T.A., Goldberg, J.B. (2005) The multifarious, multireplicon *Burkholderia cepacia* complex. *Nat Rev Microbiol. 3*, 144-156.

Maia, E.H.B, Assis, L.C., de Oliveira, T.A., da Silva, A.M., Taranto, A.G. (2020) Structure-based virtual screening: from classical to artificial intelligence. *Front Chem. 8*, 343.

Maione, D., Margarit, I., Rinaudo, C.D., Masignani, V., Mora, M., Scarselli, M., Tettelin, H., Brettoni, C., Iacobini, E.T., Rosini, R., D'Agostino, N., Miorin, L., Buccato, S., Mariani, M., Galli, G., Nogarotto, R., Nardi-Dei, V., Vegni, F., Fraser, C., Mancuso, G., Teti, G., Madoff, L.C., Paoletti, L.C., Rappuoli, R., Kasper, D.L., Telford, J.L., Grandi, G. (2005) Identification of a universal Group B *Streptococcus* vaccine by multiple genome screen. *Science*. *309*, 148-150.

Makarov, V., Riabova, O.B., Yuschenko, A., Urlyapova, N., Daudova, A., Zipfel, P.F., Möllmann, U. (2006) Synthesis and antileprosy activity of some dialkyl-dithiocarbamates. *J Antimicrob Chemother*. *57*, 1134-1138.

Makidon, P.E., Knowlton, J., Groom, J.V. 2nd, Blanco, L.P., LiPuma, J.J., Bielinska, A.U., Baker, J.R.Jr. (2010) Induction of immune response to the 17 kDa OMPA *Burkholderia cenocepacia* polypeptide and protection against pulmonary infection in mice after nasal vaccination with an OMP nanoemulsion-based vaccine. *Med Microbiol Immunol*. *199*, 81-92.

References

Malott, R.J., O'Grady, E.P., Toller, J., Inhülsen, S., Eberl, L., Sokol, P.A. (2009) A *Burkholderia cenocepacia* orphan LuxR homolog is involved in quorum-sensing regulation. *J Bacteriol*. *191*, 2447-2460.

Mankovich, A.G., Maciel, K., Kavanaugh, M., Kistler, E., Muckle, E., Weingart, C.L. (2023) Phage-antibiotic synergy reduces *Burkholderia cenocepacia* population. *BMC Microbiol. 23*, 1-12.

Martina, P., Leguizamon, M., Prieto, C.I., Sousa, S.A., Montanaro, P., Draghi, W.O., Stämmler, M., Bettiol, M., de Carvalho, C.C.C.R., Palau, J., Figoli, C., Alvarez, F., Benetti, S., Lejona, S., Vescina, C., Ferreras, J., Lasch, P., Lagares, A., Zorreguieta, A., Leitão, J.H., Yantorno, O.M., Bosch, A. (2018) *Burkholderia puraquae* sp. nov., a novel species of the *Burkholderia cepacia* complex isolated from hospital settings and agricultural soils. *Int J Syst Evol Microbiol*. *68*, 14-20.

Martin, A., Takiff, H., Vandamme, P., Swings, J., Palomino, J.C., Portaels, F. (2006) A new rapid and simple colorimetric method to detect pyrazinamide resistance in *Mycobacterium tuberculosis* using nicotinamide. *J Antimicrob Chemother. 58*, 327–331.

Martinotti, S, Ranzato, E. (2016) 2-DE Gel analysis: the spot detection. *Methods Mol Biol*. *1384*, 155-164.

Marzhoseyni, Z., Mousavi, M.J., Saffari, M., Ghotloo, S. (2023) Immune escape strategies of *Pseudomonas aeruginosa* to establish chronic infection. *Cytokine*. *163*, 156135.

Masignani, V., Pizza, M., Moxon, E.R. (2019) The development of a vaccine against meningococcus B using reverse vaccinology. *Front Immunol. 10*, 751.

Mathew, B., Hobrath, J.V., Ross, L., Connelly, M.C., Lofton, H., Rajagopalan, M., Guy, R.K., Reynolds, R.C. (2016) Screening and development of new inhibitors of FtsZ from *M. tuberculosis*. *PLoS One*. *11*, e0164100.

Matsui, T., Yamane, J., Mogi, N., Yamaguchi, H., Takemoto, H., Yao, M., Tanaka, I. (2012) Structural reorganization of the bacterial cell-division protein FtsZ from *Staphylococcus aureus*. *Acta Crystallogr D Biol Crystallogr*. *68*, 1175-1188.

Maura, D., Ballok, A.E., Rahme, L.G. (2016) Considerations and caveats in anti-virulence drug development. *Curr Opin Microbiol*. *33*, 41-46.

Mayer-Hamblett, N., Kloster, M., Rosenfeld, M., Gibson, R. L., Retsch-Bogart, G.Z., Emerson, J., Thompson, V., Ramsey, B.W. (2015) Impact of sustained eradication of new *Pseudomonas aeruginosa* infection on long-term outcomes in cystic fibrosis. *Clin Infect Dis*. *61*, 707-715.

McClean, S., Healy, M.E., Collins, C., Carberry, S., O'Shaughnessy, L., Dennehy, R., Adams, Á., Kennelly, H., Corbett, J.M., Carty, F., Cahill, L.A., Callaghan, M., English, K., Mahon, B.P., Doyle, S., Shinoy, M. (2016) Linocin and OmpW are involved in attachment of the cystic fibrosis-associated pathogen *Burkholderia cepacia* complex to lung epithelial cells and protect mice against infection. *Infect Immun*. *84*, 1424-1437.

Medina-Pascual, M.J., Valdezate, S., Villalón, P., Garrido, N., Rubio, V., Saéz-Nieto, J.A. (2012) Identification, molecular characterisation and antimicrobial susceptibility of genomovars of the *Burkholderia cepacia* complex in Spain. *Eur J Clin Microbiol Infect Dis. 31*, 3385-3396.

Ménard, G., Rouillon, A., Ghukasyan, G., Emily, M., Felden, B., Donnio, P.Y. (2021) *Galleria mellonella* larvae as an infection model to investigate sRNA-mediated pathogenesis in *Staphylococcus aureus*. *Front Cell Infect Microbiol*. 11, 631710.

Mil-Homens, D., Fialho, A.M. (2012) A BCAM0223 mutant of *Burkholderia cenocepacia* is deficient in hemagglutination, serum resistance, adhesion to epithelial cells and virulence. *PLoS One. 7*, e41747.

Mil-Homens, D., Leça, M.I., Fernandes, F., Pinto, S.N., Fialho, A.M. (2014) Characterization of BCAM0224, a multifunctional trimeric autotransporter from the human pathogen *Burkholderia cenocepacia*. *J Bacteriol. 196*, 1968-1979.

Mil-Homens, D., Pinto, S.N., Matos, R.G., Arraiano, C., Fialho, A.M. (2017) *Burkholderia cenocepacia* K56-2 trimeric autotransporter adhesin BcaA binds TNFR1 and contributes to induce airway inflammation. *Cell Microbiol*. 19.

Miller, W.R., Bayer, A.S., Arias, C.A. (2016) Mechanism of action and resistance to daptomycin in *Staphylococcus aureus* and enterococci. *Cold Spring Har*b. *6*, 1-16.

Mitri, C., Xu, Z., Bardin, P., Corvol, H., Touqui, L., Tabary, O. (2020) Novel anti-inflammatory approaches for cystic fibrosis lung disease: identification of molecular targets and design of innovative therapies. *Front Pharmacol*. *11*, 1-25.

Mogayzel, P.J., Naureckas, E.T., Robinson, K.A., Brady, C., Guill, M., Lahiri, T., Lubsch, L., Matsui, J., Oermann, C.M., Ratjen, F., Rosenfeld, M., Simon, R.H., Hazle, L., Sabadosa, K., Marshall, B.C., Mueller, G., Hadjiliadis, D., Hoag, J.B. (2014) Cystic fibrosis foundation pulmonary guideline pharmacologic approaches to prevention and eradication of initial *Pseudomonas aeruginosa* infection. *Ann Am Thorac Soc. 11*, 1640-1650.

Mohapatra, S.S., Dwibedy, S.K., Padhy, I. (2021) Polymyxins, the last-resort antibiotics: mode of action, resistance emergence, and potential solutions. *J Biosci*. *46*, 85.

Mohd-Asri, N.A., Ahmad, S., Mohamud, R., Mohd Hanafi, N., Mohd Zaidi, N.F., Irekeola, A.A., Shueb, R.H., Yee, L.C., Mohd-Noor, N., Mustafa, F.H., Yean, C.Y., Yusof, N.Y. (2021) Global prevalence of nosocomial multidrug-resistant *Klebsiella pneumoniae*: a systematic review and meta-analysis. *Antibiotics (Basel). 10*, 1508.

Moriel, D.G., Bertoldi, I., Spagnuolo, A., Marchi, S., Rosini, R., Nesta, B., Pastorello, I., Corea, V.A., Torricelli, G., Cartocci, E., Savino, S., Scarselli, M., Dobrindt, U., Hacker, J., Tettelin, H., Tallon, L.J., Sullivan, S., Wieler, L.H., Ewers, C., Pickard, D., Dougan, G., Fontana, M.R., Rappuoli, R., Pizza, M., Serino, L. (2010) Identification of protective and broadly conserved vaccine antigens from the genome of extraintestinal pathogenic *Escherichia coli*. *Proc Natl Acad Sci USA. 107*, 9072-9077.

References

Moser, C., Jensen, P.O., Kobayashi, O., Hougen, H.P., Song, Z., Rygaard, J., Kharazmi, A., N. Hoibi. (2002) Improved outcome of chronic *Pseudomonas aeruginosa* lung infection is associated with induction of a Th1-dominated cytokine response. *Clin Exp Immunol*. *127*, 206-213.

Mulani, M.S., Kamble, E.E., Kumkar, S.N., Tawre, M.S., Pardesi, K.R. (2019) Emerging strategies to combat ESKAPE pathogens in the era of antimicrobial resistance: a review. *Front Microbiol*. *10*, 539.

Mullen, T., Markey, K., Murphy, P., McClean, S., Callaghan, M. (2007) Role of lipase in *Burkholderia cepacia* complex (Bcc) invasion of lung epithelial cells. *Eur J Clin Microbiol Infect Dis*. *26*, 869-877.

Murphy, M.P., Caraher, E. (2015) Residence in biofilms allows *Burkholderia cepacia* complex (Bcc) bacteria to evade the antimicrobial activities of neutrophil-like dHL60 cells. *Pathog Dis. 73*, ftv069.

Murray, S., Charbeneau, J., Marshall, B.C., LiPuma, J.J. (2008) Impact of *Burkholderia* infection on lung transplantation in cystic fibrosis. *Am J Respir Crit Care Med. 17*, 363-371.

Nickzad A., Lépine F., Déziel E. (2015) Quorum Sensing Controls Swarming Motility of *Burkholderia glumae* through regulation of rhamnolipids. *PLoS One*. *10*, e0128509.

Nierhaus, T., McLaughlin, S.H., Bürmann, F., Kureisaite-Ciziene, D., Maslen, S.L., Skehel, J.M., Yu, C.W.H., Freund, S.M.V., Funke, L.F.H., Chin, J.W., Löwe, J. (2022) Bacterial divisome protein FtsA forms curved antiparallel double filaments when binding to FtsN. *Nat Microbiol*. *7*, 1686-1701.

Nikaido, H., Takatsuka, Y. (2009) Mechanisms of RND multidrug efflux pumps. *Biochim Biophys Acta*. *1794*, 769-781.

Nosanchuk, J.D., Casadevall, A. (2006) Impact of melanin on microbial virulence and clinical resistance to antimicrobial compounds. *Antimicrob Agents Chemother*. *50*, 3519-3528.

Nye, C., Duckers, J., Dhillon, R. (2022) Cefiderocol to manage chronic, multi-drug-resistant Burk*holderia cepacia* complex infection in a patient with cystic fibrosis: a case report. *Access Microbiol*. *4*, acmi000413.

O'Grady, E.P., Viteri, D.F., Malott, R.J., Sokol, P.A. (2009) Reciprocal regulation by the CepIR and CciIR quorum sensing systems in *Burkholderia cenocepacia*. *BMC Genom. 10*, 441.

Ong, K.S., Aw, Y.K., Lee, L.H., Yule, C.M., Cheow, Y.L., Lee, S.M. (2016) *Burkholderia paludis* sp. nov., an antibiotic-siderophore producing novel *Burkholderia cepacia* complex species, isolated from Malaysian tropical peat swamp soil. *Front Microbiol*. *7*, 2046.

Oster, P., Lennon, D., O'Hallahan, J., Mulholland, K., Reid, S., Martin, D. (2005) MeNZB: a safe and highly immunogenic tailor-made vaccine against the New Zealand *Neisseria meningitidis* serogroup B disease epidemic strain. *Vaccine*. *23*, 2191-2196.

Papadopoulos, A., Busch, M., Reiners, J., Hachani, E., Baeumers, M., Berger, J., Schmitt, L., Jaeger, K.E., Kovacic, F.., Smits, S.H.J., Kedrov, A. (2022) The periplasmic chaperone Skp prevents misfolding of the secretory lipase A from *Pseudomonas aeruginosa*. *Front Mol Biosci. 9,* 1026724.

Papaleo, M.C., Perrin, E., Maida, I., Fondi, M., Fani, R., Vandamme, P. (2010) Identification of species of the *Burkholderia cepacia* complex by sequence analysis of the *hisA* gene. *J Med Microbiol*. *59*, 1163-1170.

Parkins, M.D., Somayaji, R., Waters, V.J. (2018) Epidemiology, biology, and impact of clonal *Pseudomonas aeruginosa* infections in cystic fibrosis. *Clin Microbiol Rev*. *31*, 1-38.

Peeters, C., Zlosnik, J.E.A., Spilker, T., Hird, T.J., LiPuma, J.J., Vandamme, P. (2013) *Burkholderia pseudomultivorans* sp. nov., a novel *Burkholderia cepacia* complex species from human respiratory samples and the rhizosphere. *Syst Appl Microbiol*. *36*, 483-489.

Peleg, A.Y., Seifert, H., Paterson, D.L. (2008) *Acinetobacter baumannii*: emergence of a successful pathogen. *Clin Microbiol Rev. 21*, 538-582.

Pereira, T.C., de Barros, P.P., Fugisaki, L.R.O., Rossoni, R.D., Ribeiro, F.C., de Menezes, R.T., Junqueira, J.C., Scorzoni, L. (2018) Recent advances in the use of *Galleria mellonella* model to study immune responses against human pathogens. *J Fungi (Basel). 4*. 128.

Pilapitiya, D.H., Harris, P.W.R., Hanson-Manful, P., McGregor, R., Kowalczyk, R., Raynes, J.M., Carlton, L.H., Dobson, R.C.J., Baker, M.G., Brimble, M., Lukomski, S., Moreland, N.J. (2021) Antibody responses to collagen peptides and streptococcal collagen-like 1 proteins in acute rheumatic fever patients. *Pathog Dis.79*, ftab033.

Pimenta, A.I., Bernardes, N., Alves, M.M., Mil-Homens, D., Fialho, A.M. (2021a) *Burkholderia cenocepacia* transcriptome during the early contacts with giant plasma membrane vesicles derived from live bronchial epithelial cells. *Sci Rep*. *11*, 1-16.

Pimenta, A.I., Kilcoyne, M., Bernardes, N., Mil-Homens, D., Joshi, L., Fialho, A.M. (2021b) *Burkholderia cenocepacia* BCAM2418-induced antibody inhibits bacterial adhesion, confers protection to infection and enables identification of host glycans as adhesin targets. *Cell Microbiol*. *23*, e13340.

Piochon, M., Coulon, P.M. L., Caulet, A., Groleau, M.C., Déziel, E., Gauthier, C. (2020) Synthesis and antimicrobial activity of *Burkholderia*-related 4-Hydroxy-3-methyl-2-alkenylquinolines (HMAQs) and their N-Oxide counterparts. *J Nat Prod. 83*, 2145-2154.

Pizza, M., Scarlato, V., Masignani, V., Giuliani, M.M., Aricò, B., Comanducci, M., Jennings, G.T., Baldi, L., Bartolini, E., Capecchi, B., Galeotti, C.L., Luzzi, E., Manetti, R., Marchetti, E., Mora, M., Nuti, S., Ratti, G., Santini, L., Savino, S., Scarselli, M., Storni, E., Zuo, P., Broeker, M., Hundt, E., Knapp, B., Blair, E., Mason, T., Tettelin, H., Hood, D.W., Jeffries, A.C., Saunders, N.J., Granoff, D.M., Venter, J.C., Moxon, E.R., Grandi, G., Rappuoli, R. (2000) Identification of vaccine candidates against serogroup B meningococcus by whole-genome sequencing. *Science*. *287*, 1816-1820.

References

Pompilio, A., Scribano, D., Sarshar, M., Di Bonaventura, G., Palamara, A.T., Ambrosi, C. (2021) Gram-negative bacteria holding together in a biofilm: the *Acinetobacter baumannii* way. *Microorganisms*. *9*, 1353.

Powers, J.H. (2004) Antimicrobial drug development - The past, the present, and the future. *Clin Microbiol Infect Supplement*. *10*, 23-31.

Pradenas, G.A., Myers, J.N., Torres, A.G. (2017) Characterization of the *Burkholderia cenocepacia* TonB mutant as a potential live Attenuated vaccine. *Vaccines (Basel). 5*, 33.

Pradhan, P., Margolin, W., Beuria, T.K. (2021) Targeting the Achilles heel of FtsZ: The Interdomain cleft. *Front Microbiol*. *12*, 732796.

Prasad, P., Sun, J., Danner, R.L., Natanson, C. (2012) Excess deaths associated with tigecycline after approval based on noninferiority trials. *Clin Infect Dis*. *54*, 1699-1709.

Pritt, B., O'Brien, L., Winn, W. (2007) Mucoid *Pseudomonas* in cystic fibrosis. *Am J Clin Pathol. 128*, 32-34.

Putra, L., Natadiputri, G., Meryandini, A., Suwanto, A. (2019) Isolation, cloning and co-expression of lipase and foldase genes of *Burkholderia territorii* GP3 from mount Papandayan soil. *J Microbiol Biotechnol. 29*, 944-951.

Qiu, Y., Zhou, L., Hu, Y., Bao, Y. (2019) Discovery of promising FtsZ inhibitors by E-pharmacophore, 3D-QSAR, molecular docking study, and molecular dynamics simulation. *J Recept Signal Transduct Res*. *39*, 154-166.

Rappuoli, R. (2000) Reverse vaccinology. *Curr Opin Microbiol*. *3*, 445-450.

Rasmussen, M., Jacobsson, M., Björck, L. (2003) Genome-based identification and analysis of collagen-related structural motifs in bacterial and viral proteins. *J Biol Chem. 278*, 32313-32316.

Recio, R., Brañas, P., Martínez, M.T., Chaves, F., Orellana, M.A. (2018) Effect of respiratory *Achromobacter* spp. infection on pulmonary function in patients with cystic fibrosis. *J Med Microbiol. 67*, 952-956.

Rex, J.H., Outterson, K. (2016). Antibiotic reimbursement in a model delinked from sales: a benchmark-based worldwide approach. *Lancet Infect Dis*. *16*, 500-505.

Rhodes, K.A., Schweizer, H.P. (2016) Antibiotic resistance in *Burkholderia* species. *Drug Resist Updat*. *28*, 82-90.

Riordan, J.R., Rommens, J.M., Kerem, B., Alon, N., Rozmahel, R., Grzelczak, Z., Zielenski, J., Lok, S., Plavsic, N., Chou, J.L., Drum, M.L., Iannuzzi, M.C., Collins, F.S., Tsui, L. (1989) Identification of the cystic fibrosis gene: cloning and characterization of complementary DNA. *Science*. *245*, 1066-1073.

Riwu, K.H.P., Effendi, M.H., Rantam, F.A., Khairullah, A.R., Widodo, A. (2022) A review: virulence factors of *Klebsiella pneumonia* as emerging infection on the food chain. *Vet World*. *15*, 2172-2179.

Roesch, E.A., Nichols, D.P., Chmiel, J.F. (2018) Inflammation in cystic fibrosis: an update. *Pediatr Pulmonol*. *53*, S30-S50.

Román, F., Cantón, R., Pérez-Vázquez, M., Baquero, F., Campos, J. (2004) Dynamics of long-term colonization of respiratory tract by *Haemophilus influenzae* in cystic fibrosis patients shows a marked increase in hypermutable strains. *J Clin Microbiol. 42*, 1450-1459.

Rosales-Reyes, R., Aubert, D.F., Tolman, J.S., Amer, A.O., Valvano, M.A. (2012) *Burkholderia cenocepacia* Type VI Secretion System mediates escape of Type II secreted proteins into the cytoplasm of infected macrophages. *PLoS ONE. 7*, e41726.

Rosenau, F., Isenhardt, S., Gdynia, A., Tielker, D., Schmidt, E., Tielen, P., Schobert, M., Jahn, D., Wilhelm, S., Jaeger, K.E. (2010) Lipase LipC affects motility, biofilm formation and rhamnolipid production in *Pseudomonas aeruginosa*. *FEMS Microbiol Lett*. *309*, 25-34.

Rowe, S.M., Daines, C., Ringshausen, F.C., Kerem, E., Wilson, J., Tullis, E., Nair, N., Simard, C., Han, L., Ingenito, E.P., McKee, C., Lekstrom-Himes, J., Davies, J.C. (2017) Tezacaftor-Ivacaftor in residual-function heterozygotes with cystic fibrosis. *N Engl J Med. 377*, 2024-2035.

Rumpf, C., Lange, J., Schwartbeck, B., Kahl, B.C. (2021) *Staphylococcus aureus* and cystic fibrosis—a close relationship. What can we learn from sequencing studies? *Pathogens*. *10*, 1177.

Sajjan, S.U., Carmody, L.A., Gonzalez, C.F., LiPuma, J.J. (2008) A type IV secretion system contributes to intracellular survival and replication of *Burkholderia cenocepacia*. *Infect Immunity*. *76*, 5447-5455.

Sanivarapu, R.R., Gibson, J. (2023) Aspiration pneumonia. *StatPearls publishing.*

Santana-Molina, C., Del Saz-Navarro, D., Devos, D.P. (2023) Early origin and evolution of the FtsZ/tubulin protein family. *Front Microbiol*. 13, 1100249.

Sass, A., Marchbank, A., Tullis, E., LiPuma, J.J., Mahenthiralingam, E. (2011) Spontaneous and evolutionary changes in the antibiotic resistance of *Burkholderia cenocepacia* observed by global gene expression analysis. *BMC Genom*. *12*, 373.

Sass, P., Brötz-Oesterhelt, H. (2013) Bacterial cell division as a target for new antibiotics. *Curr Opin Microbiol*. *16*, 522-530.

Schmid, N., Suppiger, A., Steiner, E., Pessi, G., Kaever, V., Fazli, M., Tolker-Nielsen, T., Jenal, U., Eberl, L. (2017) High intracellular c-di-GMP levels antagonize quorum sensing and virulence gene expression in *Burkholderia cenocepacia* H111. *Microbiology (United Kingdom)*. *163*, 754-764.

References

Scoffone, V.C., Chiarelli, L.R., Makarov, V., Brackman, G., Israyilova, A., Azzalin, A., Forneris, F., Riabova, O., Savina, S., Coenye, T., Riccardi, G., Buroni, S. (2016) Discovery of new diketopiperazines inhibiting *Burkholderia cenocepacia* quorum sensing *in vitro* and *in vivo*. *Sci Rep. 6*, 1-11.

Scotet, V., L'Hostis, C., Férec, C. (2020) The changing epidemiology of cystic fibrosis: Incidence, survival and impact of the *CFTR* gene discovery. *Genes*. *11*, 589.

Seed, K.D., Dennis, J.J. (2008) Development of *Galleria mellonella* as an alternative infection model for the *Burkholderia cepacia* complex. *Infect Immun. 76*, 1267-1275.

Seib, K.L., Zhao, X., Rappuoli, R. (2012) Developing vaccines in the era of genomics: a decade of reverse vaccinology. *Clin Microbiol Infect. 18*, 109-116.

Seixas, A.M.M., Sousa, S.A., Feliciano, J.R., Gomes, S.C., Ferreira, M.R., Moreira, L.M., Leitão, J.H. (2021) A polyclonal antibody raised against the *Burkholderia cenocepacia* OmpA-like protein BCAL2645 impairs the bacterium adhesion and invasion of human epithelial cells *in vitro*. *Biomedicines. 29*, 9, 1788.

Shelenkov, A., Akimkin, V., Mikhaylova, Y. (2023) International clones of high risk of *Acinetobacter baumannii*-Definitions, history, properties and perspectives. *Microorganisms*. *11*, 2115.

Silverman, S.M., Moses, J.E., Sharpless, K.B. (2017) Reengineering antibiotics to combat bacterial resistance: click chemistry [1,2,3]-triazole vancomycin dimers with potent activity against MRSA and VRE. *Chem. 1*, 23, 79-83.

Sköld, O.E., Swedberg, G. (2017). Sulfonamides and trimethoprim. In: Mayers, D., Sobel, J., Ouellette, M., Kaye, K., Marchaim, D. (eds) Antimicrobial Drug Resistance. *Springer, Cham*.

Sousa, S.A., Morad, M., Feliciano, J.R., Pita, T., Nady, S., El-Hennamy, R.E., Abdel-Rahman, M., Cavaco, J., Pereira, L., Barreto, C., Leitão, J.H. (2016) The *Burkholderia cenocepacia* OmpA-like protein BCAL2958: identification, characterization, and detection of anti-BCAL2958 antibodies in serum from *B. cepacia* complex-infected cystic fibrosis patients. *AMB Express*. *6*, 41.

Sousa, S.A., Seixas, A.M.M., Mandal, M., Rodríguez-Ortega, M.J., Leitão, J.H. (2020a) Characterization of the *Burkholderia cenocepacia* J2315 surface-exposed immunoproteome. *Vaccines (Basel). 8*, 509.

Sousa, S.A., Soares-Castro, P., Seixas, A.M.M., Feliciano, J.R., Balugas, B., Barreto, C., Pereira, L., Santos, P.M., Leitão, J.H. (2020b) New insights into the immunoproteome of *B. cenocepacia* J2315 using serum samples from cystic fibrosis patients. *N Biotechnol*. *54*, 62-70.

Straus, D.C., Lonon, M.K., Hutson, J.C. (1992) Inhibition of rat alveolar macrophage phagocytic function by a *Pseudomonas cepacia* lipase. *J Med Microbiol. 37*, 335-340.

Sun, D., Jeannot, K., Xiao, Y., Knapp, C.W. (2019) Editorial: horizontal gene transfer mediated bacterial antibiotic resistance. *Front Microbiol*. *27*, 1933.

Sunman, B., Emiralioglu, N., Hazirolan, G., Ademhan Tural, D., Ozsezen, B., Nayir Buyuksahin, H., Guzelkas, I., Yalcin, E., Dogru, D., Özçelik, U., Kiper, N. (2022) Impact of *Achromobacter* spp. isolation on clinical outcomes in children with cystic fibrosis. *Pediatr Pulmonol*. *57*, 658-666.

Sun, N., Chan, F.Y., Lu, Y.J., Neves, M.A., Lui, H.K., Wang, Y., Chow, K.Y., Chan, K.F., Yan, S.C., Leung, Y.C., Abagyan, R., Chan, T.H., Wong, K.Y. (2014) Rational design of berberine-based FtsZ inhibitors with broad-spectrum antibacterial activity. *PLoS One*. *139*, e97514.

Tavares, M., Kozak, M., Balola, A., Sá-Correia, I. (2020) *Burkholderia cepacia* complex bacteria: a feared contamination risk in water-based pharmaceutical products. *Clin Microbiol Rev. 33*, 1-25.

Tetart, M., Wallet, F., Kyheng, M., Leroy, S., Perez, T., Le Rouzic, O., Wallaert, B., Prevotat, A. (2019) Impact of *Achromobacter xylosoxidans* isolation on the respiratory function of adult patients with cystic fibrosis. *ERJ Open Res. 5,* 00051.

Thibau, A., Dichter, A.A., Vaca, D.J., Linke, D., Goldman, A., Kempf, V.A.J. (2020) Immunogenicity of trimeric autotransporter adhesins and their potential as vaccine targets. *Med Microbiol Immunol*. *209*, 243-263.

Thiolas, A., Bollet, C., La Scola, B., Raoult, D., Pagès, J.M. (2005) Successive emergence of *Enterobacter aerogenes* strains resistant to imipenem and colistin in a patient. *Antimicrob Agents Chemother*. *49*, 1354-1358.

Thornton, C.S., Parkins, M.D. (2023) Microbial epidemiology of the cystic fibrosis airways: past, present, and future. *Semin Respir Crit Care Med. 44*, 269-286.

Tielen, P., Kuhn, H., Rosenau, F., Jaeger, K.E., Flemming, H.C., Wingender, J. (2013) Interaction between extracellular lipase LipA and the polysaccharide alginate of *Pseudomonas aeruginosa*. *BMC Microbiol. 13*, 159.

Toyofuku, M., Schild, S., Kaparakis-Liaskos, M., Eberl, L. (2023) Composition and functions of bacterial membrane vesicles. *Nat Rev Microbiol*. *21*, 415-430.

Treggiari, M.M., Retsch-Bogart, G., Mayer-Hamblett, N., Khan, U., Kulich, M., Kronmal, R., Williams, J., Hiatt, P., Gibson, R.L., Spencer, T., Orenstein, D., Chatfield, B.A., Froh, D.K., Burns, J.L., Rosenfeld, M., Ramsey, B.W. (2011) Comparative efficacy and safety of 4 randomized regimens to treat early *Pseudomonas aeruginosa* infection in children with cystic fibrosis. *Arch Pediatr Adolesc Med. 165*, 847-856.

Trespidi, G., Scoffone, V.C., Barbieri, G., Marchesini, F., Abualsha'ar, A., Coenye, T., Ungaro, F., Makarov, V., Migliavacca, R., De Rossi, E., Buroni, S. (2021) Antistaphylococcal activity of the FtsZ inhibitor C109. *Pathogens*. *10*, 886.

Tripathy, S., Sahu, S.K. (2019) FtsZ inhibitors as a new genera of antibacterial agents. *Bioorg Chem. 91*, 103169.

References

Tsai, C.J., Loh, J.M., Proft, T. (2016) *Galleria mellonella* infection models for the study of bacterial diseases and for antimicrobial drug testing. *Virulence. 7*, 214-229.

Tullis, D.E., Burns, J.L., Retsch-Bogart, G.Z., Bresnik, M., Henig, N.R., Lewis, S.A., LiPuma, J.J. (2014). Inhaled aztreonam for chronic *Burkholderia* infection in cystic fibrosis: a placebo-controlled trial. *J Cyst Fibros*. *13*, 296-305.

Tusnády, G.E., Simon, I. (2001) The HMMTOP transmembrane topology prediction server. *Bioinformatics. 17*, 849-850.

Van Acker, H., Sass, A., Dhondt, I., Nelis, H J., Coenye, T. (2014) Involvement of toxin-antitoxin modules in *Burkholderia cenocepacia* biofilm persistence. *Pathog Dis*. *71*, 326-335.

Vandamme, P., Henry, D., Coenye, T., Nzula, S., Vancanneyt, M., LiPuma, J.J., Speert, D.P., Govan, J.R., Mahenthiralingam, E. (2002) *Burkholderia anthina* sp. nov. and *Burkholderia pyrrocinia*, two additional *Burkholderia cepacia* complex bacteria, may confound results of new molecular diagnostic tools. *FEMS Immunol Med Microbiol*. *33*, 143-149.

Vandamme, P., Holmes, B., Coenye, T., Goris, J., Mahenthiralingam, E., LiPuma, J.J., Govan, J.R. (2003) *Burkholderia cenocepacia* sp. nov.-a new twist to an old story. *Res Microbiol*. *154*, 91-96.

Vandamme, P., Mahenthiralingam, E., Holmes, B., Coenye, T., Hoste, B., De Vos, P., Henry, D., Speert, D.P. (2000) Identification and population structure of *Burkholderia stabilis* sp. nov. (formerly *Burkholderia cepacia* genomovar IV). *J Clin Microbiol. 38*, 1042-1047.

Vandamme, P., Revets, H., Gent, U., Brussel, V.U., Ziekenhuis, A., Public, C., Kingdom, U. (1997) Occurrence of multiple genomovars of *Burkholderia cepacia* in cystic fibrosis patients and proposal of *Burkholderia multivorans* sp. nov. *Int J Syst Bacteriol*. *1*, 1188-1200.

Vandecandelaere, I., Van Acker, H., Coenye, T. (2016) A Microplate-Based System as In Vitro Model of Biofilm Growth and Quantification. *Methods Mol Biol*. *1333*, 53–66.

Vanlaere, E., Baldwin, A., Gevers, D., Henry, D., De Brandt, E., LiPuma, J.J., Mahenthiralingam, E., Speert, D.P., Dowson, C., Vandamme, P. (2009) Taxon K, a complex within the *Burkholderia cepacia* complex, comprises at least two novel species, *Burkholderia contaminans* sp. nov. and *Burkholderia lata* sp. nov. *Int J Syst Evol Microbiol*. *59*, 102-111.

Vanlaere, E., Lipuma, J.J., Baldwin, A., Henry, D., De Brandt, E., Mahenthiralingam, E., Speert, D., Dowson, C., Vandamme, P. (2008) *Burkholderia latens* sp. nov., *Burkholderia diffusa* sp. nov., *Burkholderia arboris* sp. nov., *Burkholderia seminalis* sp. nov. and *Burkholderia metallica* sp. nov., novel species within the *Burkholderia cepacia* complex. *Int J Syst Evol Microbiol*. *58*, 1580-1590.

Varrassi, G., Pergolizzi, J.V., Dowling, P., Paladini, A. (2020) Ibuprofen safety at the golden anniversary: are all NSAIDs the same? A narrative review. *Adv Ther. 37*, 61-82.

Vázquez-Laslop, N., Mankin, A.S. (2018) How macrolide antibiotics work. *Trends Biochem Sci*. *43*, 668-684.

Vemula, D., Maddi, D.R., Bhandari, V. (2023) Homology modeling, virtual screening, molecular docking, and dynamics studies for discovering *Staphylococcus epidermidis* FtsZ inhibitors. *Front Mol Biosci. 3*, 1087676.

Ventola, C.L. (2015) The antibiotic resistance crisis: part 1: causes and threats. *P T. 40*, 277-83.

Vermis, K., Coenye, T., LiPuma, J.J., Mahenthiralingam, E., Nelis, H.J., Vandamme, P. (2004) Proposal to accommodate *Burkholderia cepacia* genomovar VI as *Burkholderia dolosa* sp. nov. *Int J Syst Evol Microbiol*. *54*, 689-691.

Vesikari, T., Esposito, S., Prymula, R., Ypma, E., Kohl, I., Toneatto, D., Dull, P., Kimura, A., EU Meningococcal B Infant Vaccine Study group. (2013) Immunogenicity and safety of an investigational multicomponent, recombinant, meningococcal serogroup B vaccine (4CMenB) administered concomitantly with routine infant and child vaccinations: results of two randomised trials. *Lancet*. *381*, 825-835.

Visca, P., Pisa, F., Imperi, F. (2019) The antimetabolite 3-bromopyruvate selectively inhibits *Staphylococcus aureus*. *Int J Antimicrob Agents*. *53*, 449-455.

Visser, M.B., Majumdar, S., Hani, E., Sokol, P.A. (2004) Importance of the ornibactin and pyochelin siderophore transport systems in *Burkholderia cenocepacia* lung infections. *Infect Immun. 72*, 2850-2857.

Waglechner, N., Wright, G.D. (2017) Antibiotic resistance: It's bad, but why isn't it worse? *BMC Biol. 15*, 1-8.

Wainwright, C.E., Elborn, J.S., Ramsey, B.W., Marigowda, G., Huang, X., Cipolli, M., Colombo, C., Davies, J.C., De Boeck, K., Flume, P. A., Konstan, M.W., McColley, S.A., McCoy, K., McKone, E.F., Munck, A., Ratjen, F., Rowe, S.M., Waltz, D., Boyle, M.P. (2015) Lumacaftor-Ivacaftor in patients with cystic fibrosis homozygous for Phe508del CFTR . *N Engl J Med*. *373*, 220-231.

Wang, G., Li, X., Zasloff, M. (2010) A database view of naturally occurring antimicrobial peptides: nomenclature, classification and amino acid sequence analysis. *Adv Mol Cell Microbiol. 18,* 1-21.

Wang, G., Zarodkiewicz, P., Valvano, M.A. (2020) Current advances in *Burkholderia* vaccines development. *Cells. 9*, 2671.

Wang, M., Ridderberg, W., Hansen, C.R., Høiby, N., Jensen-Fangel, S., Olesen, H.V., Skov, M., Lemming, L.E., Pressler, T., Johansen, H. K., Nørskov-Lauritsen, N. (2013) Early treatment with inhaled antibiotics postpones next occurrence of *Achromobacter* in cystic fibrosis. *J Cyst Fibros. 12*, 638-643.

References

Waters, V., Yau, Y., Beaudoin, T., Wettlaufer, J., Tom, S.K., McDonald, N., Rizvi, L., Klingel, M., Ratjen, F., Tullis, E. (2017) Pilot trial of tobramycin inhalation powder in cystic fibrosis patients with chronic *Burkholderia cepacia* complex infection. *J Cyst Fibros. 16*, 492-495.

Waters, V., Yau, Y., Prasad, S., Lu, A., Atenafu, E., Crandall, I., Tom, S., Tullis, E., Ratjen, F. (2011) *Stenotrophomonas maltophilia* in cystic fibrosis: Serologic response and effect on lung disease. *Am J Resp and Crit Care Med*. *183*, 635-640.

Watkins, R.R. (2022) Antibiotic stewardship in the era of precision medicine. *JAC Antimicrob Resist*. *4*, dlac066.

Wilhelm, S., Gdynia, A., Tielen, P., Rosenau, F., Jaeger, K.E. (2007)The autotransporter esterase EstA of *Pseudomonas aeruginosa* is required for rhamnolipid production, cell motility, and biofilm formation. *J Bacteriol*. *189*, 6695-6703.

Wong, F., Krishnan, A., Zheng, E.J., Stärk, H., Manson, A.L., Earl, A.M., Jaakkola, T., Collins, J.J. (2022) Benchmarking AlphaFold -enabled molecular docking predictions for antibiotic discovery. *Mol Syst Biol*. *18*, 1-20.

World Health Organization. (2017). Global priority list of antibiotic resistant bacteria to guide research, discovery, and development of new antibiotics. http://www.who.int/medicines/publications/WHO-PPL-Short_Summary_25Feb-ET_NM_WHO.pdf?ua=1.

World Health Organization. (2017) One Health. https://www.who.int/features/qa/one-health/en/.

Wu, L.J., Errington, J. (2004) Coordination of cell division and chromosome segregation by a nucleoid occlusion protein in *Bacillus subtilis*. *Cell.* 117, 915-925.

Yabuuchi, E., Kawamura, Y., Ezaki, T., Ikedo, M., Dejsirilert, S., Fujiwara, N., Naka, T., Kobayashi, K. **(2000)** *Burkholderia uboniae* sp. nov., L-arabinose-assimilating but different from *Burkholderia thailandensis* and *Burkholderia vietnamiensis*. *Microbiol Immunol*. *44*, 307-317.

Yabuuchi, E., Kosako, Y., Oyaizu, H., Yano, I., Hotta, H., Hashimoto, Y., Ezaki, T., Arakawa, M. (1992) Proposal of *Burkholderia* gen. nov. and transfer of seven species of the genus *Pseudomonas* homology group II to the new genus, with the type species *Burkholderia cepacia* (Palleroni and Holmes 1981) comb. nov. *Microbiol Immunol*. *36*, 1251-1275.

Yu, E., Sharma, S. (2022) Cystic Fibrosis. *StatPearls Publishing*.

Yu, N.Y., Wagner, J.R., Laird, M.R., Melli, G., Rey, S., Lo, R., Dao, P., Sahinalp, S.C., Ester, M., Foster, L.J., Brinkman, F.S. (2010) PSORTb 3.0: improved protein subcellular localization prediction with refined

localization subcategories and predictive capabilities for all prokaryotes. *Bioinformatics. 26*, 1608-1615.

Zeng, D., Debabov, D., Hartsell, T.L., Cano, R.J., Adams, S., Schuyler, J.A., McMillan, R., Pace, J.L. (2016) Approved glycopeptide antibacterial drugs: mechanism of action and resistance. *Cold Spring Harb Perspect Med. 6*, 1-16.

Novel approaches to manage antimicrobial resistances: a story of vaccine research and divisome inhibition.

List of original manuscripts

Full papers:

Scoffone, V.C., Trespidi, G., Barbieri, G., **Irudal, S.**, Perrin, E., Buroni, S. (2021) Role of RND efflux pumps in drug resistance of cystic fibrosis pathogens. *Antibiotics (Basel). 10*, 863. **IF**: **5.22**

Scoffone, V.C., Trespidi, G., Barbieri, G., **Irudal, S.**, Israyilova, A., Buroni, S. (2021) Methodological tools to study species of the genus *Burkholderia*. *Appl Microbiol Biotechnol. 105*, 9019-9034. **IF**: **5**

Scoffone, V.C., **Irudal, S.**, AbuAlshaar, A., Piazza, A., Trespidi, G., Barbieri, G., Makarov, V., Migliavacca, R., De Rossi, E., Buroni, S. (2022) Bactericidal and anti-biofilm activity of the FtsZ inhibitor C109 against *Acinetobacter baumannii*. *Antibiotics (Basel). 11*, 1571. **IF**: **5.22 (enclosed)**

Irudal, S., Scoffone, V.C., Trespidi, G., Barbieri, G., D'Amato, M., Viglio, S., Pizza, M., Scarselli, M., Riccardi, G., Buroni, S. (2023) Identification by reverse vaccinology of three virulence factors in Burkholderia cenocepacia that may represent ideal vaccine antigens. *Vaccines (Basel). 11,* 1039. **IF**: **7.8 (enclosed)**

Scoffone, V.C., Barbieri, G., **Irudal, S.**, Trespidi, G., Buroni, S. (2024) New antimicrobial strategies to treat multi-drug resistant infections caused by Gram-negatives in cystic fibrosis. *Antibiotics (Basel). 13*, 71. **IF: 5.22**

Bonacorsi, A., Trespidi, G., Scoffone, V.C., **Irudal, S.**, Barbieri ,G., Riabova, O., Monakhova, N., Makarov, V., Buroni, S. (2024) Characterization of the dispirotripiperazine derivative PDSTP as antibiotic adjuvant and antivirulence compound against *Pseudomonas aeruginosa*. *Front Microbiol. 15,* 1357708. **IF: 6.064**

Abstract:

Irudal S, Scoffone VC, Trespidi G, Bonacorsi A, Pellegrini A, Barbieri G, Buroni S. Reverse vaccinology as a tool to fight cystic fibrosis pathogens. Poster presentation at XXXII ECCMID congress, Lisbon, 23rd-26th April 2022.

Pellegrini A, Lentini G, Famà A, Bonacorsi A, Scoffone VC, Buroni S, Trespidi G, **Irudal S**, Postiglione U, Sassera D, Manai F, Pietracola G, Firon A, Biondo C, Teti G, Beninati C, Barbieri G. The CodY global regulator controls metabolism and virulence in Group B Streptococcus. Poster presentation at XXXII ECCMID congress, Lisbon, 23rd-26th April 2022.

Irudal S. Identification of novel antigen candidates to develop a vaccine for Burkholderia cenocepacia. Oral presentation at Cortona Procarioti 2022, Cortona (AR), 23rd-25th June 2022.

Irudal S, Scoffone VC, Trespidi G, Barbieri G, Buroni S. First application of reverse vaccinology on Burkholderia cepacia complex: identification and characterization of antigen candidates for the development of a vaccine. Poster presentation at X FEMS congress, Hamburg, 9th-13th July 2023.

Scoffone VC, **Irudal S**, Trespidi G, Barbieri G, Coluccia A, Buroni S. Virtual screening-based approach to identify novel inhibitors of FtsZ active against Staphylococcus aureus. Poster presentation at XXXIV SIMGBM congress, Cagliari, 21st-24th September 2023.

Irudal S, Scoffone VC, Trespidi G, Barbieri G, Buroni S. Reverse vaccinology: unveiling antigen candidates for the development of a vaccine against the Burkholderia cepacia complex. Poster presentation at XXXIV SIMGBM congress, Cagliari, 21st-24th September 2023.

Pellegrini A, Scoffone VC, Trespidi G, **Irudal S**, Bonacorsi A, Pietrocola G, Buroni S, Barbieri G. Interplay of CodY and CovR in regulating gene expression in Group B Streptococcus. Poster presentation at XXXIV SIMGBM congress, Cagliari, 21st-24th September 2023.

Trespidi G, Bonacorsi A, Scoffone VC, **Irudal S**, Barbieri G, Makarov V, Pasca MP, Buroni S. Exploiting dispirotripiperazines as a novel strategy to fight Pseudomonas aeruginosa infections in cystic fibrosis. Poster presentation at XXXIV SIMGBM congress, Cagliari, 21st-24th September 2023.

Novel approaches to manage antimicrobial resistances: a story of vaccine research and divisome inhibition.

antibiotics

MDPI

Article

Bactericidal and Anti-Biofilm Activity of the FtsZ Inhibitor C109 against *Acinetobacter baumannii*

Viola Camilla Scoffone [1], Samuele Irudal [1], Aseel AbuAlshaar [2], Aurora Piazza [2], Gabriele Trespidi [1], Giulia Barbieri [1], Vadim Makarov [3], Roberta Migliavacca [2], Edda De Rossi [1] and Silvia Buroni [1,*]

[1] Department of Biology and Biotechnology "Lazzaro Spallanzani", University of Pavia, 27100 Pavia, Italy
[2] Unit of Microbiology and Clinical Microbiology, Department of Clinical-Surgical, Diagnostic and Pediatric Sciences, University of Pavia, 27100 Pavia, Italy
[3] Research Center of Biotechnology RAS, 119071 Moscow, Russia
* Correspondence: silvia.buroni@unipv.it; Tel.: +39-0382-985574

Abstract: In the last few years, *Acinetobacter baumannii* has ranked as a number one priority due to its Multi Drug Resistant phenotype. The different metabolic states, such as the one adopted when growing as biofilm, help the bacterium to resist a wide variety of compounds, placing the discovery of new molecules able to counteract this pathogen as a topic of utmost importance. In this context, bacterial cell division machinery and the conserved protein FtsZ are considered very interesting cellular targets. The benzothiadiazole compound C109 is able to inhibit bacterial growth and to block FtsZ GTPase and polymerization activities in *Burkholderia cenocepacia*, *Pseudomonas aeruginosa*, and *Staphylococcus aureus*. In this work, the activity of C109 was tested against a panel of antibiotic sensitive and resistant *A. baumannii* strains. Its ability to inhibit biofilm formation was explored, together with its activity against the *A. baumannii* FtsZ purified protein. Our results indicated that C109 has good MIC values against *A. baumannii* clinical isolates. Moreover, its antibiofilm activity makes it an interesting alternative treatment, effective against diverse metabolic states. Finally, its activity was confirmed against *A. baumannii* FtsZ.

Keywords: *Acinetobacter baumannii*; drug resistance; biofilm; FtsZ

Citation: Scoffone, V.C.; Irudal, S.; AbuAlshaar, A.; Piazza, A.; Trespidi, G.; Barbieri, G.; Makarov, V.; Migliavacca, R.; De Rossi, E.; Buroni, S. Bactericidal and Anti-Biofilm Activity of the FtsZ Inhibitor C109 against *Acinetobacter baumannii*. *Antibiotics* **2022**, *11*, 1571. https://doi.org/10.3390/antibiotics11111571

Academic Editor: Marc Maresca

Received: 26 October 2022
Accepted: 5 November 2022
Published: 8 November 2022

1. Introduction

Acinetobacter baumannii is raising concern due to its extensive drug resistance and high mortality rate [1], especially for Intensive Care Units patients [2,3]. This Gram-negative bacterium, belonging to the ESKAPE group, usually causes ventilator-associated pneumonia [4] and infections involving skin and soft tissue, urinary tract, and bloodstream [1]. Its ability to acquire plasmids, transposons and integrons facilitates high adaptability, and the diffusion of resistance genes [5]. The increase in the use of beta-lactams has contributed to the spread of Multi Drug Resistant (MDR) strains, the prevalence of which is estimated to be 79.9% in pneumonia patients [5], requiring treatment with the last-resort antibiotic carbapenem. However, the emergence of carbapenem resistant-*A. baumannii* (CR-Ab) poses an additional threat [6]. Indeed, in 2018 CR-Ab ranked as the number one priority, according to the WHO, due to carbapenem resistance being associated with a broad range of co-resistance against other classes of antibiotics [7]. A different alternative is now provided by the novel cefiderocol cephalosporin, which showed promising activity against ESKAPE and *A. baumannii* isolates. A high percentage of unstable heteroresistence still arose after monotherapy treatment, highlighting how important combination therapy is [8]. Conversely, high loading dose colistin monotherapy successfully eradicated MDR-*A. baumannii* infections [9].

Along with its virulence factors, such as outer membrane proteins, capsular polysaccharides, and iron acquisition systems [10], the genetic array of this pathogen allows its survival and diffusion in a hostile environment, such as clinical settings [11]. Therefore,

research is nowadays focusing on alternative treatments which could dampen antimicrobial resistance by decreasing antibiotic assumption. Bacteriophages are harmless to humans and a strain-specific weapon, capable of precisely hijacking bacterial metabolism, leading to cell lysis [12–14]. Still, concern arises about the possibility of interbacterial DNA transfer by phage diffusion and the rise of phage-resistant strains [15]. To note, the phage-resistant phenotype is associated with a decrease in antibiotic resistance when combined treatments are performed [14]. Bacteriocins, a class of Antimicrobial Peptides (AMPs), are host-produced peptides possessing bactericidal and immunomodulatory properties [16]. Recent interest has emerged in these compounds, as they show a low tendency to select resistant strains, broad-spectrum activity, rapid killing action, and high clinical efficacy against different MDR strains [17–20]. These properties result from their membrane disruptive capacity or by their ability to hit internal targets [16]. Unfortunately, their clinical application is often limited by side effects, including hemolytic activity, immunogenicity, and drug resistance after long-term use [21]. However, both bacteriophages and AMPs can be used in combination with antibiotics, enhancing their potency and even decreasing their administration dose [22,23]. Another issue directly related to the metabolic state of the bacterium is its ability to form biofilms, which are noteworthy as being less susceptible to the effects of standard treatments.

In this light, bacterial division machinery has acquired more and more importance [24–26], since it could represent the ideal target for the development of new compounds effective against MDR bacteria. Several molecules have been found to interfere with the divisome, mainly targeting the conserved protein FtsZ, "Filamenting temperature-sensitive mutant Z", involved in the midpoint Z ring formation needed for cell division [27,28]. In the last few years, a broad-spectrum compound, methyl [(4-nitro-2,1,3-benzothiadiazol-5-yl)thio]acetate, named C109 (Figure 1), has surprised researchers with its ability to inhibit purified FtsZ, preventing both its GTPase and polymerization activities and being active at low concentrations against different Gram-negative and Gram-positive bacteria, including *Burkholderia cenocepacia*, *Pseudomonas aeruginosa* and *Staphylococcus aureus* [29–33].

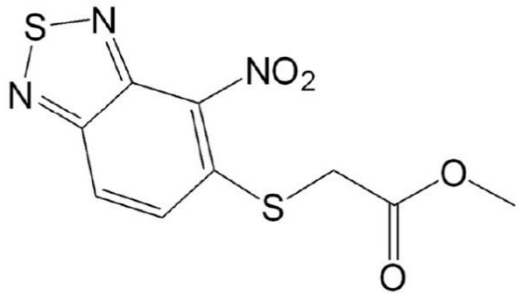

Figure 1. Chemical structure of C109 compound.

Considering the urgent need for new treatment against *A. baumannii*, the effect of C109 against sensitive and resistant strains was explored, together with its biofilm inhibitory activity. Finally, *A. baumannii* FtsZ was expressed and purified to evaluate GTPase and polymerization inhibition in the presence of the compound.

Novel approaches to manage antimicrobial resistances: a story of vaccine research and divisome inhibition.

2. Results

2.1. Activity of C109 against Sensitive and Resistant *A. baumannii* Strains

The activity of C109 was tested against a total of 108 *A. baumannii* strains by means of the microdilution method in Mueller Hinton (MH) broth. The bacterial load was always between 3.1×10^3 and 2.1×10^5 CFU/ml. The minimal inhibitory concentration (MIC) of C109 against the reference strain *A. baumannii* ATCC19606 was 8–16 mg/L and 8–32 mg/L for the clinical strain, while the minimal bactericidal concentration (MBC) was 16 mg/L.

Among the 108 clinical isolates, *A. baumannii* strains 52 (48.1%), 39 (36.1%), and 17 (15.7%) displayed MIC values of 8, 16, and 32 mg/L, respectively (Figure 2A). These results showed that the most representative MIC values among clinical isolates were equal to, or lower than, those of the reference strains, i.e., 16 mg/L. The MBCs for the same *A. baumannii* (n = 108) strains were 8, 16, 32, and 64 mg/L for 10 (9.3%), 53 (49.1%), 35 (32.4%), and 10 (9.3%) strains, respectively (Figure 2A), demonstrating that 16 mg/L, the most represented value for the MBC, was the same for the reference strains. In fact, C109 showed a bactericidal effect in 99% (n = 107/108) of the cases, with MBC being not more than fourfold higher than the MIC (Figure 2B). C109 did not show the bactericidal effect on one isolate (1%).

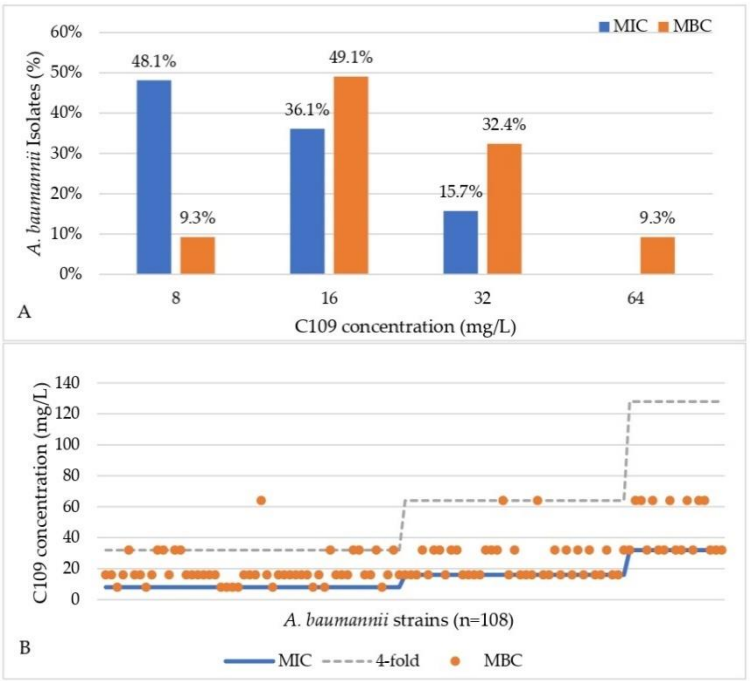

Figure 2. (**A**) MIC and MBC values of C109 obtained for *A. baumannii* strains (n = 108). (**B**) the bactericidal effect of C109 on *A. baumannii* isolates (n = 107/108).

2.2. C109 Biofilm Inhibitory Activity against A. baumannii Strains

To test the biofilm inhibitory acitivity of C109, *A. baumannii* ATCC19606 and three strains, not clonally related by Pulsed-Field Gel Electrophoresis (PFGE) and Multi-Locus Sequence Typing (MLST), were selected as representatives for all the strains. *A. baumannii* ATCC19606 belongs to the ST52 group, MO5 belongs to ST78, ST for HU5 is unkown, while the strain 560380 belongs to the ST2.

The biofilm inhibitory activity of the compound C109 against *A. baumannii* strains was first determined using a 96-well microplate crystal violet assay [34]. C109 was tested at increasing concentrations, ranging from 2 to 256 mg/L. Under the tested conditions, the biofilm formation ability of the *A. baumannii* ATCC19606 and MO5 strains significantly decreased in the presence of 128 mg/L of C109, while that of the *A. baumannii* HU5 strain significantly reduced only in the presence of 256 mg/L of C109. The biofilm of the 560380 strain was already significantly altered in the presence of 64 mg/L of the compound (Figure 3).

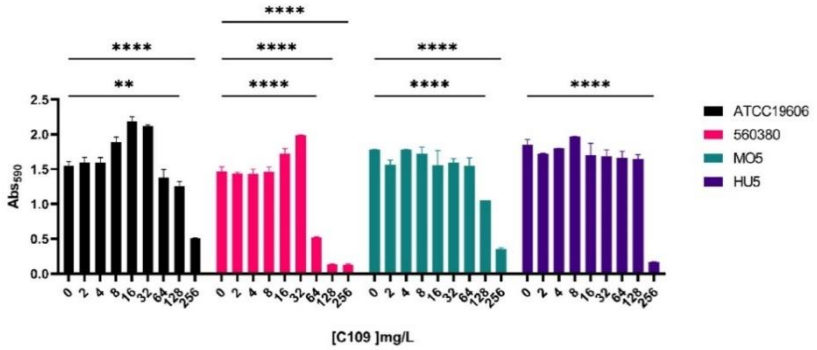

Figure 3. Effect of increasing concentration of C109 against biofilm formation ability of *A. baumannii* strains: ATCC19606 (**in black**), 560380 (**in pink**), MO5 (**in green**) and HU5 (**in purple**). The C109 concentration is indicated below each bar in mg/L. Mean ± standard error, n = 2. ** $p < 0.01$; **** $p < 0.0001$ (two-way ANOVA test).

Confocal laser scanning microscopy (CLSM) analysis was used to better characterize the effect of the C109 on *A. baumannii* biofilm morphology. *A. baumannii* strains ATCC196060, 560380, MO5 and HU5 were grown as static cultures in four-well chambered coverslips in the absence, or in the presence, of different concentrations of C109 (16, 64 and 256 mg/L) at 37 °C. Biofilms were stained with Syto 9, staining nucleic acids of all cells. Representative 3D image reconstructions of biofilms formed by each strain in the presence of 0 (untreated), 16 and 64 mg/L of C109 are reported in Figure 4. The images show that, from a qualitative point of view, the biofilm produced by the *A. baumannii* strains ATCC19606, 560380 and MO5 was already reduced at 16 mg/L of C109. In the case of the strain HU5, the same effect was observed only at 64 mg/L, in accordance with its lower susceptibility to the compound (Figure 3).

A specific biofilm morphology analysis was carried out with COMSTAT 2. These analyses showed that the biomass of the biofilm produced by ATCC19606 had already decreased significantly in the presence of 16 mg/L C109 (Figure 5A), while that of the strain 560380 decreased significantly only in the presence of 256 mg/L of C109 (Figure 5A). The biomass of the biofilm formed by the MO5 strain showed only a slight decrease in the presence of 256 mg/L of C109 (Figure 5A). On the other hand, the biomass of the

biofilm produced by the HU5 strain was not altered in the presence of C109 at the tested concentrations (Figure 5A). However, the last two strains had the ability to form a biomass which was lower in respect to the first two.

The average thickness of the biofilm produced by the *A. baumannii* ATCC19606 significantly decreased in the presence of increasing concentrations of C109 (Figure 5B). At the same time, the average thickness of the biofilm 560380 had already significantly decreased in the presence of 16 mg/L of C109 (Figure 5B). The average thickness of the biofilm formed by the strain MO5 showed a decrease, which was not statistically significant (Figure 5B). The C109 treatment did not affect the average thickness of the biofilms formed by the strains HU5 (Figure 5B). In this case, the thickness of the biofilm formed by MO5 and HU5 was lower compared to the ATCC19606 and 560380 strains.

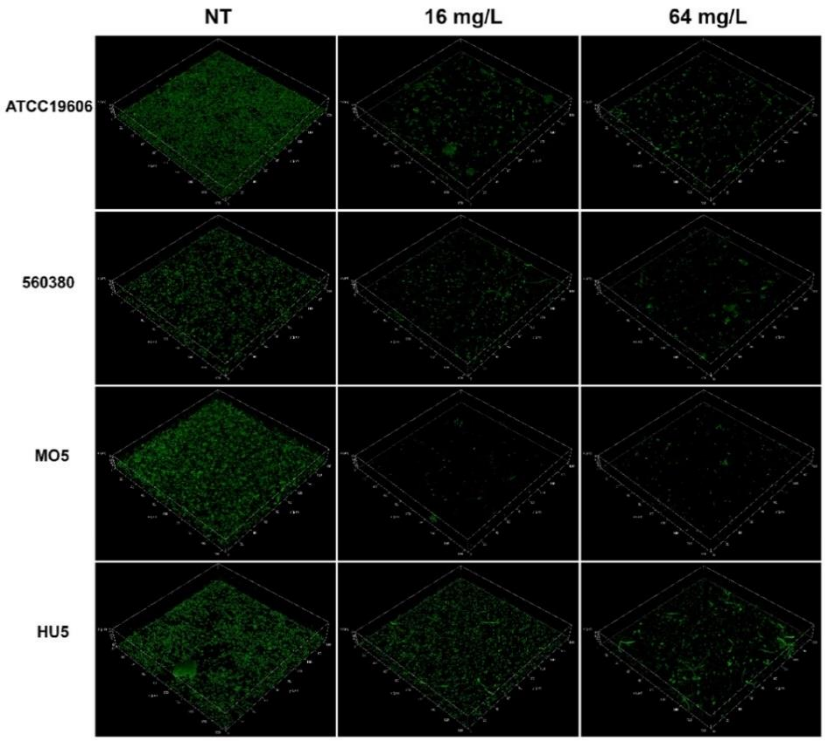

Figure 4. CLSM images of *A. baumannii* biofilms grown in four-well chambered coverslips. Pictures were taken with an overall magnification of 400×. Cells were grown overnight at 37 °C in MH with no C109 (NT), 16 mg/L of C109 or 64 mg/L of C109. Seventy planes at equal distances along the Z-axis of the biofilm were imaged by CLSM. 2D images were stacked to reconstruct the 3D biofilm image. Scale bar represents 28 µm.

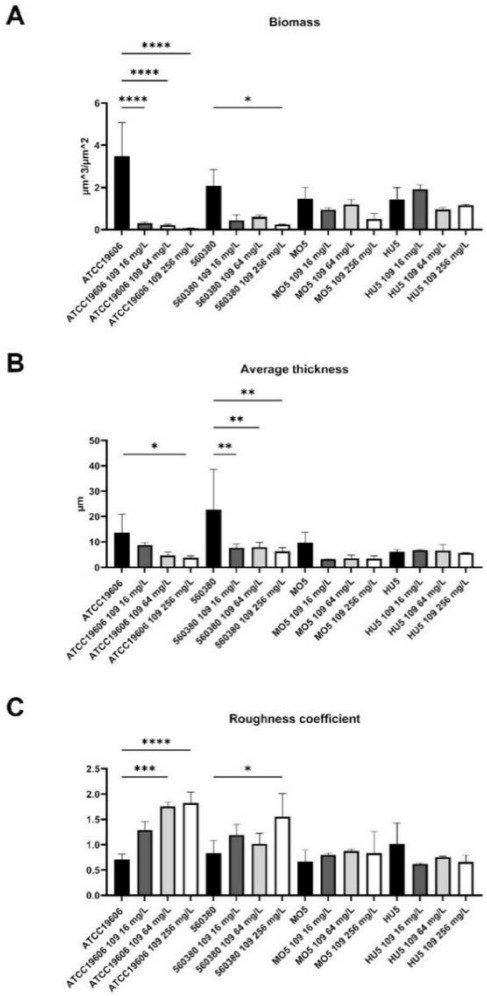

Figure 5. Analysis of biofilm properties by COMSTAT 2. (**A**) Measurements of total biomass, (**B**) average thickness, and (**C**) roughness coefficient. Data are the mean ± SD of the results from three independent replicates. * $p < 0.1$, ** $p < 0.01$, *** $p < 0.001$, **** $p < 0.0001$ (two-way ANOVA test).

Using COMSTAT, the roughness coefficient (variation in thickness calculated from the distribution of the biofilm thickness) was also analyzed, which provided an indicator of biofilm heterogeneity. The data showed that, in the case of the ATCC19606 strain, the C109

treatment induced an increase in the roughness coefficient, suggesting that the biofilm was less homogeneous (Figure 5C). The roughness of the biofilm formed by the strain 560380 increased significantly only in the presence of 256 mg/L of C109 (Figure 5C). In the case of the two clinical isolates, MO5 and HU5, the roughness coefficient of the biofilms was not affected by the compound C109 (Figure 5C).

The biofilm distribution on the *Z*-axis of the treated samples changed drastically in the strains ATCC19606 and 560380, while the biofilm distribution of the strain MO5 was less affected by the treatment with 16 mg/L C109 (Figure 6A–C). On the other hand, the biofilm of the HU5 strain was only partially altered in the presence of 256 mg/L C109 (Figure 6D).

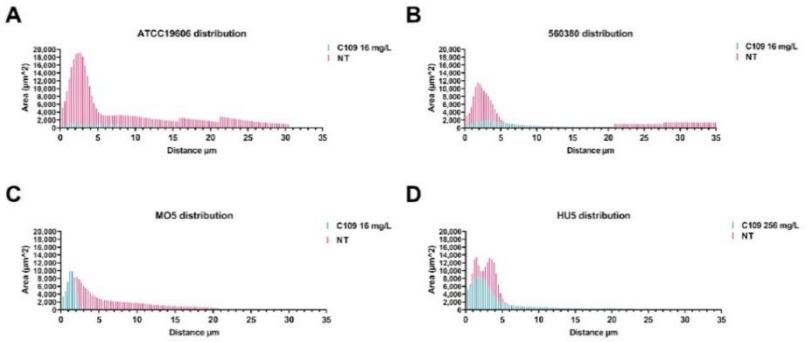

Figure 6. Analysis of biofilm properties by COMSTAT 2% of the area occupied by biofilm distribution, (**A**) ATCC19606, (**B**) 560380, (**C**) MO5 and (**D**) HU5. Data are the mean ± SD of the results from three independent replicates.

2.3. C109 Activity on Purified A. baumannii FtsZ

FtsZ is the cellular target of the compound C109 [30]. C109 is able to block the GTPase activity and the polymerization of FtsZ in *B. cenocepacia* and *P. aeruginosa*, while in *S. aureus* it blocks only the GTPase activity [31,33]. To evaluate its activity against the *A. baumannii* FtsZ, the protein was expressed and purified, as described in the Materials and Methods Section 4.5. The GTPase activity of the recombinant FtsZ of *A. baumannii* ATCC19606 was evaluated, as previously described [30], with minor modifications. The achieved results showed that C109 inhibited the FtsZ GTPase activity with a 50% inhibitory concentration (IC_{50}) of 11.84 µM (Figure 7A), which indicated that the GTPase activity of FtsZ was impaired by the compound C109. In order to understand if C109 was also able to block FtsZ polymerization in *A. baumannii*, an in vitro sedimentation assay was performed [30]. *A. baumannii* FtsZ polimerized in vitro in the presence of GTP (its substrate) and not in the presence of GDP (its product). When C109 was added to the reaction at increasing concentration (50 and 100 µM), the polymerization was already blocked at the lowest concentration used (Figure 7B,C).

These results demonstrated that the compound C109 blocked both the GTPase and the polymerization activity of FtsZ of *A. baumannii*, as previously described regarding *B. cenocepacia* and *P. aeruginosa* [30,31].

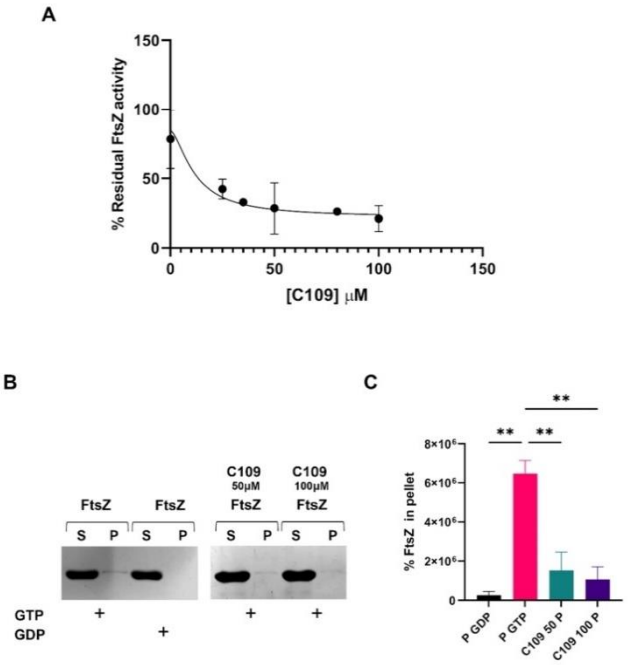

Figure 7. GTPase activity and polymerization assays on *A. baumannii* FtsZ in the presence of C109. (**A**) IC_{50} of C109 against *A. baumannii* FtsZ. (**B**) Sedimentation assay of FtsZ in the presence, or absence, of C109, GTP and GDP. P, insoluble fraction (pellet); S, soluble fraction (supernatant). (**C**) Relative quantification of FtsZ percentage in the pellet of the indicated samples obtained by densitometry analysis. Data are the mean ± SD of the results from three different replicates; images are representative of at least three different experiments. ** $p < 0.01$ (one-way ANOVA test).

3. Discussion

Recently, the WHO has recommended a global strategy to decrease the appearance of antibiotic resistant isolates and to identify new treatments. The development of new compounds active against Carbapenem-resistant *A. baumannii* is a priority. *A. baumannii* is the causative agent of 2% of healthcare-associated infections [35]. In particular, the most frequent infections with the highest mortality rates are ventilator-associated pneumonia and bacteremia, identified in patients with prolonged periods of hospitalization [36]. Of note, *A. baumannii* has been detected in sputum cultures and tracheal aspirates from COVID-19 mechanically ventilated patients [37].

The ability of this bacterium to persist on abiotic surfaces and to resist hostile environments, such as clinical settings, make it a dangerous pathogen. Therefore, focusing attention on alternative treatments is extremely relevant. In this context, weapons that hit the bacterium during different metabolic states are of the most importance. It is noteworthy that bacteria growing as biofilm show different susceptibility to antibiotics, due to their metabolism being different with respect to planktonic cells. Hence, bacterial cell division machinery and the conserved protein FtsZ are considered very interesting cellular targets.

Novel approaches to manage antimicrobial resistances: a story of vaccine research and divisome inhibition.

The benzothiadiazole derivative C109 inhibits FtsZ GTPase and polymerization activities in *B. cenocepacia* and *P. aeruginosa*, while only affecting the GTPase activity in *S. aureus* FtsZ. To face the problem of drug resistance in *A. baumannii*, the activity of C109 was tested against a panel of sensitive and resistant strains. The results showed that C109 MIC and MBC against the *A. baumannii* ATCC19606 reference strain ranged between 8 and 16 mg/L. So, 107 clinical isolates were tested and the most representative MIC and MBC values were 8 and 16 mg/L. The compound C109 showed a bactericidal effect in 99% of the cases. The obtained MIC and MBC values were considered good values, also taking into account the high number of resistant clinical isolates identified [7].

Moreover, in *A. baumannii*, the ability to form biofilm facilitates tolerance toward external stress, desiccation and antimicrobials [38]. The C109 biofilm inhibitory activity was assessed against ATCC19606 and the clinical strains 560380 (MIC = 16 mg/L), MO5 (MIC = 32 mg/L) and HU5 (MIC = 16 mg/L). The results showed that a concentration of C109 four-fold higher than the MIC decreased biofilm formation of the ATCC19606 and MO5 strains, while for the 560380 strain a concentration 2-fold higher than the MIC was sufficient. On the contrary, for the HU5 strain, a concentration of 8-fold the MIC was required to inhibit biofilm formation. To better characterize the biofilm formed by these strains in the presence of the compound C109, a CLSM analysis was performed, revealing that, for the strains ATCC19606, 560380 and MO5, the biofilm was already altered at a low concentration of C109 (16 mg/L), while, as previously shown by the other experiment, the HU5 was less sensitive.

The biofilm morphology was studied using the COMSTAT software and the analyses confirmed the previous results: the ATCC19606 reference strain and the two clinical isolates 560380 and MO5 were sensitive to the compound C109, since the biomass, the average thickness, the roughness and the distribution of the biofilms were perturbed. The clinical isolate MO5 was less sensitive and a higher dose of C109 was required to show biofilm alteration (256 mg/L).

These results are interesting since C109 treatment was shown to also alter biofilm formation in clinical isolates. Considering the main problem of biofilm formation in the nosocomial infections caused by *A. baumannii*, these findings are very promising, establishing C109 as an effective compound at different metabolic states of the bacteria. Moreover, its combination with currently used therapies could further increase its efficacy.

C109 activity was also fully characterized from an in vitro perspective. The cellular target of this compound was identified as the protein FtsZ in Gram-negative and -positive bacteria, *B. cenocepacia*, *P. aeruginosa* and *S. aureus* [30,31,33]. The GTPase activity of *A. baumannii* FtsZ was indeed inhibited by the compound, showing an IC_{50} of 11.84 µM. This value was good, if compared to the previously described compounds derived from cinnamaldehyde [39]. Moreover, C109 also blocked FtsZ polymerization in *B. cenocepacia* and in *P. aeruginosa*. Further structural studies could help to better elucidate C109 molecular interaction with FtsZ. The data presented here demonstrated that C109 interacted with the *A. baumannii* FtsZ inhibiting both functions: the GTPase activity and the polymerization.

In conclusion, our results showed that C109 is one of the first FtsZ inhibitors described as active against the Gram-negative bacterium *A. baumannii* and with good MIC values against clinical isolates. The compound is also characterized by an interesting antibiofilm activity making it an interesting alternative treatment, effective against diverse metabolic states.

4. Materials and Methods

4.1. Bacterial Strains and Culture Media

Acinetobacter baumannii ATCC19606 and 107 *A. baumannii* isolates strains were used. Bacteria were grown aerobically in Mueller-Hinton (MH, Difco, BD, Franklin Lakes, NJ, USA) or Luria-Bertani (LB, Difco, BD, Franklin Lakes, NJ, USA) broth at 37 °C at 200 rpm. *Escherichia coli* BL21(DE3) strain (laboratory collection) was grown in LBbroth at 37 °C with shaking or on LB agar plates and used for recombinant protein expression. Kanamycin

(PanReac, AppliChem, ITW Reagent, Glenview, IL, USA) was used at 50 mg/L for plasmid selection and maintenance.

4.2. A. baumannii Clinical Isolates Minimum Inhibitory Concentration (MIC) and Minimum Bactericidal Concentration (MBC) Determination

Minimum inhibitory concentrations (MICs) were determined in quadruplicates for a total of 107 *A. baumannii* clinical isolates and *A. baumannii* ATCC19606, using the broth microdilution method, according to EUCAST guidelines, in Muller–Hinton (MH, Difco, BD, Franklin Lakes, NJ, USA) broth [40]. C109 was dissolved in pure DMSO (≥99.9%). Two-fold serial dilutions of C109 in concentrations ranging from 64 to 0.125 mg/L, with a final inoculum of 5×10^5 CFU/mL, were dispensed in each well of the 96-well culture plate. After incubation for 24 h at 35 °C, 30 µL of 0.015% resazurin (Merck, Readington, NJ, USA) was added to all wells, and the culture was further incubated for 2–4 h for the observation of blue to pink color change, indicating bacterial growth [41]. MICs were determined from visual reading before and after adding resazurin as the lowest concentration able to inhibit microbial growth. All experiments were performed by two workers in quadruplicate, and either the *A. baumannii* ATCC19606 strain or clinical strain *A. baumannii* 15C32 were included in each plate as control strains.

Viable colony counts were performed in duplicates for each strain by diluting 2.5 µL from the growth-control well, after inoculation, in 50 µL of sterile distilled water and spreading on MH agar. Plate count was made by counting the colony-forming units (CFUs) after incubation for 24 h at 35 °C. The minimum bactericidal concentrations (MBCs) of C109 were determined for all *A. baumannii* strains (n = 108) by subculturing 10 µL of bacterial culture from wells, corresponding to the MIC value, and two concentrations higher than the MIC value, on MH agar plates. After 24 h of incubation in aerobic conditions at 35 °C, the lowest concentration of C109 that yielded no visible bacterial growth on MH agar plates was recorded as the MBC value [42].

4.3. In Vitro Biofilm Inhibition Test in 96-Well Microtiter Plates

Biofilm formation inhibitory activity of C109 compound was tested on *A. baumannii* ATCC19606, 560380, MO5 and HU5 strains using the crystal violet staining method [34]. Bacterial cultures grown for 18 h in MH broth were diluted to OD600 of 0.02 in MH and incubated in 96-well microtiter plates, either in the absence or presence of different concentrations of C109 (2–256 mg/L). After 3 hours of incubation, the supernatant (containing nonadherent cells) was removed and 200 µL of fresh sterile medium (with the same C109 concentrations) was added to each well and incubated for 20 h at 37 °C. Biofilms were quantified by staining with crystal violet. Briefly, planktonic cells were removed, attached cells were washed with sterile saline solution, biofilms were treated with 90% methanol for 15 min, methanol was removed and the plates were air-dried. Plates were stained with 150 µL of 0.1% crystal violet for 20 min. Wells were gently washed twice with water and the surface-associated dye was dissolved in 150 µL of 33% acetic acid. The absorbance measurements at OD600nm were measured in the Glomax (Promega Madison, WI, USA) plate reader.

4.4. Biofilm Evaluation by Confocal Laser Scanning Microscopy

Bacteria were cultured O/N in MH and diluted to an OD600 = 0.01 in the same medium. Bacteria were incubated in a four-well chambered coverslip µ-Slide (Ibidi) at 37 °C, in the presence of different concentrations of C109 (16, 64 and 256 mg/L). The compound C109 was dissolved in pure DMSO (≥99.9%), and the volume of C109 added was always 1/200 of the final volume, since this amount of DMSO was shown not to affect biofilm formation. After three hours of incubation the medium was removed, along with nonadherent cells, and fresh medium containing the same C109 concentrations, was added to the chambers. After over-night incubation, the medium was removed, and biofilms were washed with PBS 1X and stained with Syto 9 (Invitrogen, Waltham, MA, USA) at the final

concentration of 5 μM. A 63X oil immersion objective Leica DMi8 with 500- to 530-nm (green fluorescence representing Syto 9) emission filters were used to take five snapshots randomly at different positions in the confocal field of each chamber. The Z-slices were obtained every 0.3 microns. For visualization and processing of biofilm images, ImageJ was used. The thickness, biomass, roughness coefficient, and biofilm distribution were measured using the COMSTAT 2 software [43]. All confocal scanning laser microscopy experiments were performed three times, and standard deviations were measured.

4.5. Cloning, Expression and Purification of the A. baumannii FtsZ Protein

The full-length (1176 bp) *ftsZ* gene of *A. baumannii* ATCC19606 was amplified from the genomic DNA by PCR using the primers: FtsZSUMOABfor (5′- CAGAGAACAGATTGGTG GTATGGCCTCATTTGAATTTATAGAAG-3′) and FtsZSUMOABrev (5′-ATAAATACCTAAG CTTGTCTTTACTTACGTTGCTGATTTTTCAAG-3′). Primers were designed following the Gibson ® assembly kit instructions (NEB). The PCR product was cloned into the linearized pET-SUMO vector (Invitrogen, Waltham, MA, USA), using the Gibson® assembly kit (New England Biolabs, Ipswich, MA, USA), according to the manufacturer's instructions. The pET-SUMOFtsZAB vector was transformed into the *E. coli* BL21(DE3) competent cells to express the recombinant protein. After transformation bacteria were grown O/N, 1/50 of the inoculum was inoculated in 3 L of LB, supplemented with kanamycin (50 mg/L), and incubated at 37 °C with shaking until OD600 = 0.6 was reached. The FtsZ expression was induced with 0.5 mM of isopropyl-β-D-thiogalactopyranoside (IPTG, BioChemica, PanReac, AppliChem). The temperature was set at 18 °C and the culture was grown O/N. Cells were collected by centrifugation. The pellet was resuspended in lysis buffer (50 mM Tris-HCl pH 8, 300 mM KCl, 2.5 mM $MgCl_2$, 1 mM Dithiothreitol [DTT], 5 mM imidazole and 10% glycerol), supplemented with 1 mM of the nonspecific protease inhibitor phenyl-methanesulfonyl fluoride (PMSF, Merck, Readington, NJ, USA), and lysed by sonication. The lysate was centrifuged at 48,000× *g* for 1 hour and the clarified supernatant was loaded on a 1 mL His Trap FF nickel column (1 mL, GE Healthcare, Chicago, IL, USA). The protein was eluted with the lysis buffer with 250 mM imidazole added. The molecular weight of the protein with the SUMO tag was 55.4 kDa. To cleave the SUMO tag from the purified FtsZ, sample was dialyzed O/N at 4 °C, against Buffer A (20 mM Tris-HCl pH 7.8, 100 mM KCl, 2.5 mM $MgCl_2$ and 10% glycerol) and the SUMO protease was added to the dialysis. The SUMO tag was removed using a reverse-IMAC. The molecular weight of the protein without the SUMO tag was 42 kDa. The protein was quantified using Qubit Fluorometric Quantification (Thermo Fisher Scientific Inc. Waltham, MA, USA) concentrated to 4 mg/mL and samples were stored at −80 °C.

4.6. In Vitro FtsZ GTPase Activity

GTPase activity was assayed at 30 °C using a pyruvate kinase-L-lactic dehydrogenase (PK/LDH) spectrophotometric coupled assay, as previously described in [30], with minor modifications. The reaction mixture contained 50 mM MES (pH 6.5), 5 mM $Mg(CH_3COO)_2$, 100 mM CH3CO2K, 10 U PK/LDH, 0.25 mM NADH, 0.25 mM phosphoenolpyruvate, and 4.8 μM of FtsZ. The assay was initiated by the addition of 1 mM GTP. The experiments were performed in triplicate, and the kinetic constants were determined by fitting the data to the Michaelis–Menten equation using Prism 9. C109 was added in concentrations ranging from 0.5 to 100 μM, and the inhibitory concentration that reduced the enzymatic activity by half (IC_{50}) was determined using Prism 9.

4.7. In Vitro FtsZ Polymerization Assay

The polymerization of FtsZ was assessed in vitro using a sedimentation protocol, as previously described in [30]. The reaction mixture was set up to contain 50 mM MES (pH 6.5), 5 mM $Mg(CH_3COO)_2$, 100 mM CH_3CO_2K, 12 μM SaFtsZ, and 2 mM GTP or GDP. The reaction mixtures were incubated for 10 min at 30 °C and 300 rpm to allow the polymerization to occur. Subsequently, samples were ultracentrifuged at 350,000× *g*

for 10 min at 25 °C, and the supernatant was immediately separated from the pellet, which contained the protein polymers. The samples were analyzed by SDS-PAGE on 12% polyacrylamide gels. The in vitro polymerization of FtsZ protein was tested in the presence of increasing concentrations of the compound C109.

4.8. Statistical Methods

Analyses were performed using Prism 9.0 (GraphPad). Comparison of more than two groups were performed with the one-way or two-way ANOVA. P values < 0.1 were considered statistically significant ($p < 0.1$, ** $p < 0.01$, *** $p < 0.001$, **** $p < 0.0001$).

Author Contributions: Conceptualization, S.B. and E.D.R.; methodology, V.C.S., S.I. and R.M.; software, V.C.S.; validation, V.C.S., G.T. and G.B.; formal analysis, A.A. and A.P.; resources, V.M.; data curation, V.C.S., A.A. and A.P.; writing—original draft preparation, A.A., A.P., V.C.S. and S.I.; writing—review and editing, S.B., V.C.S., A.P. and R.M.; supervision, R.M., S.B. and E.D.R.; project administration, S.B. and E.D.R. All authors have read and agreed to the published version of the manuscript.

Funding: This research was funded by PRIN 2017 grant prot. 20177J5Y3P, by PRIN 2020 grant prot. 20208LLXEJ, by the Italian Ministry of Education, University and Research (MIUR) (Dipartimenti di Eccellenza, Program 2018–2022) of the Department of Biology and Biotechnology, "L. Spallanzani", University of Pavia, and by the FWO Biofilm Community W000921N.

Institutional Review Board Statement: Not applicable.

Informed Consent Statement: Not applicable.

Data Availability Statement: Not applicable.

Acknowledgments: We thank Amanda Oldani and Patrizia Vaghi (Centro Grandi Strumenti, University of Pavia, Italy) for technical assistance with confocal microscopy.

Conflicts of Interest: The authors declare no conflict of interest.

References

1. Ibrahim, S.; Al-Saryi, N.; Al-Kadmy, I.M.S.; Aziz, S.N. Multidrug-resistant *Acinetobacter baumannii* as an emerging concern in hospitals. *Mol. Biol. Rep.* **2021**, *48*, 6987–6998. [CrossRef]
2. Brasiliense, D.; Cayô, R.; Streling, A.P.; Nodari, C.S.; Souza, C.; Leal, C.; Gales, A.C. Outbreak of *Acinetobacter colistiniresistens* bloodstream infections in a neonatal intensive care unit. *J. Glob. Antimicrob. Resist.* **2021**, *24*, 257–259. [CrossRef]
3. Durán-Manuel, E.M.; Cruz-Cruz, C.; Ibáñez-Cervantes, G.; Bravata-Alcantará, J.C.; Sosa-Hernández, O.; Delgado-Balbuena, L.; León-García, G.; Cortés-Ortíz, I.A.; Cureño-Díaz, M.A.; Castro-Escarpulli, G.; et al. Clonal dispersion of *Acinetobacter baumannii* in an intensive care unit designed to patients COVID-19. *J. Infect. Dev. Ctries* **2021**, *15*, 58–68. [CrossRef]
4. Jean, S.S.; Chang, Y.C.; Lin, W.C.; Lee, W.S.; Hsueh, P.R.; Hsu, C.W. Epidemiology, treatment, and prevention of nosocomial bacterial pneumonia. *J. Clin. Med.* **2020**, *9*, 275. [CrossRef]
5. Kyriakidis, I.; Vasileiou, E.; Pana, Z.D.; Tragiannidis, A. *Acinetobacter baumannii* antibiotic resistance mechanisms. *Pathogens.* **2021**, *10*, 373. [CrossRef]
6. Hassan, R.M.; Salem, S.T.; Hassan, S.I.M.; Hegab, A.S.; Elkholy, Y.S. Molecular characterization of carbapenem-resistant *Acinetobacter baumannii* clinical isolates from Egyptian patients. *PLoS ONE* **2021**, *16*, e0251508. [CrossRef]
7. Tacconelli, E.; Carrara, E.; Savoldi, A.; Harbarth, S.; Mendelson, M.; Monnet, D.L.; Pulcini, C.; Kahlmeter, G.; Kluytmans, J.; Carmeli, Y.; et al. Discovery, research, and development of new antibiotics: The WHO priority list of antibiotic-resistant bacteria and tuberculosis. *Lancet Infect Dis.* **2018**, *18*, 318–327. [CrossRef]
8. Stracquadanio, S.; Bonomo, C.; Marino, A.; Bongiorno, D.; Privitera, G.F.; Bivona, D.A.; Mirabile, A.; Bonacci, P.G.; Stefani, S. *Acinetobacter baumannii* and cefiderocol, between cidality and adaptability. *Microbiol. Spectr.* **2022**, *10*, e0234722. [CrossRef]
9. Katip, W.; Meechoui, M.; Thawornwittayakom, P.; Chinwong, D.; Oberdorfer, P. Efficacy and safety of high loading dose of colistin in Multidrug-Resistant *Acinetobacter baumannii*: A prospective cohort study. *J. Intensive Care Med.* **2019**, *34*, 996–1002. [CrossRef]
10. Sheldon, J.R.; Skaar, E.P. *Acinetobacter baumannii* can use multiple siderophores for iron acquisition, but only acinetobactin is required for virulence. *PLoS Pathog.* **2020**, *16*, e1008995. [CrossRef]
11. Kumar, S.; Answer, R.; Azzi, A. Virulence potential and treatment options of multidrug-resistant (MDR) *Acinetobacter baumannii*. *Microorganisms* **2021**, *9*, 2104. [CrossRef]
12. Kim, S.; Lee, D.W.; Jin, J.S.; Kim, J. Antimicrobial activity of LysSS, a novel phage endolysin, against *Acinetobacter baumannii* and *Pseudomonas aeruginosa*. *J. Glob. Antimicrob. Resist.* **2020**, *22*, 32–39. [CrossRef]

Novel approaches to manage antimicrobial resistances: a story of vaccine research and divisome inhibition.

13. Styles, K.M.; Thummeepak, R.; Leungtongkam, U.; Smith, S.E.; Christie, G.S.; Millard, A.; Moat, J.; Dowson, C.G.; Wellington, E.M.H.; Sitthisak, S.; et al. Investigating bacteriophages targeting the opportunistic pathogen *Acinetobacter baumannii*. *Antibiotics* **2020**, *9*, 200. [CrossRef]
14. Schooley, R.T.; Biswas, B.; Gill, J.J.; Hernandez-Morales, A.; Lancaster, J.; Lessor, L.; Barr, J.J.; Reed, S.L.; Rohwer, F.; Benler, S.; et al. Development and use of personalized bacteriophage-based therapeutic cocktails to treat a patient with a disseminated resistant *Acinetobacter baumannii* Infection. *Antimicrob. Agents Chemother.* **2017**, *61*, e00954-17. [CrossRef]
15. Wachino, J.I.; Jin, W.; Kimura, K.; Arakawa, Y. Intercellular transfer of chromosomal antimicrobial resistance genes between *Acinetobacter baumannii* strains mediated by prophages. *Antimicrob. Agents Chemother.* **2019**, *63*, e00334-19. [CrossRef]
16. Mwangi, J.; Hao, X.; Lai, R.; Zhang, Z.Y. Antimicrobial peptides: New hope in the war against multidrug resistance. *Zool. Res.* **2019**, *40*, 488–505. [CrossRef]
17. Chen, S.P.; Chen, E.H.; Yang, S.Y.; Kuo, P.S.; Jan, H.M.; Yang, T.C.; Hsieh, M.Y.; Lee, K.T.; Lin, C.H.; Chen, R.P. A systematic study of the stability, safety, and efficacy of the de novo designed antimicrobial peptide PepD2 and its modified derivatives against *Acinetobacter baumannii*. *Front. Microbiol.* **2021**, *12*, 678330. [CrossRef]
18. Xiong, Y.Q.; Li, L.; Zhou, Y.; Kraus, C.N. Efficacy of ARV-1502, a proline-rich antimicrobial peptide, in a murine model of bacteremia caused by Multi-Drug Resistant (MDR) *Acinetobacter baumannii*. *Molecules.* **2019**, *24*, 2820. [CrossRef]
19. de Breij, A.; Riool, M.; Cordfunke, R.A.; Malanovic, N.; de Boer, L.; Koning, R.I.; Ravensbergen, E.; Franken, M.; van der Heijde, T.; Boekema, B.K.; et al. The antimicrobial peptide SAAP-148 combats drug-resistant bacteria and biofilms. *Sci. Transl. Med.* **2018**, *10*, eaan4044. [CrossRef]
20. Spencer, J.J.; Pitts, R.E.; Pearson, R.A.; King, L.B. The effects of antimicrobial peptides WAM-1 and LL-37 on multidrug-resistant *Acinetobacter baumannii*. *Pathog. Dis.* **2018**, *76*, fty007. [CrossRef]
21. Lei, J.; Sun, L.; Huang, S.; Zhu, C.; Li, P.; He, J.; Mackey, V.; Coy, D.H.; He, Q. The antimicrobial peptides and their potential clinical applications. *Am. J. Transl. Res.* **2019**, *11*, 3919–3931. [PubMed]
22. Grygorcewicz, B.; Roszak, M.; Golec, P.; Śleboda-Taront, D.; Łubowska, N.; Górska, M.; Jursa-Kulesza, J.; Rakoczy, R.; Wojciuk, B.; Dołęgowska, B. Antibiotics act with vB_AbaP_AGC01 phage against *Acinetobacter baumannii* in human heat-inactivated plasma blood and *Galleria mellonella* models. *Int. J. Mol. Sci.* **2020**, *21*, 4390. [CrossRef] [PubMed]
23. Zharkova, M.S.; Orlov, D.S.; Golubeva, O.Y.; Chakchir, O.B.; Eliseev, I.E.; Grinchuk, T.M.; Shamova, O.V. Application of antimicrobial peptides of the innate immune system in combination with conventional antibiotics-A novel way to combat antibiotic resistance? *Front. Cell Infect Microbiol.* **2019**, *9*, 128. [CrossRef] [PubMed]
24. Paulussen, F.M.; Schouten, G.K.; Moertl, C.; Verheul, J.; Hoekstra, I.; Koningstein, G.M.; Hutchins, G.H.; Alkir, A.; Luirink, R.A.; Geerke, D.P.; et al. Covalent proteomimetic inhibitor of the bacterial FtsQB divisome complex. *J. Am. Chem. Soc.* **2022**, *144*, 15303–15313. [CrossRef] [PubMed]
25. Di Somma, A.; Avitabile, C.; Cirillo, A.; Moretta, A.; Merlino, A.; Paduano, L.; Duilio, A.; Romanelli, A. The antimicrobial peptide Temporin L impairs *E. coli* cell division by interacting with FtsZ and the divisome complex. *Biochim. Biophys. Acta Gen. Subj.* **2020**, *1864*, 129606. [CrossRef] [PubMed]
26. Trespidi, G.; Scoffone, V.C.; Barbieri, G.; Riccardi, G.; De Rossi, E.; Buroni, S. Molecular characterization of the *Burkholderia cenocepacia dcw* operon and FtsZ interactors as new targets for novel antimicrobial design. *Antibiotics* **2020**, *9*, 841. [CrossRef]
27. Kumar, M.; Mathur, T.; Barman, T.K.; Chaira, T.; Kumar, R.; Joshi, V.; Pandya, M.; Sharma, L.; Fujii, K.; Bandgar, M.; et al. Novel FtsZ inhibitor with potent activity against *Staphylococcus aureus*. *J. Antimicrob. Chemother.* **2021**, *76*, 2867–2874. [CrossRef]
28. Monterroso, B.; Zorrilla, S.; Sobrinos-Sanguino, M.; Robles-Ramos, M.A.; López-Álvarez, M.; Margolin, W.; Keating, C.D.; Rivas, G. Bacterial FtsZ protein forms phase-separated condensates with its nucleoid-associated inhibitor SlmA. *EMBO Rep.* **2019**, *20*, e45946. [CrossRef]
29. Scoffone, V.C.; Ryabova, O.; Makarov, V.; Iadarola, P.; Fumagalli, M.; Fondi, M.; Fani, R.; De Rossi, E.; Riccardi, G.; Buroni, S. Efflux-mediated resistance to a benzothiadiazol derivative effective against *Burkholderia cenocepacia*. *Front. Microbiol.* **2015**, *6*, 815. [CrossRef]
30. Hogan, A.M.; Scoffone, V.C.; Makarov, V.; Gislason, A.S.; Tesfu, H.; Stietz, M.S.; Brassinga, A.K.C.; Domaratzki, M.; Li, X.; Azzalin, A.; et al. Competitive fitness of essential gene knockdowns reveals a broad-spectrum antibacterial inhibitor of the cell division protein FtsZ. *Antimicrob. Agents Chemother.* **2018**, *62*, e01231-18. [CrossRef]
31. Chiarelli, L.R.; Scoffone, V.C.; Trespidi, G.; Barbieri, G.; Riabova, O.; Monakhova, N.; Porta, A.; Manina, G.; Riccardi, G.; Makarov, V.; et al. Chemical, Metabolic, and Cellular Characterization of a FtsZ Inhibitor Effective Against *Burkholderia cenocepacia*. *Front. Microbiol.* **2020**, *11*, 562. [CrossRef]
32. Costabile, G.; Provenzano, R.; Azzalin, A.; Scoffone, V.C.; Chiarelli, L.R.; Rondelli, V.; Grillo, I.; Zinn, T.; Lepioshkin, A.; Savina, S.; et al. PEGylated mucus-penetrating nanocrystals for lung delivery of a new FtsZ inhibitor against *Burkholderia cenocepacia* infection. *Nanomed. J.* **2020**, *23*, 102–113. [CrossRef]
33. Trespidi, G.; Scoffone, V.C.; Barbieri, G.; Marchesini, F.; Abualsha'ar, A.; Coenye, T.; Ungaro, F.; Makarov, V.; Migliavacca, R.; De Rossi, E.; et al. Antistaphylococcal activity of the FtsZ inhibitor C109. *Pathogens* **2021**, *10*, 886. [CrossRef]
34. Vandecandelaere, I.; Van Acker, H.; Coenye, T. A microplate-based system as in vitro model of biofilm growth and quantification. *Methods Mol. Biol.* **2016**, *1333*, 53–66.
35. Harding, C.M.; Hennon, S.W.; Feldman, M.F. Uncovering the mechanisms of *Acinetobacter baumannii* virulence. *Nat. Rev. Microbiol.* **2018**, *16*, 91–102. [CrossRef]

36. Peleg, A.Y.; Seifert, H.; Paterson, D.L. *Acinetobacter baumannii*: Emergence of a successful pathogen. *Clin. Microbiol. Rev.* **2008**, *21*, 538–582. [CrossRef]
37. Hughes, S.; Troise, O.; Donaldson, H.; Mughal, N.; Moore, L.S.P. Bacterial and fungal coinfection among hospitalized patients with COVID-19: A retrospective cohort study in a UK secondary-care setting. *Clin. Microbiol. Infect.* **2020**, *26*, 1395–1399. [CrossRef]
38. Tomlinson, B.R.; Denham, G.A.; Torres, N.J.; Brzozowski, R.S.; Allen, J.L.; Jackson, J.K.; Eswara, P.J.; Shaw, L.N. Assessing the role of cold-shock protein C: A novel regulator of *Acinetobacter baumannii* biofilm formation and virulence. *Infect. Immun.* **2022**, *90*, e0037622. [CrossRef]
39. Chai, W.C.; Whittall, J.J.; Polyak, S.W.; Foo, K.; Li, X.; Dutschke, C.J.; Ogunniyi, A.D.; Ma, S.; Sykes, M.J.; Semple, S.J.; et al. Cinnamaldehyde derivatives act as antimicrobial agents against *Acinetobacter baumannii* through the inhibition of cell division. *Front. Microbiol.* **2022**, *29*, 967949. [CrossRef]
40. The European Committee on Antimicrobial Susceptibility Testing. EUCAST Reading Guide for Broth Microdilution. Version 2.0. 2022. Available online: https://www.eucast.org/fileadmin/src/media/PDFs/EUCAST_files/Disk_test_documents/2022_manuals/Reading_guide_BMD_v_4.0_2022.pdf (accessed on 1 January 2022).
41. Elshikh, M.; Ahmed, S.; Funston, S.; Dunlop, P.; McGaw, M.; Marchant, R.; Banat, I.M. Resazurin-based 96-well plate microdilution method for the determination of minimum inhibitory concentration of biosurfactants. *Biotechnol. Lett.* **2016**, *38*, 1015–1019. [CrossRef]
42. Eales, M.G.; Ferrari, E.; Goddard, A.D.; Lancaster, L.; Sanderson, P.; Miller, C. Mechanistic and phenotypic studies of bicarinalin, BP100 and colistin action on *Acinetobacter baumannii*. *Res. Microbiol.* **2018**, *169*, 296–302. [CrossRef] [PubMed]
43. Heydorn, A.; Nielsen, A.T.; Hentzer, M.; Sternberg, C.; Givskov, M.; Ersbøll, B.K.; Molin, S. Quantification of biofilm structures by the novel computer program COMSTAT. *Microbiology* **2000**, *146*, 2395–2407. [CrossRef] [PubMed]

Novel approaches to manage antimicrobial resistances: a story of vaccine research and divisome inhibition.

vaccines

MDPI

Article

Identification by Reverse Vaccinology of Three Virulence Factors in *Burkholderia cenocepacia* That May Represent Ideal Vaccine Antigens

Samuele Irudal [1], Viola Camilla Scoffone [1], Gabriele Trespidi [1], Giulia Barbieri [1], Maura D'Amato [2], Simona Viglio [2], Mariagrazia Pizza [3], Maria Scarselli [4], Giovanna Riccardi [1] and Silvia Buroni [1,*]

[1] Department of Biology and Biotechnology "Lazzaro Spallanzani", University of Pavia, 27100 Pavia, Italy; samuele.irudal@iusspavia.it (S.I.); viola.scoffone@unipv.it (V.C.S.); gabriele.trespidi01@universitadipavia.it (G.T.); giulia.barbieri@unipv.it (G.B.); giovanna.riccardi@unipv.it (G.R.)
[2] Department of Molecular Medicine, University of Pavia, 27100 Pavia, Italy; maura.damato01@universitadipavia.it (M.D.); simona.viglio@unipv.it (S.V.)
[3] Imperial College South Kensington Campus, London SW7 2AZ, UK; m.pizza@imperial.ac.uk
[4] GlaxoSmithKline, 53100 Siena, Italy; maria.x.scarselli@gsk.com
* Correspondence: silvia.buroni@unipv.it; Tel.: +39-0382-985574

Abstract: The *Burkholderia cepacia* complex comprises environmental and clinical Gram-negative bacteria that infect particularly debilitated people, such as those with cystic fibrosis. Their high level of antibiotic resistance makes empirical treatments often ineffective, increasing the risk of worst outcomes and the diffusion of multi-drug resistance. However, the discovery of new antibiotics is not trivial, so an alternative can be the use of vaccination. Here, the reverse vaccinology approach has been used to identify antigen candidates, obtaining a short-list of 24 proteins. The localization and different aspects of virulence were investigated for three of them—BCAL1524, BCAM0949, and BCAS0335. The three antigens were localized in the outer membrane vesicles confirming that they are surface exposed. We showed that BCAL1524, a collagen-like protein, promotes bacteria auto-aggregation and plays an important role in virulence, in the *Galleria mellonella* model. BCAM0949, an extracellular lipase, mediates piperacillin resistance, biofilm formation in Luria Bertani and artificial sputum medium, rhamnolipid production, and swimming motility; its predicted lipolytic activity was also experimentally confirmed. BCAS0335, a trimeric adhesin, promotes minocycline resistance, biofilm organization in LB, and virulence in *G. mellonella*. Their important role in virulence necessitates further investigations to shed light on the usefulness of these proteins as antigen candidates.

Keywords: *Burkholderia cepacia* complex; reverse vaccinology

check for updates

Citation: Irudal, S.; Scoffone, V.C.; Trespidi, G.; Barbieri, G.; D'Amato, M.; Viglio, S.; Pizza, M.; Scarselli, M.; Riccardi, G.; Buroni, S. Identification by Reverse Vaccinology of Three Virulence Factors in *Burkholderia cenocepacia* That May Represent Ideal Vaccine Antigens. *Vaccines* **2023**, *11*, 1039. https://doi.org/10.3390/vaccines11061039

Academic Editor: Alan Cross

Received: 19 April 2023
Revised: 24 May 2023
Accepted: 26 May 2023
Published: 30 May 2023

1. Introduction

Burkholderia cepacia complex (Bcc) is a group of Gram-negative aerobic bacteria comprising 24 different species, isolated from both environmental and clinical settings [1,2]. While they can promote plant growth and provide protection from phytopathogens [3,4], they pose an important threat not only to people affected by cystic fibrosis (CF) and chronic granulomatous disease (CGD) [5], but even to patients exposed to other risk factors, such as diabetes or renal affections [6,7]. When lungs are involved, recurrent infections can lead to a progressive loss of functions, which will eventually produce episodes of pulmonary exacerbation [8], or even a diffuse systemic infection associated with a fatal and rapid necrotizing pneumonia, called "cepacia syndrome" [9]. A growing concern is represented by an increasing number of outbreaks caused by contaminated disinfectant solutions and medical devices, leading to large and multi-structure breakouts [10–12]. Choosing a proper antibiotic treatment is usually difficult and relies on circumstances, as empirical treatments

often fail thus leading to unfavorable outcomes and eventually to the rise of further resistant strains [13]. In this light, the need for novel strategies to control these bacteria becomes mandatory, moving the attention from infection treatment to infection prevention [11,14].

Prophylactic vaccination appears to be a valuable strategy to protect fragile populations and minimize both transmission and antibiotic resistance spread, providing an alternative to expensive and burdensome drug treatments. Today, there is no vaccine available against Bcc [15], but many groups have focused on this issue, e.g., on live attenuated formulations. A *B. cenocepacia tonB* mutant was able to induce protection from acute and lethal infection in mice, with a survival of 87.5% after 6 days [16]. Conversely, higher efforts have been undertaken toward subunit vaccines, as multiple membrane proteins could be identified using bioinformatics tools and genome-available information. For example, a mixture of OMPs and a 17 kDa OmpA-like protein complexed with mucosal adjuvant were able to induce mucosal protection against *Burkholderia multivorans* and *B. cenocepacia*, while in some cases a balanced Th1/Th2 response was observed [17,18]. Furthermore, purified OmpA-like protein BCAL2958 was able to react to serum from CF patients infected with Bcc strains, leading to IgG production and an increase in neutrophils activation markers [19]. Finally, OmpW and linocin-immunized mice were able to induce both antigen-specific responses and cytokines production, conferring protection against *B. cenocepacia* and *B. multivorans* [20].

Regarding antigens' discovery, a combination of protein prediction tool and surface-protein shaving approach led to the identification of 16 extracellular proteins [21]; 3 proteins reacted to serum from Bcc-infected CF patients, thus confirming their immunogenicity. BCAL2645, one of the three identified proteins, was later proven to be involved in CFBE41o- cells adhesion and invasion [22]. Similarly, Sousa et al., [23] identified nine extracellular proteins conserved inside Bcc by reacting culture supernatant to serum from chronically infected CF patients.

In another study, a peptidoglycan-associated lipoprotein deletion mutant was produced in *B. cenocepacia* [24] and showed a reduced mortality in *Galleria mellonella*, decreased adhesion to epithelial cells, sensitivity to polimyxin and lower proinflammatory stimulation compared to the WT, all traits making it a valuable therapeutic target.

Proteins belonging to trimeric autotransporter adhesin [TAA] category were characterized by Pimenta et al. [25] who proved the role of BCAM2418 in adhesion to mucins and host cells. An antibody generated against its N-terminal was able to prevent this interaction and to successfully protect *G. mellonella* larvae after *B. cenocepacia* K56-2 challenge. In addition, Mil-Homens et al. [26] characterized the TAA BCAM0224 as involved in biofilm formation and swarming motility, immunoevasion and interaction with epithelial cells.

In this article, we applied, for the first time, the "reverse vaccinology" approach [27] to *B. cenocepacia* to identify novel antigen candidates. Applying prediction tools and strains conservation analysis, we identified 24 new antigens and selected 2 of them for further analysis.

2. Materials and Methods

2.1. Bioinformatic Analysis

The complete genomes of the strains listed in Table 1 were annotated using the Rapid Annotation Subsystem Technology (RAST) tool [28]. The *B. cenocepacia* J2315 genome was compared with each analyzed genome and with the annotated genome of *Escherichia coli* K12.

Proteins were selected according to the following parameters: conservation among the compared *Burkholderia* strains had to be >65%; conservation into the non-pathogenic *E. coli* K12 strain had to be <30% to prioritize Bcc-specific proteins; length of the amino acid sequence had to be >230 residues to drive the selection toward multidomain and presumably multi-function antigens; and finally, proteins with an identity of 100% in all pathogenic strains were excluded, because they did not undergo immunity selective pressure [29]. Localization prediction was performed using pSORT [30]. The functional prediction was performed using InterProScan [31]. To exclude proteins with a homology similar to human

Novel approaches to manage antimicrobial resistances: a story of vaccine research and divisome inhibition.

ones, a BLAST analysis was used [32]. TMHMM, Phobius and HMMTOP were employed to predict transmembrane domains and to exclude proteins with more than one transmembrane domain [33–35]. Proteins were analyzed using Vaxign [36] and VaxiJen [37] and the antigenicity score values were accepted when ≥90.9 or ≥0.5, respectively. Structural information, if available, was collected from RCSB PDB [38].

Table 1. List of the *Burkholderia* genomes used for the annotation.

Strain	Source
B. ambifaria AMMD	cell culture
B. anthina AZ-4-10-S1-D7	soil
B. cepacia ATCC25416	wash glove
B. cenocepacia J2315	CF sputum
B. cenocepacia DDS-22E-1	aerosol sample
B. cenocepacia H111	CF patient
B. cenocepacia HI12424	cell culture
B. cenocepacia MSMB384WGS	water
B. cenocepacia VC12308	CF sputum
B. cenocepacia YG-3	cell culture
B. contaminans SK875	pig with swine respiratory disease
B. diffusa RF2-nonBP9	soil
B. dolosa AU0158	CF patient
B. lata A05	blood of patient with cepacia syndrome
B. latens AU17928	CF Maxillary Sinus
B. gladioli ATCC10248	plant
B. glumae 257SH-1	rice panicles
B. metallica FL-6-5-30-S1-D7	soil
B. multivorans ATCCBAA-247	CF patient
B. pyrrocinia DSM10685	soil
B. seminalis FL-5-4-10S1-D7	soil
B. stabilis ATCC BAA-67	CF sputum
B. stagnalis MSMB735WGS	soil
B. territorii RF8-non-BP5	soil
B. ubonensis MSMB1471WGS	soil
B. vietnamiensis AU1233	CF blood

2.2. Bacterial Strains and Plasmids

The strains used in this work are listed in Table S1. *E. coli* and *B. cenocepacia* strains were grown in Luria–Bertani (LB) broth (Difco) or in artificial sputum medium (ASM) [39], with shaking at 200 rpm, or on LB agar plates at 37 °C. When necessary, cultures were supplemented with antibiotics: tetracycline (20 µg/mL for *E. coli* and 250 µg/mL for *B. cenocepacia*), kanamycin (40 µg/mL), trimethoprim (50 µg/mL for *E. coli* and 200 µg/mL for *B. cenocepacia*), chloramphenicol (30 µg/mL for *E. coli* and 400 µg/mL for *B. cenocepacia*) and ampicillin (200 µg/mL).

2.3. General Molecular Biology Techniques

Upstream and downstream DNA sequences (about 500 bp each) flanking the deletion target genes were amplified using a template *B. cenocepacia* K56-2 genomic DNA. The PCR amplifications were performed using HotStar HiFidelity Polymerase kit (Qiagen, Hilden, Germany); primers sequences are listed in Table S2. Fragments were cloned into the suicide vector pGPI-SceI-X_{cm} *Bam*HI/*Xba*I, using Gibson® assembly kit (NEB, Ipswich, MA, USA). Gene deletions were performed as previously described by Hamad et al. [40]. Deletions were confirmed via PCR amplification with the primers pairs listed in Table S2, and sequencing. The curing of the mutant strains was obtained by growth in LB medium. To complement each deleted strain, *BCAL1524* (1674 bp), *BCAM0949* (1099 bp) and *BCAS0335* (3595 bp) genes were amplified using *B. cenocepacia* K56-2 DNA as template and the primers pairs are listed in Table S3. Fragments were cloned into the vectors pAP20 (*Eco*RI/*Xba*I) [41] and pSCrhaB2 (*Nde*I/*Xba*I) [42] using the Gibson® assembly kit. The

complementation plasmids were introduced into the mutants by conjugation. The growth of all the mutants was measured by culturing the strains in LB or ASM and measuring the OD600 and plating the cultures every 60 min for 24 h. Complementation experiments with the inducible vector pSCrhaB2 were carried out with 0.01% of rhamnose.

2.4. Proteomic Analysis

B. cenocepacia mutant strains were grown in 50 mL of LB medium or ASM for 18 h. Cells were harvested and pellets were used for membrane extraction, while supernatants were used for outer membrane vesicles (OMVs) purification. Membrane fractions were prepared as previously described [43]. For OMV purification, supernatants were collected and, to completely remove the bacterial cells from the supernatant, they were filtered through a 0.45 µm cellulose membrane. The cell-free supernatants were ultrafiltrated using a centrifugal filter Amicon® (Merck Millipore, Burlington, MA, USA) with 100,000 Da NMWL, until a final volume of 1 mL, removing the non-OMV-associated proteins, such as flagella [44].

The analysis of the membrane fractions and of the OMVs was performed as previously described, via 2D gel electrophoresis [45]. Samples were precipitated with 10:1 2.7 M trichloroacetic acid, incubated in ice for 30′ and centrifuged for 15′ at 14,000 rpm. Pellets were then resuspended in 125 µL of 8M Urea, 4% CHAPS, 0.1 M Dithioerythritol (UCD), and 0.625 µL of 0.5% bromophenol blue and 0.7 µL of IPG buffer pH 3–10 (GE-Healthcare, Chicago, IL, USA) were added. Samples were then incubated for 1 h on an isoelectric focusing strip (pH 3–10). Isoelectric focusing was performed at 20 °C according to the program described in Table 2.

Table 2. Isoelectric focusing program.

Time	Voltage (V)
1 h	0
8 h	30
1 h	12
30 min	300
3 h	Up to 3500
10 min	500
Overnight	7950

Next morning, strips were equilibrated for 12 min with buffer A (6 M Urea, 2% SDS, 50 mM TRIS-HCl pH 6.8, 30% Glycerol, and 0.1 M Dithioerythritol) and then for 5 min in buffer B (6 M Urea, 2% SDS, 50 mM Tris-HCl pH 6.8, 30% Glycerol, 0.1 M Iodoacetamide, and 125 µL of 0.5% bromophenol blue). Mass weight separation (second dimension) was performed on a polyacrylamide gel formed by a 12.5% running gel and a 5% stacking gel. Briefly, 0.5% agarose was dissolved in running buffer to immobilize the strips.

Gels were digitalized using the ChemiDoc XRS system (Biorad, Hercules, CA, USA); spots were detected using PDQuest Advanced 8.0.1 program (Biorad, Hercules, CA, USA) [46]. Experiments were performed in triplicate.

2.5. Antimicrobial Susceptibility Testing for Planktonic Cells

MICs were determined in triplicate according to the EUCAST broth microdilution method [47] in U-bottom 96-well microtiter plates using LB and ASM. Nalidixic acid, amikacin, aztreonam, ciprofloxacin, minocycline, piperacillin and tobramycin were obtained from Sigma-Aldrich (Merck Millipore, Burlington, MA, USA). Levofloxacin and sparfloxacin were obtained from Honeywell Fluka™ (Charlotte, NC, USA) and Meropenem from AstraZeneca (Cambridge, UK). The MIC was determined via the resazurin method [48].

Novel approaches to manage antimicrobial resistances: a story of vaccine research and divisome inhibition.

2.6. Bacterial Autoaggregation Assay

Bacterial aggregation was measured according to Bhargava et al. [49], with some modifications. Bacterial cultures were grown in LB broth, at 37 °C and 200 rpm, up to the late-exponential phase. Samples were centrifuged, cells were resuspended in Phosphate Buffer Saline (PBS) (PanReac-Applichem, Darmstadt, Germany) and optical density at 600 nm was measured and adjusted to 3. Samples were incubated at room temperature for 16 h in static conditions. After incubation, 50 µL were removed from the air–liquid interface and the OD600 was measured. The aggregation was expressed as the percentage respect to the starting OD600 = 3.

2.7. In Vitro Biofilm Formation Test in 96-Well Microtiter Plates

The biofilm formation of *B. cenocepacia* K56-2, mutant and complemented strains was tested using the crystal violet staining method [50]. The bacterial cells were cultured in LB or ASM O/N at 37 °C and diluted to OD600 equal to 0.05 (about 1×10^7 CFU/mL). Then, 200 µL of culture were pipetted into the microtiter plate. After 4 h of incubation, the supernatant (containing nonadherent cells) was removed and 200 µL of fresh sterile medium were added to each well and incubated for an additional 20 h at 37 °C. Biofilm biomass was quantified by staining with crystal violet and taking absorbance measurements at OD595. Results were expressed as the ratio between biofilm absorbance and planktonic bacteria absorbance.

2.8. Biofilm Evaluation by Confocal Laser Scanning Microscopy

B. cenocepacia K56-2 and the ΔBCAM0949 strains were cultured O/N in LB and diluted to an OD600 = 0.05 in the same medium. Bacterial suspension was added to the µSlide four chambered coverslip (Ibidi, Gräfelfing, Germany) for 4 h in LB, at 37 °C. The medium was removed and fresh LB medium was added. After overnight incubation, the medium was removed, and biofilms were washed twice with physiological solution and stained with Syto 9 (Invitrogen, Waltham, MA, USA) at a final concentration of 5 µM. A 63× oil immersion objective and a Leica (Wetzlar, Germany) DMi8 with 500 to 530 nm (green fluorescence representing Syto 9) emission filters were used to take five snapshots randomly at different positions in the confocal field of each chamber. The Z-slices were obtained every 0.3 microns. For visualization and processing of biofilm images, ImageJ was used. The thickness, biomass, roughness coefficient, and biofilm distribution were measured using the COMSTAT 2 software [51]. All confocal scanning laser microscopy experiments were performed three times, and standard deviations were measured.

2.9. Swimming Motility Assay

Motility assays were performed as previously described [52]. Briefly, 1 µL of the overnight culture was spotted in the middle of a swimming plate (agar 0.3%), allowed to dry for 30 min at room temperature and incubated for 16 h at 37 °C. Diameters of swimming halos were measured.

2.10. Infection in Galleria Mellonella

Strains were grown in LB broth, at 37 °C, 200 rpm, until OD_{600} = 0.5. Each larva was then infected with 10^5 CFU/mL in physiological solution (PS) [53], with an injection volume of 10 µL; control was performed by injecting PS. Larvae were placed in Petri dishes and kept in the dark at 30 °C. Live/dead count and health index scores [53,54] were registered after 24 h, 48 h and 72 h. For each experiment, at least 10 larvae per group were injected.

2.11. Lipase Activity Assay

Tributyrin agar plates (LB medium, 0.5% tributyrin, and 1.5% agar) were used for lipase activity detection [55]. Halos formed by the lipase activity around colonies were measured.

2.12. Rhamnolipid Analysis

Strains were inoculated in 10 mL of LB for 48 h at 37 °C at 200 rpm. To quantify the amount of rhamnolipids in the culture supernatant, the colorimetric orcinol assay was used [56]. A volume of the supernatant (50 to 500 µL) was diluted with water to reach the volume of 500 µL. Samples were extracted twice with 2 volumes of diethyl ether. The ether fractions were evaporated and the pellets were dissolved in 100 µL of distilled water and mixed with 100 µL 1.6% orcinol and 800 µL of 60% sulfuric acid. Samples were incubated at 80 °C at 175 rpm for 30 min. After incubation, the OD421 was measured. The rhamnolipid concentration was calculated using a standard concentration curve with rhamnose standards on the assumption that 1 µg of rhamnose corresponds to 2.5 µg of rhamnolipid [57].

2.13. Statistical Methods

Analyses were performed using Prism 9.0 (GraphPad). Comparison of more than two groups were performed with the unpaired *t*-test, one-way or two-way ANOVA.

3. Results and Discussion

3.1. In Silico Identification of Antigen Candidates

The identification of antigen candidates was performed using the "reverse vaccinology" approach [27]. The scheme of the workflow is depicted in Figure 1. The genome of *B. cenocepacia* J2315 was used as reference [58], and annotated with the Rapid Annotation using Subsystem Technology (RAST) pipeline, a fully automated annotation engine for archaeal and bacterial genomes [28]. RAST identifies protein coding genes, assigns functions and gives a prediction of subsystems present in the genomes.

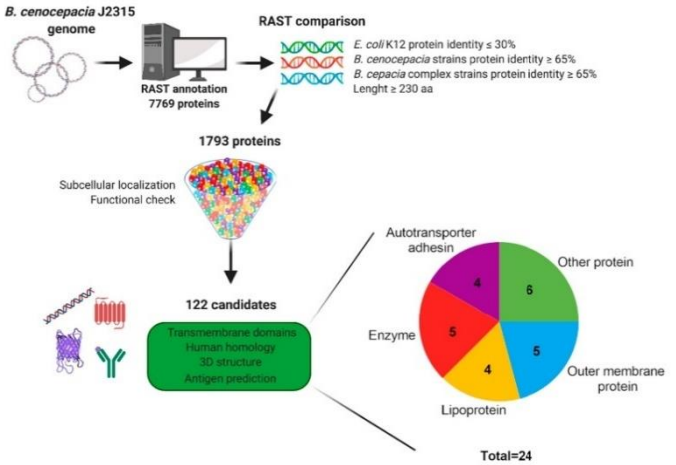

Figure 1. Schematic workflow of the in silico analysis. Reverse vaccinology was applied to the *B. cenocepacia* proteome to select novel vaccine candidates. The process starts with RAST software annotation and comparison, which led to the selection of 1793 candidates from 7769 proteins. These candidates were analyzed via different bioinformatics tools and bibliographic information, which further selected 122 proteins. At the end, 24 antigen candidates were selected based on the presence and number of transmembrane domains, low homology with human proteins, 3D structure and antigenicity prediction (created with BioRender.com, accessed on 5 May 2023).

Novel approaches to manage antimicrobial resistances: a story of vaccine research and divisome inhibition.

The annotation of *B. cenocepacia* J2315 genome provided 7769 protein encoding genes as an output. Each genome was compared with the annotated genome of *E. coli* K-12 and with the genomes of six *B. cenocepacia* strains and eighteen Bcc strains (Table 1). The parameters to select putative antigen candidates were as follows: identity with *E. coli* K-12 proteins less or equal to 30% and identity with the proteins of *B. cenocepacia* and Bcc strains higher than 65%. Since immunogenic proteins are generally localized on the outer membrane and have more complex structures created by multiple domains, (e.g., transmembrane and extracellular domains), only proteins longer than 230 amino acids were selected. Using these parameters, a pool of 1793 proteins was obtained and analyzed for subcellular localization and putative function. The pool was reduced to 122 candidates predicted to be outer-membrane or extracellular, potentially involved in cell adhesion, virulence or with unknown function. Further analyses were performed to evaluate the transmembrane domains prediction, the homology with human proteins and the prediction of the antigenicity of the candidates as described in the "Materials and methods" section. The result is a short list of 24 antigen candidates belonging to different protein classes: 4 lipoproteins, 4 autotransporter adhesin proteins, 5 enzymes, 5 outer membrane proteins and 6 other proteins (Table 3, Figure 1).

Table 3. Selected antigen candidates.

Protein Name	Functional Prediction	Protein Type	Length aa	Cellular Localization Prediction	N° of Predicted TMD	VaxiJen Score	Vaxign-ML Score
BCAL0151	ABC-type branched-chain amino acid transport systems, periplasmic component	Extracellular ligand binding protein	381	unknown	Signal peptide	0.5863	98.9
BCAL0198	Outer membrane protein, OmpW	Putative outer membrane protein	278	unknown	8	0.6727	90.9
BCAL0199	DUF2957 domain-containing protein, putatative lipoprotein	Lipoprotein	414	unknown	Signal peptide	0.6030	95.2
BCAL0200	DUF2957 domain-containing protein, putative lipoprotein	Lipoprotein	477	extracellular	≤1	0.7576	90.9
BCAL0358	peptidase M1 family M1 metalopeptidase	Enzyme	723	extracellular	≤1	0.4835	99.7
BCAL1524	Collagen-like triple helix repeat-containing protein	Lipoprotein	558	extracellular	≤1	0.9966	90.9
BCAL2229	Beta-propeller fold lactonase family protein, surface antigen	Enzyme	330	extracellular	≤1	0.3297	90.9
BCAL2615	Putative exported outer membrane porin protein	Putative outer membrane protein	359	outermembrane	16	0.6883	91.0
BCAL3279	DUF3971 domain-containing protein, Possible exported protein	Hypothetical protein	1400	extracellular	1	0.5901	90.9
BCAL3353	Putative outer membrane autotransporter	Autotransporter/ adhesin protein	1772	outermembrane/ extracellular	≤1	0.8135	94.9
BCAM0949	LipA triacylglycerol lipase	Enzyme	365	extracellular	1	0.4937	90.9
BCAM1514	Outer membrane protein	Other protein	294	outermembrane	≥1	0.6875	90.9
BCAM1737	Alpha-2-macroglobulin	Other protein	2021	outermembrane	1	0.6400	97.7

Table 3. *Cont.*

Protein Name	Functional Prediction	Protein Type	Length aa	Cellular Localization Prediction	N° of Predicted TMD	VaxiJen Score	Vaxign-ML Score
BCAM1740	Adhesin	Lipoprotein	233	extracellular	≥1	0.6559	90.9
BCAM1931	Outer membrane porin	Putative outer membrane protein	360	outermembrane	16	0.6868	92.5
BCAM2311	Outer membrane porin OmpC	Putative outer membrane protein	380	outermembrane	16	0.5846	91.4
BCAM2328	Coagulation factor 5/8 type-like protein	Other protein	470	extracellular	1	0.5850	95.4
BCAM2418	Cell surface protein putative haemagglutinin-related autotransporter/adhesin protein	Autotransporter/ adhesin protein	558	extracellular	1	0.9141	93.5
BCAM2444	NHL-superfamily, Six-bladed beta-propeller, TolB-like	Other protein	643	extracellular	≤1	0.5015	95.0
BCAS0147	YncE super family, beta-propeller fold lactonase family protein	Enzyme	397	outermembrane/ extracellular	1	0.6027	90.9
BCAS0236	putative haemagglutinin-related autotransporter/adhesin protein	Autotransporter/ adhesin protein	1497	outermembrane/ extracellular	≤1	0.8682	92.2
BCAS0321	Autotransporter	Autotransporter/ adhesin protein	4250	outermembrane	≥1	1.115	90.9
BCAS0335	putative haemagglutinin-related autotransporter/adhesin protein	Autotransporter/ adhesin protein	1198	extracellular	≤1	0.8436	98.9
BCAS0409	M4 family metallopeptidase	Enzyme	566	extracellular	≤1	0.6513	95.0
BCAS0641	phosphatase PAP2 family protein	Enzyme	464	unknown	≤1	0.6073	93.9

Among them, BCAM0949, BCAM2418, BCAS0409 and BCAS0236 were previously described as being involved in virulence and cell adhesion [25,59–61]. BCAS0147 was described as surface exposed [21]; BCAM1514 and BCAS0409 were localized in the outer membrane fraction in the CF niche [62].

Three antigens, the collage-like protein BCAL1524, the lipase LipA BCAM0949 and the autotransporter adhesin BCAS0335 were selected for further analysis. The rationale for the selection is described below. Collagen-like proteins, characterized by a collagen-like (CL) domain containing Gly-Xaa-Yaa amino acid repetition and organized in a triple helix-structure, are widespread in pathogenic bacteria and highly resemble human collagen [63]. Due to their structure, they can interact with different host factors promoting adhesion, inflammation and immunoreaction [64,65]. Additionally, Grund et al., [66] described the high Th2 immune response induced in mice immunized with *B. pseudomallei* collagen-like protein 8 (Bucl8) antigens, while studies on the role of these proteins in *B. cenocepacia* are still lacking. Lipases are commonly found in clinical *B. cepacia* complex isolates [67]. While evidence of their involvement in Bcc infection is still nominal [67,68], multiple studies reported their role in virulence and pathogenesis in *P. aeruginosa* [56,69,70]. Trimeric autotransporter adhesins are known to play a key role in virulence for a wide range of bacteria [71]; Pimenta et al. [25] and Mil-Homens et al. [26,72] extensively described their

role in adhesion and inflammation in epidemic *B. cenocepacia* epidemic strain K56-2, thus highlighting the putative role they may play as protective antigens.

3.2. Construction of Deletion Mutants of the Selected Antigen Candidates

To investigate the roles of these proteins in virulence and host pathogen interaction, deletion mutants were constructed in *B. cenocepacia* K56-2, since the amino acid sequence of the corresponding proteins was identical to J2315 and this strain is most amenable to genetic manipulation. The growth of the mutants and complemented strains was comparable to that of the WT K56-2 both in LB and in ASM media (Figure S1).

3.3. Analysis of Protein Localization

To demonstrate that the antigen candidates selected are localized on the bacterial surface, a proteomic analysis of Outer Membrane Vesicles (OMV) derived from K56-2 and deleted strains was performed. As shown in Figure 2, when analyzed via the 2D electrophoresis, in the OMVs of the ΔBCAL1524 isogenic mutant strain, no spots were identified at the coordinate value corresponding to the BCAL1524 protein (isoelectric point 8.55 and molecular weight 49 kDa) (Figure 2B). In the OMVs of the K56-2 wild-type strain, a spot numbered 7308 with intensity of 27,944.8 mAu was identified at these coordinates (Figure 2A,C).

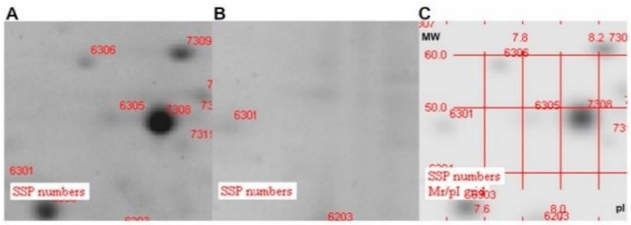

Figure 2. Zoom-in of two-dimensional gel electrophoresis (2DE)-stained gel with Coomassie. (**A**) 2D gel of K56-2 OMVs; (**B**) 2D gel of ΔBCAL1524 OMVs and (**C**) the 2D gels of OMV proteins superimposed with K56-2 and ΔBCAL1524. (MW: molecular weight; pI: isoelectric point).

The same applied to the OMV of ΔBCAM0949 and K56-2 strains electrophoresis of the OMVs of the K56-2, in which a spot numbered 4301 was identified at pI~6.4 and MW~42 kDa and intensity 3399.7 mAu, which was not present in the ΔBCAM0949 mutant OMVs (Figure 3). The MW and pI values of BCAM0949 are 38 kDa and 6.41, respectively.

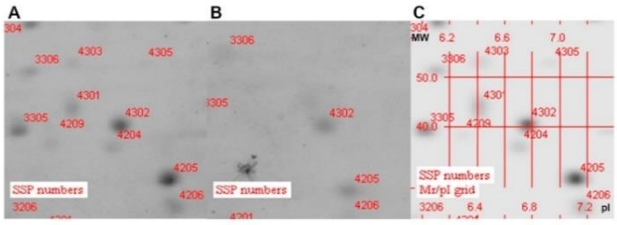

Figure 3. Zoom-in of two-dimensional gel electrophoresis (2DE)-stained gel with Coomassie. (**A**) 2D gel of K56-2 OMVs; (**B**) 2D gel of ΔBCAM0949 OMVs and (**C**) 2D gels of OMV proteins superimposed with K56-2 and ΔBCAM0949. (MW: molecular weight; pI: isoelectric point).

Finally, the OMVs 2D-electrophoresis of the K56-2 showed the spot number 3701 at pI 5.3 and MW 124 kDa with an intensity equal to 4156 mAu, lacking in the ΔBCAS0335 (Figure 4). The theoretical pI and MW of the BCAS0335 are 5.0 and 117 kDa, respectively.

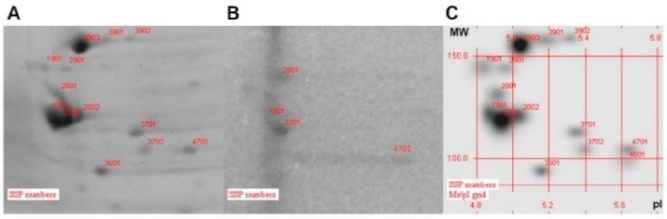

Figure 4. Zoom-in of two-dimensional gel electrophoresis (2DE)-stained gel with Coomassie. (**A**) 2D gel of K56-2 OMVs; (**B**) 2D gel of ΔBCAS0335 OMVs and (**C**) 2D gels of OMV proteins superimposed with K56-2 and ΔBCAS0335. (MW: molecular weight; pI: isoelectric point).

All these data demonstrate that the collagen-like protein BCAL1524, the lipase BCAM0949 and the trimeric-autotransporter adhesion BCAS0335 are expressed in the outer membrane vesicles compartment in the conditions tested. Two-dimensional gel electrophoresis full images are shown in Supplementary Materials (Figures S2–S5).

3.4. Antibiotic Susceptibility

To test the involvement of the selected proteins in antibiotic susceptibility, the minimal inhibitory concentration of 12 currently used antibiotics was determined against the deleted and complemented strains grown in LB. Piperacillin had an MIC which was four-fold lower in the ΔBCAM0949 strain with respect to the K56-2 in LB (32 μg/mL vs. 128 μg/mL) (in bold in Table 4). The deleted strain, complemented with the WT copy of the gene cloned into the rhamnose inducible vector pSCrhaB2, showed a reverted phenotype.

Table 4. Antimicrobial susceptibilities (μg/mL) of *B. cenocepacia* mutants and of the complemented strains.

	Antibiotics									
Strain	**AMK**	**AZT**	**CIP**	**LVX**	**MEM**	**MIN**	**NAL**	**PIP**	**SPX**	**TOB**
K56-2	≥256	≥256	2	4	8	8	16	128	4	≥256
ΔBCAL1524	≥256	256	2	4	8	4	8	128	4	≥256
ΔBCAM0949	≥256	256	2	4	4	16	16	**32**	4	≥256
ΔBCAS0335	≥256	256	4	4	8	**64**	16	128	4	≥256
ΔBCAL1524 pSCrhaB2*BCAM1524*	≥256	≥256	≤2	4	16	≤2	16	64	4	≥256
ΔBCAM0949 pSCrhaB2*BCAM0949*	≥256	≥256	≤2	4	4	≤2	4	**128**	4	≥256
ΔBCAS0335 pSCrhaB2*BCAS0335*	≥256	≥256	≤2	4	8	**4**	8	128	4	≥256

AMK, amikacin; ATM, aztreonam; CIP, ciprofloxacin; LVX, levofloxacin; MEM, meropenem; MIN, minocycline; NAL, nalidixic acid; PIP, piperacillin; SPX, sparfloxacin; TOB, tobramycin.

The MIC of minocycline was eight-fold higher in the ΔBCAS0335 strain than the K56-2 (64 μg/mL vs. 8 μg/mL) (in bold in Table 4). In this case, the complementation using the inducible vector pSCrhaB2 restored the phenotype of the K56-2 strain.

The MICs of the control strains carrying the empty pSCrhaB2 vector are listed in Table S4. It is to be noted that the presence of the empty vector did not affect strain phenotypes.

The MICs value for the ΔBCAL1524 did not show differences compared to the K56-2 in the conditions tested.

3.5. Phenotypic Characterization of the Deleted Mutant

3.5.1. Biofilm Formation

To assess the role of the three antigen candidates in sessile lifestyle, biofilm formation was evaluated using crystal violet assay in 96-well plates after 48 h of incubation. The results showed that the ΔBCAM0949 mutant strain produces a lower quantity of biofilm in both LB and ASM media with respect to the WT (Figure 5A,B). The ΔBCAS0335 mutant produced a slightly lower quantity of biofilm only in LB, compared to the K56-2 (Figure 5A). Complementation was carried out using the pAP20 constitutive vector. The complemented strains showed the reversion of the ΔBCAM0949 phenotype in LB and ASM (Figure 5C,D). Regarding the ΔBCAS0335 mutant, the mutant transformed with the empty vector did not show a significant decrease in biofilm production (Figure S6), but in the deleted strain the constitutive expression of the *BCAS0335* gene significantly increased the biofilm production in both the media tested (Figure 5C,D). The data suggest that both the lipase BCAM0949 and the autotransporter adhesin protein BCAS0335 contribute to biofilm formation. On the contrary, the collagen-like protein does not seem to have a role in this process in the condition tested. The data regarding the biofilm production in the control strains of the complementation carrying the empty pAP20 vector are reported in Figure S6.

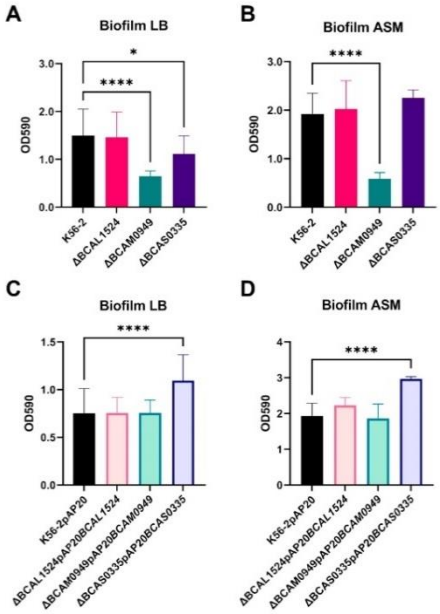

Figure 5. Graphical representation of the OD_{590} measured after the crystal violet assay comparing the biofilm formation of *B. cenocepacia* K56-2, deleted and complemented strains. (**A**) Biofilm of deleted strains in LB and (**B**) in ASM; (**C**) biofilm of complemented strains in LB and (**D**) in ASM. (* $p < 0.1$, **** $p < 0.0001$ one-way ANOVA test).

Since the difference in biofilm formation with respect to the K56-2 strain was higher in the lipase mutant, we decided to evaluate the biofilm formed by this strain using confocal laser scanning microscopy (CLSM). The obtained imaging showed that the biofilm formed by the ΔBCAM0949 mutant is less structured and thick in both conditions tested (LB and ASM) (Figure 6A).

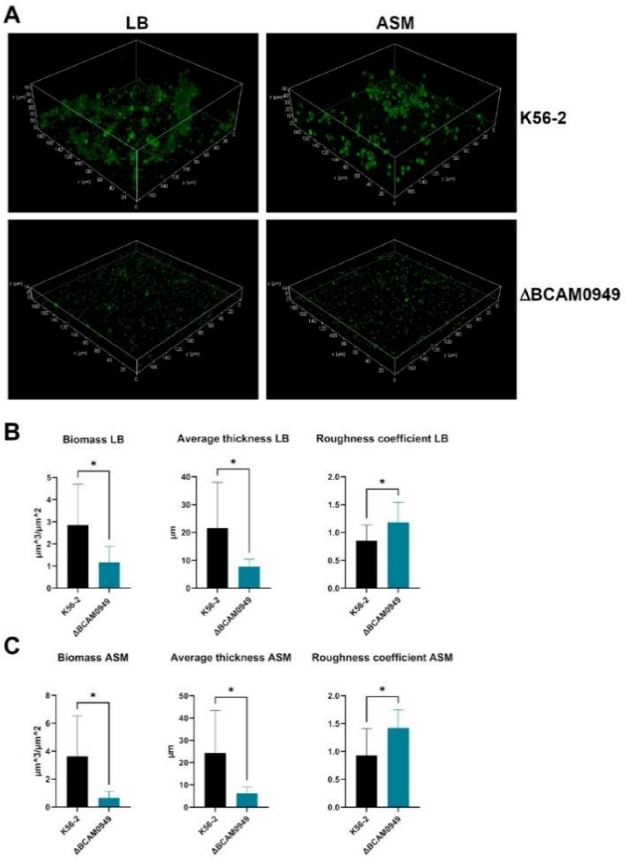

Figure 6. Biofilm evaluation using CLSM. (**A**) CLSM images of *B. cenocepacia* K56-2 and ΔBCAM0949 strains in LB and in ASM media. Biofilms were grown in chambered slides. Pictures were taken with an overall magnification of 400×. Cells were grown for 48 h at 37 °C in LB. Planes at equal distances along the Z-axis of the biofilms were imaged using CLSM. These images were stacked to reconstruct the 3D biofilm images. (**B**,**C**) Analysis of biofilm properties via COMSTAT 2. Measures of total biomass, average thickness and roughness coefficient are represented. Data are the mean ± SD of the results from three independent replicates. (* $p < 0.05$ unpaired t test).

The analysis using COMSTAT2 confirmed the qualitative evaluation of the biofilm. Biofilms formed in LB and ASM by the ΔBCAM0949 strain have a significantly lower biomass and average thickness (Figure 6B,C). Moreover, the roughness of the biofilm is significantly higher for the deleted strain (Figure 6B,C), indicating that the structure of the biofilm is altered.

All these data suggest that the lipase BCAM0949 has a role in biofilm formation and structure in the conditions tested.

3.5.2. Bacterial Autoaggregation

The involvement of the antigen candidates in bacterial autoaggregation, a process known to be involved in bacterial colonization and persistence in the host, was assessed using a precipitation-based assay. The decrease in the OD600 of the air–liquid interface after 16 h of static incubation is consistent with an increase in bacterial interaction, which promotes precipitation; on the contrary, if interactions are impaired, the OD600 is higher. The autoaggregation is expressed as the percentage of OD600 of the air–liquid interface with respect to the initial OD600 normalized to 3. For the K56-2 strain, the obtained value was 11.9%, while in the case of the ΔBCAL1524, ΔBCAM0949 and ΔBCAS0335 mutant strains it was 17.7%, 9.13% and 14.8% (Figure 7A), respectively.

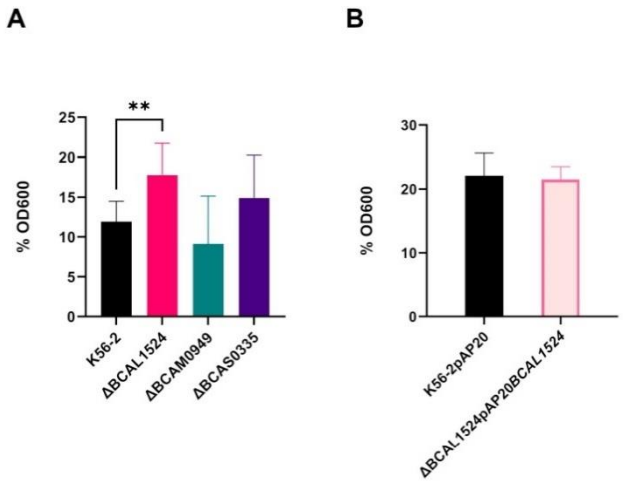

Figure 7. Quantitative autoaggregation assay. (**A**) Percentage of initial OD600 of K56-2 and deleted strains. (**B**) Percentage of initial OD600 of ΔBCAL1524 complemented strain. Data are the mean ± SD of the results from three independent replicates. (** $p < 0.01$ one-way ANOVA test).

When BCAL1524 protein was lacking, autoaggregation decreased as the percentage of residual OD600 after 16 h was increased. The proteins BCAM0949 and BCAS0335 are not involved in autoaggregation in the conditions tested.

The complementation with the pAP20*BCAL1524* vector restored a phenotype identical to the K56-2 (Figure 7B).

3.5.3. Swimming Motility

Swimming motility allows bacteria to diffuse through low viscosity medium, such as mucus, and it is considered a virulence determinant. Swimming motility of the deleted

strains was tested on 0.3% agar plates. In the ΔBCAM0949 mutant strain, the swimming phenotype was abolished (diameter of the motility halo 10.8 mm) compared to the K56-2 (27.8 mm) (Figure 8A,B). On the other hand, the two deleted mutant strains, ΔBCAL1524 and ΔBCAS0335, showed no differences compared to the K56-2 (Figure 8A,B).

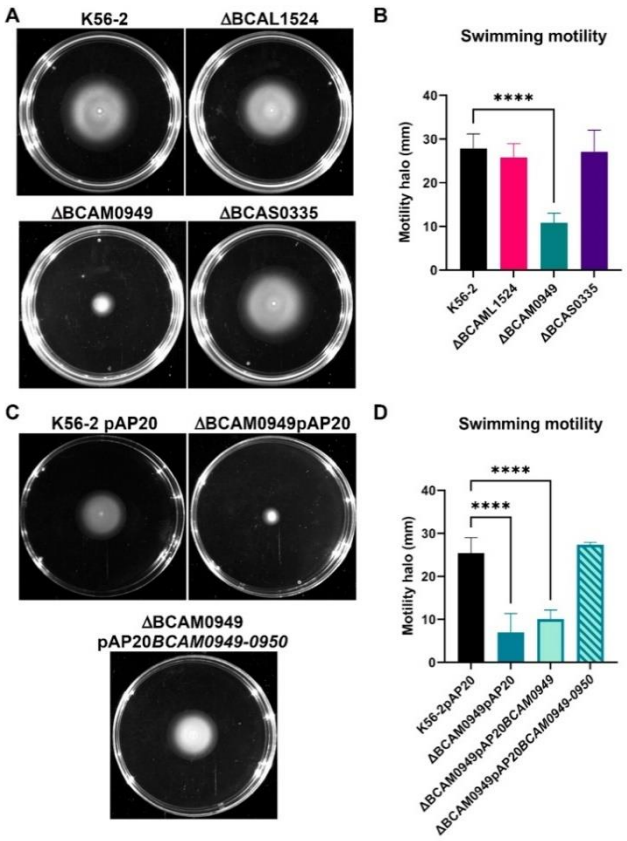

Figure 8. Swimming motility assay. (**A**) Swimming halo of K56-2 and deleted strains on LB 0.3% agar plate. (**B**) graphical representation of the swimming motility assay measurements (mm) of K56-2 and deleted strains. (**C**) Swimming halo of the complemented strains on LB 0.3% agar plate. (**D**) graphical representation of the swimming motility assay measurements (mm) of complemented strain. Data are the mean ± SD of the results from three independent replicates. (**** $p < 0.0001$ one-way ANOVA test).

The complementation was carried out using the entire *BCAM0949-BCAM0950* operon cloned into the vector pAP20 as the phenotype was not restored by expressing the only LipA (BCAM0949) protein. As reported by Papadopoulos et al. [73] and Putra et al. [74],

P. aeruginosa LipA and *Burkholderia territori* LipBT lipases have to be co-expressed with the relative foldase to avoid precipitation and to allow increased functional protein concentration, which would be required to complement some phenotypes. Indeed, upon complementation with the pAP20*BCAM0949-0950* construct, the swimming halo was restored to the diameter of the K56-2 (Figure 8C,D). The data suggest that while the proteins BCAL1524 and BCAS0335 are not involved in swimming motility, the lipase BCAM0949 has a pivotal role in this pathway in the conditions tested.

3.6. Infection in Galleria mellonella

G. mellonella larvae are a well-known invertebrate animal model for infection, as they provide a simple, fast, and cost-effective platform. After an infection with a dose of 10^3 CFU bacteria, symptoms started to appear 24 h post-infection (Figure 9A,B): at this time point, larvae infected with the ΔBCAL1524 and ΔBCAS0335 mutant strains showed a significantly higher health index score compared to the larvae infected with the K56-2. These larvae showed a lower melanization level than the larvae infected with the K56-2 (Figure 9B). On the contrary, infection with the ΔBCAM0949 mutant did not affect larval survival and health index scores compared to what was observed in larvae infected with the WT strain (K56-2).

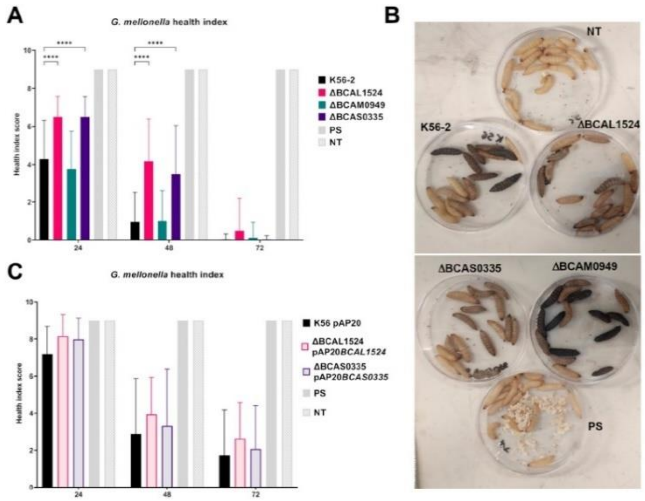

Figure 9. Graphical representation of *G. mellonella* health index. (**A**) Health index scores associated with infection with *B. cenocepacia* K56-2 and the mutants ΔBCAL1524, ΔBCAM0949, and ΔBCAS0335. Data are the mean ± SD of the results from three independent experimental replicates. (**** $p < 0.0001$ two-way ANOVA test). (**B**) *G. mellonella* larvae 24 h post treatment. PS: larvae injected with physiological solution; NT: not treated. (**C**) Health index scores associated with infection with *B. cenocepacia* K56-2 and complemented strains. Data are representative of the results of three independent experimental replicates.

To complement the observed phenotypes, the pAP20 vector was used. Complementation was achieved in the case of ΔBCAL1524 (8.15) and ΔBCAS0335 (7.9) as the K56-2 symptom score at 24 h post-infection was 7.56 (Figure 9C). The data regarding the health

index score of *G. mellonella* moths infected with the control strains of the complementation carrying the empty pAP20 vector are reported in Figure S7.

The data obtained suggest that the proteins BCAL1524 and BCAS0335 are involved in virulence in vivo, since their lack increases the health score of larvae injected with the corresponding deleted strains; thus, host immunization using these two antigens could provide protection from severe infection. On the contrary, deletion of BCAM0949 does not affect the in vivo virulence of the bacterium.

3.7. Characterization of the Lipase BCAM0949

3.7.1. Lipolytic Activity

Although the deletion of BCAM0949 has no effect on the in vivo virulence of *Burkholderia*, its amino acid sequence is characterized by a conserved domain of the triacylglycerol esterase/lipase superfamily, so we further characterized its activity. In other bacteria, such as *Pseudomonas aeruginosa*, several lipolytic enzymes are secreted or surface-exposed; among these is the EstA, which has a lipolytic activity, and is involved in rhamnolipid production and virulence [57]. To better characterize the lipase BCAM0949, the lipolytic activity of the deleted strain was compared to the K56-2 using the tributyrin agar plate assay (Figure 10).

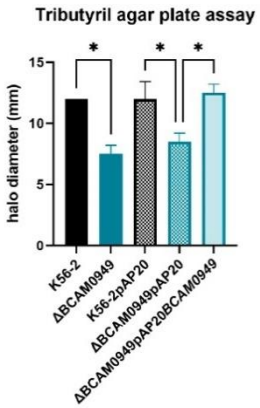

Figure 10. Lipolytic activity of K56-2, ΔBCAM0949 and complemented strains in terms of zone of hydrolysis (in mm) in tributyrin agar plate. Data are the mean ± SD of the results from three independent replicates (* $p < 0.1$ one-way ANOVA test).

The diameter of the lipolytic halo was measured and, as shown in Figure 10, the mutant strain has a lower lipolytic activity than the K56-2. The lipolytic activity is not completely blocked because the bacterium possesses other lipolytic enzymes. The complementation restored the lipolytic activity (Figure 10).

3.7.2. Rhamnolipid Production

In *P. aeruginosa*, EstA is involved in rhamnolipid production [57]. To study the involvement of the lipase BCAM0949 in rhamnolipid production, the quantity of rhamnolipids produced by the deleted strain was compared to the K56-2, showing that the deleted strain ΔBCAM0949 is impaired in their production (Figure 11).

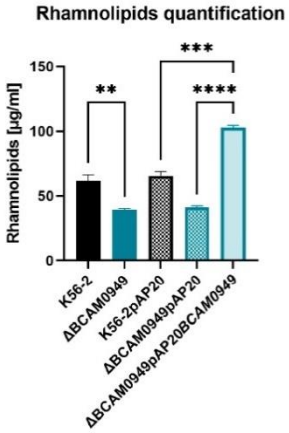

Figure 11. Quantitative determination of extracellular rhamnolipids produced by K56-2, ΔBCAM0949 and complemented strains as determined via the Orcinol test. SDs were calculated from three independent experiments. Data are the mean ± SD of the results from three independent replicates. (** $p < 0.01$, *** $p < 0.001$, **** $p < 0.0001$ one-way ANOVA test).

Complementation with the pAP20BCAM0949 vector not only restored the K56-2 phenotype, but induced an increase in rhamnolipids production (Figure 11). These results demonstrate the involvement of the protein BCAM0949 in rhamnolipid production.

All these data showed how the protein BCAM0949 has a role in the virulence pathway of rhamnolipid production. Since rhamnolipids play a role in outer membrane composition, cell motility and biofilm formation in other bacteria, BCAM0949 is also demonstrated to be involved in different virulence pathways.

4. Conclusions

In this work, reverse vaccinology was used to identify surface-exposed proteins which can be ideal antigen candidates for the development of a vaccine against the *B. cepacia* complex bacteria. We chose this strategy that previously revealed to be resolutive in cases for which the discovery of a vaccine seemed to be impossible [75]. It represents therefore a valuable option in the case of *Burkholderia* for which, despite numerous attempts to find suitable antigen candidates, a vaccine is not yet available. Starting from the bacterial genome, a short list of gene candidates, encoding extracellular proteins predicted to be ideal targets for the immune system, was selected. Among the 24 proteins identified, 3 of them were selected because of their homology with important virulence factors in other bacteria: BCAL1524, a lipoprotein containing a collagen-like triple helix repeat, able to interact with host cell adhesive proteins; BCAM0949, an extracellular lipase; BCAS0335, a trimeric autotransporter adhesin (TAAs) which interacts with the extracellular membrane components and host cell receptors and possesses hemagglutinin activity. Antigens used to develop vaccines do not necessarily have to be virulence factors, however, directing the immune response toward virulence determinants has been a successful rationale in eliciting protective immunity [76].

Hence, the role of these proteins in virulence was investigated by constructing marker-less deletion mutants of *B. cenocepacia* K56-2.

An important aspect of antigen candidates is their localization. To support the in silico prediction, a proteomic analysis of the deleted strains was performed and it demonstrated

that the three proteins are indeed localized in the outer membrane vesicle (OMV) compartments. The OMVs play a critical role in host–pathogen interaction and virulence, as they are produced in response to stress conditions and can carry bioactive molecules and virulence factors able to sustain bacterial growth and modulate host inflammation [77]; therefore, the presence of the three proteins in these compartments highlights their possible role in these pathways. Moreover, their localization on the bacterial surface could make them ideal targets for recognition by the host immune system.

The antibiotic susceptibility tests showed that BCAM0949 is involved in piperacillin resistance and BCAS0335 is involved in minocycline sensitivity. Considering the role and the localization of the two proteins, these results suggest that their absence may alter the membrane permeability, thus changing *Burkholderia* antibiotic susceptibility.

Virulence determinant analysis showed that the collagen-like protein BCAL1524 is involved in bacterial autoaggregation and has a role in *G. mellonella* infection, while the autotransporter adhesin BCAS0335 is involved in biofilm formation and promotes *G. mellonella* infection. This makes BCAL1524 and BCAS0335 suitable for further investigations as putative antigens.

On the other hand, the extracellular lipase BCAM0949 is involved in different virulence pathways: biofilm formation, autoaggregation and swimming motility. Further investigations on this protein showed its role as lipolytic enzyme and in rhamnolipid production, highlighting its similarity with the protein EstA of *P. aeruginosa* which is involved in virulence. Thus, considering their phenotypic analogy, LipA may be a homologous candidate of EstA protein, which still has not be found in *B. cenocepacia*. Hence, these data suggest that BCAM0949 could be considered as a protein which has a pivotal role in *B. cenocepacia* virulence.

Additional experiments will be fundamental to evaluate the immunogenicity of these antigens in vivo in the mouse model. On the basis of the potential role that these antigens play in virulence and their localization on the bacterial surface, it might be expected that the antibodies may impair their function by binding the antigens, thus generating the same phenotype of the isogenic mutant strains: reduction in adhesion, biofilm formation, membrane permeability and swimming motility.

Overall, this study provides the rationale for future functional characterization of novel vaccine candidates against Bcc, paving the way to discovering effective vaccines to prevent *Burkholderia* infections.

Supplementary Materials: The following supporting information can be downloaded at: https://www.mdpi.com/article/10.3390/vaccines11061039/s1, Table S1. Strains and plasmids used in this work [40–42,58,78]. Table S2. Primers used for deletion construction. Table S3. Primers used for complementation. Table S4. Antimicrobial susceptibilities (μg/mL) of *B. cenocepacia* wt, mutants and the complemented strains. Figure S1. Growth curves of WT and deleted strains. Figure S2. Two-dimensional gel electrophoresis (2DE)-stained gel with Coomassie of K56-2 OMV. Figure S3. Two-dimensional gel electrophoresis (2DE)-stained gel with Coomassie of ΔBCAL1524 OMV. Figure S4. Two-dimensional gel electrophoresis (2DE)-stained gel with Coomassie of ΔBCAM0949 OMV. Figure S5. Two-dimensional gel electrophoresis (2DE)-stained gel with Coomassie of ΔBCAS0335 OMV. Figure S6. Graphical representation of the OD590 measured after the crystal violet assay comparing the biofilm formation of *B. cenocepacia* complemented strains. (A) Biofilm of complemented strains in LB and (B) in ASM. Figure S7. Graphical representation of the *G. mellonella* health index score. *G. mellonella* moths were injected with the complemented strains or with physiological solution or not injected.

Author Contributions: Conceptualization, G.R.; methodology, S.I., V.C.S. and M.D.; software, V.C.S.; validation, G.T., G.B. and S.V.; formal analysis, S.I. and V.C.S.; investigation, S.I. and V.C.S.; resources, S.B. and S.V.; writing—original draft preparation, S.I. and V.C.S.; writing—review and editing, S.B.; visualization, M.P. and M.S.; supervision, S.B. All authors have read and agreed to the published version of the manuscript.

Funding: This research received no external funding.

Novel approaches to manage antimicrobial resistances: a story of vaccine research and divisome inhibition.

Data Availability Statement: The datasets generated and analyzed during the current study are available from the corresponding author on reasonable request.

Acknowledgments: We thank Amanda Oldani and Patrizia Vaghi (Centro Grandi Strumenti, University of Pavia, Italy) for technical assistance with confocal microscopy.

Conflicts of Interest: The authors declare no conflict of interest.

References

1. Tavares, M.; Kozak, M.; Balola, A.; Sá-Correia, I. *Burkholderia cepacia* complex bacteria: A feared contamination risk in water-based pharmaceutical products. *Clin. Microbiol. Rev.* **2020**, *33*, e00139-19. [CrossRef] [PubMed]
2. Bach, E.; Sant'Anna, F.H.; Seger, G.D.D.S.; Passaglia, L.M.P. Pangenome inventory of *Burkholderia sensu lato*, *Burkholderia sensu stricto*, and the *Burkholderia cepacia* complex reveals the uniqueness of *Burkholderia catarinensis*. *Genomics* **2022**, *114*, 398–408. [CrossRef] [PubMed]
3. Chen, J.H.; Xiang, W.; Cao, K.X.; Lu, X.; Yao, S.C.; Hung, D.; Huang, R.S.; Li, L.B. Characterization of volatile organic compounds emitted from endophytic *Burkholderia cenocepacia* ETR-B22 by SPME-GC-MS and their inhibitory activity against various plant fungal pathogens. *Molecules* **2020**, *25*, 3765. [CrossRef] [PubMed]
4. Patel, R.R.; Patel, D.D.; Bhatt, J.; Thakor, P.; Triplett, L.R.; Thakkar, V.R. Induction of pre-chorismate, jasmonate and salicylate pathways by *Burkholderia* sp. RR18 in peanut seedlings. *J. Appl. Microbiol.* **2021**, *131*, 1417–1430. [CrossRef]
5. Mahenthiralingam, E.; Baldwin, A.; Dowson, C.G. *Burkholderia cepacia* complex bacteria: Opportunistic pathogens with important natural biology. *J. Appl. Microbiol.* **2008**, *104*, 1539–1551. [CrossRef]
6. El Chakhtoura, N.G.; Saade, E.; Wilson, B.M.; Perez, F.; Papp-Wallace, K.M.; Bonomo, R.A. A 17-Year nationwide study of *Burkholderia cepacia* complex bloodstream infections among patients in the United States Veterans Health Administration. *Clin. Infect. Dis.* **2017**, *65*, 1253–1259. [CrossRef]
7. Tüfekci, S.; Şafak, B.; Nalbantoğlu, B.; Samancı, N.; Kiraz, N. *Burkholderia cepacia* complex bacteremia outbreaks among non-cystic fibrosis patients in the pediatric unit of a university hospital. *Turk. J. Pediatr.* **2021**, *63*, 218–222. [CrossRef]
8. Lubovich, S.; Zaragoza, S.; Rodríguez, V.; Buendía, J.; Camargo Vargas, B.; Alchundia Moreira, J.; Galanternik, L.; Ratto, P.; Teper, A. Risk factors associated with pulmonary exacerbations in pediatric patients with cystic fibrosis. *Arch. Argent. Pediatr.* **2019**, *117*, e466–e472.
9. Somayaji, R.; Yau, Y.C.W.; Tullis, E.; LiPuma, J.J.; Ratjen, F.; Waters, V. Clinical outcomes associated with *Burkholderia cepacia* complex infection in patients with cystic fibrosis. *Ann. Am. Thorac. Soc.* **2020**, *17*, 1542–1548. [CrossRef]
10. Akinboyo, I.C.; Sick-Samuels, A.C.; Singeltary, E.; Fackler, J.; Ascenzi, J.; Carroll, K.C.; Maldonado, Y.; Brooks, R.B.; Benowitz, I.; Wilson, L.E.; et al. Multistate outbreak of an emerging *Burkholderia cepacia* complex strain associated with contaminated oral liquid docusate sodium. *Infect. Control Hosp. Epidemiol.* **2018**, *39*, 237–239. [CrossRef]
11. Wong, S.C.Y.; Wong, S.C.; Chen, J.H.K.; Poon, R.W.S.; Hung, D.L.L.; Chiu, K.H.Y.; So, S.Y.C.; Leung, W.S.; Chan, T.M.; Yap, D.Y.H.; et al. Polyclonal *Burkholderia cepacia* complex outbreak in peritoneal dialysis patients caused by contaminated aqueous chlorhexidine. *Emerg. Infect. Dis.* **2020**, *26*, 1987–1997. [CrossRef]
12. Bharara, T.; Chakravarti, A.; Sharma, M.; Agarwal, P. Investigation of *Burkholderia cepacia* complex bacteremia outbreak in a neonatal intensive care unit: A case series. *J. Med. Case Rep.* **2020**, *14*, 76. [CrossRef]
13. Lord, R.; Jones, A.M.; Horsley, A. Antibiotic treatment for *Burkholderia cepacia* complex in people with cystic fibrosis experiencing a pulmonary exacerbation. *Cochrane Database Syst. Rev.* **2020**, *4*, CD009529. [CrossRef]
14. Sousa, S.A.; Seixas, A.M.M.; Leitão, J.H. Postgenomic approaches and bioinformatics tools to advance the development of vaccines against bacteria of the *Burkholderia cepacia* complex. *Vaccines* **2018**, *6*, 34. [CrossRef]
15. Scoffone, V.C.; Barbieri, G.; Buroni, S.; Scarselli, M.; Pizza, M.; Rappuoli, R.; Riccardi, G. Vaccines to Overcome Antibiotic Resistance: The Challenge of *Burkholderia cenocepacia*. *Trends Microbiol.* **2020**, *28*, 315–326. [CrossRef]
16. Pradenas, G.A.; Myers, J.N.; Torres, A.G. Characterization of the *Burkholderia cenocepacia* tonB mutant as a potential live attenuated vaccine. *Vaccines* **2017**, *5*, 33. [CrossRef]
17. Bertot, G.M.; Restelli, M.A.; Galanternik, L.; Aranibar Urey, R.C.; Valvano, M.A.; Grinstein, S. Nasal immunization with *Burkholderia multivorans* outer membrane proteins and the mucosal adjuvant adamantylamide dipeptide confers efficient protection against experimental lung infections with *B. multivorans* and *B. cenocepacia*. *Infect. Immun.* **2007**, *75*, 2740–2752. [CrossRef]
18. Makidon, P.E.; Knowlton, J.; Groom, J.V., 2nd; Blanco, L.P.; LiPuma, J.J.; Bielinska, A.U.; Baker, J.R., Jr. Induction of immune response to the 17 kDa OMPA *Burkholderia cenocepacia* polypeptide and protection against pulmonary infection in mice after nasal vaccination with an OMP nanoemulsion-based vaccine. *Med. Microbiol. Immunol.* **2010**, *199*, 81–92. [CrossRef]
19. Sousa, S.A.; Morad, M.; Feliciano, J.R.; Pita, T.; Nady, S.; El-Hennamy, R.E.; Abdel-Rahman, M.; Cavaco, J.; Pereira, L.; Barreto, C.; et al. The *Burkholderia cenocepacia* OmpA-like protein BCAL2958: Identification, characterization, and detection of anti-BCAL2958 antibodies in serum from *B. cepacia* complex-infected Cystic Fibrosis patients. *AMB Express* **2016**, *6*, 41. [CrossRef]
20. McClean, S.; Healy, M.E.; Collins, C.; Carberry, S.; O'Shaughnessy, L.; Dennehy, R.; Adams, Á.; Kennelly, H.; Corbett, J.M.; Carty, F.; et al. Linocin and OmpW are involved in attachment of the cystic fibrosis-associated pathogen *Burkholderia cepacia* complex to lung epithelial cells and protect mice against infection. *Infect. Immun.* **2016**, *84*, 1424–1437. [CrossRef]

21. Sousa, S.A.; Seixas, A.M.M.; Mandal, M.; Rodríguez-Ortega, M.J.; Leitão, J.H. Characterization of the *Burkholderia cenocepacia* J2315 surface-exposed immunoproteome. *Vaccines* **2020**, *8*, 509. [CrossRef]
22. Seixas, A.M.M.; Sousa, S.A.; Feliciano, J.R.; Gomes, S.C.; Ferreira, M.R.; Moreira, L.M.; Leitão, J.H. A polyclonal antibody raised against the *Burkholderia cenocepacia* OmpA-like protein BCAL2645 impairs the bacterium adhesion and invasion of human epithelial cells in vitro. *Biomedicines* **2021**, *9*, 1788. [CrossRef]
23. Sousa, S.A.; Soares-Castro, P.; Seixas, A.M.M.; Feliciano, J.R.; Balugas, B.; Barreto, C.; Pereira, L.; Santos, P.M.; Leitão, J.H. New insights into the immunoproteome of *B. cenocepacia* J2315 using serum samples from cystic fibrosis patients. *N. Biotechnol.* **2020**, *54*, 62–70. [CrossRef]
24. Dennehy, R.; Romano, M.; Ruggiero, A.; Mohamed, Y.F.; Dignam, S.L.; Mujica Troncoso, C.; Callaghan, M.; Valvano, M.A.; Berisio, R.; McClean, S. The *Burkholderia cenocepacia* peptidoglycan-associated lipoprotein is involved in epithelial cell attachment and elicitation of inflammation. *Cell Microbiol.* **2017**, *19*, e12691. [CrossRef]
25. Pimenta, A.I.; Mil-Homens, D.; Fialho, A.M. *Burkholderia cenocepacia*-host cell contact controls the transcription activity of the trimeric autotransporter adhesin BCAM2418 gene. *Microbiologyopen* **2020**, *9*, e998. [CrossRef]
26. Mil-Homens, D.; Leça, M.I.; Fernandes, F.; Pinto, S.N.; Fialho, A.M. Characterization of BCAM0224, a multifunctional trimeric autotransporter from the human pathogen *Burkholderia cenocepacia*. *J. Bacteriol.* **2014**, *196*, 1968–1979. [CrossRef]
27. Rappuoli, R. Reverse vaccinology. *Curr. Opin. Microbiol.* **2000**, *3*, 445–450. [CrossRef]
28. Aziz, R.K.; Bartels, D.; Best, A.A.; DeJongh, M.; Disz, T.; Edwards, R.A.; Formsma, K.; Gerdes, S.; Glass, E.M.; Kubal, M.; et al. The RAST Server: Rapid annotations using subsystems technology. *BMC Genom.* **2008**, *9*, 75. [CrossRef]
29. Sette, A.; Rappuoli, R. Reverse vaccinology: Developing vaccines in the era of genomics. *Immunity* **2010**, *33*, 530–541. [CrossRef]
30. Yu, N.Y.; Wagner, J.R.; Laird, M.R.; Melli, G.; Rey, S.; Lo, R.; Dao, P.; Sahinalp, S.C.; Ester, M.; Foster, L.J.; et al. PSORTb 3.0: Improved protein subcellular localization prediction with refined localization subcategories and predictive capabilities for all prokaryotes. *Bioinformatics* **2010**, *26*, 1608–1615. [CrossRef]
31. Jones, P.; Binns, D.; Chang, H.Y.; Fraser, M.; Li, W.; McAnulla, C.; McWilliam, H.; Maslen, J.; Mitchell, A.; Nuka, G.; et al. InterProScan 5: Genome-scale protein function classification. *Bioinformatics* **2014**, *30*, 1236–1240. [CrossRef]
32. Altschul, S.F.; Gish, W.; Miller, W.; Myers, E.W.; Lipman, D.J. Basic local alignment search tool. *J. Mol. Biol.* **1990**, *215*, 403–410. [CrossRef]
33. Krogh, A.; Larsson, B.; von Heijne, G.; Sonnhammer, E.L. Predicting transmembrane protein topology with a hidden Markov model: Application to complete genomes. *J. Mol. Biol.* **2001**, *305*, 567–580. [CrossRef]
34. Käll, L.; Krogh, A.; Sonnhammer, E.L. A combined transmembrane topology and signal peptide prediction method. *J. Mol. Biol.* **2004**, *338*, 1027–1036. [CrossRef]
35. Tusnády, G.E.; Simon, I. The HMMTOP transmembrane topology prediction server. *Bioinformatics* **2001**, *17*, 849–850. [CrossRef]
36. He, Y.; Xiang, Z.; Mobley, H.L. Vaxign: The first web-based vaccine design program for reverse vaccinology and applications for vaccine development. *J. Biomed. Biotechnol.* **2010**, *2010*, 297505. [CrossRef]
37. Doytchinova, I.A.; Flower, D.R. VaxiJen: A server for prediction of protective antigens, tumour antigens and subunit vaccines. *BMC Bioinform.* **2007**, *8*, 4. [CrossRef]
38. Berman, H.M.; Westbrook, J.; Feng, Z.; Gilliland, G.; Bhat, T.N.; Weissig, H.; Shindyalov, I.N.; Bourne, P.E. The Protein Data Bank. *Nucleic Acids Res.* **2000**, *28*, 235–242. [CrossRef]
39. Kirchner, S.; Fothergill, J.L.; Wright, E.A.; James, C.E.; Mowat, E.; Winstanley, C. Use of artificial sputum medium to test antibiotic efficacy against *Pseudomonas aeruginosa* in conditions more relevant to the cystic fibrosis lung. *J. Vis. Exp.* **2012**, *64*, e3857.
40. Hamad, M.A.; Skeldon, A.M.; Valvano, M.A. Construction of aminoglycoside-sensitive *Burkholderia cenocepacia* strains for use in studies of intracellular bacteria with the gentamicin protection assay. *Appl. Environ. Microbiol.* **2010**, *76*, 3170–3176. [CrossRef]
41. Law, R.J.; Hamlin, J.N.; Sivro, A.; McCorrister, S.J.; Cardama, G.A.; Cardona, S.T. A functional phenylacetic acid catabolic pathway is required for full pathogenicity of *Burkholderia cenocepacia* in the *Caenorhabditis elegans* host model. *J. Bacteriol.* **2008**, *190*, 7209–7218. [CrossRef] [PubMed]
42. Cardona, S.T.; Valvano, M.A. An expression vector containing a rhamnose-inducible promoter provides tightly regulated gene expression in *Burkholderia cenocepacia*. *Plasmid* **2005**, *54*, 219–228. [CrossRef]
43. Biot, F.V.; Lopez, M.M.; Poyot, T.; Neulat-Ripoll, F.; Lignon, S.; Caclard, A.; Thibault, F.M.; Peinnequin, A.; Pagès, J.M.; Valade, E. Interplay between three RND efflux pumps in doxycycline-selected strains of *Burkholderia thailandensis*. *PLoS ONE* **2013**, *8*, e84068. [CrossRef]
44. Klimentová, J.; Stulík, J. Methods of isolation and purification of outer membrane vesicles from gram-negative bacteria. *Microbiol. Res.* **2015**, *170*, 1–9. [CrossRef] [PubMed]
45. Buroni, S.; Scoffone, V.C.; Fumagalli, M.; Makarov, V.; Cagnone, M.; Trespidi, G.; De Rossi, E.; Forneris, F.; Riccardi, G.; Chiarelli, L.R. Investigating the mechanism of action of diketopiperazines inhibitors of the *Burkholderia cenocepacia* quorum sensing synthase CepI: A site-directed mutagenesis study. *Front. Pharmacol.* **2018**, *9*, 836. [CrossRef]
46. Martinotti, S.; Ranzato, E. 2-DE Gel analysis: The spot detection. *Methods Mol. Biol.* **2016**, *1384*, 155–164. [PubMed]
47. EUCAST. Determination of minimum inhibitory concentrations (MICs) of antibacterial agents by broth dilution. *Clin. Microbiol. Infect.* **2003**, *9*, 509–515.
48. Martin, A.; Takiff, H.; Vandamme, P.; Swings, J.; Palomino, J.C.; Portaels, F. A new rapid and simple colorimetric method to detect pyrazinamide resistance in *Mycobacterium tuberculosis* using nicotinamide. *J. Antimicrob. Chemother.* **2006**, *58*, 327–331. [CrossRef]

Novel approaches to manage antimicrobial resistances: a story of vaccine research and divisome inhibition.

49. Bhargava, S.; Johnson, B.B.; Hwang, J.; Harris, T.A.; George, A.S.; Muir, A.; Dorff, J.; Okeke, I.N. Heat-resistant agglutinin 1 is an accessory enteroaggregative *Escherichia coli* colonization factor. *J. Bacteriol.* **2009**, *191*, 4934–4942. [CrossRef]
50. Vandecandelaere, I.; Van Acker, H.; Coenye, T. A Microplate-Based System as In Vitro Model of Biofilm Growth and Quantification. *Methods Mol. Biol.* **2016**, *1333*, 53–66.
51. Heydorn, A.; Nielsen, A.T.; Hentzer, M.; Sternberg, C.; Givskov, M.; Ersbøll, B.K.; Molin, S. Quantification of biofilm structures by the novel computer program COMSTAT. *Microbiol. Read.* **2000**, *146*, 2395–2407. [CrossRef] [PubMed]
52. Bernier, S.P.; Sokol, P.A. Use of suppression-subtractive hybridization to identify genes in the *Burkholderia cepacia* complex that are unique to *Burkholderia cenocepacia*. *J. Bacteriol.* **2005**, *187*, 5278–5291. [CrossRef] [PubMed]
53. Seed, K.D.; Dennis, J.J. Development of *Galleria mellonella* as an alternative infection model for the *Burkholderia cepacia* complex. *Infect. Immun.* **2008**, *76*, 1267–1275. [CrossRef] [PubMed]
54. Tsai, C.J.; Loh, J.M.; Proft, T. *Galleria mellonella* infection models for the study of bacterial diseases and for antimicrobial drug testing. *Virulence* **2016**, *7*, 214–229. [CrossRef] [PubMed]
55. Kugimiya, W.; Otani, Y.; Hashimoto, Y.; Takagi, Y. Molecular cloning and nucleotide sequence of the lipase gene from *Pseudomonas fragi*. *Biochem. Biophys. Res. Commun.* **1986**, *141*, 185–190. [CrossRef]
56. Rosenau, F.; Isenhardt, S.; Gdynia, A.; Tielker, D.; Schmidt, E.; Tielen, P.; Schobert, M.; Jahn, D.; Wilhelm, S.; Jaeger, K.E. Lipase LipC affects motility, biofilm formation and rhamnolipid production in *Pseudomonas aeruginosa*. *FEMS Microbiol. Lett.* **2010**, *309*, 25–34. [CrossRef]
57. Wilhelm, S.; Gdynia, A.; Tielen, P.; Rosenau, F.; Jaeger, K.E. The autotransporter esterase EstA of *Pseudomonas aeruginosa* is required for rhamnolipid production, cell motility, and biofilm formation. *J. Bacteriol.* **2007**, *189*, 6695–6703. [CrossRef]
58. Holden, M.T.; Seth-Smith, H.M.; Crossman, L.C.; Sebaihia, M.; Bentley, S.D.; Cerdeño-Tárraga, A.M.; Thomson, N.R.; Bason, N.; Quail, M.A.; Sharp, S.; et al. The genome of *Burkholderia cenocepacia* J2315, an epidemic pathogen of cystic fibrosis patients. *J. Bacteriol.* **2009**, *191*, 261–277. [CrossRef] [PubMed]
59. Guo, F.B.; Xiong, L.; Zhang, K.Y.; Dong, C.; Zhang, F.Z.; Woo, P.C. Identification and analysis of genomic islands in *Burkholderia cenocepacia* AU 1054 with emphasis on pathogenicity islands. *BMC Microbiol.* **2017**, *17*, 73. [CrossRef]
60. Rosales-Reyes, R.; Aubert, D.F.; Tolman, J.S.; Amer, A.O.; Valvano, M.A. *Burkholderia cenocepacia* Type VI Secretion System mediates escape of Type II secreted proteins into the cytoplasm of infected macrophages. *PLoS ONE* **2012**, *7*, e41726. [CrossRef]
61. Pimenta, A.I.; Kilcoyne, M.; Bernardes, N.; Mil-Homens, D.; Joshi, L.; Fialho, A.M. *Burkholderia cenocepacia* BCAM2418-induced antibody inhibits bacterial adhesion, confers protection to infection and enables identification of host glycans as adhesin targets. *Cell Microbiol.* **2021**, *23*, e13340. [CrossRef] [PubMed]
62. Liu, H.; Ibrahim, M.; Qiu, H.; Kausar, S.; Ilyas, M.; Cui, Z.; Hussain, A.; Li, B.; Waheed, A.; Zhu, B.; et al. Protein profiling analyses of the outer membrane of *Burkholderia cenocepacia* reveal a niche-specific proteome. *Microb. Ecol.* **2015**, *69*, 75–83. [CrossRef] [PubMed]
63. Rasmussen, M.; Jacobsson, M.; Björck, L. Genome-based identification and analysis of collagen-related structural motifs in bacterial and viral proteins. *J. Biol. Chem.* **2003**, *278*, 32313–32316. [CrossRef]
64. Pilapitiya, D.H.; Harris, P.W.R.; Hanson-Manful, P.; McGregor, R.; Kowalczyk, R.; Raynes, J.M.; Carlton, L.H.; Dobson, R.C.J.; Baker, M.G.; Brimble, M.; et al. Antibody responses to collagen peptides and streptococcal collagen-like 1 proteins in acute rheumatic fever patients. *Pathog. Dis.* **2021**, *79*, ftab033. [CrossRef] [PubMed]
65. Bachert, B.A.; Choi, S.J.; Snyder, A.K.; Rio, R.V.; Durney, B.C.; Holland, L.A.; Amemiya, K.; Welkos, S.L.; Bozue, J.A.; Cote, C.K.; et al. A unique set of the *Burkholderia* collagen-like proteins provides insight into pathogenesis, genome evolution and niche adaptation, and infection detection. *PLoS ONE* **2015**, *10*, e0137578. [CrossRef]
66. Grund, M.E.; Kramarska, E.; Choi, S.J.; McNitt, D.H.; Klimko, C.P.; Rill, N.O.; Dankmeyer, J.L.; Shoe, J.L.; Hunter, M.; Fetterer, D.P.; et al. Predictive and experimental immunogenicity of *Burkholderia* collagen-like protein 8-derived antigens. *Vaccines* **2021**, *9*, 1219. [CrossRef]
67. Mullen, T.; Markey, K.; Murphy, P.; McClean, S.; Callaghan, M. Role of lipase in *Burkholderia cepacia* complex (Bcc) invasion of lung epithelial cells. *Eur. J. Clin. Microbiol. Infect. Dis.* **2007**, *26*, 869–877. [CrossRef]
68. Straus, D.C.; Lonon, M.K.; Hutson, J.C. Inhibition of rat alveolar macrophage phagocytic function by a *Pseudomonas cepacia* lipase. *J. Med. Microbiol.* **1992**, *37*, 335–340. [CrossRef]
69. Tielen, P.; Kuhn, H.; Rosenau, F.; Jaeger, K.E.; Flemming, H.C.; Wingender, J. Interaction between extracellular lipase LipA and the polysaccharide alginate of *Pseudomonas aeruginosa*. *BMC Microbiol.* **2013**, *13*, 159. [CrossRef]
70. Funken, H.; Knapp, A.; Vasil, M.L.; Wilhelm, S.; Jaeger, K.E.; Rosenau, F. The lipase LipA (PA2862) but not LipC (PA4813) from *Pseudomonas aeruginosa* influences regulation of pyoverdine production and expression of the sigma factor PvdS. *J. Bacteriol.* **2011**, *193*, 5858–5860. [CrossRef]
71. Kiessling, A.R.; Malik, A.; Goldman, A. Recent advances in the understanding of trimeric autotransporter adhesins. *Med. Microbiol. Immunol.* **2020**, *209*, 233–242. [CrossRef] [PubMed]
72. Mil-Homens, D.; Pinto, S.N.; Matos, R.G.; Arraiano, C.; Fialho, A.M. *Burkholderia cenocepacia* K56-2 trimeric autotransporter adhesin BcaA binds TNFR1 and contributes to induce airway inflammation. *Cell Microbiol.* **2017**, *19*, e12677. [CrossRef] [PubMed]
73. Papadopoulos, A.; Busch, M.; Reiners, J.; Hachani, E.; Baeumers, M.; Berger, J.; Schmitt, L.; Jaeger, K.E.; Kovacic, F.; Smits, S.H.J.; et al. The periplasmic chaperone Skp prevents misfolding of the secretory lipase A from *Pseudomonas aeruginosa*. *Front. Mol. Biosci.* **2022**, *9*, 1026724. [CrossRef] [PubMed]

74. Putra, L.; Natadiputri, G.; Meryandini, A.; Suwanto, A. Isolation, cloning and co-expression of lipase and foldase genes of *Burkholderia territorii* GP3 from mount Papandayan soil. *J. Microbiol. Biotechnol.* **2019**, *29*, 944–951. [CrossRef] [PubMed]
75. Masignani, V.; Pizza, M.; Moxon, E.R. The Development of a Vaccine against Meningococcus B Using Reverse Vaccinology. *Front. Immunol.* **2019**, *10*, 751. [CrossRef] [PubMed]
76. Delany, I.; Rappuoli, R.; Seib, K.L. Vaccines, reverse vaccinology, and bacterial pathogenesis. *Cold Spring Harb. Perspect. Med.* **2013**, *3*, a012476. [CrossRef] [PubMed]
77. Toyofuku, M.; Schild, S.; Kaparakis-Liaskos, M.; Eberl, L. Composition and functions of bacterial membrane vesicles. *Nat. Rev. Microbiol.* 2023, *Online ahead of print*.
78. Figurski, D.H.; Helinski, D.R. Replication of an origin-containing derivative of plasmid RK2 dependent on a plasmid function provided in trans. *Proc. Natl. Acad. Sci. USA* **1979**, *76*, 1648–1652. [CrossRef] [PubMed]